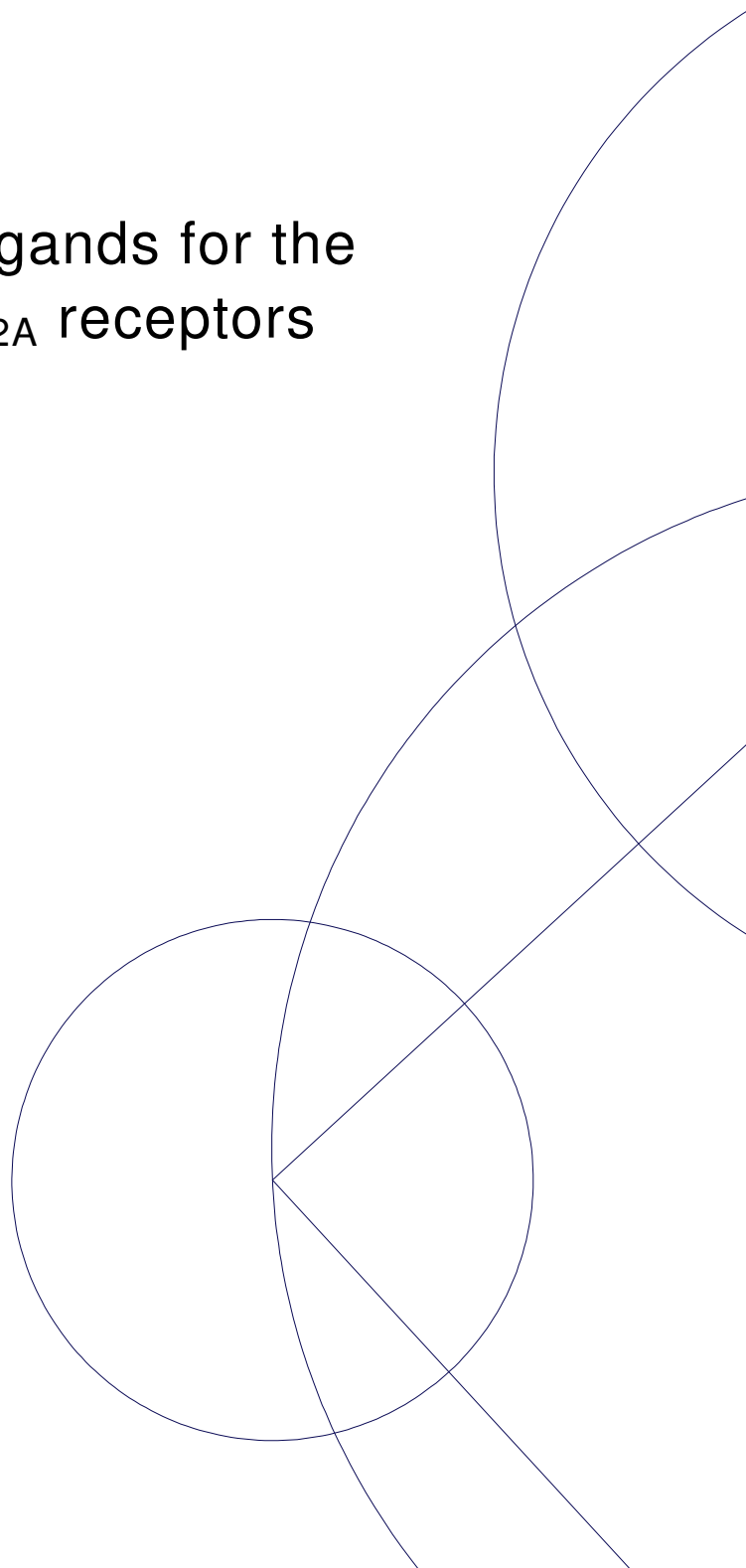## PhD thesis

Hanne Demant Hansen

Evaluation of PET radioligands for the cerebral 5-HT$_7$ and 5-HT$_{2A}$ receptors

Academic advisor: Gitte Moos Knudsen

Submitted: 31/05/2013

Title: Evaluation of PET radioligands for the cerebral 5-HT$_7$ and 5-HT$_{2A}$ receptors

Author: Hanne Demant Hansen, M.Sc. Molecular Biology

Department: Neurobiology Research Unit, Neuroscience Center, Copenhagen University Hospital Rigshospitalet, Denmark

Institution: Faculty of Health and Medical Sciences, University of Copenhagen, Denmark

Date of Submission: May 31st, 2013

Principal supervisor:

Professor Gitte Moos Knudsen, Neurobiology Research Unit and Center for Integrated Molecular Brain Imaging

Review committee:

Assistant professor Petrine Welledorph (Chairperson), Department of Medicinal Chemistry, University of Copenhagen, Denmark

Professor David Brooks, Department of Clinical Medicine, Aarhus University, Denmark

Professor Christer Halldin, Department of Clinical Neuroscience, Karolinska Institute, Sweden.

The PhD thesis defence will take place on October 11th, 2013 at 2 PM in Auditorium 93 at Rigshospitalet, Copenhagen.

This thesis has been submitted to the Graduate School of The Faculty of Health and Medical Sciences, University of Copenhagen.

List of manuscripts

The thesis is based on the following manuscripts and published papers, which in the text are referred to by their Roman numerals:

I. **Hansen HD**, Ettrup A, Herth MM, Dyssegaard A, Ratner C, Gillings N, Knudsen GM. Direct comparison of [^{18}F]MH.MZ and [^{18}F]altanserin for 5-HT$_{2A}$ receptor imaging with PET. *Synapse*. 2013 Jun;67(6):328-37.

II. **Hansen HD**, Lacivita E, Di Pilato P, Herth MM, Lehel S, Ettrup A, Andersen VL, Dyssegaard A, De Giorgio P, Perrone R, Berardi F, Colabufo NA, Niso M, Knudsen GM, Leopoldo M. Synthesis, Radiolabeling and In Vivo Evaluation of [^{11}C](*R*)-1-[4-[2-(4-methoxyphenyl)phenyl]piperazin-1-yl]-3-pyrazin-2-yloxy]-2-propanol, a Potential PET Radioligand for the 5-HT$_7$ Receptor. *Manuscript*

III. Herth MM*, **Hansen HD***, Ettrup A, Dyssegaard A, Lehel S, Kristensen J, Knudsen GM. Synthesis and evaluation of [^{11}C]Cimbi-806 as a potential PET ligand for 5-HT$_7$ receptor imaging. *Bioorganic & Medicinal Chemistry*. 2012 Jul 15;20(14):4574-81.
* Equal contributions.

IV. **Hansen HD**, Herth MM, Ettrup A, Andersen VL, Lehel S, Dyssegaard A, Kristensen JL, Knudsen GM. Radiosynthesis and in vivo evaluation of novel radioligands for PET imaging of 5-HT$_7$ receptors. *Journal of Nuclear Medicine*, *submitted April 2013*.

The following papers and manuscripts are related to the work described, but not included in the thesis:

1. Risgaard R, Ettrup A, Balle T, Dyssegaard A, **Hansen HD**, Lehel S, Madsen J, Pedersen H, Püschl A, Badolo L, Bang-Andersen B, Knudsen GM, Kristensen JL. Radiolabelling and PET brain imaging of the α$_1$-adrenoceptor antagonist Lu AE43936. *Nuclear Medecine and Biology*. 2013 Jan;40(1):135-40.

2. Pinborg LH, Feng L, Haahr ME, Gillings N, Dyssegaard A, Madsen J, Svarer C, Yndgaard S, Kjaer TW, Parsey RV, **Hansen HD**, Ettrup A, Paulson OB, Knudsen GM. No change in [^{11}C]CUMI-101 binding to 5-HT$_{1A}$ receptors after intravenous citalopram in human. *Synapse*. 2012 Oct;66(10):880-4.

Acknowledgements

First and foremost I would like to sincerely thank my supervisor Gitte Moos Knudsen for scientific advice, guidance and encouragement. Your scientific understanding and visions are truly impressive and inspiring.

Secondly, I would like to thank the entire NRU staff for creating a professional, inspiring and yet very sociable work environment - I feel privileged to have worked here for three years. Whether the daily breaks revolve around science or snacks you always brighten my day. A special thanks to my practical supervisor Anders Ettrup who has taught me so much science, been the editor on both manuscripts and this thesis, and been a true support all the way through this thesis work.

This work could not have been possible without the generous help and assistance from many people. Thank you all for your continuous flexibility and for working long hours. Thanks to Mette Værum Olsen and Letty Klarskov at the Department of Experimental Medicine, for preparing the pigs for a day in the PET scanner. Bente Dall, Camilla Knudsen, Anna Ljunggren are thanked for preparing and operating the HRRT scanner. Thanks also to the radiochemists Jacob Madsen, Szabolcs Lehel and Nic Gillings for assisting in or producing the radioligands, to Lasse Bech, Mikkel Schiødt and Agnete Dyssegaard for performing the HPLC analysis of the many blood samples, and to Sune Keller for helping with the more troublesome image reconstructions. A special thanks also to Matthias M. Herth and Valdemar L. Andersen for synthesizing the reference compounds and precursors, for radiolabeling these, and for fruitful discussions about experimental design and the results.

Lastly, I would like to thank my family and friends for endless support, encouragement and patience during three years with many joyful and preoccupied moment spiced with a few stressful moments as well.

Hanne Demant Hansen, Copenhagen, May 2013

Table of contents

Summary in English

The brain serotonin (5-HT) system plays a key role in modulating behavioural effects such as mood, appetite and sleep. Accordingly, dysfunction in the serotonergic system has been implicated in the pathophysiology of a wide range of neuropsychiatric disorders. Positron emission tomography (PET) is an imaging modality that is widely used clinically to measure metabolic activity and in brain research, PET can be utilized to map and quantify molecular targets in the different neurotransmitter systems. PET thereby allows for studies of the specific serotonergic targets related to certain neuropsychiatric disorders in both animals and humans. Currently, PET radioligands are available for the serotonin transporter (5-HTT) and for the 5-HT_{1A}, 5-HT_{1B}, 5-HT_{2A}, 5-HT_4 and 5-HT_6 receptors, but no well-validated PET radioligand currently exists for the 5-HT_7 receptor. The functional importance of this receptor is still unclear; however its involvement in neurological disorders such as depression and schizophrenia makes it an interesting target for both drug discovery and PET radioligand development.

The aim of this Ph.D. thesis was 1) to compare two existing PET radioligands for the 5-HT_{2A} receptor: $[^{18}\text{F}]$altanserin and $[^{18}\text{F}]$MH.MZ, 2) to determine the 5-HT_7 receptor distribution in post mortem pig brain using autoradiography and 3) to evaluate novel PET radioligands for the 5-HT_7 receptor.

In the direct comparison between $[^{18}\text{F}]$altanserin and $[^{18}\text{F}]$MH.MZ, we found that $[^{18}\text{F}]$MH.MZ had a more reproducible metabolism than $[^{18}\text{F}]$altanserin in the pig and furthermore, no radiolabeled metabolites of $[^{18}\text{F}]$MH.MZ were found to cross the blood-brain barrier (BBB). However, $[^{18}\text{F}]$MH.MZ displayed very slow tracer kinetics which complicated the kinetic modeling. $[^{18}\text{F}]$Altanserin had reversible tracer kinetics but it is well-known that metabolites are generated that cross the BBB and interfere with the signal from the parent compound in the brain.

We tested eight different compounds in three different structural classes as possible PET radioligands for the 5-HT_7 receptor. Of these eight radioligands, two were substrates for P-glycoprotein, a BBB efflux protein, and therefore showed no brain uptake. Four other radioligands failed as 5-HT_7 receptor PET radioligands because their binding could not be blocked by the 5-HT_7 receptor specific antagonist SB-269970. Lastly, the two radioligands $[^{11}\text{C}]$Cimbi-712 and $[^{11}\text{C}]$Cimbi-717 had high brain uptake and showed specific binding to the 5-HT_7 receptor as binding could be blocked by preadministration of SB-269970, indicating that these radioligand candidates bound specifically to the 5-HT_7 receptor. Contrary to $[^{11}\text{C}]$Cimbi-712, $[^{11}\text{C}]$Cimbi-717 displayed reversible tracer kinetics and therefore we continued with the validation of this radioligand. With

[^{11}C]Cimbi-717 we found a dose-dependent relationship between administered SB-269970 and the measured receptor occupancy. Also we found good agreement between the 5-HT$_7$ receptor distribution found with [^{3}H]SB-269970 autoradiography in post mortem pig brain tissue and the *in vivo* binding distribution of [^{11}C]Cimbi-717.

In summary, the work comprised in this thesis describes the advantages and disadvantages of the two 5-HT$_{2A}$ receptor radioligands [^{18}F]altanserin and [^{18}F]MH.MZ. Furthermore, it describes the evaluation of a number of PET radioligands for the cerebral 5-HT$_7$ receptor. [^{11}C]Cimbi-717 being the most promising of the tested candidates may be a useful radiotracer for *in vivo* imaging of the 5-HT$_7$ receptors in the human brain.

Resumé på dansk

Hjernens serotonin (5-HT) system spiller en afgørende rolle i reguleringen af adfærdsmæssige aspekter så som humør, appetit og søvn. Dysfunktion af det serotonerge system er endvidere af patofysiologisk betydning for en lang række neuropsykiatriske sygdomme. Positron emission tomografi (PET) er en billeddannelses-teknik, der anvendes meget klinisk til at måle metabolsk aktivitet, og indenfor hjerneforskning kan PET bruges til at kortlægge og måle mængden af receptorer og andre proteiner inden for forskellige neurotransmittersystemer. De specifikke serotonerge targets, der er relateret til de neuropsykiatriske sygdomme, kan således studeres i både dyr og mennesker med PET. I øjeblikket eksisterer der PET sporstoffer for 5-HT transporteren og for $5-HT_{1A}$, $5-HT_{2A}$, $5-HT_4$ og $5-HT_6$ receptorerne, men der eksisterer ikke noget velvalideret PET sporstof for $5-HT_7$ receptoren. Den funktionelle betydning af denne receptor er stadig uklar, men dens implikation i hjernesygdomme såsom depression og skizofreni gør denne receptor til et interessant mål for både lægemiddel- og sporstofsudvikling.

Formålet med denne Ph.D. afhandling var 1) at sammenligne to eksisterende PET sporstoffer for $5-HT_{2A}$ receptoren: $[^{18}F]$altanserin og $[^{18}F]$MH.MZ, 2) at bestemme distributionen af $5-HT_7$ receptorer i post mortem grisehjerne og 3) at evaluere hidtil ukendte PET sporstoffer for $5-HT_7$ receptoren.

I den direkte sammenligning af $[^{18}F]$altanserin og $[^{18}F]$MH.MZ fandt vi, at $[^{18}F]$MH.MZ havde en mere reproducerbar metabolisme i grisen end $[^{18}F]$altanserin, og ydermere fandt vi, at ingen af de radiomærkede metabolitter af $[^{18}F]$MH.MZ krydsede blod-hjerne barrieren. $[^{18}F]$MH.MZ havde dog en meget langsom farmakokinetik i hjernen, hvilket komplicerer den kinetiske modellering. $[^{18}F]$Altanserin havde reversibel farmakokinetik, men det er velkendt, at der dannes lipofile radiomærkede metabolitter, der krydser blod-hjerne barrieren og forstyrrer signalet fra $[^{18}F]$altanserin.

Vi testede otte stoffer i tre forskellige strukturelle klasser som mulige PET sporstoffer for $5-HT_7$ receptoren. Af disse otte havde to sporstoffer intet hjerneoptag som følge af at være substrater for P-glycoprotein, som er et blod-hjerne barriere efflux protein. Fire andre sporstoffer fejlede som $5-HT_7$ receptor PET sporstoffer, da disse ikke kunnne blokeres med den $5-HT_7$ receptor specifikke antagonist SB-269970. De sidste to radioligander, $[^{11}C]$Cimbi-712 og $[^{11}C]$Cimbi-717, udviste høj optagelse i grisehjernen, og bindingen af disse kunne blokeres ved indgift af SB-269970 forud for sporstoffet, hvilket viser at disse radioligander binder specifikt til $5-HT_7$ receptoren. Da $[^{11}C]$Cimbi-717 i modsætning til $[^{11}C]$Cimbi-712 udviser reversibel farmakonkinetik, valgte vi at fortsætte

validering af netop denne radioligand. Med [^{11}C]Cimbi-717 fandt vi en dosis-afhængig sammenhæng mellem den indgivne mængde af SB-269970 og den målte receptorokkupans. Vi fandt også en god sammenhæng mellem hjernens regionale 5-HT$_7$ receptor distribution målt med [^{3}H]SB-269970 autoradiografi på post mortem grisehjernevæv og distributionen af [^{11}C]Cimbi-717 *in vivo*.

Denne afhandling beskriver således fordele og ulemper ved de to 5-HT$_{2A}$ receptor PET sporstoffer [^{18}F]altanserin og [^{18}F]MH.MZ. Den beskriver desuden evalueringen af en række PET sporstoffer for hjernens 5-HT$_7$ receptorer. Vi identificerede [^{11}C]Cimbi-717 som værende den bedste kandidat til *in vivo* billeddannelse af hjernens 5-HT$_7$ receptorer.

Abbreviations

1TC	One-tissue compartment	LogP	Log of partition coefficient
5-CT	5-carboxamidotryptamine	MAO	Monoamine oxidase
5-HIAA	5-hydroxindoleacetic acid	mg	Milligram
5-HT	5-hydroxytryptamine, serotonin	min	Minute(s)
5-HTP	5-hydroxytryptophan	mL	Millilitre
5-HTT	Serotonin transporter (SERT)	MRI	Magnetic resonance imaging
AADC	Aromatic amino acid decarboxylase	mRNA	Messenger ribonucleic acid
AC	Adenylate cyclase	NSB	Non-specifically bound
ANOVA	Analysis of variance	P	Plasma
BBB	Blood brain barrier	PCP	Phenylcyclinidine
Bmax	Receptor density	pCPA	p-chlorophenylalanine
BP	Binding potential	PET	Positron emission tomography
BP_{ND}	Binding potential related to the nondisplaceable radioligand in tissue	P-gp	P-glycoprotein
BP_P	Binding potential related to the plasma concentration of radioligand	PIB	Pittsburgh compound B
Bq	Becquerel	PIP_2	Phosphatidylinisotol-4,5-biphosphate
°C	Degree celcius	PPI	Prepulse inhibition
CNS	Central nervous system	PSL	Photostimulated luminescence
C_P	Concentration of radioligand in plasma	ROI	Region of interest
C_T	Concentration of radioligand in tissue	rpm	Revolutions per minute
CsA	Cyclosporine A	SB	Specific binding
F	Free radioligand	sec	Second(s)
ΔF_{NT}	Difference in neurotransmitter concentration	SERT	Serotonin transporter (5-HTT)
fMRI	Functional magnetic resonance imaging	SNP	Short nucleotide polymorphism
F_{NT}	Neurotransmitter concentration	SPECT	Single-proton emission computed tomography
FST	Forced swim test	SSRI	Selective serotonin reuptake inhibitor
g	Gram	SUV	Standardized uptake value
GPCR	G-protein coupled receptor	$t_{1/2}$	Half-life
HPLC	High pressure liquid chromatography	TB	Total binding
HRRT	High resolution research tomography	TE	Tissue equivalent
i.v.	Intra venous	TH	Tryptophan hydroxylase
IP	Imaging plate	TRYP	Tryptophan
IP_3	Inositol-1,4,5-triphosphate	TST	Tail suspension test
kBq	KiloBecquerel	µg	Microgram
K_D	Dissociation constant	µM	Micromolar
Kg	Kilogram	V_{ND}	Non-displaceable distribution volume
K_i	Inhibition constant	VOI	Volume of interest
K_{NT}	Neurotransmitter affinity	V_T	Distribution volume

INTRODUCTION

The serotonin transmitter system

Serotonin (5-hydroxytryptamine, 5-HT) was identified in 1948 when it was characterized as a vasoconstrictive substance in serum (Rapport et al., 1948). Five years later it was also found present in the mammalian brain (Twarog and Page, 1953). Biochemically derived from the amino acid tryptophan, 5-HT act as a neurotransmitter in the central and peripheral nervous system and it also acts as a hormone in other tissues such as the gastrointestinal tract, the cardiovascular system, and in immune cells. Thus, the majority of the total body serotonin is found outside of the central nervous system (CNS) and only one out of a million CNS nerve cells produce 5-HT (Gershon and Tack, 2007). Despite this, 5-HT is involved as a neurotransmitter in a range of normal physiological processes such as perception, appetite, sex, sleep, thermoregulation, cognition, and mood (Berger et al., 2009). Dysfunction in the 5-HT system has also been implicated in a variety of CNS disorders such as anxiety, depression, migraine, obsessive compulsive disorders, and schizophrenia (Muller and Jacobs, 2010).

5-HT does not cross the BBB but is synthesized in serotonergic neurons in the raphe nuclei in the brain (Dahlstrom and Fuxe, 1964; Törk, 1990). The serotonergic neurons project to the entire cerebrum, with almost every cell in the brain being in proximity of a serotonergic fiber (Berger et al., 2009). Two distinct anatomical subdivisions of raphe nuclei in humans are recognized (Figure 1): the rostral raphe nuclei where the projections ascend toward the cerebral cortex, basal ganglia and limbic system. These serotonergic neurons are implicated in the regulation of mood, sleep, sex, appetite etc. (Gershon and Tack, 2007). Projections from the caudal raphe nuclei either terminate in the medulla or descend to the spinal cord. These projections influence spinal and brainstem mechanisms and are involved in the central modulation of pain (Sommer, 2006).
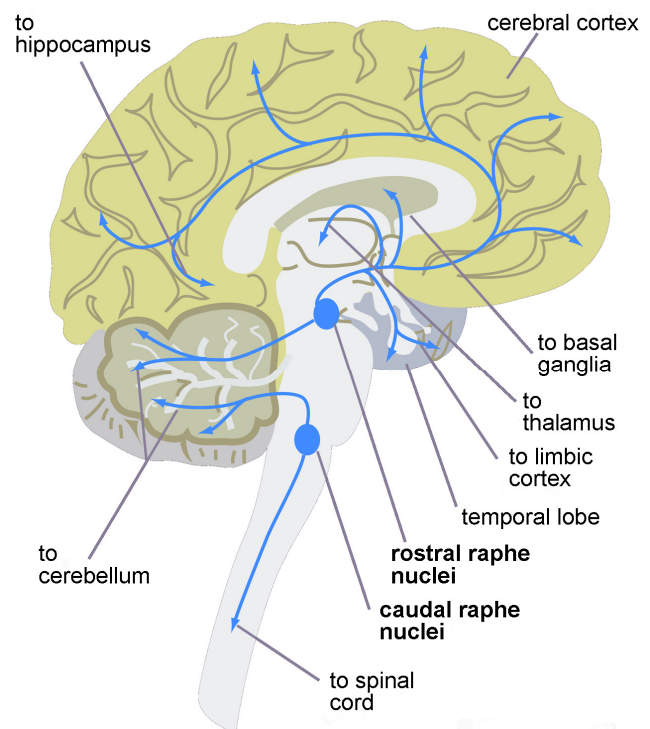

Figure 1 Serotonergic pathways in the human brain. Figure modified from: http://www.cnsforum.com/educationalresources/imagebank/

The biosynthesis of 5-HT starts by conversion of the essential amino acid L-tryptophan to 5-hydroxy-L-tryptophan (5-HTP) by tryptophan hydroxylase. 5-HTP is subsequently converted by the enzyme aromatic amino acid decarboxylase to 5-HT. After synthesis, 5-HT is packaged into terminal vesicles for release into the synaptic cleft, which occurs upon neuronal firing, i.e. when there is sufficient stimulation of the neuron. Upon release from the serotonergic neuron, 5-HT in the synapse has multiple actions: 1) 5-HT can bind to its receptor on the post-synaptic neuron, resulting in a transduction of the signal that initially stimulated the pre-synaptic serotonergic neuron. 2) 5-HT can bind to presynaptic serotonin receptors (also called autoreceptors) on the neuron from which it was released, which provides feedback and regulates firing rate of the neuron. 3) 5-HT can be taken up into the presynaptic serotonin neuron by the serotonin transporter (5-HTT, SERT) where it will be recycled for future release or broken down by monoamine oxidase to 5-hydroxyindoleacetic acid and excreted in urine (Figure 2).
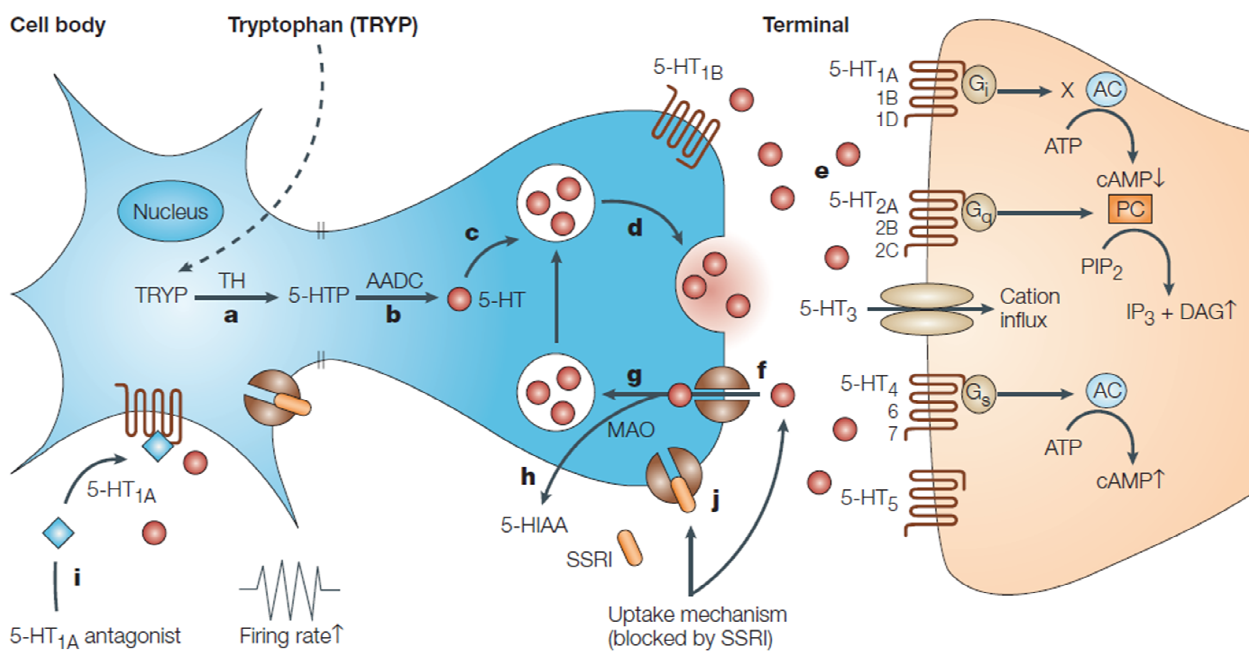

Figure 2   Schematic representation of serotonergic neurotransmission. Figure adapted from: (Wong et al., 2005) **a**) Tryptophan hydroxylase (TH) converts tryptophan (TRYP) into 5-hydroxytryptophan (5-HTP). **b**) Aromatic amino acid decarboxylase (AADC) subsequently catalyses the conversion of 5-HTP to 5-hydroxytryptamine (5-HT). **c**) 5-HT is stored in synaptic vesicles. **d**) Upon neuronal firing, 5-HT is released from the vesicles into the synaptic cleft. **e**) 5-HT can bind to one of the receptors in the seven different receptor families, which is coupled to a signal transduction system within in the postsynaptic neuron. **f**) Reuptake of 5-HT by the serotonin transporter (5-HTT, SERT). **g**) 5-HT can be stored into vesicles allowing for recycling of the neurotransmitter. **h**) Degradation of 5-HT by monoamine oxidase (MAO) into its main metabolite 5-hydroxyindoleactic acid (5-HIAA). **i**) 5-HT can bind to autoreceptors such as the $5-HT_{1A}$ receptor, resulting in a feedback loop and regulation of plasticity of the neuron. **j**) Selective serotonin-reuptake inhibitors (SSRIs) can inhibit the 5-HT transporter (5-HTT) and thereby increase the concentration of 5-HT in the synaptic cleft. AC, adenylate cyclase; ATP: adenosine triphosphate; cAMP, cyclic adenosine monophosphate; DAG, diacylglycerol; IP_3 inositiol-1,4,5-triphosphate; PIP_2, phosphatidylinositol-4,5-biphosphate.

5-HT receptors

Part of the ability of 5-HT to mediate the aforementioned wide range of actions arise from the number and diversity of 5-HT receptors. All 5-HT receptors, except the 5-HT_3 receptor, are members of the so-called Family A type G protein-coupled receptors (GPCR). Currently, 14 distinct mammalian receptor subtypes are recognized and these are divided into 7 families (5-HT_{1-7}) based on their coupling to second messengers via the G-proteins. The 5-HT_1 family receptors (5-HT_{1A}, 5-HT_{1B}, 5-HT_{1D}, 5-ht_{1e}, and 5-HT_{1F}) are coupled to $G_{i/o}$ that inhibit adenylyl cyclase and reduce cAMP levels upon activation. The 5-HT_2 receptors (5-HT_{2A}, 5-HT_{2B}, and 5-HT_{2C}) are coupled to $G_{q/11}$ which increase inositol phosphates and cytosolic $[Ca^{2+}]$. The 5-HT_4, 5-HT_6 and 5-HT_7 receptors all couple preferentially to G_s and promote cAMP formation by activation of various adenylate cyclases. The function of the 5-ht_5 receptors (5-ht_{5A} and 5-ht_{5B}) is not established and neither is its preferential coupling which may be to $G_{i/o}$ or G_s. This is why the receptor retain the lower case appellation (Hannon and Hoyer, 2008).

The 5-HT_3 receptor is a ligand-gated ion channel and has less than 10 % sequence homology with the other 5-HT receptors (Hoyer et al., 2002). The 5-HT_3 receptor mediate rapidly activating and desensitizing inward currents, which are carried primarily by Na^+ and K^+ ions but also Ca^{2+} and other small organic cations such as ammonium and choline (Lummis, 2012). The sequence homology between receptors in the same 5-HT receptor subfamily is around 50-70 %, whereas the overall amino acid sequence identity of non-related 5-HT receptors is around 30 % (Hoyer et al., 2002). Figure 3 visualizes the relationship between the fourteen different 5-HT receptors. An introduction to the two receptors relevant for this thesis – the 5-HT_{2A} and the 5-HT_7 receptors – will be presented in the following sections.
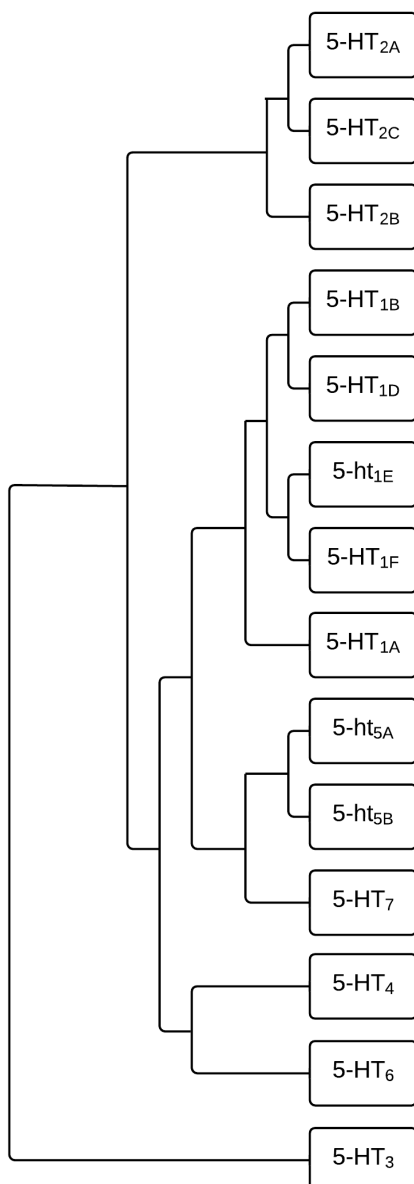

Figure 3 Dendrogram showing the evolutionary relationship between the human 5-HT receptor protein sequences (except 5-ht_5 receptors which are of murine origin). Figure modified from: (Barnes and Sharp, 1999). Annotation of the receptors is according to the IUPHAR database nomenclature guidelines.

The 5-HT$_{2A}$ receptor

The 5-HT$_{2A}$ receptors are interesting for several reasons: they are evolved in the etiology or treatment of various psychiatric disorders and they are a primary target of psychedelic drugs (González-Maeso and Sealfon, 2009; Leysen, 2004). The interest in particular 5-HT$_{2A}$ expression and function in major depression disorder is illustrated by a large number of imaging studies in this research field (Stockmeier, 2003). Meyer et al. suggested that increased 5-HT$_{2A}$ receptor binding might reflect an up-regulation of receptors in response to chronically impaired 5-HT release (Meyer et al., 2003). Furthermore, increased 5-HT$_{2A}$ receptor binding was found in patients recovered from depression suggesting that the up-regulation of 5-HT$_{2A}$ receptors continues after recovery and SSRI withdrawal (Bhagwagar et al., 2006). Consistent with these two studies, our group has shown that frontolimbic 5-HT$_{2A}$ receptor binding was positively correlated to neuroticism score, a risk factor for developing major depression (Frokjaer et al., 2008). Other *in vivo* imaging studies have shown decreased hippocampal 5-HT$_{2A}$ binding in depressed subjects (Mintun et al., 2004) and both increased and decreased 5-HT$_{2A}$ receptor binding following antidepressant treatment with SSRIs (Massou et al., 1997; Meyer et al., 2001; Yatham et al., 1999; Zanardi et al., 2001). In summary, there seems to be a not yet fully elucidated role for the 5-HT$_{2A}$ receptor in depression and other neuropsychiatric disorders.

Distribution of cerebral 5-HT$_{2A}$ receptors

The 5-HT$_{2A}$ receptor protein and mRNA have been extensively mapped in the brain by autoradiography, in situ hybridization and immunocytochemistry. A number of selective 5-HT$_{2A}$ radioligands are available for studying the 5-HT$_{2A}$ receptors, including [^{3}H]ketanserin, [^{3}H]MDL 100907 and [^{3}H]altanserin (Paterson et al., 2013). Despite differences in the *in vitro* selectivity profiles of these ligands, the binding to the 5-HT$_{2A}$ receptors are quite comparable. The 5-HT$_{2A}$ receptor is mainly found in the neocortex, but also in lower densities in central brain structures such as hippocampus and in patches of the caudate nucleus (Hall et al., 2000). Specific 5-HT$_{2A}$ receptor binding was not found in the cerebellum determined by human post mortem autoradiography using [^{3}H]MDL 100907 (Hall et al., 2000), however another study did observe non-negligible specific binding in the cerebellum with the less specific radioligand [^{3}H]ketanserin (Eastwood et al., 2001). In homogenate binding assays, Eastwood et al determined the receptor density (B$_{max}$) to 135 fmol/mg protein and 57 fmol/mg protein in the prefrontal cortex and cerebellum, respectively. The presence of 5-HT$_{2A}$ receptors in the cerebellum of rats was detected with immunohistochemistry (Geurts et al., 2002) but not with autoradiography using either [^{3}H]ketanserin or [^{3}H]MDL 100907

(López-Giménez et al., 1997). One important outcome of paper I from this thesis is the demonstration of a significant amount of 5-HT$_{2A}$ receptors in the pig cerebellum.

The importance of 5-HT$_{2A}$ receptors in the cerebellum relates to the use of this region as a reference region representing free and non-specific binding only. This is useful for quantification of the binding of a PET radioligand because reference tissue models simplify the study set-up, as arterial blood samples and subsequent HPLC analysis of the plasma is not needed.

The 5-HT$_7$ receptor

The 5-HT$_7$ receptor is the most recent discovered of 5-HT receptors and for many years the 5-HT$_7$ receptor was known to be a member of the 5-HT$_1$-like receptors, since no pharmacological tools were available to distinguish the receptors from each other. The receptor has been cloned from human (Bard et al., 1993), mouse (Plassat et al., 1993), rat (Ruat et al., 1993), guinea pig (Tsou et al., 1994), and pig (Bhalla et al., 2002a). The human 5-HT$_7$ receptor gene has two introns in the coding region allowing for alternative splicing that gives rise to different isoforms of the receptor (Heidmann et al., 1997; Stam et al., 1997). However, to date these isoforms have not been shown to differ in their pharmacology, signal transduction or tissue distribution (Heidmann et al., 1998; Krobert et al., 2001).

Distribution of cerebral 5-HT$_7$ receptors

Immunocytochemical studies have shown staining of cell bodies and proximal fibers suggesting a somatodendritic subcellular distribution of the 5-HT$_7$ receptors (Neumaier et al., 2001). The tissue distribution of 5-HT$_7$ receptors has been studied with in situ hybridization and receptors are found predominately in thalamus, hypothalamus, cerebral cortex, hippocampus and amygdala of rats and guinea pigs (Thomas and Hagan, 2004).

An important issue for any receptor is whether the expressed protein exhibits functional agonist binding. This can be determined with binding experiments in tissue homogenate or by autoradiography on post mortem brain tissue. The non-selective [^{3}H]5-CT and [^{3}H]mesulergine have been used for 5-HT$_7$ receptor autoradiography in several studies with the appropriate blocking agents to mask labeling of various other 5-HT receptors (Gustafson et al., 1996; Martin-Cora and Pazos, 2004; To et al., 1995). However, these masking compounds may also have affinity for the 5-HT$_7$ receptor, making some 5-HT$_7$ receptors unavailable for binding. With the development of the high-affinity 5-HT$_7$ receptor selective antagonist [^{3}H]SB-269970 (Thomas et al., 2000), autoradiography has been performed on post mortem human and rat tissue (Horisawa et al., 2013;

Varnas et al., 2004). Good agreement of the binding distribution was found between these autoradiography studies and also with distribution data from in situ hydridization experiments (Gustafson et al., 1996). The regions with the highest binding are the thalamus, hypothalamus, and hippocampus. The amygdala is also reported as a region with high 5-HT$_7$ receptor density in the rat brain. The two [^{3}H]SB-269970 autoradiography studies agree that there is no specific binding in the cerebellum. Discrepancies in 5-HT$_7$ receptor binding between [^{3}H]mesulergine and [^{3}H]SB-269970 was found in the striatum, where [^{3}H]mesulergine display high binding (Martin-Cora and Pazos, 2004), whereas [^{3}H]SB-269970 display only limited binding in both human and rat brain tissue (Horisawa et al., 2013; Varnas et al., 2004). This discrepancy is likely explained by difference in selectivity of the two radioligands used, where [^{3}H]mesulergine is the less selective and signal from other targets may falsely be interpreted as 5-HT$_7$ receptor binding.

In the present thesis, the 5-HT$_7$ receptor distribution in post mortem pig tissue is reported.

Therapeutic potential of the 5-HT$_7$ receptors

Advances in developing 5-HT$_7$ receptor selective antagonists and agonist and the availability of 5-HT$_7$ receptor knock-out mice have contributed to elucidating the biological significance of the 5-HT$_7$ receptor. As a result, compelling data show that 5-HT$_7$ receptors are implicated in several physiological processes and related disorders, thus their manipulation may constitute a novel target for treatment of CNS disorders.

Depression

The interaction of antidepressants with the 5-HT$_7$ receptor has been suggested to, at least in part, account for their function. Both tricyclic and selective serotonin reuptake inhibitors (SSRI) antidepressants induced *c-fos* expression in a way consistent with 5-HT$_7$ receptor activation and could be inhibited by the non-specific 5-HT$_7$ receptor antagonist ritanserin (Mullins et al., 1999). Furthermore, chronic antidepressant drug treatment led a downregulation of 5-HT$_7$ receptor expression (Mullins et al., 1999). In a more recent study of a rodent model of depression, the chronic mild stress model, an upregulation of 5-HT$_7$ receptor mRNA in the hippocampus and hypothalamus was seen, which could be reverted by flouxetine treatment, was seen (Li et al., 2009).

The forced swim test (FST) and the tail suspension test (TST) are two of the most common behavioural models for evaluating the antidepressant potential of a drug. In the FST and TST, animals are subjected to short-term inescapable stress in the form of being forced to swim in a cylinder or suspended by their tail, respectively. The outcome measure is immobility defined as the absence of initiated movements and includes passive floating or swaying. Reduction in passive

behaviour is interpreted as an antidepressant-like effect of the manipulation (Cryan et al., 2005; Slattery and Cryan, 2012).

In both the FST and TST, pharmacological blockade of the 5-HT$_7$ receptors or inactivation of the receptor gene led to an antidepressant-like behavioural profile, i.e. reduced immobility (Bonaventure et al., 2007; Guscott et al., 2005; Hedlund et al., 2005; Wesolowska et al., 2006b). Furthermore, it has been shown that there is a synergistic interaction between individual ineffective doses of the selective antagonist SB-269970 and SSRI antidepressants, leading to reduced immobility in the FST and TST (Bonaventure et al., 2007; Sarkisyan et al., 2010; Wesolowska et al., 2007).

Interestingly, two recent studies have shown that the 5-HT$_7$ receptor could be relevant for the treatment of depression. Two atypical antipsychotics, lurasidone and amisulpride, both have antidepressant effects, and these effects were previously thought to somehow rely on dopamine D$_2$/D$_3$ receptor antagonism, although the mechanism has never been satisfactorily explained. It is now known that these antipsychotics have high affinity for the 5-HT$_7$ receptor and that they cause an antidepressant-like response in the FST and TST in 5-HT$_7^{+/+}$ (wildtype) mice but not in 5-HT$_7^{-/-}$ (knock-out) mice (Abbas et al., 2009; Cates et al., 2013; Ishibashi et al., 2010).

Preclinical and clinical studies have demonstrated antidepressant properties of the compound vortioxetine (Alvarez et al., 2012; Katona et al., 2012; Mørk et al., 2013; Mørk et al., 2012), which is a multimodal serotonergic compound with affinity for 5-HT$_{3A}$, 5-HT$_7$, 5-HT$_{1D}$, 5-HT$_{1B}$, 5-HT$_{1A}$ receptors, and the 5-HTT (Bang-Andersen et al., 2011; Westrich et al., 2012). The antidepressant effect of vortioxetine is thought to be related to its multimodal pharmacological profile, but the exact mechanistic role of the individual targets is not clear.

Taken together, there is a consistent body of evidence using both pharmacological and genetic tools that implicates the 5-HT$_7$ receptor as playing a role in depression and in the mechanism of action of antidepressants.

Schizophrenia
The 5-HT$_7$ receptor is also thought to be implicated in schizophrenia and several studies have attempted to test the possible relevance of 5-HT$_7$ receptors using prepulse inhibition (PPI). Although PPI is not a complete model of schizophrenia it provides a model of the sensorimotor gating deficits seen in schizophrenic patients. One study showed that phencyclidine (PCP)-induced disruption of PPI could be counteracted by the 5-HT$_7$ selective antagonist SB-258741. Because PCP acts primarily on ionotropic glutamate receptors, it was concluded that the 5-HT$_7$ receptor could

influence the glutamatergic component of PPI (Pouzet, 2002). Other studies showed a decrease in 5-HT_7 receptor levels at both mRNA and protein levels in the dorsolateral prefrontal cortex of schizophrenic patients (Dean et al., 2006; East et al., 2002). Furthermore, two short nucleotide polymorphisms (SNP) in the 5-HT_7 receptor gene have shown to be associated with schizophrenia, but only one SNP had a functional relevance (Ikeda et al., 2006).

Anxiety disorders

Efforts have been made to link the 5-HT_7 receptor and anxiety, but so far the results have been inconclusive. Two very widely used animal modes of anxiety are the elevated plus-maze and the light/dark box tests. In the elevated plus-maze, the rodent may explore "unsecure" open arms and/or "secure" closed arms. In the light-dark box test, the animal can move between a small dark versus a large brightly lit room. Thus, the test is based on the conflict between the exploration of the whole apparatus and the aversion of the brightly lit compartment. 5-$HT_7^{-/-}$ mice had equal number of transitions between the light and dark compartments and no difference was found in the time spent exploring open arms in the elevated plus maze compared to 5-$HT_7^{+/+}$ mice (Guscott et al., 2005; Roberts et al., 2004). Thus, no implication of the 5-HT_7 receptor in anxiety was found in transgenic animals. However, pharmacological blockade of the 5-HT_7 receptor with the selective SB-269970, was associated with an anxiolytic effects in rats in the Vogel conflict drinking test (Wesolowska et al., 2006a; Wesolowska et al., 2006b). SB-269970 displayed a u-shaped dose-response effect and its anxiolytic effect was not as pronounced as the reference anxiolytic diazepam. A more recent medicinal chemistry paper identifying a series of selective 5-HT_7 receptor compounds reported anxiolytic potency of some of these compounds in both the Vogel conflict drinking and in the light-dark tests (Volk et al., 2008). We based our 5-HT_7 receptor PET radioligand development program on a lead structure from one of these compounds.

Positron emission tomography (PET)

Imaging techniques is a rapidly expanding field and techniques such as magnetic resonance imaging, x-ray, or ultrasound provide valuable information of anatomy however, it gives limited or no information about molecular events. In contrast, PET and single-photon emission computed tomography (SPECT) can offer molecular and biochemical information about physiological processes in living organisms in a quantitative manner.

PET and SPECT imaging techniques rely on the use of radioactive ligands which provide the detectable signal. These radioligands can be designed to be tissue-, cell- or protein-specific and are

administrated at tracer amounts (typically below 5 µg per injection and less than 5 % receptor occupancy) so as not to perturb normal physiology of the system. PET therefore allows the investigation of substrate-target interactions with the advantage of not having to administer an efficacious dose of a compound as is done with classical pharmacological experiments (Paterson et al., 2013).

Most PET ligands available today are antagonist. For GPCRs, antagonist radioligands label the entire population of receptors with the same affinity, thus measuring the total number of receptors, whereas agonist radioligands preferentially label the high-affinity state of the receptor that is capable of eliciting signaling events. Compared to the total number of receptors, the distribution of receptors in the high-affinity state is predicted to be a more precise outcome in studies with functional aim or studies attempting to image changes in neurotransmitter concentrations (Paterson et al., 2013) .

Receptor-ligand interactions in the dopamine and serotonin neurotransmitter systems have attracted particular interest because of their relation to the pathophysiology of psychiatric and neurological disorders, including Parkinson's disease, schizophrenia, and depression. PET studies have provided the first quantification of receptors in the living brain and thereby allowed for studies of receptor density in relation to pathophysiology (Meltzer et al., 1999; Wong et al., 1986). Significant enhancement of the clinical utility of brain PET imaging is anticipated with the development of biomarkers of pathophysiology. One such example is the use of Pittsburgh compound B ([^{11}C]PIB), a radioligand that binds to β-amyloid aggregates (Klunk et al., 2004), which are known to accumulate in brains of Alzheimer's disease patients (Hardy and Allsop, 1991).

Another utility of PET include the facilitation of drug development, where novel drugs can be tested for their occupancy at targets for which PET radioligands exist. The drug itself can also be radiolabeled and injected in doses of less than 5 µg to obtain detailed information about its biodistribution – a concept known as microdosing (Bergstrom et al., 2003).

The application of PET to study regional changes in endogenous neurotransmitter evoked by challenges that alter the synaptic neurotransmitter concentrations, was first proposed in 1984 (Friedman et al., 1984). The principle has been widely applied to the study of the dopaminergic system in which the PET ligand [^{11}C]raclopride or the SPECT ligand [^{123}I]IBZM have been combined with pharmacological challenges that elicit dopamine release (Laruelle, 2000). The clinical relevance of the methodology has been demonstrated by showing increased dopamine release in patients with schizophrenia (Breier et al., 1997; Laruelle et al., 1996). Despite the

continuous development of new radioligands for the 5-HT receptors, very few radioligands have been found suitable for studying serotonin release in clinical studies. However, a 5-HT$_{1B}$ receptor radioligand has recently been developed which shows promise for detecting endogenous 5-HT fluctuations (Finnema et al., 2012b; Nord et al., 2013).

The successful application a PET technique for changes in 5-HT levels relies on the use of a suitable radioligand. Assuming that the competition model applies, the radioligand competes directly with the neurotransmitter for binding at the target site. The competition model states that if two ligands with affinity for the same receptor are simultaneously present in the synapse, such as endogenous neurotransmitter and radioligand, they will directly compete for occupation of their target. Thus, if the concentration of neurotransmitter (F_{NT}) increases, a reduced availability for the radioligand at the target will occur, and consequently a decrease in binding potential (BP) is measured. Vice versa, the opposite would be predicted in response to neurotransmitter depletion.

The probability of measuring a difference in neurotransmitter concentration (ΔF_{NT}) in response to a pharmacological challenge is independent of radioligand characteristics, and solely depend on the affinity of the endogenous neurotransmitter for the target receptor (K_{NT}), assuming that the basal F_{NT} is not altered by the challenge (Paterson et al., 2010).

$$Occupancy = \frac{\Delta F_{NT}}{K_{NT} + F_{NT} + \Delta F_{NT}},$$

Attempting to image 5-HT fluctuations, the receptor for which 5-HT has the highest affinity should be selected as target. Among the receptors that 5-HT has the highest affinity are the 5-HT$_{1A}$ (K_i = 0.2-400 nM), 5-HT$_{1B}$ (K_i = 1-40 nM) and 5-HT$_7$ receptors (K_i = 0.3-8 nM) (Paterson et al., 2010). In this respect, the 5-HT$_7$ receptor is among the most promising target. The fact that the 5-HT$_7$ receptors are located subcortically may be an added advantage: Changes in 5-HT levels could potentially be measured with the novel 5-HT$_{2A}$ receptor agonist PET radioligand [^{11}C]Cimbi-36 (described below), where the main changes in signal will occur in the cortical regions where high 5-HT$_{2A}$ receptor density is found. As the receptor density of the 5-HT$_7$ receptor is highest subcortically in the thalamus, the 5-HT$_{2A}$ and 5-HT$_7$ receptor radioligands may in this way complement each other by measuring 5-HT changes in different regions of the brain.

Development of PET radioligands

Despite the amount of information that a PET radioligand can provide, the development of new radioligands is far from trivial. The development of novel radioligands is a complex process that requires a multidisciplinary research group including expertise in organic chemistry, radiochemistry,

pharmacology, cell biology, physics, and image analysis. The development of PET radiotracers is a time-consuming process and only a limited number of PET radioligands end up being used in clinical studies (Pike, 2009). Development of PET radioligands is comprised of a number of steps starting with the identification of a biological hypothesis and specific targets associated with this hypothesis. Subsequent to target identification and assessment of the tissue density of the target, medicinal chemistry begins to identify suitable radioligand molecules. Often lead compounds are available from the pharmaceutical industry or lead compounds can be identified through the literature. For a radioligand to be useful for quantitative PET imaging of a target, a number of criteria must be met:

1) High affinity (usually in the range of nM for the dissociation (K_D) or inhibition constant (K_i)) and high selectivity allowing for specific imaging of the target site. The affinity of the candidate tracer should be high enough that significant tissue uptake occurs, but it should be not so high that washout is delayed beyond the usable measurement time of the radionuclide.

2) The candidate compound must be able to undergo labeling with carbon-11 or fluorine-18 and subsequent purification. Precursors must therefore be available that allow for quick labeling in one (but usually no more than two) synthetic steps before final formulation for the imaging study is performed (Fumita and Innis, 2002).

3) For CNS targets, the candidate compound must be able to penetrate the blood-brain barrier. This is often dependent on the lipophilicity of the candidate tracer and in general LogP values in the range of 2.0-3.5 are desirable for optimal passive brain entry *in vivo* (Waterhouse, 2003). Generally, high lipophilicity increases the radioligand plasma protein binding, the capillary permeability surface area product, and the non-specific brain tissue binding. Low lipophilicity decreases the non-specific binding in the brain, but it also decreases blood-brain barrier permeability (Kessler et al., 1991).

The candidate tracer must also be able to circumvent the brain efflux transporters such as P-glycoprotein (P-gp) and other multidrug resistance-associated proteins. High lipophilicity, positive charge at physiological pH, and multiple aromatic groups promotes substrate affinity for P-gp. The degree to which P-gp restricts brain entry can vary across species and small structural differences can have unpredictable influence on the susceptibility to brain efflux (Pike, 2009).

4) The non-displaceable binding (or non-specific binding) should be low in order to give high signal-to-noise ratios.

5) Suitable brain pharmacokinetics (tracer kinetics) in relation to the isotopes half-life which includes observable brain uptake and washout of the radioligand (Laruelle et al., 2003). Reversible tracer kinetics enhances the likelihood of stable outcome measures when using compartment modeling for quantification of radioligand binding.

   Radioligands having very slow or even irreversible tracer kinetics can in some cases be modelled by other kinetic models such as the Gjedde-Patlak plot as seen with irreversible brain uptake of [18F]fluorodeoxyglucose ([18F]FDG) (Gjedde, 1982; Patlak et al., 1983).

6) Radiolabeled metabolites that cross the BBB complicate the analysis of the data (Mukherjee et al., 2004): radiolabeled metabolites that do not bind to the molecular target but cross the BBB will decrease the signal-to-noise measurement of the target. Active metabolites (i.e. bind to the target) will strongly confound the quantification, because the signal represents undetermined proportions of parent compound and metabolite, each of which may have different affinities for the target.

5-HT$_{2A}$ receptor PET radioligands

Several PET radioligands are available for imaging the 5-HT$_{2A}$ receptors and these have recently been reviewed (Paterson et al., 2013). Among the less selective radioligands are [18F]setoperone and [11C]NMSP, whereas [18F]altanserin and especially [11C]MDL 100907 display very high selectivity for the 5-HT$_{2A}$ receptor. All of these have successfully been tested and used in clinical studies, but the most commonly used radioligands today are [18F]altanserin and [11C]MDL 100907.

As mentioned, [11C]MDL 100907 is a highly selective PET radioligand however, it has rather slow tracer kinetics. The binding of [11C]MDL 100907 is low in the cerebellum of non-human primates and humans (Ito et al., 1998; Lundkvist et al., 1996) allowing for the use of this region as reference in reference tissue quantification methods (Meyer et al., 2010; Talbot et al., 2012). The two-tissue compartment model using arterial input remains to be superior to reference tissue models in quantifying the binding of [11C]MDL 100907 (Watabe et al., 2000).

[18F]Altanserin and the structurally related compound ketanserin have high affinity for the 5-HT$_{2A}$ receptor but also moderate affinities for the D$_2$ and α$_1$ receptors, however with the large abundance of 5-HT$_{2A}$ receptors in the brain, the majority of the signal from [18F]altanserin can be attributed to this receptor. The main disadvantage of [18F]altanserin is the formation of lipophilic metabolites that cross the BBB and interfere with the signal from the parent compound. This

complicates quantification of [18F]altanserin binding, however with the use of bolus-infusion scheme and the analysis of radiometabolites, the binding potential related to the plasma concentration of [18F]altanserin (BP_P) is used as outcome measures of [18F]altanserin binding.

In an attempt to avoid the lipophilic metabolites of [18F]altanserin, take advantage of the increased selectivity profile of [11C]MDL 100907, and to benefit from the longer half-life and spatial resolution of fluorine-18, [18F]MH.MZ was developed as an 18F-labeled analogue of MDL 100907 (Herth et al., 2008; Herth et al., 2009a; Herth et al., 2009b). In rats, [18F]MH.MZ showed high cortex-to-cerebellum ratios and no radiolabeled metabolites were detected in the brain tissue. However, [18F]MH.MZ displayed very slow tracer kinetics in the µPET studies of rats (Herth et al., 2009b). In the present thesis, a direct comparison of [18F]altanserin and [18F]MH.MZ in pigs is presented.

Whereas the above-mentioned 5-HT$_{2A}$ receptor radioligands are antagonist, a 5-HT$_{2A}$ receptor agonist radioligand is currently being validated in humans in our lab. This radioligand ([11C]Cimbi-36) has been evaluated in pigs (Ettrup et al., 2011a) and recent results show that [11C]Cimbi-36 image the 5-HT$_{2A}$ receptors in non-human primates and furthermore, that this radioligand is sensitive to changes in 5-HT levels (Finnema et al., 2012a). This sensitivity to changes in endogenous 5-HT levels has not been proven for any of the antagonist 5-HT$_{2A}$ receptor radioligands (Paterson et al., 2010). Awaiting the results of the clinical trial, [11C]Cimbi-36 has the potential to be an additional radioligand for quantification of the 5-HT$_{2A}$ receptors in humans and may present a novel tool for imaging fluctuations of 5-HT in the human brain.

Imaging of the 5-HT$_7$ receptor

An outcome measure that is very often used in PET imaging is the binding potential. This term is defined as the ratio of B_{max} and K_D. Imaging the 5-HT$_7$ receptor presents challenges related to B_{max} and K_D: The 5-HT$_7$ receptor has high sequence similarity with and the 5-HT$_{1A}$ receptor (49%) (Hoyer et al., 2002) (see Figure 3). This likely result in similar binding pockets of the two receptors, and therefore presents a challenge for the development of compounds that are selective for each receptor. *In vitro* autoradiographic studies show that the B_{max} of the 5-HT$_7$ receptor in the thalamus, which is the high binding region, is relatively low with 16 fmol/mg tissue wet weight reported in the autoradiography study (Varnas et al., 2004) and 68 fmol/mg reported in the tissue homogenate study (Thomas et al., 2002). 5-HT$_{1A}$ and 5-HT$_7$ receptors are distributed in the same brain regions such as the cortex and hippocampus (Hall et al., 1997; Kumar et al., 2013; Varnas et al., 2004). In the example below, the temporal cortex is taken as example of a region rich in 5-HT$_{1A}$ receptors

(78.6 fmol/mg tissue wet weight) and low in 5-HT$_7$ receptors (2.3 fmol/mg tissue wet weight). The prerequisite we apply for imaging the 5-HT$_7$ receptors, is that less than 10 % of the PET-signal comes from binding to the 5-HT$_{1A}$ receptor.

$$\frac{BP(5HT_{1A})}{BP(5HT_7)} \leq 0.1$$

$$\frac{B_{max}(5HT_{1A})/K_D(5HT_{1A})}{B_{max}(5HT_7)/K_D(5HT_7)} \leq 0.1$$

$$\frac{B_{max}(5HT_{1A})}{K_D(5HT_{1A})} \cdot \frac{K_D(5HT_7)}{B_{max}(5HT_7)} \leq 0.1$$

$$\frac{78.6\,fmol/mg}{K_D(5HT_{1A})} \cdot \frac{K_D(5HT_7)}{2.3\,fmol/mg} \leq 0.1$$

$$K_D(5HT_{1A}) = 342 \cdot K_D(5HT_7)$$

In conclusion, in the temporal cortex where the ratio between 5-HT$_{1A}$ and 5-HT$_7$ receptors is largest, the K$_D$ of the radioligand must be 342 times higher for the 5-HT$_{1A}$ receptor than for the 5-HT$_7$ receptor in order to allow only 10 % of the signal arising from the radioligand binding to the 5-HT$_{1A}$ receptors. Obviously, this ratio differs between regions with varying receptor densities, but that again varies depending on the radioligand used for determining the B$_{max}$ *in vitro*. In the example above, B$_{max}$ of the 5-HT$_{1A}$ receptors was determined with [^{3}H]WAY-100635, but [^{3}H]CUMI-101 has also been used for post mortem human autoradiography and in the same region B$_{max}$ was determined at 44.5 fmol/mg wet weight tissue (Kumar et al., 2013). Thus, if [^{3}H]CUMI-101 is used for this comparison, the requirements for the selectivity of the PET radioligand is lower.

5-HT$_7$ receptor PET radioligands

Only a very limited number of PET radioligands for the 5-HT$_7$ receptor has been evaluated *in vivo*. [^{11}C]DR4446 had good BBB permeability and was metabolically stable, but it only showed a minimal specific binding component (Zhang et al., 2002). The 5-HT$_7$ receptor antagonist SB-269970 has been used as lead structure for developing the ^{18}F-labeled radioligands, [^{18}F]1-{2-[(2S)-1-(phenylsulfonyl)pyrrolidin-2-yl]ethylpiperidin-4-yl-4-fluorobenzoate and [^{18}F]2FP3. These were evaluated *ex vivo* in rats and *in vivo* in cats, respectively (Andries et al., 2010; Lemoine et al., 2011). No input function was obtained while evaluating [^{18}F]2FP3 and furthermore, the 5-HT$_7$ receptor binding distribution in the cat brain is unknown, thus making it difficult to verify if the binding of

[^{18}F]2FP3 was specific to 5-HT$_7$ receptors. In the present thesis, the evaluation of eight novel 5-HT$_7$ PET radioligands in three compound classes is presented.

The pig as an experimental animal

The pig represents a useful, large experimental animal in biomedical research, surgical models and procedural training. The pig is an affordable experimental animal due to its large availability in Denmark, which is the world's largest exporter of pork. The pig is easily housed and easily trained if necessary. Compared to non-human primates, the use of pigs may potentially avoid some of the ethical dilemmas concerning the use of primates as laboratory animals (Goodman and Check, 2002).

While rodents and non-human primates have been the preferred animals studied within neuroscience, the use of pigs in neurosciences is a rapidly increasing area of research (Lind et al., 2007). There are unique advantages to the use of pigs given similar anatomic and physiological characteristics to humans. The brain of the pig is gyrencephalic as compared to the lissencephalic nature of the rodent brains, thus the pig brain more closely resembles the human brain. The weight of the adult pig brain ranges from 80 to 180 g, depending on adult body size and breed of the animal. This weight, being more than 50 times greater than that of the rat brain, makes it comparable to that of some non-human brains used for experimental purposes (Lind et al., 2007). The large size of the pig brain favours imaging techniques such as fMRI and PET and making standard clinical scanners usable. Agricultural bred pigs can reach a size of 300 kg and therefore are not very useful as experimental animal and younger pigs at a weight around 20-40 kg is therefore often used. However, pig breeds exist e.g. the Göttingen minipig that are bred for scientific purposes and especially longitudinal studies as the adult weight of these animal are 35-45 kg (Köhn et al., 2008). The Göttingen Minipig has been used as model for Parkinson's disease (Bjarkam et al., 2008; Mikkelsen et al., 1999) and attempts have also been made to establish a model for Alzheimer's disease in the Göttingen minipig (Kragh et al., 2009). The Göttingen minipig has furthermore been evaluated as an animal model for studying the effect of putative antipsychotics (van der Staay et al., 2009). This is an example of the increased interest in using other species than non-human primates for preclinical toxicology testing of pharmaceuticals.

The pig has been used as a model to study 5-HT transmission in the developing human brain (Niblock et al., 2005). A number of the serotonin receptors as well as the 5-HTT have been identified in pig brain tissue: 5-HT$_{1A}$ (Hoyer et al., 1985), 5-HT$_{1B}$ (Waeber et al., 1988), 5-HT$_{1D}$ (Heald et al., 1994; Waeber et al., 1988), 5-HT$_{1F}$ (Bhalla et al., 2002b), 5-HT$_{2A}$ (Hoyer et al., 1985), 5-HT$_{2C}$ (Pazos et al., 1984), 5-HT$_3$ (Fletcher and Barnes, 1996), 5-HT$_4$ (Schiavi et al., 1994), 5-HT$_6$

(Schoeffter and Waeber, 1994), $5\text{-}HT_7$ (Bhalla et al., 2002a), and 5-HTT (Brust et al., 1996). Autoradiography with $5\text{-}HT_{1A}$, $5\text{-}HT_{2A}$, $5\text{-}HT_4$, and 5-HTT radioligands has been reported with post mortem pig brain tissue (Ettrup et al., 2011b; Kornum et al., 2009). In the present thesis, the distribution of $5\text{-}HT_7$ receptors in post mortem pig brain is reported. Several 5-HT receptors have been assayed in brain of living pigs and below is a list of the successful PET radioligands (Table 1). Also noted are those of the PET radioligands that have been taken into humans. Many other radioligands for the 5-HT receptors that seem successful in rodent and non-human primates studies have not (yet) been evaluated in humans.

Table 1   Studies evaluating different 5-HT receptor radioligands in pigs and humans.

5-HT receptor or transporter	Radioligand(s)	Evaluated in pigs	In clinical use
$5\text{-}HT_{1A}$	[^{11}C]WAY-100635	(Cumming et al., 2007)	(Pike et al., 1995)
$5\text{-}HT_{2A}$	[^{11}C]Cimbi-5	(Ettrup et al., 2010)	
	[^{11}C]Cimbi-36	(Ettrup et al., 2011a)	(Clinical trial in progress)
	[^{18}F]altanserin	*Paper I*	(Biver et al., 1994; Pinborg et al., 2003)
	[^{18}F]MH.MZ	*Paper I*	
$5\text{-}HT_4$	[^{11}C]SB207145	(Kornum et al., 2009)	(Marner et al., 2010)
$5\text{-}HT_6$	[^{11}C]GSK215083	(Parker et al., 2012)	(Parker et al., 2012)
$5\text{-}HT_7$	[^{11}C]Cimbi-717	*Paper IV*	
5-HTT	[^{11}C]DASB	(Jensen et al., 2003)	(Houle et al., 2000)

AIMS

The aims of the present thesis were threefold:

- To compare the two 5-HT$_{2A}$ receptor PET radioligands [^{18}F]MH.MZ and [^{18}F]altanserin in the Danish Landrace pig brain.
- To determine the 5-HT$_7$ receptor distribution in the post mortem pig brain.
- To evaluate a series of novel 5-HT$_7$ receptor PET radioligands *in vivo* in the pigs, including evaluation of their regional distribution in the pig brain and evaluation of their specific binding to the 5-HT$_7$ receptors with blocking experiments with a known and structurally different 5-HT$_7$ receptor ligand.

METHODS

In the following section, a brief description of the main methods employed in this thesis is provided. For detailed experimental methods please refer to the "Materials and Methods" section in papers I-IV.

In vitro autoradiography

Autoradiography is a technique widely used to study the distribution and B_{max} of protein targets such as receptors, enzymes, or membrane transporters. The technique is based on the use of radioactive ligands with high affinity and specificity for the target in question. Since the receptor-ligand binding ratio is 1, the signal can be quantified as number of receptors. A number of different isotopes can be used for labeling of ligands, e.g. ^{125}I (half-life ($t_{1/2}$) = 59.4 days), ^{14}C ($t_{1/2}$ = 5730 years), ^{35}S ($t_{1/2}$ = 87.5 days), and ^{32}P ($t_{1/2}$ = 14.3 days). However, tritium (^{3}H, $t_{1/2}$ = 12.3 years) with its long half-life and low energy β-emission providing high spatial resolution is the most widely used isotope for labeling of ligands. The disadvantage of this low-energy emission isotope is that exposure times to ^{3}H-sensitive films can take up to several months. However, exposure time can be shortened by using ^{3}H-sensitive phospho-image plates (IP) (Pavey et al., 2002), and these are therefore used in all studies presented in this thesis. With an on-site cyclotron it is also possible to use short half-life isotopes such as ^{11}C ($t_{1/2}$ = 20.4 min) and ^{18}F ($t_{1/2}$ = 109 min) for autoradiography, although this often demands more than one production of the radioligand, because optimization of incubation and washing time is needed with novel ligands, and this can be difficult to achieve within the short time span of radiation.

Saturation studies

In vitro autoradiography can be performed as a saturation study where increasing concentrations of the radiolabeled ligand are applied to adjacent brain sections. With this approach B_{max} and the K_D, i.e. the concentration at which 50 % of the receptors are labeled, can be determined. This approach was used to determine the B_{max} of $[^{3}H]$MDL 100907 in the pig frontal cortex and the K_D of $[^{18}F]$MH.MZ in paper I.

The B_{max} of receptors can also be determined with radioligand binding assays in brain tissue homogenate. A comparison between *in vitro* binding of a known radioligand and *in vivo* binding distribution of a novel ligand can be made, if a brain is dissected into regions that are anatomically similar to regions used for quantification of PET radioligand binding and subsequently homogenized and analyzed. This has previously been done in our lab (Kornum et al., 2009), and

attempts were made to determine the B_{max} of 5-HT$_7$ receptors in pig brain homogenate binding assays with the established 5-HT$_7$ radioligand [^{3}H]SB-269970 (Lovell et al., 2000; Thomas et al., 2000). Despite large optimization efforts of the protocol, it was not possible to determine the B_{max} in the brain, regardless of the expected receptor density. Consequently, in paper IV the 5-HT$_7$ receptor distribution is reported as specific binding (SB) of [^{3}H]SB-269970 measured with autoradiography. Here we used a saturating concentration of the radioligand (4x K_D), thus the binding is interpreted as a measure of the concentration of receptors. The same approach was used to determine the 5-HT$_7$ receptor distribution in human post mortem brain tissue (Varnas et al., 2004).

Competition studies

Autoradiography can also be used to determine the K_i of a competing cold compound as shown in paper III. Here, the concentration of the radioligand is kept constant, while different concentrations of the cold compound are used. Specific radioligand was plotted as a function of concentration of the cold compound. A one-site competitive binding was fitted to the data, constraining the radioligand concentration to 5 nM and the K_D of the radioligand to 1.9 nM in this type of tissue (as determined in previous experiments).

Experimental procedure

Autoradiography was carried out on pig brain sections (approximately 2 months of age and weighing 20 kg), sectioned into sagittal and coronal plane slides of 20 µm thickness. The brain was taken out shortly after euthanasia of the animal and immediately frozen on dry ice to preserve the tissue and avoid receptor degradation. One hemisphere of the brain was sectioned on a HM500OM Cryostat and thawed-mounted on super frost plus glass slides, air-dried and stored at -80°C until further use.

For each concentration of radioligand (paper I), competing concentration of compound (paper II), or region (paper IV), a brain section was incubated with radioligand to determine the total binding (TB). Non-specific binding (NSB) is determined in anatomical adjacent sections in the presence of saturating concentrations of non-labeled structurally unrelated compound with high affinity for the same target as the radioligand. The specific binding (SB) is then determined as the TB subtracted the NSB.

The autoradiography protocol comprises four steps: pre-incubation, incubation, washing and drying. Sections are pre-incubated in assay buffer with (NSB) or without (TB) the excess of

unlabeled ligand to eliminate endogenous transmitter and remaining drugs in the tissue. Following pre-incubation, the sections are incubated in assay buffer containing the radioligand. To separate free from bound radioligand, several washes is subsequent performed with cold (4°C) buffer, followed by a brief wash in distilled water to remove excess buffer salts. The extent of washing often depends on the radioligands lipophilicity and affinity, and washing time is therefore optimized to obtain the optimal ratio between specific and non-specific binding. Finally, sections are rapidly dried to avoid dissociation of the radioligand before exposure.

Image analysis of autoradiograms

The radioligand binding in brain sections is measured by the radioactive decay of the radionuclide. Energy released by the radioactive decay is absorbed by a layer of the photostimulatory phosphor crystals inside the IPs. When later stimulated with infrared or visible radiation, the crystals emit photostimulated luminescence (PSL), the intensities of which is proportional to the absorbed radiation energy (Amemiya and Miyahara, 1988). The wavelength of the PSL can be separated by the stimulating light and collected in a photomultiplier tube, amplified and converted to a digital image. The image obtained by scanning the IPs with an image plate reader can undergo densitometric analysis because of the proportionality between the PSL and the emitted radiation. Regions of interest (ROI) were hand-drawn around anatomical landmarks, e.g. borders of sections, and for each brain region the mean pixel density was measured in each brain region as outcome. ROIs were also drawn on ^{3}H-microscales with 16 activity levels (0.07-34 nCi/mg tissue equivalents (TE)) (Amersham Biosciences, GE Healthcare, Piscataway, USA). A third-degree exponential calibration function of decay-corrected ^{3}H-microscales or a dilution row of the ^{18}F-solution (repeated after each radiotracer synthesis) was used to convert the mean pixel density to receptor binding measured in nCi/mg TE in the case of ^{3}H-autoradiography or to nM binding in the case of ^{18}F-autoradiography. Finally, the decay-corrected specific activity of the radioligand ([^{3}H]SB-269970) was used to convert nCi/mg TE to fmol/mg TE. Image analysis, calibration and quantification of binding were done with ImageJ analysis software (http://rsb.info.nih.gov/ij/).

Positron emission tomography (PET)

Principles of PET

PET employs mainly short-lived positron emitting radiopharmaceuticals. The radionuclides employed most widely are: carbon-11 ($t_{1/2}$ = 20.4 min), nitrogen-13 ($t_{1/2}$ = 10.0 min), oxygen-15 ($t_{1/2}$ = 2.03 min) and fluorine-18 ($t_{1/2}$ = 110 min) (Paans et al., 2002). Carbon, oxygen, and nitrogen are the building blocks of nearly every molecule of biological importance, whereas fluorine is rarely found in naturally occurring compounds or in pharmaceuticals and thus often complicating the search for a good radioligand that complies with the criteria discussed above. Flourine-18 with its longer half-life allows for longer scan time and the theoretical higher specific activity of fluorine-18 allows for lower injected cold doses is to prefer over carbon-11.

During the radionuclide's decay process, a positron is emitted which travels a short distance (one to a few millimetres). When the positron encounters an electron from the surrounding environment, the two particles combine and annihilate resulting in the emission of two 511 keV gamma rays (photons) travelling approximately 180° degree apart (Figure 4).
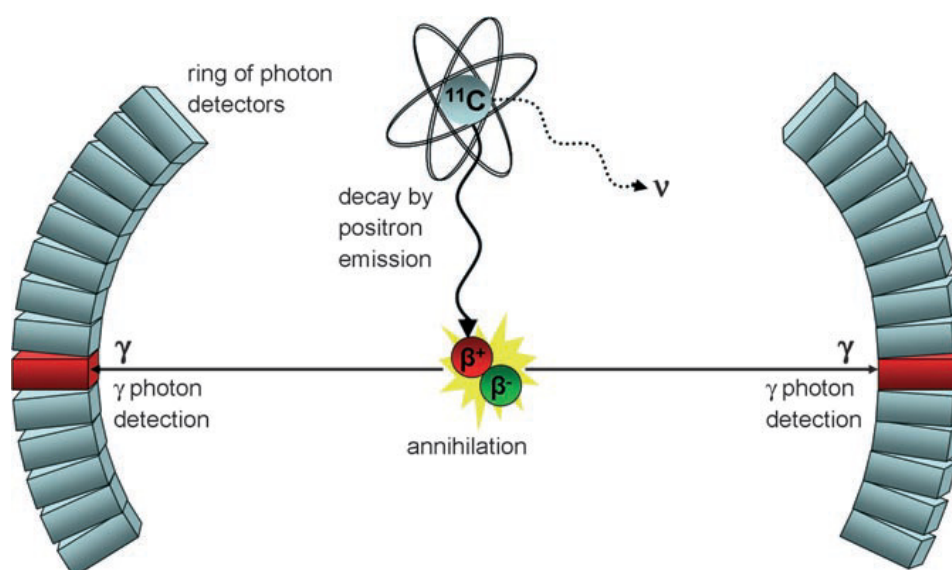

Figure 4   The principle of PET showing the decay of ^{11}C by positron emission resulting in the formation of ^{11}B atom, a positron (β^+) and a neutrino (ν). The positron then annihilates producing two photons (γ) each of 511 keV travelling in opposite directions of each other. The released photon pair can be detected as a line between the detectors and the obtained information is used to generate images of activity distribution. Figure from (Miller et al., 2008).

Due to the high energy of the two photons they have a high probability of escaping the body. When both photons hit gamma-ray detectors of the PET system, a "coincidence" event occurs. The line of response connecting the coincidence detectors are drawn through the object and is used to locate the

positron-electron annihilation and this closely resembles the location of the positron emission. Quantitative images are then obtained after reconstruction and appropriate correction for absorption, scatter, and random coincidences.

Experimental procedure

Danish Landrace pigs (approximately 2 months of age) were acquired from a vendor close to Copenhagen and housed and acclimatized for one week before the experiment at Department of Experimental Medicine, University of Copenhagen. All studies were approved by the Danish Council for Animal Ethics (Journal Nr. 2007/561-1320 and later 2012-15-2934-00156).

On the experiment day, pigs were tranquilized with an intramuscular (i.m.) injection of 0.5 mg/kg midazolam. Anaesthesia was induced by i.m. injection of a Zoletil veterinary mixture (1.25 mg/kg tiletamin, 1.25 mg/kg zolazepam, and 0.5 mg/kg midazolam; Virbac Animal Health, France). Following induction, anesthesia was maintained by intravenous (i.v.) infusion of 15 mg/kg/h propofol (B. Braun Melsugen AG). During anaesthesia, animals were endotracheally intubated and ventilated (volume 250 mL, frequency 16 min^{-1}). Venous access was granted through two catheters (Becton Dickinson) in the peripheral milk veins, and an arterial line for blood sampling measurement was obtained by a catheter in the femoral artery after a minor incision. Vital signs including blood pressure and heart rate were monitored throughout the duration of the PET scanning. Immediately after scanning, animals were euthanized by i.v. injection of pentobarbital/lidocain.

Pigs were scanned in a high resolution research tomography (HRRT) scanner (Siemens AG, Germany) at the PET and Cyclotron unit, Rigshospitalet. In all studies, a sterile physiological phosphate buffer solution (pH = 7.4) containing the radioligand was injected as a bolus (up to 14 mL) into the milk vein during 20 sec with simultaneous start of the PET acquisition. Attenuation correction was acquired before every PET measurement, with a transmission scan using a ^{137}Cs source. List mode data was continuously acquired for 90 min for ^{11}C-labeled radioligands and 150 min for ^{18}F-labeled radioligands. Reconstruction was done with increasing frame length (10 sec – 300 sec) using the ordinary Poisson-3D-ordered subset expectation maximization (OP-3D-OSEM) algorithm with point spread function.

During the first 30 min of scanning, radioactivity in whole blood was continuously measured using an ABSS autosampler (Allogg Technology) counting coincidences in a lead-shielded detector. Concurrently, blood samples were manually drawn and the radioactivity in whole blood was

measured using a well counter (Cobra 5003, Packard Instruments) that was cross-calibrated to the HRRT scanner and autosampler.

Determination of radiometabolites in plasma

The quantification of plasma parent compound and its radiolabelled metabolites was performed by direct injection of plasma in a column switching HPLC system. Whole blood samples were centrifuged (3500 rpm, 7 min) and the supernatant plasma fraction was collected and filtered through a 0.45 µM syringe filter prior to analysis with online radioactive detection, as previously described (Gillings, 2009). In the cases of fast metabolism of the radioligand, the radioactivity in the late blood samples (40-90 min post injection) could be too low for accurate measurement with online radioactive detection and consequently the fractions of the HPLC eluent were collected and counted in a gamma counter (2480 Wizard2, Perkin Elmer, Waltham, USA). The unchanged radioligand fraction was calculated by the integral of the corresponding radioactivity peak and its area was expressed as a percentage of the sum of areas of all radioactive peaks.

Quantitative analysis of PET data

Summed images of all counts in the full scan length were reconstructed for each pig and used for co-registration to a standardized MRI-based atlas of the Danish Landrace pig brain, similar to that previously published for the Göttingen minipig (Watanabe et al., 2001), using the software Register, as previously described (Kornum et al., 2009). Each registration was verified by visual inspection before final resampling of the dynamic emission sequence and subsequent extraction of time-radioactivity curves from volumes of interests (VOIs) using statistically defined volumes of interest obtained in 22 animals (Watanabe et al., 2001). Radioactivity in all VOIs was calculated as the average of radioactive concentration (Bq/mL) in the left and right sides. However, in the Lassen plot analysis, left and right regions are analysed separately. Outcome measure in the time-activity curves was radioactive concentration in VOI (in kBq/mL) normalized to the injected dose corrected for animal weight (in kBq/kg), yielding standardized uptake values (SUV) in g/mL.

For quantification of radioligand binding mathematical models are used, and these make use of the arterial input of radioligand to the brain and the brain response to the input. The input function can be determined by measuring the radioactivity in the arterial blood or estimated using reference region approaches.

Compartment modeling is regarded the golden standard for receptor binding quantification. Each compartment is characterized by the concentration of tracer within it as function of time. The

relationship between the concentrations in different compartments can be described as a set of differential equations, which describe the balance between the mass entering and leaving each compartment. Iterative calculation of these equations provides us with rate constants (micro parameters), and the ratio between these rate constants provides us with outcome measures such as distribution volumes (V_T) expressed in mL/cm^3 (macro parameter). In paper I-IV, V_T was calculated with the one-tissue compartment (1TC) model. The 1TC model is a simplified "physiological" model, where the tissue is considered to only have one compartment which means that free and non-specifically bound radioligand cannot be distinguished from the specifically bound (Innis et al., 2007). The V_T is calculated as: $V_T = \dfrac{K_1}{k_2}$.
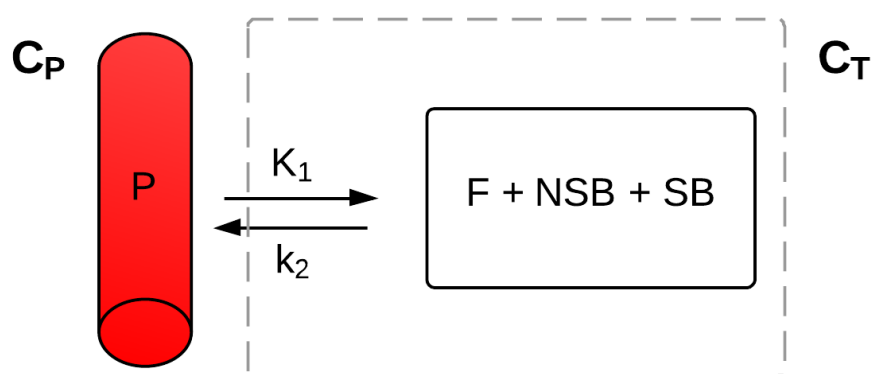

Figure 5   Schematic representation of the one-tissue compartment model (1TC). Radioligand in the plasma (P) in a given concentration (C_P) will distribute to the tissue compartment where free (F), non-specifically bound (NSB) and specifically bound (SB) radioligand contribute to the radioligand concentration in the tissue (C_T). The rate constants, K_1 and k_2, determine the influx and efflux between plasma and tissue, respectively.

The BP quantifies the equilibrium concentration of specific radioligand binding as a ratio to a reference concentration. The most commonly used reference concentration is the binding of radioligand in a region that is devoid of the target in interest, thus giving a measure of the non-displaceable binding of the radioligand (BP_{ND}). When a reference region is not available, the non-displaceable distribution volume (V_{ND}) can be estimated by a graphical method using regional estimates of V_T (Cunningham et al., 2010), although this requires a blocking experiment with the radioligand of interest. This method is based on differences in V_T before and after drug administration and the V_{ND} is extracted as the x intercept of the linear regression and the occupancy of the drug at the receptor is extracted as slope of the linear regression (Lassen et al., 1995). Based on the V_T and V_{ND}, BP_{ND} can be computed as:

$$BP_{ND} = \frac{V_T - V_{ND}}{V_{ND}}$$

The method was first introduced in 1995, however the first use of the occupancy plot (also called the Lassen plot) was not until 2007, where Pinborg et al. used it to determine the occupancy of two antipsychotic drugs at the D_2/D_3 receptors and to determine that the cerebellum was not a valid reference region for quantification of the high-affinity D_2/D_3 receptor SPECT radioligand [123]epidepride (Pinborg et al., 2007).

RESULTS AND DISCUSSION

Comparison of [^{18}F]MH.MZ and [^{18}F]altanserin

The *in vitro* and *in vivo* properties of [^{18}F]MH.MZ were evaluated in pigs and compared directly with [^{18}F]altanserin. Autoradiography on post mortem pig brain sections showed that [^{18}F]MH.MZ and [^{18}F]altanserin distribution was in accordance with the expected 5-HT$_{2A}$ receptor distribution (Ettrup et al., 2011b), and their specific binding was blocked by ketanserin. Cerebellar 5-HT$_{2A}$ receptor binding has not previously been investigated in the pig, and here we find specific binding in the cerebellum with both [^{18}F]MH.MZ and [^{3}H]MDL 100907 (Figure 6). This renders the cerebellum invalid as a reference region when quantifying the binding of 5-HT$_{2A}$ receptor radioligands in the pig brain.
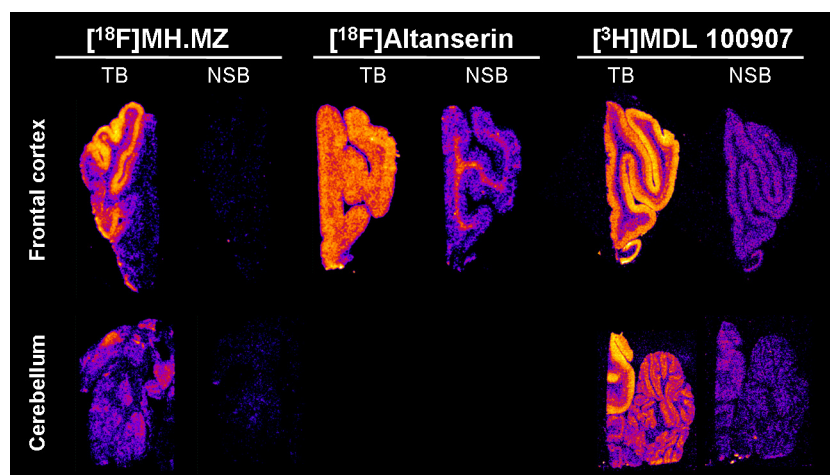

Figure 6   Autoradiographic images of 20 µm sections of pig brain incubated with 10 nM [^{18}F]MH.MZ, 2.5 nM [^{18}F]altanserin, or 2 nM [^{3}H]MDL 100907. Non-specific binding (NSB) is determined in the presence of 10 µM ketanserin. TB: Total binding.

The direct *in vivo* comparison of [^{18}F]MH.MZ and [^{18}F]altanserin showed that each radioligand has its advantages and disadvantages. The main disadvantage of [^{18}F]altanserin is the formation of lipophilic metabolites that cross the BBB and interfere with the binding signal from the parent compound as shown in rats, non-human primates, and humans (Price et al., 2001; Tan et al., 1999). The metabolism of [^{18}F]MH.MZ is more reproducible than what is seen with [^{18}F]altanserin and importantly, the metabolites do not cross the BBB. The disadvantage of [^{18}F]MH.MZ proved to be very slow tracer kinetics especially in the cortex which has high 5-HT$_{2A}$ receptor density. Despite the fact that the *in vitro* affinity of altanserin for the 5-HT$_{2A}$ receptor is higher than that of MH.MZ (see Table 2), [^{18}F]altanserin does not display slower tracer kinetics

than $[^{18}F]MH.MZ$. In fact, the kinetics of $[^{18}F]$altanserin in the pig brain was reversible in all regions investigated (Figure 7).

Table 2   Inhibition (K_i) and dissociation (K_D) constants for MH.MZ and altanserin.

Technique	Species	K_D/K_i	MH.MZ	Altanserin	Reference
Autoradiography *(in house)*	Pig	K_D	8.4 ± 5.9 nM		Paper I
Cell membrane binding assay *(in house)*	Human	K_i	9.0 ± 0.1 nM		(Herth et al., 2008)
Cell membrane binding assay *(PDSP)*	Human	K_i	3.0 ± 0 nM		http://pdsp.med.unc.edu
Brain homogenate binding assay	Rat	K_i		0.13 nM	(Leysen, 1989)

Since specific 5-HT$_{2A}$ receptor binding was found in the pig cerebellum, reference tissue models were precluded and we used compartment models for quantification of the *in vivo* binding. Slow tracer kinetics is known to be problematic for compartmental modeling of receptor binding because the rate of wash-out can be difficult to determine within the data acquisition time. The wash-out rate is necessary for the computation of outcome parameters such as V_T, and if it cannot be reliably determined from the measured TAC, it will bring large variations in the modeling and thus unacceptable bias (Laruelle et al., 2003). The modeling may also fail providing no estimates of binding of the radioligand and consequenctly the outcome parameters must be interpreted with care when quantifying radioligands with slow tracer kinetics,.

The time required for a radioligand to reach pseudo-equilibrium in the tissue is dependent on B_{max} and K_D of the radioligand (Olsson and Farde, 2001). The interest in the clinical importance of the dopamine system in extrastriatal regions led to the development of $[^{11}C]FLB$ 457 and $[^{18}F]$fallypride, both high-affinity D$_2$/D$_3$ antagonists which have the ability to image receptors in low concentrations. Contrary to $[^{11}C]$raclopride, the radioligand most often used to quantify D$_2$/D$_3$ receptors in striatal regions, $[^{11}C]FLB$ 457 reaches equilibrium in high-density regions beyond the data acquisition time. In low-density regions, however, $[^{11}C]FLB$ 457 can provide measures of D$_2$ receptor density, because equilibrium is reached within data acquisition time. The time of pseudo-equilibrium of $[^{18}F]MH.MZ$ also occurs very late in the acquisition time, likely because of a high *in vivo* affinity for the 5-HT$_{2A}$ receptors. Thus, it is possible that $[^{18}F]MH.MZ$ would be a tool for quantifying 5-HT$_{2A}$ receptors in low-density areas.
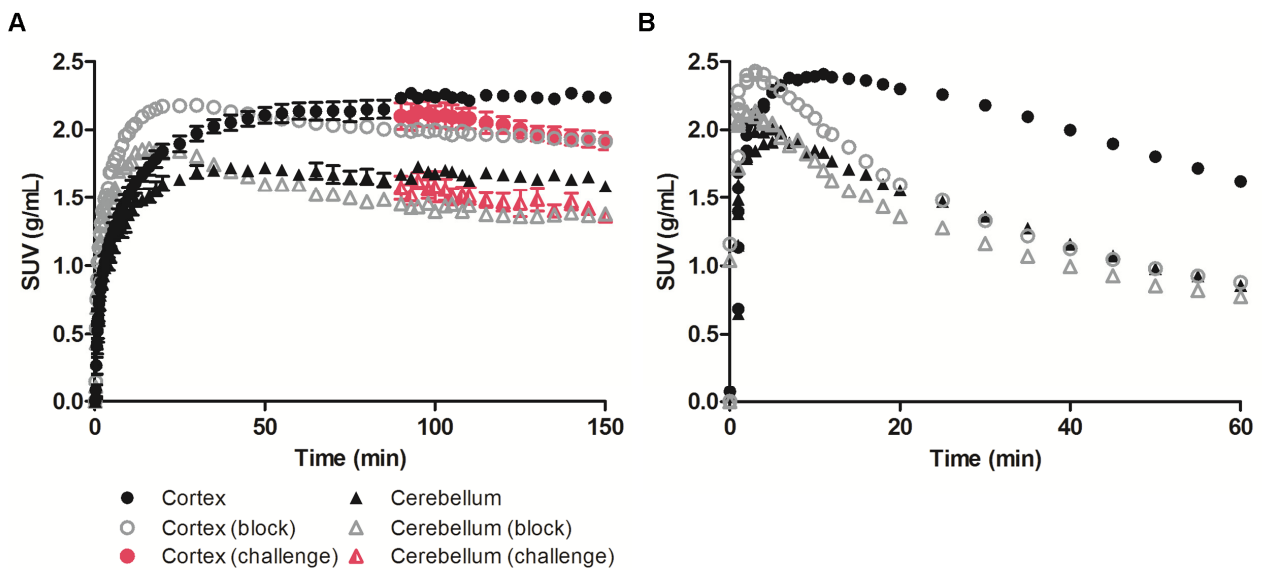
Figure 7 Regional time-activity curves for [^{18}F]MH.MZ (**A**) and [^{18}F]altanserin (**B**) at baseline (black, closed symbols), following a bolus-infusion pretreatment with ketanserin, or after an in-scan challenge of ketanserin (pink symbols).

The 5-HT$_7$ receptor distribution in the pig brain

To validate PET radioligands for the 5-HT$_7$ receptors in the pig brain, it was necessary to determine the 5-HT$_7$ receptor distribution. With autoradiography in post mortem pig brain sections using the selective 5-HT$_7$ antagonist [^{3}H]SB-269970, we found that the receptor distribution was fairly homogeneous across brain region, with only ~5 fold difference between the high and low binding region (Figure 3). Highest binding was found in the hypothalamus, thalamus, and amygdala, which is in accordance to the distribution found in rat and human tissue (Horisawa et al., 2013; Varnas et al., 2004). In the cortical regions, binding increased from the rostral to the caudal in the pig brain, with highest cortical binding found in the occipital lobe. Specific binding was also found in the cerebellum, making this region invalid as a reference region for *in vivo* data analysis.
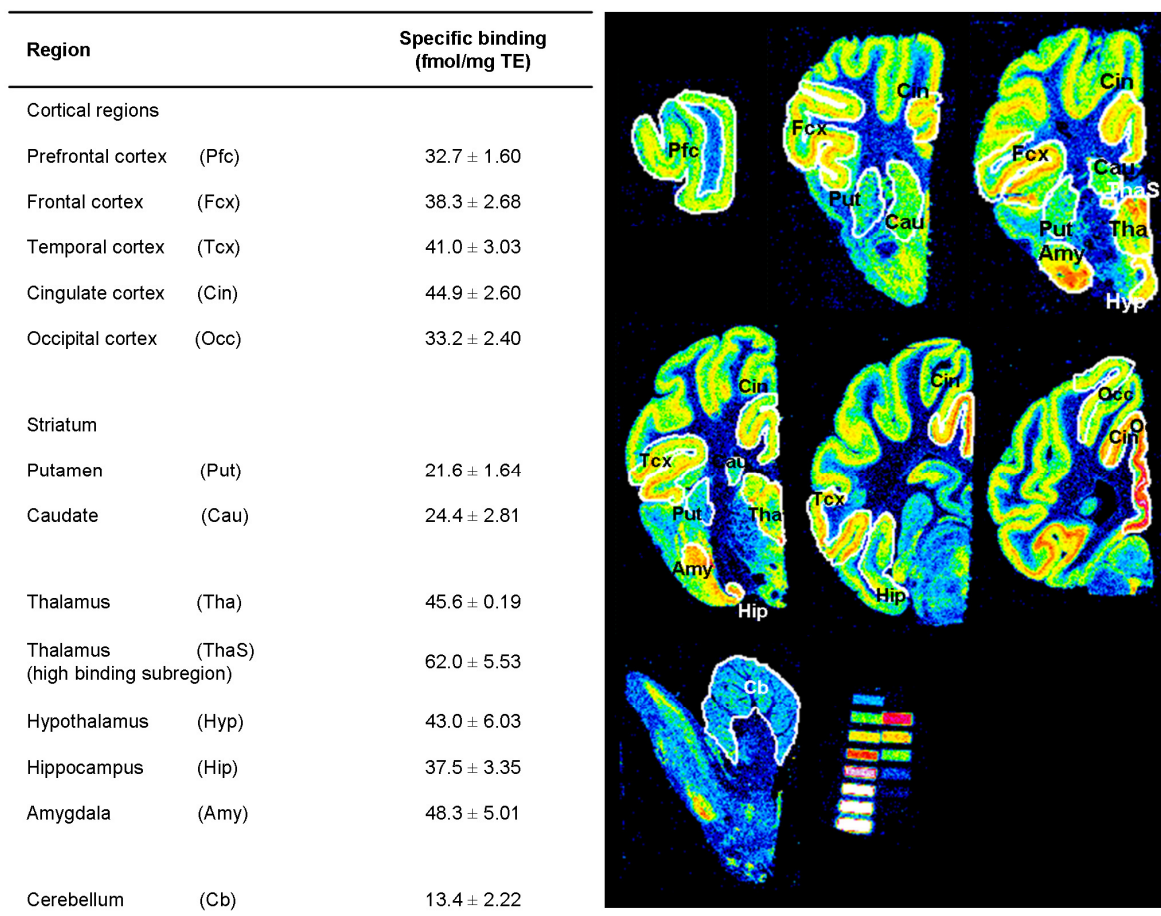
Region		Specific binding (fmol/mg TE)
Cortical regions		
Prefrontal cortex	(Pfc)	32.7 ± 1.60
Frontal cortex	(Fcx)	38.3 ± 2.68
Temporal cortex	(Tcx)	41.0 ± 3.03
Cingulate cortex	(Cin)	44.9 ± 2.60
Occipital cortex	(Occ)	33.2 ± 2.40
Striatum		
Putamen	(Put)	21.6 ± 1.64
Caudate	(Cau)	24.4 ± 2.81
Thalamus	(Tha)	45.6 ± 0.19
Thalamus (high binding subregion)	(ThaS)	62.0 ± 5.53
Hypothalamus	(Hyp)	43.0 ± 6.03
Hippocampus	(Hip)	37.5 ± 3.35
Amygdala	(Amy)	48.3 ± 5.01
Cerebellum	(Cb)	13.4 ± 2.22

Figure 8   5-HT$_7$ receptor distribution in different brain regions determined by autoradiography as specific binding of 5 nM [^{3}H]SB-269970 in fmol/mg tissue equivalent (TE). Representative pig brain sections with regions of interest indicated.

Searching for a 5-HT$_7$ PET radioligand

In the present thesis, compounds from three different structural classes were investigated for their potential as PET radioligands. These three compound classes comprise of the arylpiperazines from which PF5, PF30 and BA10 are members, the aminoethylbiphenyl class from which Cimbi-806 is a member, and finally the oxindole class from which four compounds are presented (collectively referred to as Cimbi-7xx).

The properties of the candidate PET radioligands were determined using HRRT PET scanning in Danish Landrace pigs. All candidate PET radioligands are evaluated by a 90 min baseline scan followed by the start of the 1 mg/kg/h SB-269970 infusion. After 30 min of pretreatment, the second scan is started simultaneous with a second injection of the radioligand. The infusion of SB-269970 is continued until the end of the second scan. The same dose of SB-269970 was used in all studies, allowing for comparison of occupancy at the 5-HT$_7$ receptor.

Arylpiperazines

A series of papers has been published on 4-substituted-1-arylpiperazine and the research has led to the identification of high-affinity 5-HT$_7$ receptor ligands such as LP-44, LP-12 and LP-211, all of which are agonists and some are commercial available (Leopoldo et al., 2004; Leopoldo et al., 2007; Leopoldo et al., 2008). LP-211 is now being used as a pharmacological tool for investigations of the physiological and pathophysiological roles of the cerebral 5-HT$_7$ receptors (Costa et al., 2012; Hedlund et al., 2010).
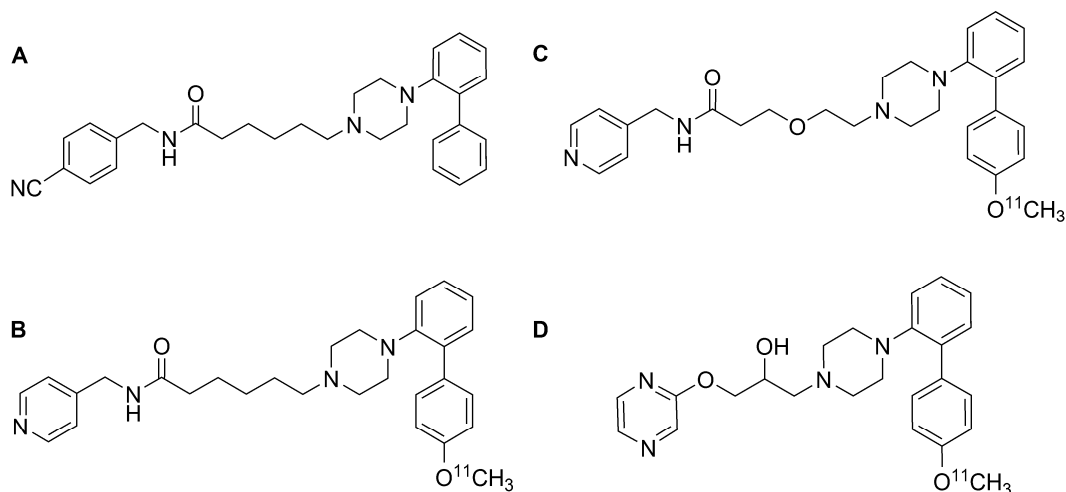
Figure 9 Structures of the lead compound LP-211 (**A**) and the candidate radioligands [^{11}C]PF5 (**B**), [^{11}C]PF30 (**C**), and [^{11}C]BA10 (**D**)

To further explore the potential of this compound class, the structure of LP-211 was modified to allow for carbon-11 labeling and subsequent evaluation of the compound as a 5-HT$_7$ receptor PET radioligand. Three compounds were developed and tested *in vivo*: [^{11}C]PF5, [^{11}C]PF30, and [^{11}C]BA10 (Figure 9).

[^{11}C]PF-5 and [^{11}C]PF-30 showed limited brain uptake and we therefore speculated that these radioligands were substrates for the BBB efflux protein, P-glycoprotein (P-gp). This was further investigated by a second scan where P-gp was inhibited with Cyclosporin A (CsA) pretreatment. The uptake of both [^{11}C]PF5 and [^{11}C]PF30 was increased after CsA pretreatment, suggesting that these compounds are in fact substrates for the P-gp. After CsA pretreatment, both radioligands displayed uniform brain uptake and slow tracer kinetics, i.e. limitied wash-out of the radioligands was observed within the 90 min acquisition time. With these drawbacks of being P-gp substrates and displaying uniform uptake across regions, we did not attempt to investigate the specificity of binding after SB-269970 pretreatment.

On the basis of 5-HT$_7$ receptor selectivity and lipophilicity of a candidate radioligand, a series of 1-arylpiperazine derivatives were screened in the search for a more appropriate radioligand candidate. The ligand BA10 (referred to as (*R*)-**16** in paper II) possessed the desired lipophilicity and a functional group for radiolabeling with carbon-11. [^{11}C]BA10 was evaluated in the pig in a similar manner as for the PF compounds. [^{11}C]BA10 was not a substrate for the P-gp transporter, as uptake was only slightly increased after CsA pretreatment and furthermore, [^{11}C]BA10 also displayed reversible tracer kinetics (Figure 10A). However, the distribution of [^{11}C]BA10 was almost uniform in the pig brain. The *in vivo* blocking study with SB-269970 showed faster wash-out of [^{11}C]BA10, which is to be expected when the cerebral receptors are blocked by SB-269970, however when quantifying the binding with the 1TC model, no significant changes were found in the V$_{TS}$ after SB-269970 pre-treatment in any region ($p>0.05$, 2-way analysis of variance (ANOVA), Bonferroni post-test) (Figure 10B). Thus, [^{11}C]BA10 had no specific binding to the 5-HT$_7$ receptor and therefore we do not consider [^{11}C]BA10 an appropriate 5-HT$_7$ receptor radioligand.
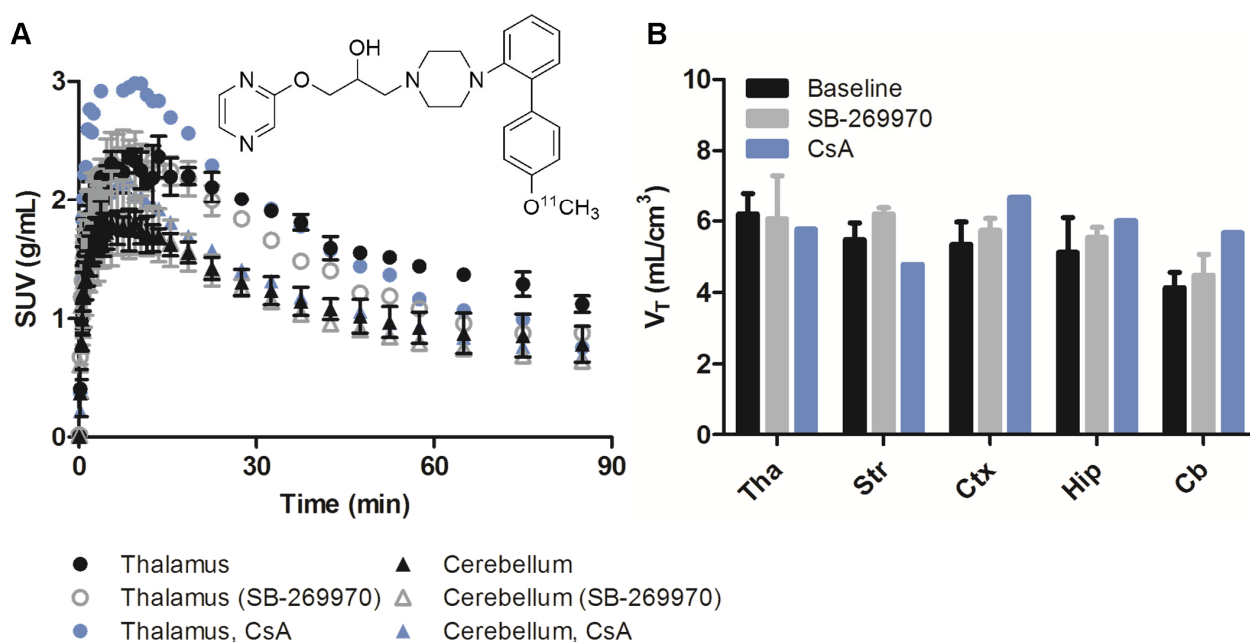

Figure 10   **A**) Regional time-activity curves for [^{11}C]BA10 at baseline (black, closed symbols), following pretreatment with 1 mg/kg/h SB-269970 (grey, open symbols), or following pretreatment with cyclosporine A (CsA) (blue closed symbols). **B**) Distribution volumes (V$_T$) for [^{11}C]BA10 quantified by one-tissue compartment modeling. Tha: thalamus, Str: striatum, Ctx: cortex, Hip: hippocampus, Cb: cerebellum.

The aminoethylbiphenyl: [^{11}C]Cimbi-806

The aminoethylbiphenyl, Cimbi-806, was synthesized and reported as a selective 5-HT$_7$ ligand (Paillet-Loilier et al., 2007). We confirmed the high *in vitro* affinity for the 5-HT$_7$ receptor using competitive autoradiography with [^{3}H]SB-269970 (K_i = 8.6 nM). *In vivo* evaluation of [^{11}C]Cimbi-806 in the pig revealed high binding in the thalamus and low binding in the cerebellum, as we expected based on the [^{3}H]SB-269970 autoradiography. However, when conducting the *in vivo* blocking experiment with SB-269970, no significant changes in V_T were found (Figure 11). This lack of reduced binding after receptor blockade, renders [^{11}C]Cimbi-806 an inappropriate 5-HT$_7$ receptor radioligand, and as a consequence we did not explore this compound class any further.
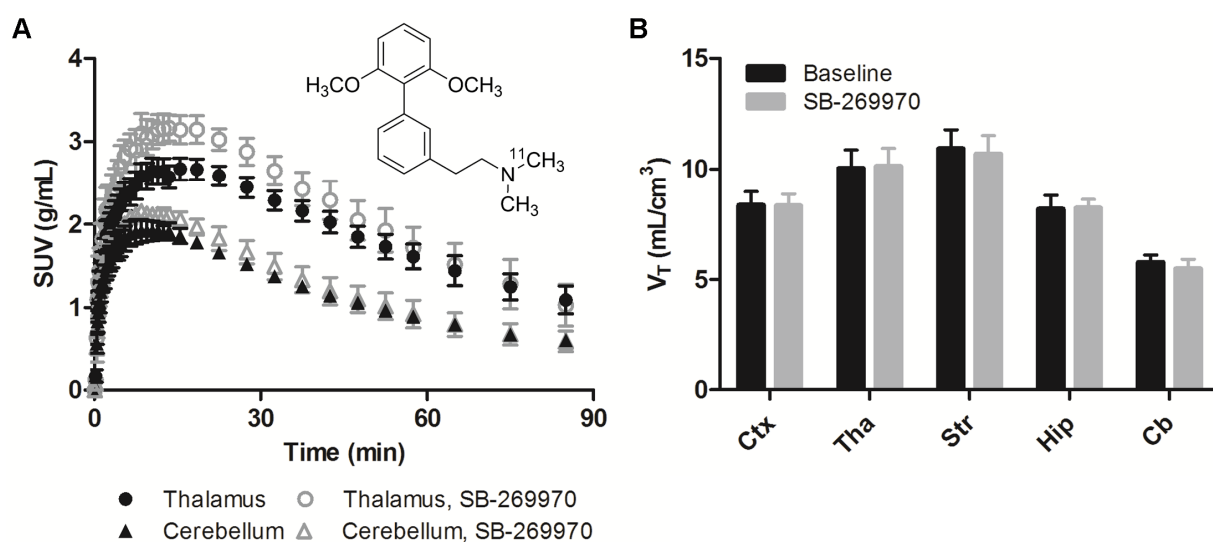

Figure 11 **A**) Regional time-activity curves for [^{11}C]Cimbi-806 at baseline (black, closed symbols) or following pretreatment with 1 mg/kg/h SB-269970 (grey, open symbols). Circles represent the thalamus and triangles represent cerebellum. **B**) Distribution volumes (V_T) for [^{11}C]Cimbi-806 quantified by one-tissue compartment modeling. Tha: thalamus, Str: striatum, Ctx: cortex, Hip: hippocampus, Cb: cerebellum.

The oxindoles: [^{11}C]Cimbi-7xx

Volk et al. reported the synthesis of a series of (phenylpiperazinyl-butyl)oxindole compounds with high affinity for the 5-HT$_7$ receptor and exhibiting antagonistic and anxiolytic properties (Volk et al., 2008). Here, the evaluation of four (phenylpiperazinyl-butyl)oxindole compounds (Figure 12) is presented: [^{11}C]Cimbi-712, [^{11}C]Cimbi-717, [^{11}C]Cimbi-772, and [^{11}C]Cimbi-775. Compounds with a methoxy moity attached to the phenylpiperazine allows for a simple methylation of the hydroxy precursor. A radiolabeling method was also developed for ^{11}C-labeling of the methyl moiety on the phenylpiperazine (Andersen et al., 2013). The final modification of the compounds was the removal of the ethyl moity at the oxindole. Uptake, tracer kinetics, and specificity of binding of the candidate radioligands are discussed below.
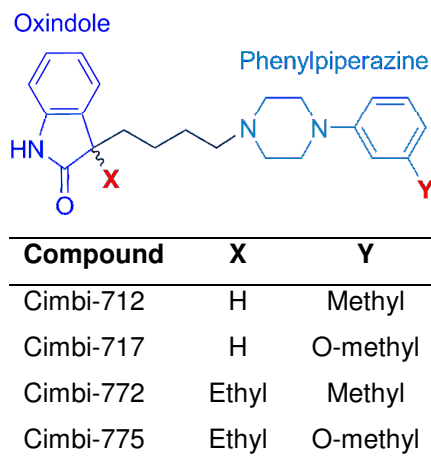
Figure 12 Structural differences of the four radioligand candidates: Cimbi-712, Cimbi-717, Cimbi-772, and Cimbi-775. The oxindole moiety is displayed in dark blue and the phenylpiperazine moity is displayed in light blue. The two positions of variability between the compounds are displayed in red and are described in the table.

[^{11}C]Cimbi-772 and [^{11}C]Cimbi-775

The ethyl-substituted radioligands, [^{11}C]Cimbi-772 and [^{11}C]Cimbi-775, readily entered the pig brain after i.v. injection. Both tracers displayed reversible tracer kinetics, however no specific binding to the 5-HT$_7$ receptors *in vivo* was observed, as neither [^{11}C]Cimbi-772 nor [^{11}C]Cimbi-775 could be blocked by SB-269970 (Figure 13). As with [^{11}C]BA10 and [^{11}C]Cimbi-806 these compounds show high *in vitro* affinity to the 5-HT$_7$ receptor (Herth et al., 2012; Volk et al., 2008), but display no specific binding to the receptor *in vivo*.
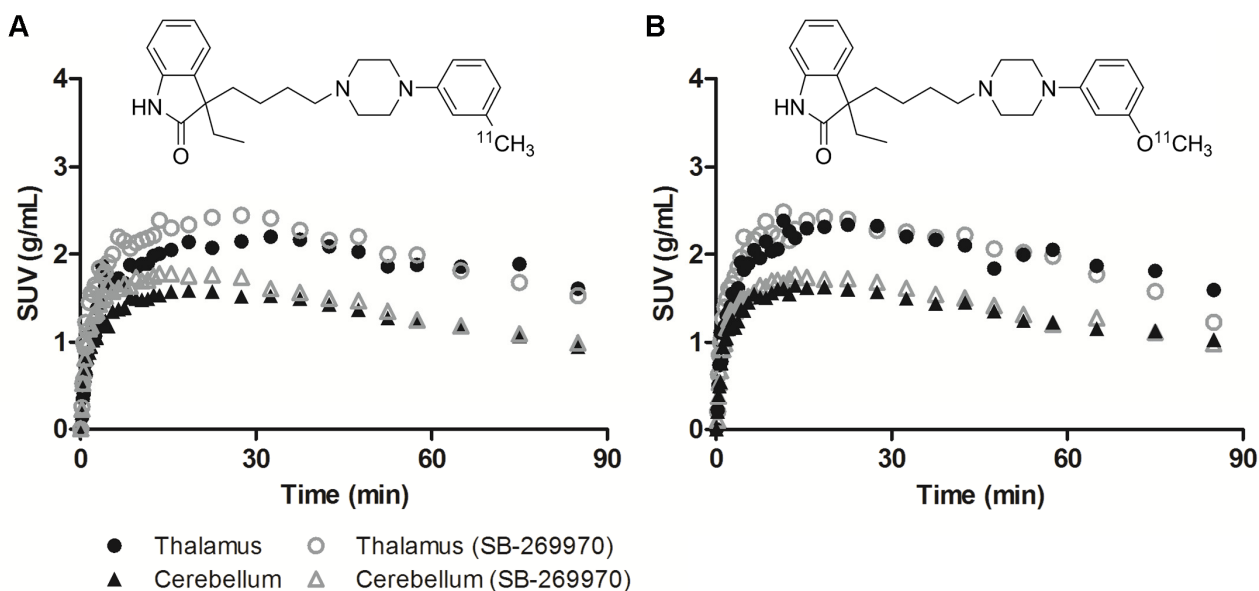

Figure 13 Regional time-activity curves for [^{11}C]Cimbi-772 (**A**) and [^{11}C]Cimbi-775 (**B**) at baseline (black, closed symbols) or following pretreatment with 1 mg/kg/h SB-269970 (grey, open symbols).

Position X on the phenylpiperazineoxindole (Figure 12) presents a chiral center, and thus enantiomeric separation was attempted for all four compounds. Different enantiomers may very well have different affinities for the 5-HT$_7$ receptor and in relation to the development of PET radioligands, imaging with the enantiomers may therefore result in different binding characteristics. We found that only the ethyl-substituted compounds were enantiomerically stable after separation (unpublished data), however due to the lack of specific binding to the 5-HT$_7$ receptor *in vivo* of the racemic [^{11}C]Cimbi-772 and [^{11}C]Cimbi-775, we chose not to evaluate these enatiomers *in vivo*.

[^{11}C]Cimbi-712 and [^{11}C]Cimbi-717

The PET radioligands [^{11}C]Cimbi-712 and [^{11}C]Cimbi-717 both readily entered the pig brain and reached a peak uptake of approximate 3 SUV. This is a slightly higher uptake than for [^{11}C]Cimbi-772 and [^{11}C]Cimbi-775, indicating that the ethyl substitution at the oxindole causes a slight decrease in the brain uptake of the radioligand. Both ligands had highest uptake in the thalamus and lowest uptake in the cerebellum in line with the 5-HT$_7$ receptor distribution found in the post mortem pig brain. The tracer kinetics of the two radioligands proved to be very different despite the close structural similarity of the compounds: [^{11}C]Cimbi-712 displayed slow tracer kinetics with a peak uptake after 50 min, and limited wash-out was seen within the data acquisition time. [^{11}C]Cimbi-717, on the other hand, displayed reversible tracer kinetics, which is important for compartmental data analysis (Figure 14).
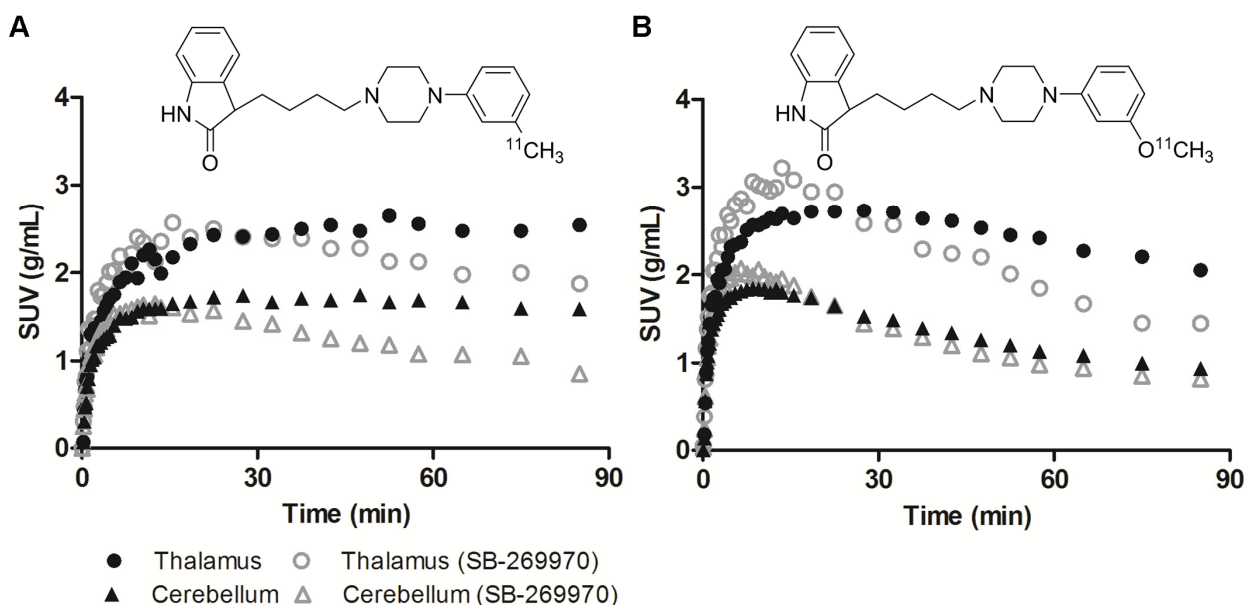

Figure 14 Regional time-activity curves for [^{11}C]Cimbi-712 (**A**) and [^{11}C]Cimbi-717 (**B**) at baseline (black, closed symbols) or following pretreatment with 1 mg/kg/h SB-269970 (grey, open symbols).

To validate the specificity of the binding of the radioligands, we conducted the *in vivo* blocking experiments with SB-269970. The concentration of both [^{11}C]Cimbi-712 and [^{11}C]Cimbi-717 in the thalamus decreased following the pretreatment with SB-269970. This indicated that the binding of the two radioligands can be attributed to binding to 5-HT$_7$ receptors in the pig brain. As expected from the autoradiography study, the *in vivo* concentration of radioligands in the cerebellum was also decreased after pretreatment, verifying the presence of 5-HT$_7$ receptors in this region.

Because of the higher reversibility of the binding in the pig brain, [^{11}C]Cimbi-717 was further evaluated *in vivo* with different doses of SB-269970. [^{11}C]Cimbi-717 binding in all scans was quantified using the 1TC model and V_Ts were highest in thalamus (16 ± 2.5 mL/cm^3) and lowest in cerebellum (6.6 ± 1.2 mL/cm^3) indicating good regional separation. A dose-dependent reduction in V_Ts was observed after SB-269970 pretreatment, with significant reductions with the doses 1.0 mg/kg/h ($p < 0.01$) and 4.2 mg/kg/h ($p < 0.001$) in all regions, except the cerebellum (Figure 15A).

As our initial affinity profile of [^{11}C]Cimbi-717 showed that binding to α_1 receptors could be a potential problem (Herth et al., 2012), we investigated this by pretreating one animal with the α_1 antagonist prazosin. The calculated V_T did not indicate any displacement of [^{11}C]Cimbi-717 and additional analysis of the binding by the occupancy plot confirmed that prazosin does not alter the binding of the [^{11}C]Cimbi-717, as the slope of the occupancy curve for prazosin was not significantly different from zero (Figure 15B). This strongly suggests that [^{11}C]Cimbi-717 does not bind to the α_1 receptors *in vivo*.
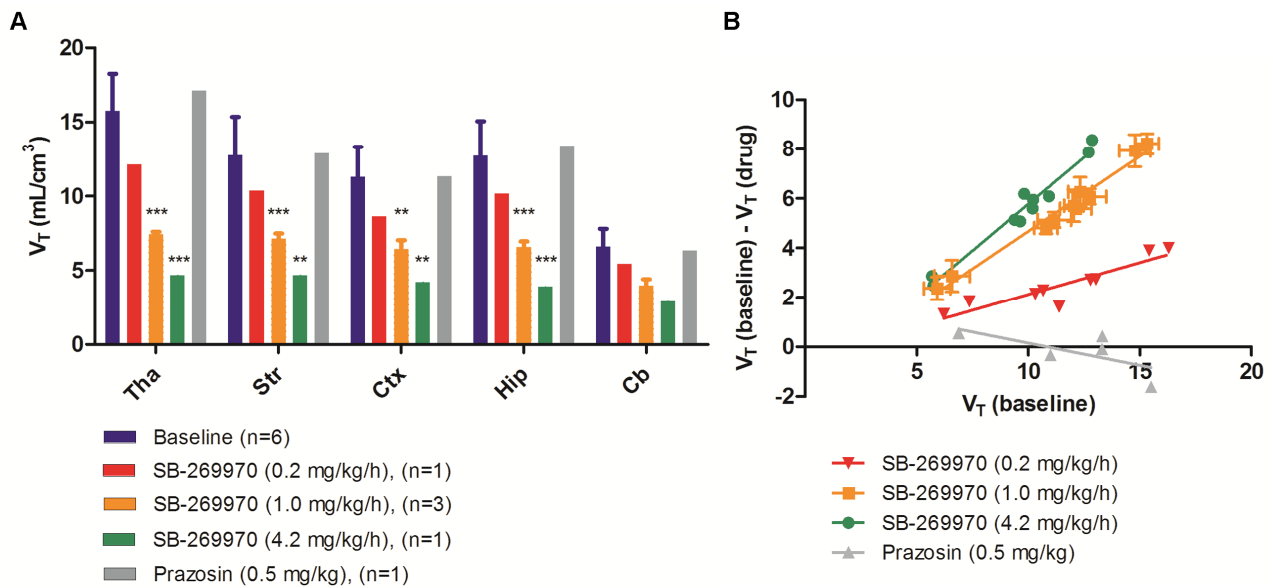
Figure 15 **A**) Distribution volumes (V_T) for $[^{11}C]$Cimbi-717 quantified by one-tissue compartment modeling. **B**) Occupancy plots for $[^{11}C]$Cimbi-717 with three different doses of SB-269970 and one dose of prazosin. Tha: thalamus, Str: striatum, Ctx: cortex, Hip: hippocampus, Cb: cerebellum. Error bars represent S.D. *** $p<0.001$, ** $p<0.01$. Two-way ANOVA with Bonferroni correction for multiple comparison.

In conclusion, $[^{11}C]$Cimbi-717 is the first well-validated 5-HT$_7$ receptor PET radioligand and we found a dose-dependent decline in cerebral binding following receptor blockade. Thus, $[^{11}C]$Cimbi-717 is currently the most promising radioligand for investigation of 5-HT$_7$ receptor binding in the living human brain.

CONCLUSION AND PERSPECTIVES

The present thesis focused on the comparison of known radioligands for the cerebral 5-HT$_{2A}$ receptors and the evaluation of novel radioligands for the cerebral 5-HT$_7$ receptors in pigs.

In paper I, we compared [^{18}F]altanserin, a clinically used 5-HT$_{2A}$ receptor radioligand, with the relatively recent developed [^{18}F]MH.MZ. We showed that both [^{18}F]altanserin and [^{18}F]MH.MZ can image the 5-HT$_{2A}$ receptors in the living pig brain. In contrast to [^{18}F]altanserin, [^{18}F]MH.MZ displayed very slow tracer kinetics in the pig brain. Additionally, we found that the cerebellum was not a valid reference region for 5-HT$_{2A}$ receptor quantification in pigs. In the lack of an appropriate reference region, we computed the BP using compartment modeling only. With the cerebellum as a validated reference region, it is possible that reference tissue models can be applied for quantification of [^{18}F]MH.MZ binding in humans. With reference region analysis, HPLC analysis of the blood can be avoided, and [^{18}F]MH.MZ may therefore be a less labour intensive alternative to [^{18}F]altanserin in humans. HPLC analysis of the blood is necessary with [^{18}F]altanserin, due to the formation of lipophilic metabolites that cross the BBB. The slow kinetics, due to what we believe is a high *in vivo* affinity, may in fact be an advantage of [^{18}F]MH.MZ since it could present the opportunity to measure 5-HT$_{2A}$ receptor quantities in subcortical regions where the B$_{max}$ of 5-HT$_{2A}$ receptors are lower. This property of [^{18}F]MH.MZ has not been tested in neither rodents nor pigs, and studies in non-human primates or humans may determine if [^{18}F]MH.MZ has potential as a 5-HT$_{2A}$ receptor radioligand in clinical settings.

In paper II, III and IV, we radiolabeled and evaluated novel 5-HT$_7$ receptor radioligands. In paper II and III, we present the unsuccessful radioligands [^{11}C]BA10 and [^{11}C]Cimbi-806. These failed because we were unable to show specific binding to the 5-HT$_7$ receptor. Two of the oxindole compounds, [^{11}C]Cimbi-772 and [^{11}C]Cimbi-775, were also unsuccessful due to lack of specific binding to the 5-HT$_7$ receptor. In spite of similar *in vitro* affinities of BA10, Cimbi-806, and the four Cimbi-7xx compounds, only two of these radioligands display specific binding to the 5-HT$_7$ receptor *in vivo*. The weakness of only considering the affinity when choosing a compound for radiolabeling and evaluation, is that only one of the the characteristics for a successful radioligand is considered with little deliberation given to the prediction of non-specific binding and optimal kinetics. Despite years of experience, the ability to predict which compounds will have the bioavailability, specificity, and kinetics required to image and quantify molecular targets in the brain remains limited. Recently, a biomathematical modeling was published that aimed to predict the *in vivo* performance of radioligands based on *in silico* and *in vitro* data such as affinity,

lipophilicity and target density (Guo et al., 2009). Adding the information that is obtained in this thesis, with evaluation of compounds in different structural classes and several compounds within one structural class to such a biomathematical model, may enable us to target the right compounds and reduce the time and costs spent on radiolabeling and *in vivo* experiments. The strength here may be the similarity of compounds in the oxindole compound class leading to differences in uptake, tracer kinetics and specificity of binding which would add a novel degree of detailing to the biomathematical model.

In paper IV, we present $[^{11}C]$Cimbi-712 and $[^{11}C]$Cimbi-717 as two promising radioligands. Due to the reversibility of $[^{11}C]$Cimbi-717, this ligand was further evaluated with different blocking agents and doses. We found a dose-dependent decrease in $[^{11}C]$Cimbi-717 binding in the pig brain supporting the 5-HT$_7$ receptor selectivity *in vivo* for $[^{11}C]$Cimbi-717. $[^{11}C]$Cimbi-717 remains our top candidate for a 5-HT$_7$ receptor PET radioligand for human use. Pending validation of $[^{11}C]$Cimbi-717 as a 5-HT$_7$ receptor specific radioligand in non-human primates and regulatory approvals, we aim at translating this radioligand into humans as we have successful done with the 5-HT$_{2A}$ receptor agonist PET radioligand $[^{11}C]$Cimbi-36 (Ettrup et al., 2013).

One of the objectives for developing a PET radioligand for the 5-HT$_7$ receptor was the theoretical potential that such as radioligand would be sensitive to fluctations in endogenous 5-HT, however it still remains to be investigated whether $[^{11}C]$Cimbi-717 is sensitive to such changes in 5-HT levels. To test this, a baseline scan with $[^{11}C]$Cimbi-717 should be compare to a second scan conducted on the same day and animal after pharmaocological challenge to change 5-HT levels. This intervention could be a 5-HT releasing agent, such as fenfluramine, or an acute dose of SSRI. Our group has also shown that it is possible to decrease the 5-HT levels in the pig brain with p-chlorophenylalanine (pCPA) (Ettrup et al., 2011b). Thus, to prove that $[^{11}C]$Cimbi-717 is sensitive to decreased levels of 5-HT, a study could be designed where $[^{11}C]$Cimbi-717 binding is measured before and after 5-HT depletion with pCPA.

Although the effect of Cimbi-712 and Cimbi-717 on the intracellular levels of the second messenger cAMP have not been tested in cellular assays, nine other compounds in the same structural class have proven to be antagonists of the 5-HT$_7$ receptor (Volk et al., 2008). This strongly indicates that Cimbi-712 and Cimbi-717 would be 5-HT$_7$ receptor antagonists, and as radioligands they would therefore label the entire pool of 5-HT$_7$ receptors. Contrary to this, an agonist would only label the high-affinity state of the receptor, thus labeling a sub-population of the available 5-HT$_7$ receptors. The B$_{max}$ of the 5-HT$_7$ receptor has been determined with both the

selective antagonist [^{3}H]SB-269970 and the agonist [^{3}H]5-CT and was found to be very similar in the two studies (Thomas et al., 2000), suggesting that the majority of 5-HT$_7$ receptors are present in an agonist high affinity state. The requirements for the K$_D$ of a PET radioligand that we apply in order to avoid signal from other receptors will therefore be equal for both agonists and antagonists.

With 10-15 % of Europeans currently inflicted with a mental disorder such as depression (Demyttenaere et al., 2004), the need to understand and treat these disorders is enormous. The possible mechanistic role of the 5-HT$_7$ receptor in the pathophysiology of depression makes this receptor an interesting target for imaging. The development of a 5-HT$_7$ receptor PET radioligand could significantly advance our understanding of these neurological disorders that are affected by 5-HT and may prove useful in monitoring therapy for patients with e.g. depression or schizophrenia. Also, the availability of a 5-HT$_7$ receptor PET radioligand would provide a predictive tool for individual drug response to 5-HT$_7$ receptor therapy and accelerate the development of new 5-HT$_7$ receptor ligands that can be used as therapeutic drugs.

REFERENCES

Abbas, A.I., P.B. Hedlund, X.P. Huang, T.B. Tran, H.Y. Meltzer, and B.L. Roth. 2009. Amisulpride is a potent 5-HT7 antagonist: relevance for antidepressant actions in vivo. *Psychopharmacology (Berl)*. 205:119-128.

Alvarez, E., V. Perez, M. Dragheim, H. Loft, and F. Artigas. 2012. A double-blind, randomized, placebo-controlled, active reference study of Lu AA21004 in patients with major depressive disorder. *Int J Neuropsychopharmacol*. 15:589-600.

Amemiya, Y., and J. Miyahara. 1988. Imaging plate illuminates many fields. *Nature*. 336:89-90.

Andersen, V.L., M.M. Herth, S. Lehel, G.M. Knudsen, and J.L. Kristensen. 2013. Palladium-mediated conversion of para-aminoarylboronic esters into para-aminoaryl-11C-methanes. *Tetrahedron Lett*. 54:213-216.

Andries, J., L. Lemoine, A. Mouchel-Blaisot, S. Tang, M. Verdurand, B.D. Le, L. Zimmer, and T. Billard. 2010. Looking for a 5-HT7 radiotracer for positron emission tomography. *Bioorg Med Chem Lett*. 20:3730-3733.

Bang-Andersen, B., T. Ruhland, M. Jorgensen, G. Smith, K. Frederiksen, K.G. Jensen, H. Zhong, S.M. Nielsen, S. Hogg, A. Mork, and T.B. Stensbol. 2011. Discovery of 1-[2-(2,4-dimethylphenylsulfanyl)phenyl]piperazine (Lu AA21004): a novel multimodal compound for the treatment of major depressive disorder. *J Med Chem*. 54:3206-3221.

Bard, J.A., J. Zgombick, N. Adham, P. Vaysse, T.A. Branchek, and R.L. Weinshank. 1993. Cloning of a novel human serotonin receptor (5-HT7) positively linked to adenylate cyclase. *J Biol Chem*. 268:23422-23426.

Barnes, N.M., and T. Sharp. 1999. A review of central 5-HT receptors and their function. *Neuropharmacology*. 38:1083-1152.

Berger, M., J.A. Gray, and B.L. Roth. 2009. The expanded biology of serotonin. *Annu Rev Med*. 60:355-366.

Bergstrom, M., A. Grahnen, and B. Langstrom. 2003. Positron emission tomography microdosing: a new concept with application in tracer and early clinical drug development. *Eur J Clin Pharmacol*. 59:357-366.

Bhagwagar, Z., R. Hinz, M. Taylor, S. Fancy, P. Cowen, and P. Grasby. 2006. Increased 5-HT(2A) receptor binding in euthymic, medication-free patients recovered from depression: a positron emission study with [(11)C]MDL 100,907. *Am J Psychiatry*. 163:1580-1587.

Bhalla, P., P.R. Saxena, and H.S. Sharma. 2002a. Molecular cloning and tissue distribution of mRNA encoding porcine 5-HT7 receptor and its comparison with the structure of other species. *Mol Cell Biochem*. 238:81-88.

Bhalla, P., H.S. Sharma, T. Wurch, P.J. Pauwels, and P.R. Saxena. 2002b. Molecular cloning and expression of the porcine trigeminal ganglion cDNA encoding a 5-ht(1F) receptor. *Eur J Pharmacol*. 436:23-33.

Biver, F., S. Goldman, A. Luxen, M. Monclus, M. Forestini, J. Mendlewicz, and F. Lotstra. 1994. Multicompartmental study of fluorine-18 altanserin binding to brain 5HT2 receptors in humans using positron emission tomography. *Eur J Nucl Med*. 21:937-946.

Bjarkam, C.R., M.S. Nielsen, A.N. Glud, F. Rosendal, P. Mogensen, D. Bender, D. Doudet, A. Moller, and J.C. Sorensen. 2008. Neuromodulation in a minipig MPTP model of Parkinson disease. *Br J Neurosurg*. 22 Suppl 1:S9-12.

Bonaventure, P., L. Kelly, L. Aluisio, J. Shelton, B. Lord, R. Galici, K. Miller, J. Atack, T.W. Lovenberg, and C. Dugovic. 2007. Selective blockade of 5-hydroxytryptamine (5-HT)7 receptors enhances 5-HT transmission, antidepressant-like behavior, and rapid eye movement sleep suppression induced by citalopram in rodents. *J Pharmacol Exp Ther*. 321:690-698.

Breier, A., T.P. Su, R. Saunders, R.E. Carson, B.S. Kolachana, A. de Bartolomeis, D.R. Weinberger, N. Weisenfeld, A.K. Malhotra, W.C. Eckelman, and D. Pickar. 1997. Schizophrenia is associated with elevated amphetamine-induced synaptic dopamine concentrations: evidence from a novel positron emission tomography method. *Proc Natl Acad Sci U S A*. 94:2569-2574.

Brust, P., R. Bergmann, and B. Johannsen. 1996. High-affinity binding of [3H]paroxetine to caudate nucleus and microvessels from porcine brain. *NeuroReport*. 7:1405-1408.

Cates, L.N., A.J. Roberts, S. Huitron-Resendiz, and P.B. Hedlund. 2013. Effects of lurasidone in behavioral models of depression. Role of the 5-HT receptor subtype. *Neuropharmacology*. 70:211-217.

Costa, L., M. Spatuzza, S. D'Antoni, C.M. Bonaccorso, C. Trovato, S.A. Musumeci, M. Leopoldo, E. Lacivita, M.V. Catania, and L. Ciranna. 2012. Activation of 5-HT7 Serotonin Receptors Reverses Metabotropic Glutamate Receptor-Mediated Synaptic Plasticity in Wild-Type and Fmr1 Knockout Mice, a Model of Fragile X Syndrome. *Biol Psychiatry*. 72:924-933.

Cryan, J.F., C. Mombereau, and A. Vassout. 2005. The tail suspension test as a model for assessing antidepressant activity: Review of pharmacological and genetic studies in mice. *Neurosci Biobehav Rev*. 29:571-625.

Cumming, P., M. Møller, K. Benda, L. Minuzzi, S. Jakobsen, S.B. Jensen, B. Pakkenberg, A.K. Stark, J.B. Gramsbergen, M.F. Andreasen, and A.K. Olsen. 2007. A PET study of effects of chronic 3,4-methylenedioxymethamphetamine (MDMA, "ecstasy") on serotonin markers in Göttingen minipig brain. *Synapse*. 61:478-487.

Cunningham, V.J., E.A. Rabiner, M. Slifstein, M. Laruelle, and R.N. Gunn. 2010. Measuring drug occupancy in the absence of a reference region: the Lassen plot re-visited. *J Cereb Blood Flow Metab*. 30:46-50.

Dahlstrom, A., and K. Fuxe. 1964. Localization of monoamines in the lower brain stem. *Experientia*. 20:398-399.

Dean, B., G. Pavey, D. Thomas, and E. Scarr. 2006. Cortical serotonin7, 1D and 1F receptors: effects of schizophrenia, suicide and antipsychotic drug treatment. *Schizophr Res*. 88:265-274.

Demyttenaere, K., R. Bruffaerts, J. Posada-Villa, I. Gasquet, V. Kovess, J.P. Lepine, M.C. Angermeyer, S. Bernert, G. de Girolamo, P. Morosini, G. Polidori, T. Kikkawa, N. Kawakami, Y. Ono, T. Takeshima, H. Uda, E.G. Karam, J.A. Fayyad, A.N. Karam, Z.N. Mneimneh, M.E. Medina-Mora, G. Borges, C. Lara, R. de Graaf, J. Ormel, O. Gureje, Y. Shen, Y. Huang, M. Zhang, J. Alonso, J.M. Haro, G. Vilagut, E.J. Bromet, S. Gluzman, C. Webb, R.C. Kessler, K.R. Merikangas, J.C. Anthony, M.R. Von Korff, P.S. Wang, T.S. Brugha, S. Aguilar-Gaxiola, S. Lee, S. Heeringa, B.E. Pennell, A.M. Zaslavsky, T.B. Ustun, and S. Chatterji. 2004. Prevalence, severity, and unmet need for treatment of mental disorders in the World Health Organization World Mental Health Surveys. *JAMA*. 291:2581-2590.

East, S.Z., P.W. Burnet, R.W. Kerwin, and P.J. Harrison. 2002. An RT-PCR study of 5-HT(6) and 5-HT(7) receptor mRNAs in the hippocampal formation and prefrontal cortex in schizophrenia. *Schizophr Res*. 57:15-26.

Eastwood, S.L., P.W.J. Burnet, R. Gittins, K. Baker, and P.J. Harrison. 2001. Expression of serotonin 5-HT2A receptors in the human cerebellum and alterations in schizophrenia. *Synapse*. 42:104-114.

Ettrup, A., S. da Cunha-Bang, B. Mc Macon, A. Dyssegaard, S. Lehel, M. Hansen, A.O. Baandrup, K. Møller, C. Svarer, J.L. Kristensen, N. Gillings, and G.M. Knudsen. 2013. Serotonin 2A receptor agonist binding in the human brain: first evaluation of [11C]Cimbi-36. *In* The 11th International Conference on Quantification of Brain Function with PET. Vol. Abstract no. 1123. Journal of Cerebral Blood Flow and Metabolism, Shanghai, China.

Ettrup, A., M. Hansen, M. Santini, J. Paine, N. Gillings, M. Palner, S. Lehel, M. Herth, J. Madsen, J. Kristensen, M. Begtrup, and G. Knudsen. 2011a. Radiosynthesis and in vivo evaluation of a series of substituted 11C-phenethylamines as 5-HT2A agonist PET tracers. *Eur J Nucl Med Mol Imaging*. 38:681-693.

Ettrup, A., B.R. Kornum, P. Weikop, and G.M. Knudsen. 2011b. An approach for serotonin depletion in pigs: effects on serotonin receptor binding. *Synapse*. 65:136-145.

Ettrup, A., M. Palner, N. Gillings, M.A. Santini, M. Hansen, B.R. Kornum, L.K. Rasmussen, K. Någren, J. Madsen, M. Begtrup, and G.M. Knudsen. 2010. Radiosynthesis and Evaluation of 11C-CIMBI-5 as a 5-HT2A Receptor Agonist Radioligand for PET. *J Nucl Med*. 51:1763-1770.

Finnema, S., A. Ettrup, V. Stepanov, R. Nakao, N. Amini, A. Varrone, G.M. Knudsen, and C. Halldin. 2012a. Characterization of [11C]Cimbi-36 as a 5-HT2A receptor agonist PET radioligand in the non-human primate brain. *J Cereb Blood Flow Metab*. 32:S64.

Finnema, S.J., A. Varrone, T.J. Hwang, C. Halldin, and L. Farde. 2012b. Confirmation of fenfluramine effect on 5-HT(1B) receptor binding of [(11)C]AZ10419369 using an equilibrium approach. *J Cereb Blood Flow Metab*. 32:685-695.

Fletcher, S., and N.M. Barnes. 1996. Distribution and characterisation of the [3H](S)-zacopride labelled 5-HT3 receptor in pig forebrain. *Brain Res*. 729:281-284.

Friedman, A.M., O.T. DeJesus, J. Revenaugh, and R.J. Dinerstein. 1984. Measurements in vivo of parameters of the dopamine system. *Ann Neurol*. 15:S66-76.

Frokjaer, V.G., E.L. Mortensen, F.A. Nielsen, S. Haugbol, L.H. Pinborg, K.H. Adams, C. Svarer, S.G. Hasselbalch, S. Holm, O.B. Paulson, and G.M. Knudsen. 2008. Frontolimbic serotonin 2A receptor binding in healthy subjects is associated with personality risk factors for affective disorder. *Biol Psychiatry*. 63:569-576.

Fumita, M., and R.B. Innis. 2002. In Vivo Molecular Imaging: Ligand Development and Research Applications. *In* Neuropsychopharmacology: The Fifth Generation of Progress. K.L. Davis, D. Cherney, J.T. Coyle, and C. Nemeroff, editors. Lippincott, Williams, & Wilkins, Philadelphia, Pensylvania. 411-425.

Gershon, M.D., and J. Tack. 2007. The Serotonin Signaling System: From Basic Understanding To Drug Development for Functional GI Disorders. *Gastroenterology*. 132:397-414.

Geurts, F.J., E. De Schutter, and J.P. Timmermans. 2002. Localization of 5-HT2A, 5-HT3, 5-HT5A and 5-HT7 receptor-like immunoreactivity in the rat cerebellum. *J Chem Neuroanat*. 24:65-74.

Gillings, N. 2009. A restricted access material for rapid analysis of [(11)C]-labeled radiopharmaceuticals and their metabolites in plasma. *Nucl Med Biol*. 36:961-965.

Gjedde, A. 1982. Calculation of cerebral glucose phosphorylation from brain uptake of glucose analogs in vivo: A re-examination. *Brain Res Rev*. 4:237-274.

González-Maeso, J., and S.C. Sealfon. 2009. Psychedelics and schizophrenia. *Trends Neurosci*. 32:225-232.

Goodman, S., and E. Check. 2002. The great primate debate. *Nature*. 417:684-687.

Guo, Q., M. Brady, and R.N. Gunn. 2009. A biomathematical modeling approach to central nervous system radioligand discovery and development. *J Nucl Med*. 50:1715-1723.

Guscott, M., L.J. Bristow, K. Hadingham, T.W. Rosahl, M.S. Beer, J.A. Stanton, F. Bromidge, A.P. Owens, I. Huscroft, J. Myers, N.M. Rupniak, S. Patel, P.J. Whiting, P.H. Hutson, K.C. Fone, S.M. Biello, J.J. Kulagowski, and G. McAllister. 2005. Genetic knockout and pharmacological blockade studies of the 5-HT7 receptor suggest therapeutic potential in depression. *Neuropharmacology*. 48:492-502.

Gustafson, E.L., M.M. Durkin, J.A. Bard, J. Zgombick, and T.A. Branchek. 1996. A receptor autoradiographic and in situ hybridization analysis of the distribution of the 5-ht7 receptor in rat brain. *Br J Pharmacol*. 117:657-666.

Hall, H., L. Farde, C. Halldin, C. Lundkvist, and G. Sedvall. 2000. Autoradiographic localization of 5-HT(2A) receptors in the human brain using [(3)H]M100907 and [(11)C]M100907. *Synapse*. 38:421-431.

Hall, H., C. Lundkvist, C. Halldin, L. Farde, V.W. Pike, J.A. McCarron, A. Fletcher, I.A. Cliffe, T. Barf, H. Wikstrom, and G. Sedvall. 1997. Autoradiographic localization of 5-HT1A receptors in the post-mortem human brain using [3H]WAY-100635 and [11C]way-100635. *Brain Res*. 745:96-108.

Hannon, J., and D. Hoyer. 2008. Molecular biology of 5-HT receptors. *Behav Brain Res*. 195:198-213.

Hardy, J., and D. Allsop. 1991. Amyloid deposition as the central event in the aetiology of Alzheimer's disease. *Trends Pharmacol Sci*. 12:383-388.

Heald, A., J.A. Stanton, S.A. Osborne, D.N. Middlemiss, and M.S. Beer. 1994. [3H]L-694,247 labels the 5-HT1D beta receptor in pig caudate membranes. *Eur J Pharmacol*. 264:213-216.

Hedlund, P.B., S. Huitron-Resendiz, S.J. Henriksen, and J.G. Sutcliffe. 2005. 5-HT7 receptor inhibition and inactivation induce antidepressantlike behavior and sleep pattern. *Biol Psychiatry*. 58:831-837.

Hedlund, P.B., M. Leopoldo, S. Caccia, G. Sarkisyan, C. Fracasso, G. Martelli, E. Lacivita, F. Berardi, and R. Perrone. 2010. LP-211 is a brain penetrant selective agonist for the serotonin 5-HT(7) receptor. *Neurosci Lett*. 481:12-16.

Heidmann, D.E., M.A. Metcalf, R. Kohen, and M.W. Hamblin. 1997. Four 5-hydroxytryptamine7 (5-HT7) receptor isoforms in human and rat produced by alternative splicing: species differences due to altered intron-exon organization. *J Neurochem*. 68:1372-1381.

Heidmann, D.E., P. Szot, R. Kohen, and M.W. Hamblin. 1998. Function and distribution of three rat 5-hydroxytryptamine7 (5-HT7) receptor isoforms produced by alternative splicing. *Neuropharmacology*. 37:1621-1632.

Herth, M.M., F. Debus, M. Piel, M. Palner, G.M. Knudsen, H. Luddens, and F. Rosch. 2008. Total synthesis and evaluation of [18F]MHMZ. *Bioorg Med Chem Lett*. 18:1515-1519.

Herth, M.M., V. Kramer, M. Piel, M. Palner, P.J. Riss, G.M. Knudsen, and F. Rosch. 2009a. Synthesis and in vitro affinities of various MDL 100907 derivatives as potential 18F-radioligands for 5-HT2A receptor imaging with PET. *Bioorg Med Chem*. 17:2989-3002.

Herth, M.M., M. Piel, F. Debus, U. Schmitt, H. Luddens, and F. Rosch. 2009b. Preliminary in vivo and ex vivo evaluation of the 5-HT2A imaging probe [(18)F]MH.MZ. *Nucl Med Biol*. 36:447-454.

Herth, M.M., B. Volk, K. Pallagi, L. Kofoed Bech, F.A. Antoni, G.M. Knudsen, and J.L. Kristensen. 2012. Synthesis and in vitro evaluation of oxindole derivatives as potential radioligands for 5-HT(7) receptor imaging with PET. *ACS Chem Neurosci*. 3:1002-1007.

Horisawa, T., T. Ishiyama, M. Ono, T. Ishibashi, and M. Taiji. 2013. Binding of lurasidone, a novel antipsychotic, to rat 5-HT7 receptor: Analysis by [3H]SB-269970 autoradiography. *Prog Neuropsychopharmacol Biol Psychiatry*. 40:132-137.

Houle, S., N. Ginovart, D. Hussey, J.H. Meyer, and A.A. Wilson. 2000. Imaging the serotonin transporter with positron emission tomography: initial human studies with [11C]DAPP and [11C]DASB. *Eur J Nucl Med*. 27:1719-1722.

Hoyer, D., G. Engel, and H.O. Kalkman. 1985. Molecular pharmacology of 5-HT1 and 5-HT2 recognition sites in rat and pig brain membranes: radioligand binding studies with [3H]5-HT, [3H]8-OH-DPAT, (-)[125I]iodocyanopindolol, [3H]mesulergine and [3H]ketanserin. *Eur J Pharmacol*. 118:13-23.

Hoyer, D., J.P. Hannon, and G.R. Martin. 2002. Molecular, pharmacological and functional diversity of 5-HT receptors. *Pharmacol Biochem Behav*. 71:533-554.

Ikeda, M., N. Iwata, T. Kitajima, T. Suzuki, Y. Yamanouchi, Y. Kinoshita, and N. Ozaki. 2006. Positive association of the serotonin 5-HT7 receptor gene with schizophrenia in a Japanese population. *Neuropsychopharmacology*. 31:866-871.

Innis, R.B., V.J. Cunningham, J. Delforge, M. Fujita, A. Gjedde, R.N. Gunn, J. Holden, S. Houle, S.C. Huang, M. Ichise, H. Iida, H. Ito, Y. Kimura, R.A. Koeppe, G.M. Knudsen, J. Knuuti, A.A. Lammertsma, M. Laruelle, J. Logan, R.P. Maguire, M.A. Mintun, E.D. Morris, R. Parsey, J.C. Price, M. Slifstein, V. Sossi, T. Suhara, J.R. Votaw, D.F. Wong, and R.E. Carson. 2007. Consensus nomenclature for in vivo imaging of reversibly binding radioligands. *J Cereb Blood Flow Metab*. 27:1533-1539.

Ishibashi, T., T. Horisawa, K. Tokuda, T. Ishiyama, M. Ogasa, R. Tagashira, K. Matsumoto, H. Nishikawa, Y. Ueda, S. Toma, H. Oki, N. Tanno, I. Saji, A. Ito, Y. Ohno, and M. Nakamura. 2010. Pharmacological profile of lurasidone, a novel antipsychotic agent with potent 5-hydroxytryptamine 7 (5-HT7) and 5-HT1A receptor activity. *J Pharmacol Exp Ther*. 334:171-181.

Ito, H., S. Nyberg, C. Halldin, C. Lundkvist, and L. Farde. 1998. PET imaging of central 5-HT2A receptors with carbon-11-MDL 100,907. *J Nucl Med*. 39:208-214.

Jensen, S.B., D.F. Smith, D. Bender, S. Jakobsen, D. Peters, E.Ø. Nielsen, G.M. Olsen, J. Scheel-Krüger, A. Wilson, and P. Cumming. 2003. [11C]-NS 4194 versus [11C]-DASB for PET imaging of serotonin transporters in living porcine brain. *Synapse*. 49:170-177.

Katona, C., T. Hansen, and C.K. Olsen. 2012. A randomized, double-blind, placebo-controlled, duloxetine-referenced, fixed-dose study comparing the efficacy and safety of Lu AA21004 in elderly patients with major depressive disorder. *Int Clin Psychopharmacol*. 27:215-223.

Kessler, R.M., M.S. Ansari, T. de Paulis, D.E. Schmidt, J.A. Clanton, H.E. Smith, R.G. Manning, D. Gillespie, and M.H. Ebert. 1991. High affinity dopamine D2 receptor radioligands. 1. Regional rat brain distribution of iodinated benzamides. *J Nucl Med*. 32:1593-1600.

Klunk, W.E., H. Engler, A. Nordberg, Y. Wang, G. Blomqvist, D.P. Holt, M. Bergstrom, I. Savitcheva, G.F. Huang, S. Estrada, B. Ausen, M.L. Debnath, J. Barletta, J.C. Price, J. Sandell, B.J. Lopresti, A. Wall, P. Koivisto, G. Antoni, C.A. Mathis, and B. Langstrom. 2004. Imaging brain amyloid in Alzheimer's disease with Pittsburgh Compound-B. *Ann Neurol*. 55:306-319.

Köhn, F., A.R. Sharifi, H. Täubert, Š. Malovrh, and H. Simianer. 2008. Breeding for low body weight in Goettingen minipigs. *J Anim Breed Genet*. 125:20-28.

Kornum, B.R., N.M. Lind, N. Gillings, L. Marner, F. Andersen, and G.M. Knudsen. 2009. Evaluation of the novel 5-HT4 receptor PET ligand [11C]SB207145 in the Gottingen minipig. *J Cereb Blood Flow Metab*. 29:186-196.

Kragh, P.M., A.L. Nielsen, J. Li, Y. Du, L. Lin, M. Schmidt, I.B. Bogh, I.E. Holm, J.E. Jakobsen, M.G. Johansen, S. Purup, L. Bolund, G. Vajta, and A.L. Jorgensen. 2009. Hemizygous minipigs produced by random gene insertion and handmade cloning express the Alzheimer's disease-causing dominant mutation APPsw. *Transgenic Res*. 18:545-558.

Krobert, K.A., T. Bach, T. Syversveen, A.M. Kvingedal, and F.O. Levy. 2001. The cloned human 5-HT7 receptor splice variants: a comparative characterization of their pharmacology, function and distribution. *Naunyn Schmiedebergs Arch Pharmacol*. 363:620-632.

Kumar, J.S., R.V. Parsey, S.A. Kassir, V.J. Majo, M.S. Milak, J. Prabhakaran, N.R. Simpson, M.D. Underwood, J.J. Mann, and V. Arango. 2013. Autoradiographic evaluation of [(3)H]CUMI-101, a novel, selective 5-HT1AR ligand in human and baboon brain. *Brain Res*. 1507:11-18.

Laruelle, M. 2000. Imaging synaptic neurotransmission with in vivo binding competition techniques: a critical review. *J Cereb Blood Flow Metab*. 20:423-451.

Laruelle, M., A. Abi-Dargham, C.H. van Dyck, R. Gil, C.D. D'Souza, J. Erdos, E. McCance, W. Rosenblatt, C. Fingado, S.S. Zoghbi, R.M. Baldwin, J.P. Seibyl, J.H. Krystal, D.S. Charney, and R.B. Innis. 1996. Single photon emission computerized tomography imaging of amphetamine-induced dopamine release in drug-free schizophrenic subjects. *Proc Natl Acad Sci U S A*. 93:9235-9240.

Laruelle, M., M. Slifstein, and Y. Huang. 2003. Relationships between radiotracer properties and image quality in molecular imaging of the brain with positron emission tomography. *Mol Imaging Biol*. 5:363-375.

Lemoine, L., J. Andries, D. Le Bars, T. Billard, and L. Zimmer. 2011. Comparison of 4 Radiolabeled Antagonists for Serotonin 5-HT7 Receptor Neuroimaging: Toward the First PET Radiotracer. *J Nucl Med*. 52:1811-1818.

Leopoldo, M., F. Berardi, N.A. Colabufo, M. Contino, E. Lacivita, M. Niso, R. Perrone, and V. Tortorella. 2004. Structure-affinity relationship study on N-(1,2,3,4-tetrahydronaphthalen-1-yl)-4-aryl-1-piperazinealkylamides, a new class of 5-hydroxytryptamine7 receptor agents. *J Med Chem*. 47:6616-6624.

Leopoldo, M., E. Lacivita, M. Contino, N.A. Colabufo, F. Berardi, and R. Perrone. 2007. Structure-activity relationship study on N-(1,2,3,4-tetrahydronaphthalen-1-yl)-4-aryl-1-piperazinehexanamides, a class of 5-HT7 receptor agents. 2. *J Med Chem*. 50:4214-4221.

Leopoldo, M., E. Lacivita, P. De Giorgio, C. Fracasso, S. Guzzetti, S. Caccia, M. Contino, N.A. Colabufo, F. Berardi, and R. Perrone. 2008. Structural modifications of N-(1,2,3,4-tetrahydronaphthalen-1-yl)-4-aryl-1-piperazinehexanamides: influence on lipophilicity and 5-HT7 receptor activity. Part III. *J Med Chem*. 51:5813-5822.

Leysen, J.E. 1989. Use of 5-HT Receptor Agonists and Antagonists for the Characterization of Their Respective Receptor Sites. *In* Drugs as Tools in Neurotransmitter Research. Vol. 12. A.A. Boulton, G.B. Baker, and A.V. Juorio, editors. 299-350.

Leysen, J.E. 2004. 5-HT2 Receptors. *Current Drug Targets - CNS & Neurological Disorders*. 3:11-26.

Li, Y.C., F.M. Wang, Y. Pan, L.Q. Qiang, G. Cheng, W.Y. Zhang, and L.D. Kong. 2009. Antidepressant-like effects of curcumin on serotonergic receptor-coupled AC-cAMP pathway in chronic unpredictable mild stress of rats. *Prog Neuropsychopharmacol Biol Psychiatry*. 33:435-449.

Lind, N.M., A. Moustgaard, J. Jelsing, G. Vajta, P. Cumming, and A.K. Hansen. 2007. The use of pigs in neuroscience: modeling brain disorders. *Neurosci Biobehav Rev*. 31:728-751.

López-Giménez, J.F., G. Mengod, J.M. Palacios, and M.T. Vilaró. 1997. Selective visualization of rat brain 5-HT2A receptors by autoradiography with [3H]MDL 100,907. *Naunyn Schmiedebergs Arch Pharmacol*. 356:446-454.

Lovell, P.J., S.M. Bromidge, S. Dabbs, D.M. Duckworth, I.T. Forbes, A.J. Jennings, F.D. King, D.N. Middlemiss, S.K. Rahman, D.V. Saunders, L.L. Collin, J.J. Hagan, G.J. Riley, and D.R. Thomas.

2000. A novel, potent, and selective 5-HT(7) antagonist: (R)-3-(2-(2-(4-methylpiperidin-1-yl)ethyl)pyrrolidine-1-sulfonyl) phen ol (SB-269970). *J Med Chem*. 43:342-345.

Lummis, S.C.R. 2012. 5-HT3 Receptors. *J Biol Chem*. 287:40239-40245.

Lundkvist, C., C. Halldin, N. Ginovart, S. Nyberg, C.-G. Swahn, A.A. Carr, F. Brunner, and L. Farde. 1996. [11C]MDL 100907, a radioligand for selective imaging of 5-HT2A receptors with positron emission tomography. *Life Sciences*. 58:187-192.

Marner, L., N. Gillings, K. Madsen, D. Erritzoe, W.F. Baare, C. Svarer, S.G. Hasselbalch, and G.M. Knudsen. 2010. Brain imaging of serotonin 4 receptors in humans with [11C]SB207145-PET. *Neuroimage*. 50:855-861.

Martin-Cora, F.J., and A. Pazos. 2004. Autoradiographic distribution of 5-HT7 receptors in the human brain using [3H]mesulergine: comparison to other mammalian species. *Br J Pharmacol*. 141:92-104.

Massou, J.M., C. Trichard, D. Attar-Levy, A. Feline, E. Corruble, B. Beaufils, and J.L. Martinot. 1997. Frontal 5-HT2A receptors studied in depressive patients during chronic treatment by selective serotonin reuptake inhibitors. *Psychopharmacology (Berl)*. 133:99-101.

Meltzer, C.C., J.C. Price, C.A. Mathis, P.J. Greer, M.N. Cantwell, P.R. Houck, B.H. Mulsant, D. Ben-Eliezer, B. Lopresti, S.T. DeKosky, and C.F. Reynolds, 3rd. 1999. PET imaging of serotonin type 2A receptors in late-life neuropsychiatric disorders. *Am J Psychiatry*. 156:1871-1878.

Meyer, J.H., S. Kapur, B. Eisfeld, G.M. Brown, S. Houle, J. DaSilva, A.A. Wilson, S. Rafi-Tari, H.S. Mayberg, and S.H. Kennedy. 2001. The effect of paroxetine on 5-HT(2A) receptors in depression: an [(18)F]setoperone PET imaging study. *Am J Psychiatry*. 158:78-85.

Meyer, J.H., S. McMain, S.H. Kennedy, L. Korman, G.M. Brown, J.N. DaSilva, A.A. Wilson, T. Blak, R. Eynan-Harvey, V.S. Goulding, S. Houle, and P. Links. 2003. Dysfunctional attitudes and 5-HT2 receptors during depression and self-harm. *Am J Psychiatry*. 160:90-99.

Meyer, P.T., Z. Bhagwagar, P.J. Cowen, V.J. Cunningham, P.M. Grasby, and R. Hinz. 2010. Simplified quantification of 5-HT2A receptors in the human brain with [11C]MDL 100,907 PET and non-invasive kinetic analyses. *Neuroimage*. 50:984-993.

Mikkelsen, M., A. Moller, L.H. Jensen, A. Pedersen, J.B. Harajehi, and H. Pakkenberg. 1999. MPTP-induced Parkinsonism in minipigs: A behavioral, biochemical, and histological study. *Neurotoxicol Teratol*. 21:169-175.

Miller, P.W., N.J. Long, R. Vilar, and A.D. Gee. 2008. Synthesis of 11C, 18F, 15O, and 13N Radiolabels for Positron Emission Tomography. *Angew Chem Int Ed*. 47:8998-9033.

Mintun, M.A., Y.I. Sheline, S.M. Moerlein, A.G. Vlassenko, Y. Huang, and A.Z. Snyder. 2004. Decreased hippocampal 5-HT2A receptor binding in major depressive disorder: in vivo measurement with [18F]altanserin positron emission tomography. *Biol Psychiatry*. 55:217-224.

Mørk, A., L.P. Montezinho, S. Miller, C. Trippodi-Murphy, N. Plath, Y. Li, M. Gulinello, and C. Sanchez. 2013. Vortioxetine (Lu AA21004), a novel multimodal antidepressant, enhances memory in rats. *Pharmacol Biochem Behav*. 105:41-50.

Mørk, A., A. Pehrson, L.T. Brennum, S.M. Nielsen, H. Zhong, A.B. Lassen, S. Miller, L. Westrich, N.J. Boyle, C. Sánchez, C.W. Fischer, N. Liebenberg, G. Wegener, C. Bundgaard, S. Hogg, B. Bang-Andersen, and T.B. Stensbøl. 2012. Pharmacological Effects of Lu AA21004: A Novel Multimodal Compound for the Treatment of Major Depressive Disorder. *J Pharmacol Exp Ther*. 340:666-675.

Mukherjee, J., B. Shi, T.K. Narayanan, B.T. Christian, and Y. Zhi-Ying. 2004. Chapter 5 - Radiopharmaceuticals for Imaging the Brain. *In* Emission Tomography. N.W. Miles, Ph.D, and P.D. John N. Aarsvold, editors. Academic Press, San Diego. 89-101.

Muller, C.P., and B.L. Jacobs. 2010. Handbook of the Behavioral Neurobiology of Serotonin. Vol. 21. Academic Press.

Mullins, U.L., G. Gianutsos, and A.S. Eison. 1999. Effects of antidepressants on 5-HT7 receptor regulation in the rat hypothalamus. *Neuropsychopharmacology*. 21:352-367.

Neumaier, J.F., T.J. Sexton, J. Yracheta, A.M. Diaz, and M. Brownfield. 2001. Localization of 5-HT7 receptors in rat brain by immunocytochemistry, in situ hybridization, and agonist stimulated cFos expression. *J Chem Neuroanat*. 21:63-73.

Niblock, M.M., C.J. Luce, R.A. Belliveau, D.S. Paterson, M.L. Kelly, L.A. Sleeper, J.J. Filiano, and H.C. Kinney. 2005. Comparative anatomical assessment of the piglet as a model for the developing human medullary serotonergic system. *Brain Res Rev*. 50:169-183.

Nord, M., S.J. Finnema, C. Halldin, and L. Farde. 2013. Effect of a single dose of escitalopram on serotonin concentration in the non-human and human primate brain. *Int J Neuropsychopharmacol*. FirstView:1-10.

Olsson, H., and L. Farde. 2001. Potentials and Pitfalls Using High Affinity Radioligands in PET and SPET Determinations on Regional Drug Induced D2 Receptor Occupancy—A Simulation Study Based on Experimental Data. *Neuroimage*. 14:936-945.

Paans, A.M.J., A. van Waarde, P.H. Elsinga, A.T.M. Willemsen, and W. Vaalburg. 2002. Positron emission tomography: the conceptual idea using a multidisciplinary approach. *Methods*. 27:195-207.

Paillet-Loilier, M., F. Fabis, A. Lepailleur, R. Bureau, S. Butt-Gueulle, F. Dauphin, A. Lesnard, C. Delarue, H. Vaudry, and S. Rault. 2007. Novel aminoethylbiphenyls as 5-HT7 receptor ligands. *Bioorg Med Chem Lett*. 17:3018-3022.

Parker, C.A., R.N. Gunn, E.A. Rabiner, M. Slifstein, R. Comley, C. Salinas, C.N. Johnson, S. Jakobsen, S. Houle, M. Laruelle, V.J. Cunningham, and L. Martarello. 2012. Radiosynthesis and Characterization of 11C-GSK215083 as a PET Radioligand for the 5-HT6 Receptor. *J Nucl Med*. 53:295-303.

Paterson, L.M., B.R. Kornum, D.J. Nutt, V.W. Pike, and G.M. Knudsen. 2013. 5-HT radioligands for human brain imaging with PET and SPECT. *Med Res Rev*. 33:54-111.

Paterson, L.M., R.J. Tyacke, D.J. Nutt, and G.M. Knudsen. 2010. Measuring endogenous 5-HT release by emission tomography: promises and pitfalls. *J Cereb Blood Flow Metab*. 30:1682-1706.

Patlak, C.S., R.G. Blasberg, and J.D. Fenstermacher. 1983. Graphical evaluation of blood-to-brain transfer constants from multiple-time uptake data. *J Cereb Blood Flow Metab*. 3:1-7.

Pavey, G.M., D.L. Copolov, and B. Dean. 2002. High-resolution phosphor imaging: validation for use with human brain tissue sections to determine the affinity and density of radioligand binding. *J Neurosci Methods*. 116:157-163.

Pazos, A., D. Hoyer, and J.M. Palacios. 1984. The binding of serotonergic ligands to the porcine choroid plexus: characterization of a new type of serotonin recognition site. *Eur J Pharmacol*. 106:539-546.

Pike, V.W. 2009. PET radiotracers: crossing the blood-brain barrier and surviving metabolism. *Trends Pharmacol Sci*. 30:431-440.

Pike, V.W., J.A. McCarron, A.A. Lammerstma, S.P. Hume, K. Poole, P.M. Grasby, A. Malizia, I.A. Cliffe, A. Fletcher, and C.J. Bench. 1995. First delineation of 5-HT1A receptors in human brain with PET and [11C]WAY-100635. *Eur J Pharmacol*. 283:R1-R3.

Pinborg, L.H., K.H. Adams, C. Svarer, S. Holm, S.G. Hasselbalch, S. Haugbol, J. Madsen, and G.M. Knudsen. 2003. Quantification of 5-HT2A receptors in the human brain using [18F]altanserin-PET and the bolus/infusion approach. *J Cereb Blood Flow Metab*. 23:985-996.

Pinborg, L.H., C. Videbaek, M. Ziebell, T. Mackeprang, L. Friberg, H. Rasmussen, G.M. Knudsen, and B.Y. Glenthoj. 2007. [123I]epidepride binding to cerebellar dopamine D2/D3 receptors is displaceable: implications for the use of cerebellum as a reference region. *Neuroimage*. 34:1450-1453.

Plassat, J.L., N. Amlaiky, and R. Hen. 1993. Molecular cloning of a mammalian serotonin receptor that activates adenylate cyclase. *Mol Pharmacol*. 44:229-236.

Pouzet, B. 2002. SB-258741: a 5-HT7 receptor antagonist of potential clinical interest. *CNS Drug Rev*. 8:90-100.

Price, J.C., B.J. Lopresti, N.S. Mason, D.P. Holt, Y. Huang, and C.A. Mathis. 2001. Analyses of [(18)F]altanserin bolus injection PET data. I: consideration of radiolabeled metabolites in baboons. *Synapse*. 41:1-10.

Rapport, M.M., A.A. Green, and I.H. Page. 1948. Serum vasoconstrictor, serotonin; isolation and characterization. *J Biol Chem*. 176:1243-1251.

Roberts, A.J., T. Krucker, C.L. Levy, K.A. Slanina, J.G. Sutcliffe, and P.B. Hedlund. 2004. Mice lacking 5-HT receptors show specific impairments in contextual learning. *Eur J Neurosci*. 19:1913-1922.

Ruat, M., E. Traiffort, R. Leurs, J. Tardivel-Lacombe, J. Diaz, J.M. Arrang, and J.C. Schwartz. 1993. Molecular cloning, characterization, and localization of a high-affinity serotonin receptor (5-HT7) activating cAMP formation. *Proc Natl Acad Sci U S A*. 90:8547-8551.

Sarkisyan, G., A.J. Roberts, and P.B. Hedlund. 2010. The 5-HT(7) receptor as a mediator and modulator of antidepressant-like behavior. *Behav Brain Res*. 209:99-108.

Schiavi, G.B., S. Brunet, C.A. Rizzi, and H. Ladinsky. 1994. Identification of serotonin 5-HT4 recognition sites in the porcine caudate nucleus by radioligand binding. *Neuropharmacology*. 33:543-549.

Schoeffter, P., and C. Waeber. 1994. 5-Hydroxytryptamine receptors with a 5-HT6 receptor-like profile stimulating adenylyl cyclase activity in pig caudate membranes. *Naunyn Schmiedebergs Arch Pharmacol*. 350:356-360.

Slattery, D.A., and J.F. Cryan. 2012. Using the rat forced swim test to assess antidepressant-like activity in rodents. *Nat Protoc*. 7:1009-1014.

Sommer, C. 2006. Is serotonin hyperalgesic or analgesic? *Curr Pain Headache Rep*. 10:101-106.

Stam, N.J., C. Roesink, F. Dijcks, A. Garritsen, A. van Herpen, and W. Olijve. 1997. Human serotonin 5-HT7 receptor: cloning and pharmacological characterisation of two receptor variants. *FEBS Letters*. 413:489-494.

Stockmeier, C.A. 2003. Involvement of serotonin in depression: evidence from postmortem and imaging studies of serotonin receptors and the serotonin transporter. *J Psychiatr Res*. 37:357-373.

Talbot, P.S., M. Slifstein, D.-R. Hwang, Y. Huang, E. Scher, A. Abi-Dargham, and M. Laruelle. 2012. Extended characterisation of the serotonin 2A (5-HT2A) receptor-selective PET radiotracer 11C-MDL100907 in humans: Quantitative analysis, test–retest reproducibility, and vulnerability to endogenous 5-HT tone. *Neuroimage*. 59:271-285.

Tan, P.Z., R.M. Baldwin, C.H. Van Dyck, M. Al-Tikriti, B. Roth, N. Khan, D.S. Charney, and R.B. Innis. 1999. Characterization of radioactive metabolites of 5-HT2A receptor PET ligand [18F]altanserin in human and rodent. *Nucl Med Biol*. 26:601-608.

Thomas, D.R., P.J. Atkinson, P.G. Hastie, J.C. Roberts, D.N. Middlemiss, and G.W. Price. 2002. [3H]-SB-269970 radiolabels 5-HT7 receptors in rodent, pig and primate brain tissues. *Neuropharmacology*. 42:74-81.

Thomas, D.R., P.J. Atkinson, M. Ho, S.M. Bromidge, P.J. Lovell, A.J. Villani, J.J. Hagan, D.N. Middlemiss, and G.W. Price. 2000. [(3)H]-SB-269970--A selective antagonist radioligand for 5-HT(7) receptors. *Br J Pharmacol*. 130:409-417.

Thomas, D.R., and J.J. Hagan. 2004. 5-HT7 receptors. *Curr Drug Targets CNS Neurol Disord*. 3:81-90.

To, Z.P., D.W. Bonhaus, R.M. Eglen, and L.B. Jakeman. 1995. Characterization and distribution of putative 5-ht7 receptors in guinea-pig brain. *Br J Pharmacol*. 115:107-116.

Törk, I. 1990. Anatomy of the Serotonergic System. *Annals of the New York Academy of Sciences*. 600:9-34.

Tsou, A.P., A. Kosaka, C. Bach, P. Zuppan, C. Yee, L. Tom, R. Alvarez, S. Ramsey, D.W. Bonhaus, E. Stefanich, and et al. 1994. Cloning and expression of a 5-hydroxytryptamine7 receptor positively coupled to adenylyl cyclase. *J Neurochem*. 63:456-464.

Twarog, B.M., and I.H. Page. 1953. Serotonin content of some mammalian tissues and urine and a method for its determination. *Am J Physiol*. 175:157-161.

van der Staay, F.J., B. Pouzet, M. Mahieu, R.E. Nordquist, and T. Schuurman. 2009. The d-amphetamine-treated Gottingen miniature pig: an animal model for assessing behavioral effects of antipsychotics. *Psychopharmacology (Berl)*. 206:715-729.

Varnas, K., D.R. Thomas, E. Tupala, J. Tiihonen, and H. Hall. 2004. Distribution of 5-HT7 receptors in the human brain: a preliminary autoradiographic study using [3H]SB-269970. *Neurosci.Lett*. 367:313-316.

Volk, B., J. Barkoczy, E. Hegedus, S. Udvari, I. Gacsalyi, T. Mezei, K. Pallagi, H. Kompagne, G. Levay, A. Egyed, L.G. Harsing, Jr., M. Spedding, and G. Simig. 2008. (Phenylpiperazinyl-butyl)oxindoles as selective 5-HT7 receptor antagonists. *J Med Chem*. 51:2522-2532.

Waeber, C., P. Schoeffter, J.M. Palacios, and D. Hoyer. 1988. Molecular pharmacology of 5-HT1D recognition sites: Radioligand binding studies in human, pig and calf brain membranes. *Naunyn Schmiedebergs Arch Pharmacol*. 337:595-601.

Watabe, H., M.A. Channing, M.G. Der, H.R. Adams, E. Jagoda, P. Herscovitch, W.C. Eckelman, and R.E. Carson. 2000. Kinetic analysis of the 5-HT2A ligand [11C]MDL 100,907. *J Cereb Blood Flow Metab*. 20:899-909.

Watanabe, H., F. Andersen, C.Z. Simonsen, S.M. Evans, A. Gjedde, and P. Cumming. 2001. MR-based statistical atlas of the Gottingen minipig brain. *Neuroimage*. 14:1089-1096.

Waterhouse, R.N. 2003. Determination of lipophilicity and its use as a predictor of blood-brain barrier penetration of molecular imaging agents. *Mol Imaging Biol*. 5:376-389.

Wesolowska, A., A. Nikiforuk, and K. Stachowicz. 2006a. Potential anxiolytic and antidepressant effects of the selective 5-HT7 receptor antagonist SB 269970 after intrahippocampal administration to rats. *Eur J Pharmacol*. 553:185-190.

Wesolowska, A., A. Nikiforuk, K. Stachowicz, and E. Tatarczynska. 2006b. Effect of the selective 5-HT7 receptor antagonist SB 269970 in animal models of anxiety and depression. *Neuropharmacology*. 51:578-586.

Wesolowska, A., E. Tatarczynska, A. Nikiforuk, and E. Chojnacka-Wojcik. 2007. Enhancement of the anti-immobility action of antidepressants by a selective 5-HT7 receptor antagonist in the forced swimming test in mice. *Eur J Pharmacol*. 555:43-47.

Westrich, L., A. Pehrson, H. Zhong, S.M. Nielsen, K. Frederiksen, T.B. Stensbøl, N. Boyle, M. Hentzer, and C. Sanchez. 2012. In vitro and in vivo effects of the multimodal antidepressant vortioxetine (Lu AA21004) at human and rat targets. *In* International Journal of Psychiatry in Clinical Practice. Vol. 16. 47.

Wong, D.F., H.N. Wagner, Jr., L.E. Tune, R.F. Dannals, G.D. Pearlson, J.M. Links, C.A. Tamminga, E.P. Broussolle, H.T. Ravert, A.A. Wilson, J.K. Toung, J. Malat, J.A. Williams, L.A. O'Tuama, S.H. Snyder, M.J. Kuhar, and A. Gjedde. 1986. Positron emission tomography reveals elevated D2 dopamine receptors in drug-naive schizophrenics. *Science*. 234:1558-1563.

Wong, D.T., K.W. Perry, and F.P. Bymaster. 2005. Case history: the discovery of fluoxetine hydrochloride (Prozac). *Nat Rev Drug Discov*. 4:764-774.

Yatham, L.N., P.F. Liddle, J. Dennie, I.S. Shiah, M.J. Adam, C.J. Lane, R.W. Lam, and T.J. Ruth. 1999. Decrease in brain serotonin 2 receptor binding in patients with major depression following desipramine treatment: a positron emission tomography study with fluorine-18-labeled setoperone. *Arch Gen Psychiatry*. 56:705-711.

Zanardi, R., F. Artigas, R. Moresco, C. Colombo, C. Messa, C. Gobbo, E. Smeraldi, and F. Fazio. 2001. Increased 5-hydroxytryptamine-2 receptor binding in the frontal cortex of depressed patients responding to paroxetine treatment: a positron emission tomography scan study. *J Clin Psychopharmacol*. 21:53-58.

Zhang, M.-R., T. Haradahira, J. Maeda, T. Okauchi, T. Kida, S. Obayashi, K. Suzuki, and T. Suhara. 2002. Synthesis and preliminary PET study of the 5-HT7 receptor antagonist [11C]DR4446. *J. Labelled Cpd. Radiopharm*. 45:857-866.

Paper I

Hansen HD, Ettrup A, Herth MM, Dyssegaard A, Ratner C, Gillings N, and Knudsen GM.

Direct comparison of [^{18}F]MH.MZ and [^{18}F]altanserin for 5-HT$_{2A}$ receptor imaging with PET.

Direct Comparison of [18F]MH.MZ and [18F]altanserin for 5-HT$_{2A}$ Receptor Imaging with PET

HANNE D. HANSEN,[1] ANDERS ETTRUP,[1] MATTHIAS M. HERTH,[1,2] AGNETE DYSSEGAARD,[1] CECILIA RATNER,[1] NIC GILLINGS,[2] AND GITTE M. KNUDSEN[1]*

[1]*Neurobiology Research Unit and Center for Integrated Molecular Brain Imaging, Copenhagen University Hospital Rigshospitalet, Blegdamsvej 9, Copenhagen DK-2100, Denmark*
[2]*PET and Cyclotron Unit, Copenhagen University Hospital Rigshospitalet, Blegdamsvej 9, Copenhagen DK-2100, Denmark*

ABSTRACT   Imaging the cerebral serotonin 2A (5-HT$_{2A}$) receptors with positron emission tomography (PET) has been carried out in humans with [11C]MDL 100907 and [18F]altanserin. Recently, the MDL 100907 analogue [18F]MH.MZ was developed combining the selectivity profile of MDL 100907 and the favourable radiophysical properties of fluorine-18. Here, we present a direct comparison of [18F]altanserin and [18F]MH.MZ. 5-HT$_{2A}$ receptor binding in pig cortex and cerebellum was investigated by autoradiography with [3H]MDL 100907, [18F]MH.MZ, and [18F]altanserin. [18F]MH.MZ and [18F]altanserin were investigated in Danish Landrace pigs by brain PET scanning at baseline and after i.v. administration of blocking doses of ketanserin. Full arterial input function and high performance liquid chromatography (HPLC) analysis allowed for tissue-compartment kinetic modeling of PET data. In vitro autoradiography showed high binding in cortical regions with both [18F]MH.MZ and [18F]altanserin. Significant 5-HT$_{2A}$ receptor binding was also found in the pig cerebellum, thus making this region unsuitable as a reference region for in vivo data analysis in this species. The cortical binding of [18F]MH.MZ and [18F]altanserin was blocked by ketanserin supporting that both radioligands bind to 5-HT$_{2A}$ receptors in the pig brain. In the HPLC analysis of pig plasma, [18F]MH.MZ displayed a fast and reproducible metabolism resulting in hydrophilic radiometabolites only whereas the metabolic profile of [18F]altanserin as expected showed lipophilic radiometabolites. Due to the slow kinetics of [18F]MH.MZ in high-binding regions in vivo, we suggest that [18F]MH.MZ will be an appropriate tracer for low binding regions where kinetics will be faster, whereas [18F]altanserin is a suitable tracer for high-binding regions. **Synapse 67:328–337, 2013.** © 2013 Wiley Periodicals, Inc.

INTRODUCTION

Serotonin (5-hydroxytryptamine, 5-HT) 2A receptors has been implicated in various physiological functions and pathological conditions including depression, Alzheimer's disease, and schizophrenia (Naughton et al., 2000) and is thus of significant clinical interest. Evidence for the role of 5-HT$_{2A}$ receptors in the brain disorders comes both from post-mortem studies and brain imaging studies (Hasselbalch et al., 2008; McKeith et al., 1987; Rasmussen et al., 2010).

Positron emission tomography (PET) is a widely used in vivo brain imaging technique, where the pharmacological parameters of ligand-neuroreceptor interactions can be quantified and in vivo PET studies of cerebral 5-HT$_{2A}$ receptors and occupancy by

therapeutic drugs, e.g. antipsychotics, have provided a significant advance in the understanding of the living human brain.

The two clinically used PET-tracers for the 5-HT$_{2A}$ receptor are [18F]altanserin and [11C]MDL 100907

(Paterson et al., 2011) both of which have high affinity for the 5-HT$_{2A}$ receptor (Herth et al., 2009a; Kehne et al., 1996; Leysen, 1989). However, these PET-tracers have limitations: [^{18}F]altanserin generates blood brain-barrier (BBB) crossing lipophilic radiometabolites and has lower receptor selectivity (Leysen, 1989; Price et al., 2001b) and [^{11}C]MDL 100907 has slow kinetics which makes it hard to quantify reliably (Watabe et al., 2000).

In an attempt to avoid the lipophilic metabolites of altanserin and take advantage of the increased selectivity profile of MDL 100907, an ^{18}F-labelled analogue of MDL 100907, [^{18}F]MH.MZ was developed (Herth et al., 2008, 2009a,b). In vitro and in vivo studies in rodents showed that this radioligand combines the selectivity of MDL 100907 with the isotopic properties of 18-fluorine.

The aim of this study was to evaluate the binding characteristics of [^{18}F]MH.MZ in the brain of a large experimental animal; the in vitro and in vivo properties of [^{18}F]MH.MZ was evaluated in pigs and compared directly with [^{18}F]altanserin.

MATERIALS AND METHODS
Radiochemistry

[^{18}F]MH.MZ and [^{18}F]altanserin were prepared as previously reported (Herth et al., 2012).

In vitro autoradiography

Twenty micrometer coronal and sagittal sections of pig brain (approximately 3 months of age and weight 19 kg) were sectioned on a HM500OM Cryostat (Microm Intl GmbH, Walldorf, Germany) and thawed-mounted on super frost plus glass slides (Thermo Scientific, Braunschweig, Germany), air-dried and stored at −80°C

Abbreviations

Kd	Dissociation constant
BPND	Non-displaceable binding potential
TB	Total binding
VOI	Volume of interest
VT	Total distribution volume
VND	Non-displaceable distribution volume
i.v.	intra venous
5-HT	5-hydroxytryptamine
Bmax	receptor density
SB	Specific binding
HRRT	High resolution research tomography
BBB	blood brain-barrier
COV	coefficient variance
HPLC	high performance liquid chromatography
IP	imaging plates
NSB	non-specific binding
PET	positron emission tomography
SUV	standardized uptake values
TAC	time–activity curves
TC	tissue compartment.

until further use. Autoradiography was conducted at room temperature in assay buffer (50 mM Tris-HCl, pH 7.4) with varying concentrations of [^{18}F]MH.MZ (0.78–100 nM) or [^{18}F]altanserin (1.25 nM). Non-specific binding (NSB) was determined with 10 μM ketanserin (Sigma-Aldrigh, Brøndby, Denmark). Blocking experiments with [^{18}F]MH.MZ (at a ligand concentration of 10 nM) were carried out with 10 μM ketanserin or MDL 100907, while [^{18}F]altanserin blocking experiments (at a ligand concentration of 2.5 nM) were carried out with 10 μM ketanserin, MDL 100907, raclopride or prazosin (Sigma-Aldrigh, Brøndby, Denmark). Sections were pre-incubated in buffer for approximately 30 min, then incubated with ^{18}F-labelled compounds for 1 h at RT, washed for 2 × 5 min ([^{18}F]MH.MZ) or for 3 × 5 min ([^{18}F]altanserin) in ice-cold assay buffer, and finally washed for 20 sec in ice-cold water (dH$_2$O). Sections were then dried and exposed to Fuji imaging plates (Fujifilm Europe GmbH, Düsseldorf, Germany) for 5 min ([^{18}F]altanserin) or 8 h ([^{18}F]MH.MZ).

The autoradiographic protocol for [^{3}H]MDL 100907 (kindly provided by Prof. Christer Halldin, Karolinska Institute, Stockholm, Sweden) was as follows: Sections were pre-incubated for 15 min in 50 mM Tris-HCl buffer containing 0.01% ascorbic acid (pH 7.4) at room temperature. Sections were then incubated for 1 h in assay buffer containing 2 nM [^{3}H]MDL 100907 at room temperature. NSB was determined in the presence of 10 μM ketanserin. Slides were washed in ice-cold 50 mM Tris-HCl (pH 7.4) for 2 × 5 min followed by a 20 sec dip in ice-cold dH$_2$O water. Slides were then dried before being fixed in a PFA vapor overnight at 4°C. Hereafter, slides were exposed to BAS TR2040 TR-imaging plates (Science Imaging Scandinavia AB, Nacka, Sweden) for 7 days at 4°C along with two sets of high and low activity [^{3}H]microscales and then scanned. A saturation study was performed to determine K_d and B_{max} of [^{3}H]MDL 100907. Concentrations of 0.125, 0.25, 0.5, 1, and 2 nM [^{3}H]MDL 100907 were used. The remaining protocol was as described above except for a shorter washing time of 2 × 20 sec followed by a 20 sec dip in dH$_2$O.

Calibration, quantification, and data evaluation of all autoradiography images were done with ImageJ analysis software (http://rsb.info.nih.gov/ij/). Regions of interest were hand-drawn around anatomical landmarks, e.g., borders of sections, for each brain region and the mean pixel density was measured in each brain region as outcome. A third-degree exponential calibration function of either decay-corrected [^{3}H]microscales or a dilution series of the ^{18}F-solution (repeated after each radiotracer synthesis) was used to convert the mean pixel density to radioactivity.

Animal procedures

Six female Danish Landrace pigs (mean weight was 20.0 ± 1 kg) were used in this study. Animal

procedures were carried out as previously published (Ettrup et al., 2010). All animal procedures were approved by the Danish Council for Animal Ethics (Journal No. 2007/561–1320).

PET scanning protocol

[^{18}F]MH.MZ ($n = 4$) and [^{18}F]altanserin ($n = 2$) were given as intravenous (i.v.) bolus injections, and the pigs were subsequently PET-scanned for 150 min (with [^{18}F]MH.MZ) and 60 min (with [^{18}F]altanserin) in a high-resolution research tomography (HRRT) scanner. Data acquisition began at the time of injection. An average of 215 ± 172 MBq of [^{18}F]MH.MZ (range 69–462 MBq) was injected, the average specific activity (A_s) at the time of injection was 19.8 ± 30.9 GBq/µmol (range 0.90–65.9 GBq/µmol), and the average mass injected was 17.8 ± 15.5 µg (range 3.5–37.8 µg). An average of 588 MBq of [^{18}F]altanserin (632 and 543 MBq) was injected, the average specific activity at the time of injection was 426 GBq/µmol (420 and 431 GBq/µmol) and average injected mass was 0.78 µg (0.84 and 0.70 µg).

For in vivo challenge studies, ketanserin was administered 90 min after [^{18}F]MH.MZ bolus injection in two pigs, 5 mg/kg bolus followed by 3 mg/kg/h infusion for the remaining of the scan. In the in vivo pre-treatment studies, 5 mg/kg ketanserin was administered 30 min before injection of ^{18}F-tracer and 3 mg/kg/h ketanserin infusion was continued throughout the scan.

During the first 30 min of the scanning, radioactivity in whole blood was continuously measured using an ABSS autosampler (Allogg Technology, Mariefred, Sweden) counting coincidences in a lead-shielded detector. Concurrently, blood samples were manually drawn at 2.5, 5, 10, 20, 30, 40, 50, 70, 90, 120, and 150 min and the radioactivity in whole blood and plasma was measured using a well counter (Cobra 5003, Packard Instruments, PerkinElmer, Skovlunde, Denmark) that was cross-calibrated to the HRRT scanner and autosampler.

High performance liquid chromatography (HPLC) analysis of pig plasma and pig brain tissue

[^{18}F]MH.MZ was separated from its radiolabeled metabolite by direct injection of plasma in a column switching HPLC system (Dionex Ultimate 3000 HPLC system consisting of a DGP-3600SD pump and an online Posi-Ram Radio Flow-Through Detector). Whole blood samples were centrifuged (3500 rpm, 7 min) and the supernatant plasma fraction was collected and filtered through a 0.45 µM syringe filter prior to analysis with online radioactive detection, as previously described (Gillings, 2009). We also examined the pig brain for the presence of radioactive metabolites of [^{18}F]MH.MZ: At the end of the scan-

ning session (2.5 h after injection of tracer), the pigs were sacrificed by i.v. injection of pentobarbital and the brains were removed. Within an hour after completion of scanning, brain tissue was homogenized in 0.1 N perchloric acid saturated with sodium-EDTA for 2×30 sec using a polytron. After centrifugation ($3500g$, 7 min), pH of the supernatant adjusted to 10 using a 25% (v/v) ammonia solution, filtered (0.45 µm), and analyzed by radio-HPLC as described for plasma samples.

To determine the fraction of unmetabolized [^{18}F]altanserin in plasma the samples were processed by off-line solid phase extraction followed by HPLC analysis as previously described (Pinborg et al., 2003). The free, non-protein bound fraction of [^{18}F]MH.MZ and [^{18}F]altanserin in pig plasma, f_p, was estimated using an equilibrium dialysis chamber method as previously described (Kornum et al., 2009).

Quantification of PET data

For [^{18}F]MH.MZ, 150-min HRRT list-mode PET data were reconstructed into 58 dynamic frames of increasing length (6×10, 6×20, 6×30, 6×60, 4×120, 14×300, 8×150, 8×300 sec). For [^{18}F]altanserin, 60-min HRRT list-mode PET data were reconstructed into 36 dynamic frames of increasing length (6×10, 6×20, 6×30, 6×60, 4×120, 8×300). Images consisted of 207 planes of 256×256 voxels of $1.22 \times 1.22 \times 1.22$ mm. Summed images of all counts in the time frame 0–150 min ([^{18}F]MH.MZ) or 0–60 min ([^{18}F]altanserin) were reconstructed for each pig and used for co-registration to a standardized MRI-based atlas of the Danish Landrace pig brain, similar to that previously published for the Göttingen minipig (Watanabe et al., 2001), using the software Register, as previously described (Kornum et al., 2009). Each registration was verified by visual inspection before final resampling of the dynamic emission sequence, before the extraction of time-radioactivity curves from cerebral cortex, striatum, and cerebellum using statistically defined volumes of interest obtained in 22 animals (Watanabe et al., 2001). Activity in striatum was averaged over the caudate nucleus and the putamen. Radioactivity in all volume of interests (VOIs) was calculated as the average of radioactive concentration (Bq/mL) in the left and right sides. Outcome measure in the time–activity curves (TAC) was calculated as radioactive concentration in VOI (in kBq/mL) normalized to the injected dose corrected for animal weight (in kBq/kg), yielding standardized uptake values (SUV) in g/mL.

In all pigs, distribution volumes (V_T) for the VOIs were calculated on the basis on the one-tissue compartment (1TC) model. The parent compound fraction was for both [^{18}F]MH.MZ and [^{18}F]altanserin fitted to a biexponential function that was used to correct the radioactive concentration in plasma. The V_T of
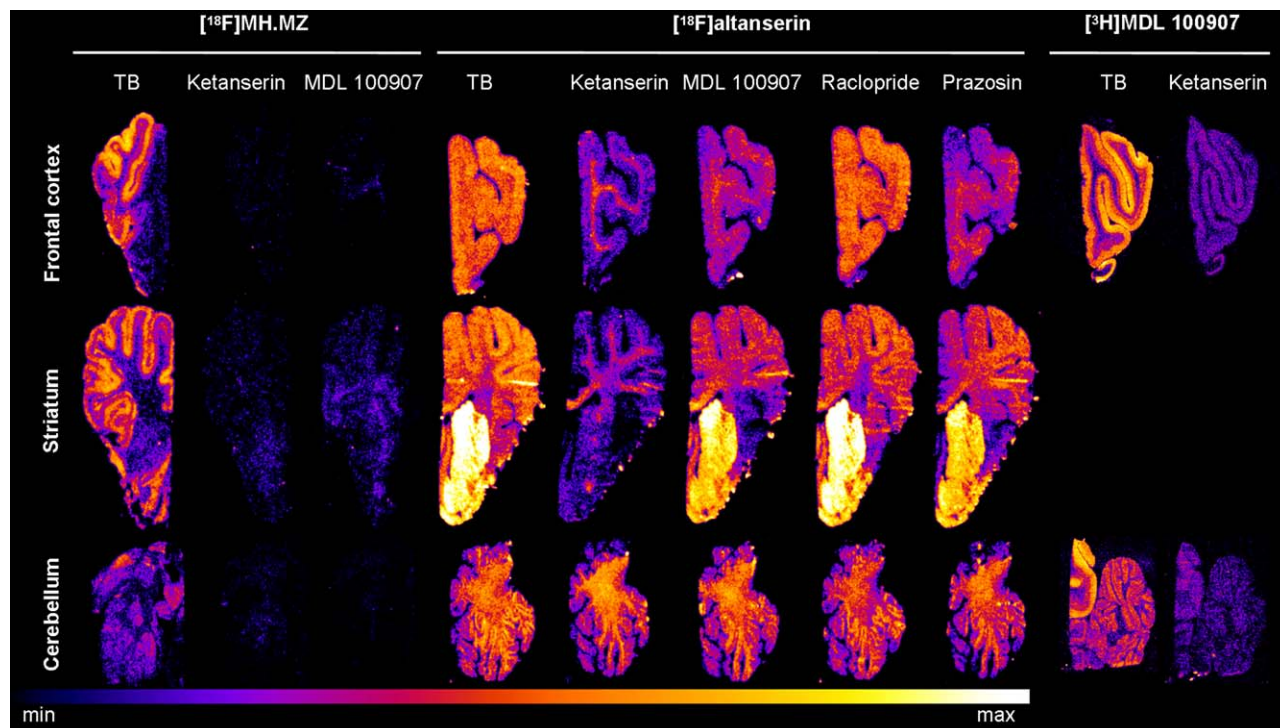
Fig. 1. Autoradiographic images of 20 μm sections of pig brain incubated with 10 nM [^{18}F]MH.MZ, 2.5 nM [^{18}F]altanserin or 2 nM [^{3}H]MDL 100907. Inhibition of [^{18}F]MH.MZ, [^{18}F]altanserin, or [^{3}H]MDL 100907 binding is determined in the presence of 10 μM ketanserin, MDL 100907, raclopride, or prazosin. TB: Total binding.

baseline and pre-treated (ketanserin) conditions was used to determine the non-displaceable distribution volume (V_{ND}) by use of the Lassen plot allowing for calculation of binding potentials (Cunningham et al., 2010). For the Lassen plot analysis, the baseline V_Ts from three pigs were compared with blocked V_Ts from one ketanserin pre-treated pig. Determination of the V_{ND} for [^{18}F]altanserin is done in a similar manner plotting one baseline scan against one ketanserin pre-treated scan.

$$BP_{ND} = \frac{V_T - V_{ND}}{V_{ND}}$$

Modeling was performed on 0–90 min data for [^{18}F]MH.MZ and 0–60 min for [^{18}F]altanserin. All modeling is done with same starting parameters, and standard deviation coefficient variance (COV) was below 15% for macroparameters (K_1 and V_T). Data sets that did not fulfil this criterion were not included in the results. Kinetic modeling was performed with PMOD software (version 3.0; PMOD Technologies, Zürich, Switzerland).

RESULTS
In vitro autoradiography

[^{18}F]MH.MZ and [^{18}F]altanserin distribution in pig brain slices (Fig. 1) was in accordance with the expected 5-HT$_{2A}$ receptor distribution (Ettrup et al.,

2011b). The K_d value of [^{18}F]MH.MZ for 5-HT$_{2A}$ receptors in pig frontal cortex was determined to be 8.4 ± 5.9 nM (Fig. 2B). Ketanserin blocked all specific binding of both [^{18}F]MH.MZ and [^{18}F]altanserin. Significant NSB of [^{18}F]altanserin was observed in the white matter, while NSB was considerably lower for [^{18}F]MH.MZ.

Complete displacement of [^{18}F]MH.MZ binding in the pig brain was found with the 5-HT$_{2A}$ receptor antagonists ketanserin and MDL100907, and some displaceable binding was also observed in the cerebellum. Autoradiography with [^{3}H]MDL 100907 revealed high specific binding in the frontal cortex (29.0 ± 3.24 fmol/mg TE, $n = 4$), but also identified specific binding in the pig cerebellum (14.7 ± 0.6 fmol/mg TE, $n = 4$) (Fig. 1). Thus, the 5-HT$_{2A}$ binding in pig cerebellum constituted around 50% of that in frontal cortex. From the saturation curve of [^{3}H]MDL 100907, a B_{max} of 31 fmol/mg TE in pig frontal cortex was determined (Fig. 2A).

Specific binding of [^{18}F]altanserin was displaceable by ketanserin in all brain regions, whereas the more selective 5-HT$_{2A}$ receptor ligand MDL 100907 did not displace the high binding in striatum. Raclopride as well as prazosin (D$_2$- and α_1-receptor blocking) had only minimal, if any effect on [^{18}F]altanserin binding in any region. In vitro cortex-to-cerebellum ratios for [^{18}F]MH.MZ and [^{18}F]altanserin in the pig brain were 2.95 ± 0.44 ($n = 3$) and 1.51 ± 0.32 ($n = 2$), respectively.
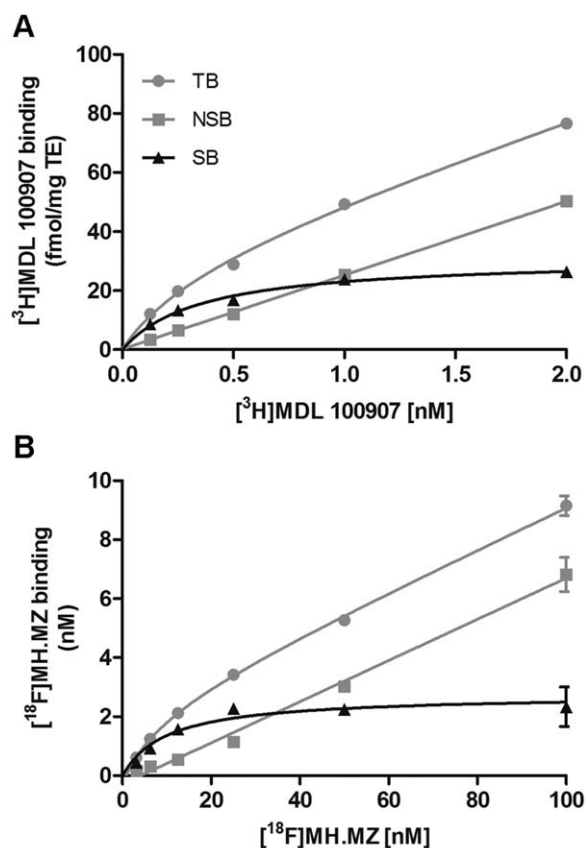
Fig. 2. Saturation plots of [³H]MDL 100907 (**A**) and [¹⁸F]MH.MZ (**B**) showing total (TB), non-specific (NSB), and specific binding (SB) at different concentrations of the respective radiotracer.

In vivo PET imaging

After bolus injection of [¹⁸F]MH.MZ and [¹⁸F]altanserin, there was a rapid uptake of radioactivity in brain tissue and the highest accumulation was observed in cortical regions with lower accumulation in cerebellum (Fig. 3).

Tissue TAC of [¹⁸F]MH.MZ and [¹⁸F]altanserin showed that [¹⁸F]altanserin displayed faster kinetics than [¹⁸F]MH.MZ, whereas limited wash-out of radioactivity of [¹⁸F]MH.MZ was observed in the high-binding cortical region. Thus, [¹⁸F]MH.MZ displayed very slow PET-tracer kinetics in high-binding brain regions (Figs. 3A and 3B).

A challenge experiment with 5 mg/kg (bolus) + 3 mg/kg/h (infusion) ketanserin given 90 min after [¹⁸F]MH.MZ injection resulted in a decrease in cortical binding of [¹⁸F]MH.MZ binding, with an effect that reached pre-treatment levels after 150 min scan time (Fig. 3A).

From the Lassen plot analyses (Fig. 4), the V_{ND} for MH.MZ was computed to 17.8 ± 1.06 mL/cm³ (average based on three plots). The V_{ND} of [¹⁸F]altanserin was 3.14 mL/cm³. Drug occupancy after pre-treatment with ketanserin was on average $72 \pm 13\%$ for [¹⁸F]MH.MZ and 78% for [¹⁸F]altanserin.

The BP_{ND} values for [¹⁸F]MH.MZ were up to five times higher than for [¹⁸F]altanserin (Table I), and a reduction in [¹⁸F]MH.MZ binding by pre-treatment with ketanserin was seen in all regions, whilst a reduction in [¹⁸F]altanserin binding was only observed in cortex. With [¹⁸F]MH.MZ, specific binding was observed in the cerebellum as the BP_{ND} was reduced by 92%.

[¹⁸F]MH.MZ underwent fast metabolism, with 50% parent fraction remaining after 5 min (Fig. 5A) and only polar metabolites were found in plasma (Fig. 5B). Metabolism of [¹⁸F]altanserin was less reproducible and noisy average data is produced despite large injected doses (Fig. 5C). Up to three radiometabolites of [¹⁸F]altanserin could be identified in the HPLC radiochromatograms, all of which had a more lipophilic character (Fig. 5D).

HPLC analysis of pig cortex following injection of [¹⁸F]MH.MZ revealed that the tissue radioactivity was predominantly present as parent compound (Fig. 6B). Only trace amounts of a polar metabolite were detected. In comparison, the pig plasma contained only about 5% parent compound at this time point (150 min) (Fig. 6A). Plasma protein binding in pig blood was determined ($n = 3$) for both tracers using the equilibrium dialysis method. At equilibrium, the free plasma fraction of radioactivity (f_P) was $22.9 \pm 4.6\%$ for [¹⁸F]MH.MZ and $1.0 \pm 0.2\%$ for [¹⁸F]altanserin.

DISCUSSION

The in vitro autoradiography confirmed high binding of both [¹⁸F]MH.MZ and [¹⁸F]altanserin in the pig cerebral cortex in accordance with previous results (Ettrup et al., 2011b). Whereas ketanserin blocked [¹⁸F]MH.MZ binding in the pig frontal cortex completely, some NSB of [¹⁸F]altanserin remained in white matter, which is in contrast to expectations based on the higher lipophilicity of MH.MZ as compared with altanserin (Herth et al., 2009a). Blocking with ketanserin and MDL 100907 led to a large reduction in [¹⁸F]MH.MZ binding in frontal cortex and a moderate reduction in striatum, which is a region with relatively low 5-HT$_{2A}$ receptor density (Ettrup et al., 2011b). In contrast to [¹⁸F]MH.MZ, high [¹⁸F]altanserin binding was observed in the striatum and we suggest that this can be attributed to binding to targets other than the 5-HT$_{2A}$ receptor, since blocking with a structurally similar compound led to a reduction of [¹⁸F]altanserin binding of approximately 50% in striatum, whereas blocking with the more 5-HT$_{2A}$ receptor selective ligand, MDL 100907, only led to a minor reduction in binding. Based on the selectivity profile of [¹⁸F]altanserin, we attempted blocking of D$_2$ and α_1 receptors, but this only lead to minor reductions in binding, suggesting that the striatal binding cannot alone be attributed to D$_2$ or α_1-receptors. Contrary to our expectations,
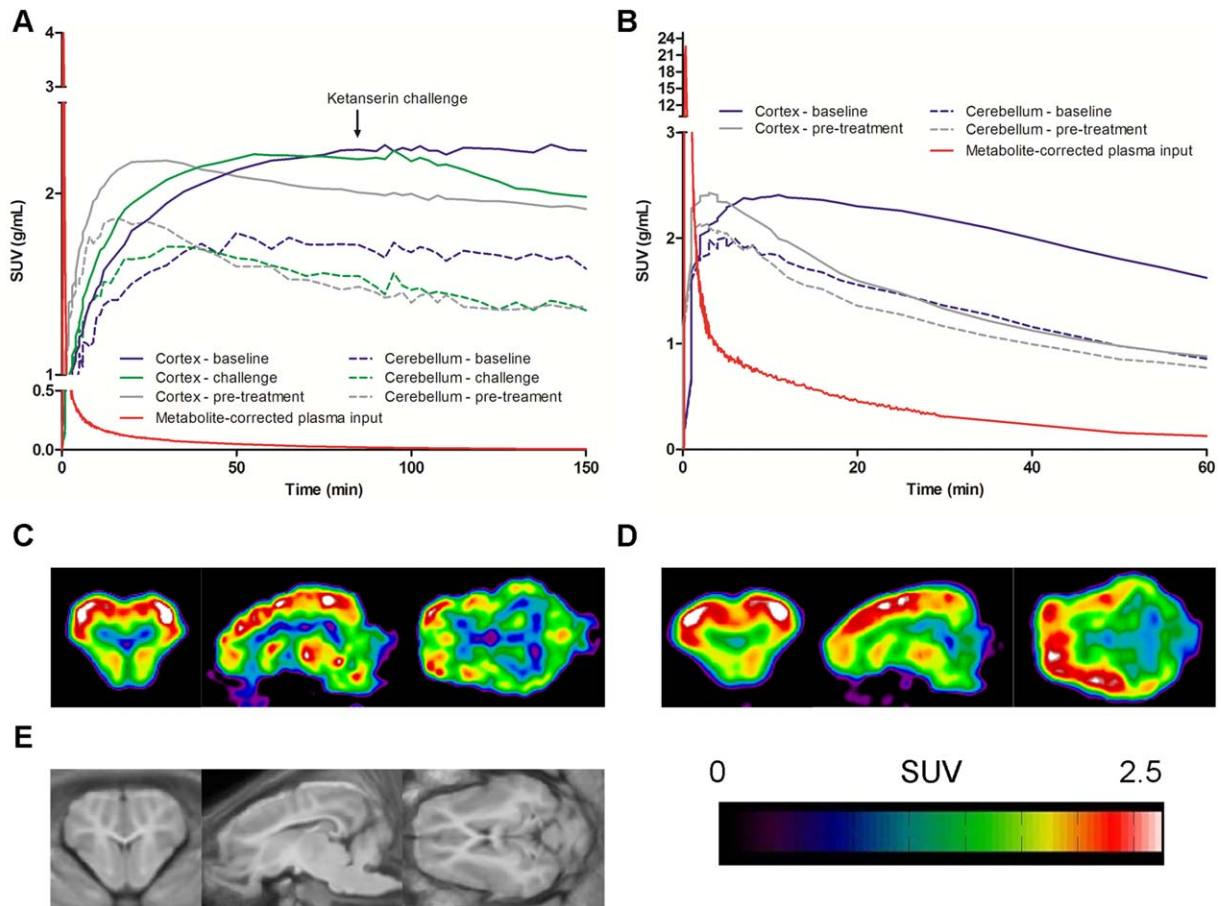
Fig. 3. TACs and metabolism-corrected input curves for [^{18}F]MH.MZ (**A**) and [^{18}F]altanserin (**B**). Data are presented as SUV. [^{18}F]MH.MZ: Baseline ($n = 1$), challenge ($n = 2$), pre-treatment ($n = 1$). [^{18}F]Altanserin: Baseline ($n = 1$), pre-treatment ($n = 1$). PET images of the mean decay-corrected activity concentration after bolus injection of [^{18}F]MH.MZ (**C**) and [^{18}F]altanserin (**D**), summed between 0 and 60 min after injection of the radioligands. (**E**) MRI-based atlas of the pig brain.

since other species are almost devoid of 5-HT$_{2A}$ receptors in cerebellum (Hall et al., 2000; Lopez-Gimenez et al., 1997), we found significant binding both with [^{18}F]altanserin and [^{18}F]MH.MZ in the pig cerebellum; about 50% of the [^{18}F]MH.MZ binding was displaceable with MDL 100907. Our subsequent [^{3}H]MDL 100907 autoradiography studies confirmed the presence of significant 5-HT$_{2A}$ receptor binding in pig cerebellum, reaching levels of specific binding up to 50% of that in frontal cortex. To support the relatively high abundance of 5-HT$_{2A}$ receptors in pig cerebellum, cortex-to-cerebellum ratios on pig sections for [^{18}F]MH.MZ and [^{18}F]altanserin were compared with those determined in rat, where the cerebellum is devoid of 5-HT$_{2A}$ receptors (Biver et al., 1997; Debus et al., 2010). As expected, lower cortex-to-cerebellum ratios were detected in the pig brain. Based on our autoradiography studies, we conclude that the pig cerebellum is not a valid reference region and therefore we refrained from using reference tissue models to analyse the in vivo data.
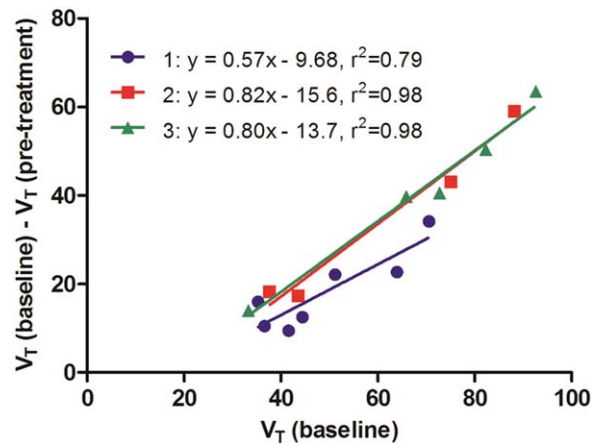

Fig. 4. Lassen plot of [^{18}F]MH.MZ distribution volumes (V_T) at baseline and in pre-treated scan. V_Ts from the one pre-treated pig are subtracted from the V_Ts from each baseline experiments. Fraction of 5-HT$_{2A}$ receptor occupancy is measured as the slope of the regression line, and [^{18}F]MH.MZ non-displaceble binding (V_{ND}) is the intercept at y-axis. Goodness of fit (R^2) also listed for each plot.

TABLE I. BP_{ND} values for [^{18}F]MH.MZ and [^{18}F]altanserin at baseline and ketanserin pre-treatment conditions determined by arterial input modeling with one-tissue compartment model and determination of V_{ND} by Lassen plot analysis

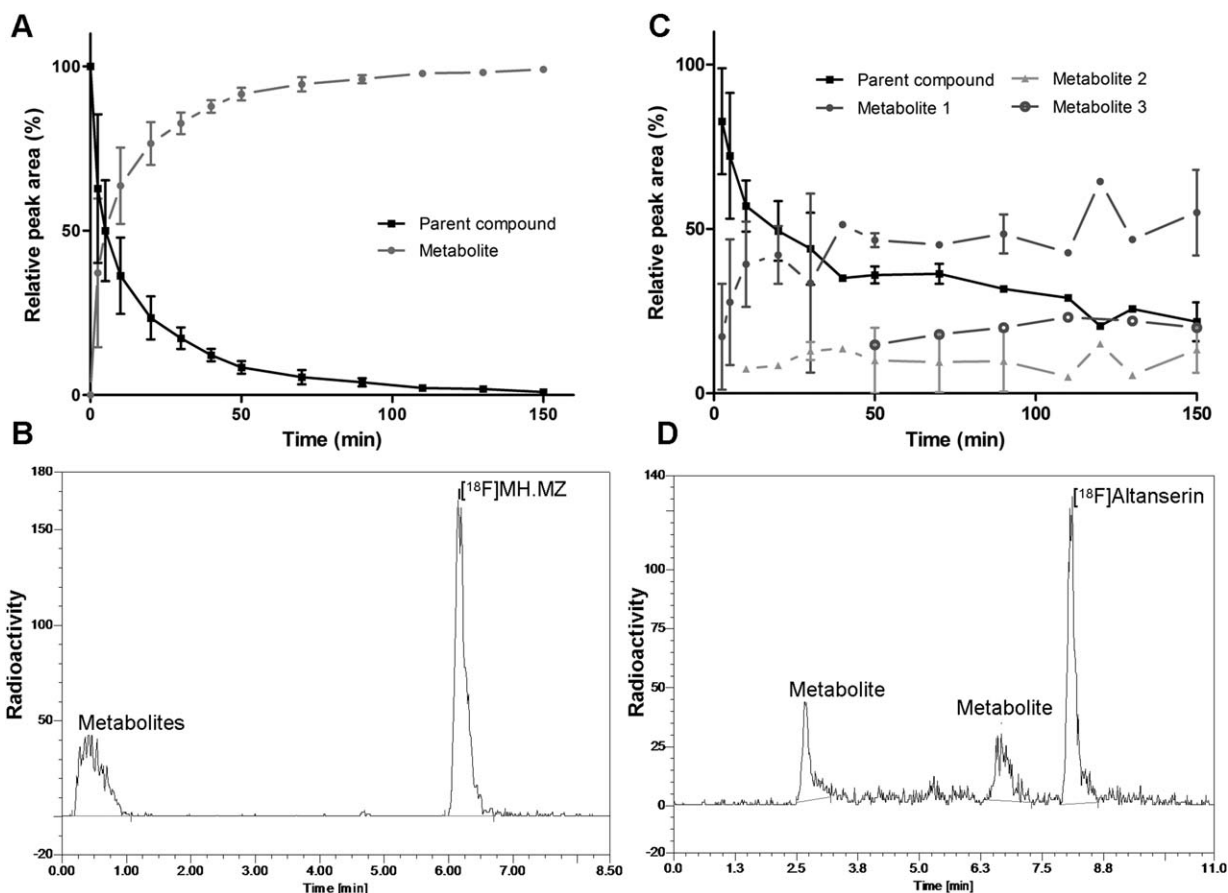| | [^{18}F]MH.MZ | | | [^{18}F]altanserin | | |
	Baseline ($n = 3$)	Ketanserin ($n = 1$)	% reduction	Baseline ($n = 1$)	Ketanserin ($n = 1$)	% reduction
Cortex	3.3 ± 1.3	0.63	81	0.68	0.15	78
Striatum	2.8	1.2	58	0.59	0.60	0
Cerebellum	1.0 ± 0.12	0.08	92	ND	ND	ND

ND: not determined.

Fig. 5. (**A**) HPLC analysis of the radioactive metabolites in pig plasma after i.v. injection of [^{18}F]MH.MZ ($n = 3$). (**B**) HPLC radiochromatogram of pig plasma 5 min post-injection of [^{18}F]MH.MZ. (**C**) HPLC analysis of the radioactive metabolites in pig plasma after i.v. injection of [^{18}F]altanserin ($n = 2$). (**D**) HPLC radiochromatogram of pig plasma 50 min after injection of [^{18}F]altanserin. For (A) and (C): Parent compound (black) and metabolites (shades of grey) are given as percent of total radioactivity (average $\pm$ S.D).

Comparing with previously published data, it is evident that there are species differences with regard to striatal and cerebellum binding, since low binding potentials are shown in these regions with [^{18}F]altanserin in humans (Adams et al., 2004; Price et al., 2001b). Low binding in the cerebellum but high binding in striatum of [^{18}F]altanserin is shown in rats with in vitro autoradiography (Herth et al., 2008). [^{18}F]MH.MZ showed no specific binding in the cerebellum in rats (in vitro autoradiography and microPET studies), but did show some striatal binding in rat autoradiography (Herth et al., 2009b), in accordance with the in vivo binding in pigs.

After intravenous injection, [^{18}F]MH.MZ underwent a fast metabolism and only polar metabolites were found in plasma, in accordance with findings in the rat (Debus et al., 2010; Herth et al., 2008, 2009a,b). We consider the most likely metabolic pathway of MH.MZ to be through cleavage of the fluoroethoxy group, similar to the metabolism of MDL 100907 (Scott and Heath, 1998). The time course of metabolism was quite reproducible between pigs, which shows promise for a population-based metabolite correction of the arterial input function, as this input function is required in the absence of a reference region. As expected, radiolabeled polar
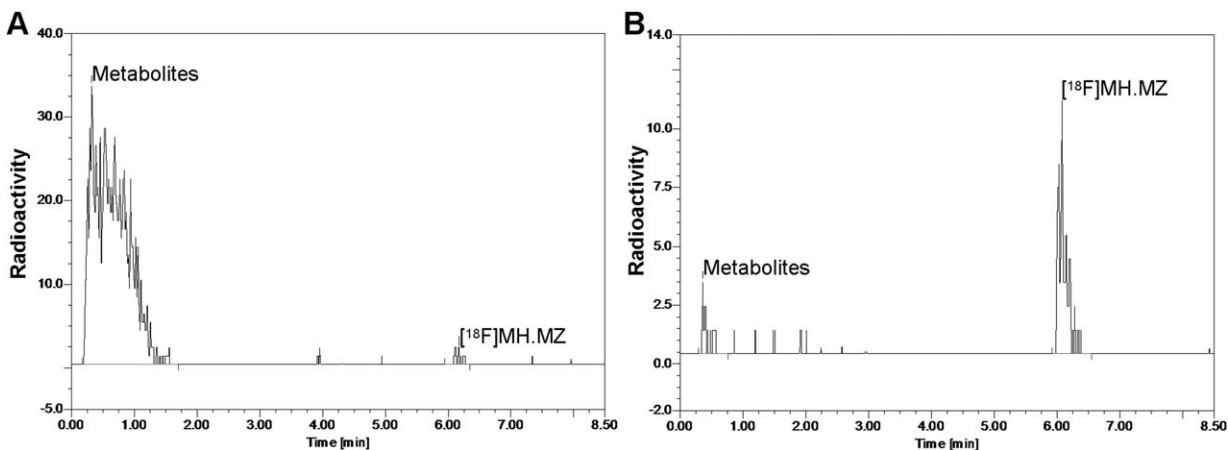
Fig. 6. HPLC radiochromatograms of plasma (**A**) and frontal cortex extract (**B**) 150 min after injection of [^{18}F]MH.MZ.

metabolites were not found in frontal cortex brain homogenate confirming that they do not cross the BBB. In line with findings in humans, non-human primates, and rats, lipophilic metabolites of [^{18}F]altanserin were generated, and we speculate that these metabolites can cross the BBB and interfere with the PET signal (Price et al., 2001a; Tan et al., 1999). The metabolic rates of [^{18}F]altanserin showed high inter-individual variation in pigs, complicating population-based metabolic rate approaches for modeling purposes. The f_P for [^{18}F]MH.MZ was substantially higher than for [^{18}F]altanserin ($23 \pm 5\%$ versus $1 \pm 0.2\%$) which means the measurement accuracy is higher for [^{18}F]MH.MZ and this is required for computation of individual BP$_F$ values.

Kinetic modeling with arterial input is considered the gold standard for quantification of radioligand binding (Innis et al., 2007). The 1TC model was chosen to determine the total distribution volumes (V_T) because of the simplicity of the model and because it more often resulted in successful fitting. The slow kinetics of [^{18}F]MH.MZ presented a challenge for the kinetic modeling: of seven VOIs analyzed in three pigs, six fits failed to converge, whereas 15 fulfilled the criteria set, as described in the experimental section. Kinetic modeling with 1TC model computed the highest V_T in cortex and lowest in cerebellum for both [^{18}F]MH.MZ and [^{18}F]altanserin, in line with previously published data (Debus et al., 2010; Ettrup et al., 2011a; Herth et al., 2008, 2009a,b). By use of V_{ND} extrapolated from the Lassen plot, the resulting BP$_{ND}$ values were 3.3 for [^{18}F]MH.MZ and 0.68 for [^{18}F]altanserin in cortex. Using the enantiomer, (R)-[^{18}F]MH.MZ rather than the racemate would probably increase the BP$_{ND}$ (Debus et al., 2010). (R)-MH.MZ has an in vitro 5-HT$_{2A}$ receptor affinity (0.72 nM) that is very similar to that of [^{18}F]altanserin (0.12 nM). Although (S)-MH.MZ has a non-negligible

affinity for the 5-HT$_{2A}$ receptor, based on the affinities of MH.MZ and (R)-MH.MZ (9.02 nM versus 0.72 nM, respectively), we consider it unlikely that (S)-MH.MZ alone can be ascribed to the slow kinetics seen with [^{18}F]MH.MZ, as (R)-[^{18}F]MH.MZ displayed a similar kinetic profile to [^{18}F]MH.MZ when evaluated in rats (Debus et al., 2010). We speculate that the lower BP$_{ND}$ of [^{18}F]altanserin is caused by BBB-crossing metabolites. To accommodate the lipophilic metabolites of [^{18}F]altanserin in the kinetic modeling, a dual input model is required whereas a single-input compartment model, as used in this study, will underestimate binding potentials by up to 2.5 times (Price et al., 2001b). Although we did not ascertain the BBB passage of metabolites into the pig brain, [^{18}F]altanserin metabolites are known to cross the BBB in other species (Price et al., 2001a) and this would contribute to a larger V_{ND}. A potential limitation of the design was that the occupancy plot was not based on rescan data from the same pig and this might have induced some noise in the determination of V_{ND}. Futhermore, lipophilic metabolites in the pig brain could influence the V_T and V_{ND} values of [^{18}F]altanserin, which contributes to noise on the V_{ND} measures.

The slow kinetic behaviour of [^{18}F]MH.MZ suggests that this tracer has high in vivo affinity for the 5-HT$_{2A}$ receptor, however, we cannot be sure that the in vivo affinity is the same in pigs and humans, therefore a study is warranted to establish whether the same slow kinetics is observed in humans. Kinetics are often seen slower in humans than in animals, and since B_{max} of 5-HT$_{2A}$ receptors in the cortex of humans is more than twice as high as in pigs [$\sim$70 fmol/mg (Hall et al., 2000) versus 31 fmol/mg], slow kinetics of [^{18}F]MH.MZ would be expected. In regions where B_{max} is lower, the kinetics of the tracer is expected to be faster, because occupancy is

reached faster. In humans, MH.MZ could be used to quantify binding in e.g. the striatum, where B_{max} is $\sim$20 fmol/mg, thus lower than B_{max} in pig cortex. In humans, reference tissue modeling will be applicable and slow kinetics will therefore be less problematic. Slow kinetics is known to be problematic for compartmental modeling as used in this study, but because a reference region is not available in the pig our data could not be thus analyzed.

Pre-treatment with ketanserin reduced BP_{ND} of both [18F]MH.MZ and [18F]altanserin to a similar degree in the pig cerebral cortex, whereas in cerebellum we only observed a reduction in [18F]MH.MZ binding and not in [18F]altanserin binding. This difference is most likely due to the low specific versus NSB of [18F]altanserin in these regions, making [18F]altanserin less sensitive to detection of changes in low-density regions. Based on these data, we conclude that in the pig brain [18F]MH.MZ is better suited to the determination of 5-HT$_{2A}$ binding in regions outside the cortex than [18F]altanserin.

Interestingly, in vivo both radiotracers had a high striatal binding with BP_{ND}s $\sim$15% lower than BP_{ND}s in the pig cortex. In vitro data also showed high striatal binding for [18F]altanserin, but only minor binding in the striatum for [18F]MH.MZ. This difference between in vitro and in vivo data may be explained by autoradiography only assessing binding in one cross-section of the striatum, whereas PET detects the activity in the entire region. In addition, the PET experiments involved use of tracer doses, whereas concentrations around K_d were applied in vitro. That is, the autoradiography signal in striatum could be influenced by binding to receptors to which the tracer has only low affinity. This could possibly explain the discrepancy between the relatively high in vitro binding of [18F]altanserin in striatum compared with the observed in vivo binding.

CONCLUSION

Both [18F]MH.MZ and [18F]altanserin successfully imaged 5-HT$_{2A}$ receptors in pig brain both in vitro with autoradiography and in vivo with PET scanning.

Since in vitro autoradiography with [3H]MDL 100907 showed specific 5-HT$_{2A}$ receptor binding in the pig cerebellum, this region cannot serve as a valid reference region for quantification of 5-HT$_{2A}$ receptor binding in pigs via modeling approaches.

In areas with high 5-HT$_{2A}$ receptor density, [18F]MH.MZ displayed very slow kinetics which complicated modeling. [18F]altanserin, in contrast has faster kinetics, but has lower specific to NSB and a problematic metabolic profile compared with [18F]MH.MZ, thus also complicating modeling and quantification of 5-HT$_{2A}$ receptors. We speculate that [18F]MH.MZ can be used for quantification of 5-HT$_{2A}$ receptors in humans in brain regions with low 5-HT$_{2A}$ receptor density and where reference tissue modeling will also the ease the quantification. Studies are warranted to assess the suitability of [18F]MH.MZ or its enantiomer for clinical use.

REFERENCES

Adams KH, Pinborg LH, Svarer C, Hasselbalch SG, Holm S, Haugbol S, Madsen K, Frokjaer V, Martiny L, Paulson OB, Knudsen GM. 2004. A database of [(18)F]-altanserin binding to 5-HT(2A) receptors in normal volunteers: Normative data and relationship to physiological and demographic variables. Neuroimage 21:1105–1113.

Biver F, Lotstra F, Monclus M, Dethy S, Damhaut P, Wikler D, Luxen A, Goldman S. 1997. In vivo binding of [18F]altanserin to rat brain 5HT2 receptors: A film and electronic autoradiographic study. Nucl Med Biol 24:357–360.

Cunningham VJ, Rabiner EA, Slifstein M, Laruelle M, Gunn RN. 2010. Measuring drug occupancy in the absence of a reference region: The Lassen plot re-visited. J Cereb Blood Flow Metab 30:46–50.

Debus F, Herth MM, Piel M, Buchholz HG, Bausbacher N, Kramer V, Luddens H, Rosch F. 2010. 18F-labeling and evaluation of novel MDL 100907 derivatives as potential 5-HT2A antagonists for molecular imaging. Nucl Med Biol 37:487–495.

Ettrup A, Palner M, Gillings N, Santini MA, Hansen M, Kornum BR, Rasmussen LK, Nagren K, Madsen J, Begtrup M, Knudsen GM. 2010. Radiosynthesis and evaluation of 11C-CIMBI-5 as a 5-HT2A receptor agonist radioligand for PET. J Nucl Med 51:1763–1770.

Ettrup A, Hansen M, Santini MA, Paine J, Gillings N, Palner M, Lehel S, Herth MM, Madsen J, Kristensen J, Begtrup M, Knudsen GM. 2011a. Radiosynthesis and in vivo evaluation of a series of substituted 11C-phenethylamines as 5-HT (2A) agonist PET tracers. Eur J Nucl Med Mol Imaging 38:681–693.

Ettrup A, Kornum BR, Weikop P, Knudsen GM. 2011b. An approach for serotonin depletion in pigs: Effects on serotonin receptor binding. Synapse 65:136–145.

Gillings N. 2009. A restricted access material for rapid analysis of [(11)C]-labeled radiopharmaceuticals and their metabolites in plasma. Nucl Med Biol 36:961–965.

Hall H, Farde L, Halldin C, Lundkvist C, Sedvall G. 2000. Autoradiographic localization of 5-HT(2A) receptors in the human brain using [(3)H]M100907 and [(11)C]M100907. Synapse 38:421–431.

Hasselbalch SG, Madsen K, Svarer C, Pinborg LH, Holm S, Paulson OB, Waldemar G, Knudsen GM. 2008. Reduced 5-HT2A receptor binding in patients with mild cognitive impairment. Neurobiol Aging 29:1830–1838.

Herth MM, Debus F, Piel M, Palner M, Knudsen GM, Luddens H, Rosch F. 2008. Total synthesis and evaluation of [18F]MHMZ. Bioorg Med Chem Lett 18:1515–1519.

Herth MM, Kramer V, Piel M, Palner M, Riss PJ, Knudsen GM, Rosch F. 2009a. Synthesis and in vitro affinities of various MDL 100907 derivatives as potential 18F-radioligands for 5-HT2A receptor imaging with PET. Bioorg Med Chem 17:2989–3002.

Herth MM, Piel M, Debus F, Schmitt U, Luddens H, Rosch F. 2009b. Preliminary in vivo and ex vivo evaluation of the 5-HT2A imaging probe [(18)F]MH.MZ. Nucl Med Biol 36:447–454.

Herth MM, Kramer V, Gillings N, Rösch F, Knudsen GM. 2012. Direct radiofluorination of [18F]MH.MZ for 5-HT2A receptor molecular imaging with PET. J Label Comp Rad 55:354–358.

Innis RB, Cunningham VJ, Delforge J, Fujita M, Gjedde A, Gunn RN, Holden J, Houle S, Huang SC, Ichise M, Iida H, Ito H, Kimura Y, Koeppe RA, Knudsen GM, Knuuti J, Lammertsma AA,

Laruelle M, Logan J, Maguire RP, Mintun MA, Morris ED, Parsey R, Price JC, Slifstein M, Sossi V, Suhara T, Votaw JR, Wong DF, Carson RE. 2007. Consensus nomenclature for in vivo imaging of reversibly binding radioligands. J Cereb Blood Flow Metab 27:1533–1539.

Kehne JH, Baron BM, Carr AA, Chaney SF, Elands J, Feldman DJ, Frank RA, van Giersbergen PL, McCloskey TC, Johnson MP, McCarty DR, Poirot M, Senyah Y, Siegel BW, Widmaier C. 1996. Preclinical characterization of the potential of the putative atypical antipsychotic MDL 100,907 as a potent 5-HT2A antagonist with a favorable CNS safety profile. J Pharmacol Exp Ther 277:968–981.

Kornum BR, Lind NM, Gillings N, Marner L, Andersen F, Knudsen GM. 2009. Evaluation of the novel 5-HT4 receptor PET ligand [11C]SB207145 in the Gottingen minipig. J Cereb Blood Flow Metab 29:186–196.

Leysen JE. 1989. Use of 5-HT receptor agonists and antagonists for the characterization of their respective receptor sites. In: Boulton A, Baker G, Juorio A, editors. Drugs as tools in neurotransmitter research: Humana Press, New York, USA. p 299–350.

Lopez-Gimenez JF, Mengod G, Palacios JM, Vilaro MT. 1997. Selective visualization of rat brain 5-HT2A receptors by autoradiography with [3H]MDL 100,907. Naunyn Schmiedebergs Arch Pharmacol 356:446–454.

McKeith IG, Marshall EF, Ferrier IN, Armstrong MM, Kennedy WN, Perry RH, Perry EK, Eccleston D. 1987. 5-HT receptor binding in post-mortem brain from patients with affective disorder. J Affect Disord 13:67–74.

Naughton M, Mulrooney JB, Leonard BE. 2000. A review of the role of serotonin receptors in psychiatric disorders. Hum Psychopharmacol Clin Exp 15:397–415.

Paterson LM, Kornum BR, Nutt DJ, Pike VW, Knudsen GM. 2011. 5-HT radioligands for human brain imaging with PET and SPECT. Med Res Rev 2013;33:54–111.

Pinborg LH, Adams KH, Svarer C, Holm S, Hasselbalch SG, Haugbol S, Madsen J, Knudsen GM. 2003. Quantification of 5-HT2A receptors in the human brain using [18F]altanserin-PET and the bolus/infusion approach. J Cereb Blood Flow Metab 23:985–996.

Price JC, Lopresti BJ, Mason NS, Holt DP, Huang Y, Mathis CA. 2001a. Analyses of [(18)F] altanserin bolus injection PET data. I: Consideration of radiolabeled metabolites in baboons. Synapse 41:1–10.

Price JC, Lopresti BJ, Meltzer CC, Smith GS, Mason NS, Huang Y, Holt DP, Gunn RN, Mathis CA. 2001b. Analyses of [(18)F]altanserin bolus injection PET data. II: Consideration of radiolabeled metabolites in humans. Synapse 41:11–21.

Rasmussen H, Erritzoe D, Andersen R, Ebdrup BH, Aggernaes B, Oranje B, Kalbitzer J, Madsen J, Pinborg LH, Baare W, Svarer C, Lublin H, Knudsen GM, Glenthoj B. 2010. Decreased frontal serotonin2A receptor binding in antipsychotic-naive patients with first-episode schizophrenia. Arch Gen Psychiatry 67:9–16.

Scott DO, Heath TG. 1998. Investigation of the CNS penetration of a potent 5-HT2a receptor antagonist (MDL 100,907) and an active metabolite (MDL 105,725) using in vivo microdialysis sampling in the rat. J Pharm Biomed Anal 17:17–25.

Tan P-Z, Baldwin RM, Fu T, Charney DS, Innis RB. 1999. Rapid synthesis of F-18 and H-2 dual-labeled altanserin, a metabolically resistant PET ligand for 5-HT2a receptors. J Label Comp Rad 42:457–467.

Watabe H, Channing MA, Der MG, Adams HR, Jagoda E, Herscovitch P, Eckelman WC, Carson RE. 2000. Kinetic analysis of the 5-HT2A ligand [11C]MDL 100,907. J Cereb Blood Flow Metab 20:899–909.

Watanabe H, Andersen F, Simonsen CZ, Evans SM, Gjedde A, Cumming P. 2001. MR-based statistical atlas of the Gottingen minipig brain. Neuroimage 14:1089–1096.

Paper II

Hansen HD, Lacivita E, Di Pilato P, Herth MM, Lehel S, Ettrup A, Andersen VL, Dyssegaard A, De Giorgio P, Perrone R, Berardi F, Colabufo NA, Niso M, Knudsen GM, and Leopoldo M.

Synthesis, radiolabeling and in vivo evaluation of [^{11}C](R)-1-[4-[2-(4-methoxyphenyl)phenyl]piperazin-1-yl]-3-(2-pyrazinyloxy)-2-propanol, a potential PET radioligand for the 5-HT$_7$ receptor.

Manuscript

Synthesis, Radiolabeling and In Vivo Evaluation of [11C](*R*)-1-[4-[2-(4-methoxyphenyl)phenyl]piperazin-1-yl]-3-(2-pyrazinyloxy)-2-propanol, a Potential PET Radioligand for the 5-HT7 Receptor.

Hanne D. Hansen[a,b], Enza Lacivita[c], Pantaleo Di Pilato[c], Matthias M. Herth[a,b,d], Szabolcs Lehel[d], Anders Ettrup[a,b], Valdemar L. Andersen[a,b,d], Agnete Dyssegaard[a,b], Paola De Giorgio[c], Roberto Perrone[c], Francesco Berardi[c], Nicola Antonio Colabufo[c], Niso Mauro[c], Gitte M. Knudsen[a,b], and Marcello Leopoldo[c]

a) *Center for Integrated Molecular Brain Imaging, Rigshospitalet, Blegdamsvej 9, 2100 Copenhagen, Denmark*

b) *Neurobiology Research Unit, Rigshospitalet and University of Copenhagen, Blegdamsvej 9, 2100 Copenhagen, Denmark*

c) *Dipartimento di Farmacia – Scienze del Farmaco, Università degli Studi di Bari A. Moro, via Orabona, 4, 70125 Bari, Italy*

d) *PET and Cyclotron Unit, Rigshospitalet, Blegdamsvej 9, 2100 Copenhagen, Denmark*

CORRESPONDING AUTHOR:

Gitte M. Knudsen

Center for Integrated Molecular Brain Imaging

Copenhagen University Hospital, Rigshospitalet

Blegdamsvej 9

DK-2100 Copenhagen, Denmark

Phone: (+45) 3545 6720   Fax: (+45) 3545 6713

Email: gmk@nru.dk

ABSTRACT

In the search for a novel serotonin 7 (5-HT$_7$) receptor PET radioligand we synthesized and evaluated a new series of biphenylpiperazine derivatives *in vitro*. Among the studied compounds, (*R*)-1-[4-[2-(4-methoxyphenyl)phenyl]piperazin-1-yl]-3-(2-pyrazinyloxy)-2-propanol ((*R*)-**16**), showed the best combination of affinity, selectivity, and lipophilicity, and was thus chosen for carbon-11 labelling and evaluation in pigs. After intravenous injection, [^{11}C](*R*)-**16** entered the pig brain and displayed reversible tracer kinetics. Pretreatment with the 5-HT$_7$ receptor selective antagonist SB-269970 (**1**) slightly decreased the binding of [^{11}C](*R*)-**16**, suggesting that this radioligand has limited potential for imaging the brain 5-HT$_7$ receptor *in vivo* but it may serve as a lead compound for novel 5-HT$_7$ receptor PET radioligands.

INTRODUCTION

The 5-HT$_7$ subtype is the most recently discovered receptor in the serotonin (5-HT) receptor family. It was identified in 1993 through a homology cloning strategy and has been cloned from several species including humans[1-3]. Since its identification, the 5-HT$_7$ receptor has been the subject of intense research efforts driven by the accumulating evidence suggesting the involvement of the 5-HT$_7$ receptor in both physiological processes and in several brain disorders such as depression and schizophrenia[4, 5]. Several atypical anti-psychotics have high affinity for the 5-HT$_7$ receptor[6], and they also have antidepressant effects that may be mediated through the 5-HT$_7$ receptor[7-9]. The receptor's involvement in mood disorders and other psychiatric and neurodevelopmental disorders is still a subject to intense research[10, 11] and pharmacological and genetic tools such as the 5-HT$_7$ selective antagonist **1** (SB-269970, Figure 1) and 5-HT$_7$ receptor knock-out mice[12-16] are important tools for elucidating the receptor's functional role.

In vivo studies of cerebral 5-HT$_7$ receptor binding would greatly improve the understanding of its role in CNS disorders. Especially, the *in vivo* molecular imaging technique, positron emission tomography (PET), allows for the quantification of neuroreceptor binding *in vivo* and to study drug-neuroreceptor interactions[17]. Therefore, the availability of an appropriate 5-HT$_7$ receptor PET radioligand would be of particular interest.

The literature presents some examples of 5-HT$_7$ receptor PET radioligands (Figure 1), however most of them display questionable or no specific binding to the receptor. No specific binding was observed for [^{11}C]1-methyl-2a-[4-(4,5,6,7-tetrahydrothieno[3,2-*c*]pyridine-5-yl)butyl]-2*a*,3,4,5-tetrahydro-1H-benz[*cd*]indole-2-one (**2**, [^{11}C]DR4446)[18] and [^{11}C]-2-(2',6'-dimethoxy-[1,1'-biphenyl]-3-yl)-*N*,*N*-dimethylethanamine (**3**, [^{11}C]Cimbi-806)[19]. Recently, **1** has been used as template for developing ^{18}F-labeled radioligands, however 1-(2-{(2R)-1-[(2-fluorophenyl)sulfonyl]pyrrolidin-2-yl}ethyl)-4-methylpiperidine (**4**, [^{18}F]2FP3) had a questionable specific binding component and with the lack of an arterial input function no quantification of the binding was attempted[20]. Very recently, two compounds with an oxindole backbone were evaluated in pigs[21]. Of the two compounds evaluated, 3-{4-[4-(3-methoxyphenyl)piperazine-1-yl]butyl}-1,3-dihydro-2H-indol-2-one (**5**, [^{11}C]Cimbi-717) had the highest uptake, favourable tracer kinetics, and dose-dependent occupancy decline in cerebral binding upon receptor blockade. [^{11}C]1-(4-Methoxybiphenyl-2-yl)piperazine (**6**, [^{11}C]PM20) is another recently developed 5-HT$_7$ radioligand, that originated from structure-activity relationship studies on 1-arylpiperazine derivatives carried out by the research group at the University of Bari[22-25]. [^{11}C]**6** showed accumulation in 5-HT$_7$

receptor regions in autoradiography studies. However, subsequent studies in monkey brain displayed homogenous binding in the brain that could be attributed to high degree of non-specific binding[26].

In the search of a lead compound for the development of a PET radioligand for the visualization of cerebral 5-HT$_7$ receptors, we screened a series of 1-arylpiperazine derivatives previously prepared in our laboratory. Important for the selection of an appropriate radioligand candidate, is the a high selectivity for the 5-HT$_7$ receptor since 5-HT$_{1A}$ and 5-HT$_7$ receptors largely share their cerebral distribution[27]. We identified compound **7** (Table 1), which showed 5-HT$_7$ affinity value in the nanomolar range (K_i= 1.31 nM) along with a 100-fold selectivity over 5-HT$_{1A}$ receptors. While the pharmacodynamic profile of **7** was promising, its calculated lipophilicity (clogD$_{7.4}$= 5.30) was well above the optimal range for high BBB permeation and low non-specific binding (2.0 < logP < 3.5)[28,29]. Moreover, **7** did not present a functional group that could allow the insertion of a positron emitter isotope in the molecule. Therefore, we designed a set of analogues of **7** possessing the desired lipophilicity and a functional group for radiolabeling with carbon-11.

Here, we describe the synthesis and *in vitro* characterization of a series of 5-HT$_7$ receptor ligands rationally designed specifically for use as a PET radiotracer starting from our lead compound **7** (Table 1). We selected (*R*)-**16** as the most promising candidate for carbon-11 radiolabeling and *in vivo* evaluation in pigs.

RESULTS AND DISCUSSION

Chemistry

The preparation of the target compounds required several synthetic routes depicted in Schemes 1-4. The final compounds required 1-(2-biphenyl)piperazine[20], 1-[2-(4-methoxyphenyl)phenyl]piperazine[20], and 1-bipyridylpiperazines **20-22** and **27-29** were prepared according to Schemes 1 and 2. Commercially available pinacolate esters **17** were coupled with 2-bromopyridine by Suzuki cross-coupling reaction under microwave irradiation to give *N*-Boc protected derivative **18** which was subsequently deprotected with trifluoroacetic acid to yield the piperazine **20**. Piperazines **21** and **22** were prepared from 1-(3-bromo-2-pyridyl)piperazine (**19**)[30] and 3- or 4-pyridineboronic acid, respectively, by Suzuki cross-coupling (Scheme 1). The preparation of 1-[(pyridyl)-3-pyridyl]piperazines is depicted in Scheme 2. Piperazine **27** was prepared by condensing 3-amino-2,2'-bipyridile[31] (**23**) with bis-(2-chloroethyl)amine. Synthesis of piperazines **28** and **29** started from the key intermediate *t*-butyl 4-(2-chloro-3-pyridyl)piperazine-1-carboxylate[32] (**24**), which was cross-coupled with 3- or 4-pyridineboronic acid to afford the *N*-Boc protected derivatives **25** and **26**, respectively. These were deprotected with trifluoroacetic acid to afford the desired piperazines **28** and **29**.

The synthesis of racemic final compounds is depicted in Scheme 3. Oxiranes **33** and **34** were prepared by alkylation of phenol or 4-methoxyphenol, respectively, with epichloridin according to literature methods[33, 34], whereas **35-37** were synthetized from arylchlorides **30-32** that were condensed with glycydol in presence of NaH. The target compounds **7-16** were obtained by reacting the appropriate 1-arylpiperazine with oxiranes **33-37**.

Enantiomers (*R*)- and (*S*)-**13**, (*R*) and (*S*)-**16** were prepared according to Scheme 4. 4-Methoxyphenol was treated with NaH to form the corresponding sodium salt, which in turn reacted with the commercially available (*R*)- or (*S*)-glycidyl nosilate to afford oxiranes (*R*)-**34** and (*S*)-**34**, respectively. Ring opening of the latters by piperazine **29** gave compounds (*R*)-**13** and (*S*)-**13**. In a similar manner, 2-chloropyrazine reacted with (*R*)- or (*S*)-glycidol in presence of NaH to give the epoxides (*S*)-**37** and (*R*)-**37**, respectively. These compounds reacted with 1-[2-(4-methoxyphenyl)phenyl]piperazine to afford final compounds (*S*)-**16** and (*R*)-**16**.

Structure-Activity Relationships for 5-HT₇ Receptor

The insertion of a functional group amenable for radiolabeling on the scaffold of compound **7** was accomplished by placing a methoxy group on the phenoxy ring, because previous SAR studies on

1-arylpiperazine-based 5-HT$_7$ receptor ligands indicated that this part of the molecule was less sensitive to structural modifications. Moreover, the insertion of the labeling group in this part of the molecule would not lead to the formation of radioactive metabolite capable to bind to 5-HT$_7$ receptors. Published data on the metabolism of 4-substituted-1-arylpiperazine derivatives indicate that this class of compounds undergo *N*-dealkylation leading to the formation of unsubstituted 1-arylpiperazines that are capable to enter the brain[35, 36]. In order to obtain compounds less lipophilic than **7**, we replaced the biphenyl moiety with a bipyridyl system. To this end, literature data indicated that the insertion of one or two aza group(s) in the aromatic group linked to the piperazine could be well tolerated[30, 37]. Therefore, we inserted one aza group in 2- or 3-position on the phenyl ring directly linked to the piperazine, whereas a second aza group was inserted in the second phenyl (distal) ring. We evaluated 2-, 3- or 4-pyridyl substituents in order to find the most favourable bipyridyl system for the interaction with 5-HT$_7$ receptors, because our previous SAR studies on the 1-(2-biphenyl)piperazines indicated that this part of the molecule interacts with a lipophilic pocket in the 5-HT$_7$ binding site[38]. This structural modification fulfilled our goal of decreasing lipophilicity: all the compounds showed clogD$_{7.4}$ values within the optimal range for brain penetrance (Table 1).

Binding affinity data indicated that the replacement of the biphenyl moiety with a bipyridyl group led to a decrease of 5-HT$_7$ receptor binding affinity. In particular, among the 2-pyridylpiperazine derivatives, **9** and **10**, bearing respectively a 3- or a 4-pyridyl ring as distal aryl ring, respectively, showed a 20-fold decrease of 5-HT$_7$ affinity as compared to **7**, whereas a more marked decrease was shown by the 2-(2-pyridyl)pyridyl derivative **8** (80-fold). As for the 3-pyridylpiperazine derivatives **11-13**, a wide range of 5-HT$_7$ receptor affinity can be observed: **13** showed acceptable affinity (K$_i$= 16.8 nM) whereas **11** was completely devoid of affinity. Moreover, the introduction of two aza groups on the right end of **7** did not lead to an improvement of the selectivity for the 5-HT$_7$ receptor over the 5-HT$_{1A}$ receptor.

On the basis of these results, we modified **7** to design a PET tracer candidate. The two aza groups required to obtain compounds having the desired lipophilicity were inserted in the "left end" of **7** by replacing the phenoxy group with different heteroaryloxy rings. Instead, the functional group for the labeling with carbon-11 was introduced on the biphenyl ring, resembling the 1-(4-methoxybiphenyl-2-yl)piperazine motif of **6**. The second approach proved successful. All compounds showed clogD$_{7.4}$ values very close to the optimal range for a PET tracer and, more interestingly, they showed 5-HT$_7$ receptor affinities in the low nanomolar range. In particular, **16**

showed an affinity profile comparable to that of **7** along with a marked decrease in lipophilicity. Moreover, the introduction of the 1-(4-methoxybiphenyl) group improved the selectivity over 5-HT$_{1A}$ receptor, thus **16** was the most selective compound of the series (145-fold). These data confirmed that the lipophilicity of the aryl moiety linked to the piperazine ring is crucial for optimal interaction with 5-HT$_7$ receptor.

Since compounds **7-16,** which contain a chiral carbon atom, were synthesized and tested as racemates, we wondered if differences in the affinity profile could be shown by the pure enatiomers. Therefore, we prepared and tested the enantiomers of **13** and **16**, due to their affinity and selectivity profile, whereas **14** and **15** were not studied further due to them being unstable and decomposed on standing. Binding affinity data indicated that the enantiomers of both **13** and **16** showed only slight enantiopreference, being the eutomer 3-fold more potent than the distomer. In both cases, the (*R*)-enantiomer showed higher 5-HT$_7$ affinity than the (*S*)-enantiomer. Interestingly, (*R*)-**16** showed high selectivity over 5-HT$_{1A}$ (200-fold). Since (*R*)-**16** showed the best compromise between affinity, selectivity and lipophilicity, it was thus chosen for radiolabeling with carbon-11.

Radiochemistry

Derivative (*R*)-**39**, the desmethyl precursor for ^{11}C-radiolabeling, was prepared as shown in Scheme 5. The 1-(4-methoxybiphenyl-2-yl)piperazine was demethylated with HBr 48% to afford the 1-[(4-hydroxyphenyl)phenyl]piperazine **38** that was condensed with (*R*)-**37** to obtain (*R*)-**39** in 56% yield.

Radiolabeling of [^{11}C](*R*)-**16** succeeded applying standard ^{11}C-labeling conditions (Scheme 5). The precursor eluted ~600 sec prior to the radiolabeled product as indicated by the UV-absorption chromatogram (supplementary information). The radiosynthesis including HPLC purification and formulation generated an injectable solution of [^{11}C](*R*)-**16** (radiochemical purity > >98%) within 70-80 min. Typically, 250–500 MBq (RCY > 35%) of [^{11}C](*R*)-**16** was isolated with a specific activity (A$_s$) of 60–150 GBq/µmol at the end of synthesis.

PET imaging of [^{11}C](*R*)-16 in pigs

The ability of [^{11}C](*R*)-**16** to image brain 5-HT$_7$ receptors *in vivo* was tested with PET in pigs. After intravenous bolus injection of [^{11}C](*R*)-**16** in the pig, the radioligand successfully entered the brain with a peak standardized uptake value (SUV) of ~2.5 g/mL (Figure 2). The subsequent rapid washout of radioactivity indicated reversible tracer kinetics of [^{11}C](*R*)-**16**. Highest brain uptake of

[^{11}C](R)-**16** was found in the thalamus and lowest uptake found in the cerebellum, which is in accordance with the 5-HT$_7$ receptor distribution in pigs (unpublished data) and humans[39].

We also tested whether [^{11}C](R)-**16** was a P-gp substrate by pre-administering one pig with the P-gp transporter inhibitor cyclosporine (CsA). CsA administration only led to a minor increase in brain uptake of [^{11}C](R)-**16**, indicating that [^{11}C](R)-**16** is not a strong substrate for P-gP (Figure 3B).

To investigate the selectivity of [^{11}C](R)-**16** *in vivo*, blocking experiments with **1** were performed in two pigs that first had an unblocked baseline scan performed. After pre-treatment with **1**, average PET images of the pig brain (Figure 4) still displayed a high level of radioactivity, especially in thalamus and in cortical regions. Scans from the corresponding pre-blocked experiments show a similar distribution of radioligand, indicating a limited blocking effect by pre-treatment with this 5-HT$_7$ receptor antagonist.

The binding of [^{11}C](R)-**16** at baseline and after pre-treatment with 1 mg/kg/h of **1** was quantified by arterial input modelling with the one-tissue compartment model. The calculated distribution volumes (V_T) revealed a uniform distribution of binding between the different regions at baseline (Figure 5A) and no significant decrease in V_Ts was observed after pretreatment with **1**, suggesting that [^{11}C](R)-**16** does not bind specifically to the 5-HT$_7$ receptor. Because of technical difficulties we did not obtain HPLC data from one animal (baseline and blocked scan), but in order to quantify the binding of [^{11}C](R)-**16** in this animal, we applied the metabolite correction obtained from the second animal. Based on the V_Ts generated before and after pretreatment with **1**, occupancy plots with all included regions were created (Figure 5B). From the occupancy plots, the non-displaceable volume (V_{ND}) and occupancy of **1** was extracted from the linear regression of the data points[40]. The slope of the linear regression in the occupancy plot of one animal was not significantly different from zero, indicating no blocking effect of **1**. In the occupancy plot of the second animal, the slope of the linear regression was significantly different from zero (p = 0.011), indicating that **1** did indeed block the binding of [^{11}C](R)-**16**, however the occupancy of **1** was low (18%) compared to the high dose of **1** used, and this indicates that [^{11}C](R)-**16** has a limited 5-HT$_7$ receptor specificity. The V_{ND} of [^{11}C](R)-**16** was determined to 2.1 mL/cm^3 in the pig, where we had the accompanying metabolite correction, and thus comprised of about 33 % of the V_T in the high-binding regions (thalamus, 6.2 mL/cm^3). This ratio of specific-to non-specific binding is similar to a successful α_7 nicotinic acetylcholine receptor PET radioligand evaluated in the pig[41]. The non-displaceable binding potential (BP_{ND}) of [^{11}C](R)-**16** in the high binding region (thalamus)

was calculated to 0.94 ($BP_{ND} = ((V_T-V_{ND}))/V_{ND}$). Although the $clogD_{7.4}$ value of (*R*)-**16** ($clogD_{7.4}$ = 3.72) is significantly lower than the lead compound **7** ($clogD_{7.4}$ = 5.30) it might still be too high and promote high non-specific binding caused by hydrophobic interactions with lipids and proteins[28]. Taken together, [^{11}C](*R*)-16 has very limited specific binding to the 5-HT$_7$ receptors in the pig brain.

Radiometabolism of [^{11}C](*R*)-16

After the i.v. injection of [^{11}C](*R*)-**16** into pigs, the parent radioligand component reduced rapidly (Figure 6), with only 40% parent compound remaining after 10 min. The identities of the metabolites are currently unknown, as well as their ability to penetrate the blood-brain barrier. Their lower lipophilicities (retention time of 0.5 and 5.3 min) relative to the radioligand (retention time 6.0 min) suggest that they do not cross the BBB to any major extent. We were in this sample unable to detect differences in the parent compound metabolism after pre-treatment with CsA or **1**. However, it seemed as if CsA influenced the rate of accumulation for one of the metabolites of [^{11}C](*R*)-**16**, as increased amounts of the less polar metabolite was observed after CsA pretreatment. The underlying mechanism is likely that CsA inhibits the enzymes responsible of phase 2 metabolites (conjugates).

CONCLUSION

In summary, we have synthesized a series of biphenylpiperazines suitable as PET radioligands for imaging cerebral 5-HT$_7$ receptors. Starting from our high-affinity ligand **7** and guided in part by previous structure-activity relationship studies, we designed a set of compounds possessing chemical features amenable to carbon-11 labeling and $clogD_{7.4}$ values within the range that is considered optimal for PET radioligands. Compound (*R*)-**16** had high *in vitro* affinity for the 5-HT$_7$ receptor (K_i= 1.1 nM) and 200 fold selectivity over the 5-HT$_{1A}$ receptor (K_i= 242 nM). Carbon-11 labeling of the precursor (*R*)-**39** resulted in [^{11}C](*R*)-**16** in sufficient radiochemical yields allowing for *in vivo* PET experiments in pigs. When tested *in vivo* in pigs, [^{11}C](*R*)-**16** readily entered the brain and displayed desirable reversible tracer kinetics. Pretreatment with cyclosporine A did not increase the brain uptake of [^{11}C](*R*)-**16**, suggesting that this radioligand is not a P-gp substrate. When pre-treating with the 5-HT$_7$ receptor selective antagonist **1** (SB-269970), only limited specific binding of [^{11}C](*R*)-**16** to the 5-HT$_7$ receptors was found. From the occupancy plot, it was found that the non-specific binding was acceptable. Based on the outcome of the [^{11}C](*R*)-**16** imaging data, the pharmacokinetics of [^{11}C](*R*)-**16** suggests that the compound easily crosses the blood brain

barrier, has a high brain uptake, and its binding cannot be blocked by a structurally different 5-HT$_7$ receptor compound. That is, although the compound does not have ideal properties for PET imaging of the 5-HT$_7$ receptors, it may possess good pharmacological properties. It is possible that further optimization of this compound could lead to the finding of a 5-HT$_7$ receptor specific PET radioligand.

EXPERIMENTAL SECTION

Chemistry

The purity of the tested compounds **7-16** has been assessed by RP-HPLC and combustion analysis. All compounds showed ≥ 95% purity. Column chromatography was performed with 1:30 Merck silica gel 60A (63-200 µm) as the stationary phase. Melting points were determined in open capillaries on a Gallenkamp electrothermal apparatus. Reactions under microwave irradiation were performed with a Biotage Initiator+ synthetizer. Elemental analyses (C,H,N) were performed on Eurovector Euro EA 3000 analyzer; the analytical results were within ±0.4% of the theoretical values for the formula given. ^{1}H NMR spectra were recorded at 300 MHz on a Varian Mercury-VX spectrometer. All spectra were recorded on free bases. All chemical shift values are reported in ppm (δ). Recording of mass spectra was done on an HP6890-5973 MSD gas chromatograph/mass spectrometer; only significant *m/z* peaks, with their percentage of relative intensity in parentheses, are reported. All spectra were in accordance with the assigned structures. RP-HPLC analysis was performed on a Perkin-Elmer series 200 LC instrument using a Phenomenex Prodigy ODS-3 RP-18 column, (250 × 4.6 mm, 5 µm particle size) and equipped with a Perkin-Elmer 785A UV/VIS detector setting λ= 254 nm. Compounds **7-16** were eluted with $CH_3OH/H_2O/Et_3N$, 7:3:0.01, v/v at a flow rate of 0.8 mL/min. The enantiomeric excesses of compounds (*R*)-**13**, (*S*)-**13**, (*R*)-**16** and (*S*)-**16** were determined by HPLC analysis on Chiralcel OD (4.6 mm i.d. x 250 mm, Daicel Chemical Industries Ltd, Tokyo, Japan). Compounds (*R*)-**13** and (*S*)-**13** were eluted with *n*-hexane/EtOH/Et_2NH, 8:2:0.01, v/v at a flow rate of 0.8 mL/min. Compounds (*R*)-**16** and (*S*)-**16** were eluted with *n*-hexane/*i*-propanol/Et_2NH, 8:2:0.01, v/v at a flow rate of 0.8 mL/min. All compounds showed enantiomeric excesses ≥ 95%. Optical rotations were measured with a Perkin-Elmer 341 polarimeter at room temperature (20 °C), concentrations are expressed as g/100 mL.

The following compounds were prepared according to literature methods: 1-(2-biphenyl)piperazine[38], 1-[2-(4-methoxyphenyl)phenyl]piperazine[38], 1-(3-bromo-2-pyridyl)piperazine[30]; *t*-butyl 4-(2-chloro-3-pyridyl)piperazine-1-carboxylate[32]; 3-amino-2,2'-bipyridile[31]; 2-[(4-methoxyphenoxy)methyl]oxirane[33]; 3-chloropyridazine[42].

_t_-Butyl 4-[3-(2-pyridyl)-2-pyridyl]piperazine-1-carboxylate (18).

To a degassed mixture of 2-bromopyridine (0.08 g, 0.5 mmol), 2-(4-Boc-1-piperazinyl)pyridine-3-boronic acid pinacolate ester (0.2 g, 0.5 mmol), K_2CO_3 (0.16 g, 0.1 mmol) in a mixture of 1,2-dimethoxyethane and H_2O (1:1, v/v, 4 mL) was added tetrakis(triphenylphosphino)palladium(0)

(0.03 g, 0.11 mmol) under argon atmosphere. The mixture was heated at 100 °C for 3 min under microwave irradiation. After cooling, the solvent was distilled off in vacuo and the residue was taken up with $CHCl_3$ (30 mL) and filtered over a celite pad. The residue was concentrated and chromatographed on a silica gel column(petroleum ether/AcOEt, 3:2, as eluent) to afford pure compound as a yellow solid (0.08 g, quantitative yield). ^{1}H NMR ($CDCl_3$): δ 1.44 (s, 9H), 3.06-3.09 (m, 4H), 3.35-3.38 (m, 4H), 6.98 (dd, 1H, J= 7.4 Hz), 7.20-7.25 (m, 1H), 7.71 (dt, 1H, J= 1.6 and 7.4 Hz), 7.83 (dd, 1H, J= 1.9 and 7.4 Hz), 7.90 (dt, 1H, J= 1.1 and 8.0 Hz), 8.27 (dd, 1H, J= 1.9 and 4.9 Hz), 8.69-8.72 (m, 1H). ESI-MS m/z 341 (M+H)[+]. ESI-MS/MS m/z 285 (100), 241 (21).

General Procedure for the Preparation of Compounds 21, 22, 25, 26.

To a degassed mixture of the appropriate halopyridine (2.5 mmol), the appropriate pyridineboronic acid (2.73) and 2M aqueous Na_2CO_3 (2.67 mL) in 1,2-dimethoxyethane (10 mL) was added tetrakis(triphenylphosphino)palladium(0) (0.12 mmol) under argon atmosphere. The mixture was refluxed for 18-20 h. After cooling, the solvent was distilled off in vacuo and the residue was taken up with AcOEt (30 mL) and washed first with H_2O and then with brine. The organic layer was separated, dried over anhydrous Na_2SO_4 and concentrated. The crude residue was chromatographed on a silica gel column as detailed below to give pure compound as oil.

1-[3-(3-Pyridyl)-2-pyridyl]piperazine (21). Eluted with $CHCl_3$/MeOH, 9:1. 53% Yield. ^{1}H NMR ($CDCl_3$): δ 1.79 (s, 1H, D_2O exchanged), 2.79 (app t, 4H), 3.04 (app t, 4H), 6.96 (dd, 1H, J= 7.4 Hz), 7.35 (dd, 1H, J= 7.7 and 8.0 Hz), 7.46 (dd, 1H, J= 1.9 and 7.4 Hz), 7.97 (dt, 1H, J= 1.9 and 7.7 Hz), 8.28 (dd, 1H, J= 1.9 and 4.9 Hz), 8.56 (dd, 1H, J= 1.7 and 4.9 Hz), 8.82 (d, 1H, J= 1.7). GC/MS m/z 241 (M[+] +1, 3), 240 (M[+], 16), 198 (28), 184 (63), 172 (100).

1-[3-(4-Pyridyl)-2-pyridyl]piperazine (22). Eluted with $CHCl_3$/MeOH, 9:1. 23% Yield. ^{1}H NMR ($CDCl_3$): δ 1.95 (br s, 1H, D_2O exchanged), 2.81 (app t, 4H), 3.07 (app t, 4H), 6.95 (dd, 1H, J= 7.4 Hz), 7.48 (dd, 1H, J= 1.9 and 7.48 Hz), 7.56 (dd, 2H, J= 1.7 and 4.7 Hz), 8.28 (dd, 1H, J= 1.9 and 4.9Hz), 8.65 (dd, 2H, J= 1.7 and 4.7 Hz). GC/MS m/z 241 (M[+] +1, 3), 240 (M[+], 14), 198 (34), 184 (61), 172 (100).

_t_-Butyl 4-[2-(3-pyridyl)-3-pyridyl]piperazine-1-carboxylate (25). Eluted with $CHCl_3$/AcOEt, 9:1. 50% Yield. ^{1}H NMR ($CDCl_3$): δ 1.44 (s, 9H), 2.81 (br s, 4H), 3.40 (br s, 4H), 7.23-7.25 (m, 1H),

7.35-7.40 (m, 2H), 8.25 (dt, 1H, $J=$ 2.2 and 8.0 Hz), 8.40 (dd, 1H, $J=$ 1.7 and 4.7 Hz), 8.60 (dd, 1H, $J=$ 1.7 and 4.9 Hz), 9.23 (dd, 1H, $J=$ 0.8 and 2.2 Hz). ESI-MS m/z 341 (M+H)$^+$. ESI-MS/MS m/z 285 (100), 241 (14).

_t_-Butyl 4-[2-(4-pyridyl)-3-pyridyl]piperazine-1-carboxylate (26). Eluted with CHCl$_3$/AcOEt, 9:1. 35% Yield. ^{1}H NMR (CDCl$_3$): δ 1.44 (s, 9H), 2.82 (br s, 4H), 3.42 (br s, 4H), 7.26-7.29 (m, 1H), 7.38 (dd, 1H, $J=$ 1.4 and 8.3 Hz), 7.90-7.92 (m, 2H), 8.40 (dd, 1H, $J=$ 1.4 and 4.4 Hz), 8.68-8.70 (m, 2H). ESI-MS m/z 341 (M+H)$^+$. ESI-MS/MS m/z 285 (100), 241 (9).

General Procedure for the Preparation of Piperazines 20, 28, 29.
To a solution of the appropriate *N*-Boc-1-arylpiperazine (1.0 mmol) in CH$_2$Cl$_2$ (10 mL) was added trifluoroacetic acid (2.5 mL). The mixture was stirred at room temperature for 3-4 h. The mixture was neutralized with aqueous 5M NaOH and extracted with CHCl$_3$ (2 x 20 mL). The organic layers were collected, dried over Na$_2$SO$_4$ and concentrated under reduced pressure. The crude residue was chromatographed (CHCl$_3$/MeOH, 9:1, as eluent) to give pure compound as an oil.

1-[3-(2-Pyridyl)-2-pyridyl]piperazine (20). 90% Yield. ^{1}H NMR (CDCl$_3$): δ 1.57 (s, 1H, D$_2$O exchanged), 2.83 (app t, 4H), 3.08 (app t, 4H), 6.96 (dd, 1H, , $J=$ 7.4 Hz), 7.19-7.22 (m, 1H), 7.71 (dt, 1H, $J=$ 1.9 and 7.7 Hz), 7.84 (dd, 1H, $J=$ 1.9 and 7.4 Hz), 7.93-7.96 (m, 1H), 8.28 (dd, 1H, $J=$ 1.9 and 5.0 Hz), 8.68-8.71 (m, 1H). GC/MS m/z 241 (M$^+$+1, 3), 240 (M$^+$, 19), 210 (70), 184 (100), 155 (65).

1-[2-(3-Pyridyl)-3-pyridyl]piperazine (28). 90% Yield. ^{1}H NMR (CDCl$_3$): δ 1.62 (s, 1H, D$_2$O exchanged), 2.85 (br s, 8H), 7.22-7.25 (m, 1H), 7.34-7.42 (m, 2H), 8.28 (dt, 1H, $J=$ 1.7 and 7.7 Hz), 8.38 (dd, 1H, $J=$ 1.7 and 4.7 Hz), 8.58 (dd, 1H, $J=$ 1.9 and 4.7 Hz), 9.25-9.26 (m, 1H). GC/MS m/z 241 (M$^+$+1, 10), 240 (M$^+$, 58), 198 (59), 182 (100), 155 (18).

1-[2-(4-Pyridyl)-3-pyridyl]piperazine (29). 35% Yield. ^{1}H NMR (CDCl$_3$): δ 1.68 (br s, 1H, D$_2$O exchanged), 2.85 (br s, 8H), 7.24-7.28 (m, 1H), 7.39 (d, 1H, $J=$ 8.1 Hz), 7.93 (d, 2H, $J=$ 5.5 Hz), 8.37 (d, 1H, $J=$ 4.4 Hz), 8.68 (d, 2H, $J=$ 5.1 Hz). GC/MS m/z 241 (M$^+$+1, 10), 240 (M$^+$, 57), 198 (100), 182 (36), 170 (28).

1-[2-(2-Pyridyl)-3-pyridyl]piperazine (27). A mixture of 3-amino-2,2'-bipyridile (0.12 g, 0.7 mmol), bis(2-chloroethyl)amine hydrochloride (0.13 g, 0.7 mmol), K_2CO_3 (0.1 g, 0.7 mmol) and KI (0.12 g, 0.7 mmol) in xylene (20 mL) was refluxed for 48 h. After cooling, the solvent was distilled off in vacuo and the residue was partitioned between AcOEt (30 mL) and 5% aqueous NaOH solution (30 mL). The organic phase was separated and, then, washed with brine. The organic phase was dried over Na_2SO_4 and concentrated under reduced pressure. The crude residue was chromatographed (CHCl$_3$/MeOH, 9:1, as eluent) to give the desired compound as a brown oil (0.07 g, 21% yield). ^{1}H NMR (CDCl$_3$): δ 1.79 (s, 1H, D$_2$O exchanged), 2.79 (app t, 4H), 3.04 (app t, 4H), 7.02-7.19 (m, 2H), 7.20-7.24 (m, 1H), 7.78-7.81 (m, 1H), 8.06 (dd, 1H, J= 1.5 and 4.0 Hz), 8.48-8.58 (m, 2H). GC/MS m/z 241 (M$^+$+1, 3), 240 (M$^+$, 20), 210 (43), 184 (100), 156 (64).

General Procedure for the Preparation of Epoxides 35-37.

To a suspension of NaH (1.1 mmol) in anhydrous DMF, cooled at 0 °C, a solution of the appropriate aryl chloride (1.0 mmol) and of the appropriate glycidol (1.0 mmol) in the same solvent was added dropwise. The reaction mixture was stirred at room temperature overnight, quenched with H$_2$O and extracted with AcOEt (3 x 20 mL). The organic layers were collected, dried over Na$_2$SO$_4$ and concentrated under reduced pressure. The crude was purified on a silica gel column (CHCl$_3$/AcOEt, 9:1 as eluent) to give pure compound as an oil.

2-[(Oxiran-2-yl)methoxy]pyrimidine (35). 94% Yield. ^{1}H NMR (CDCl$_3$): δ 2.74-2.79 (m, 2H), 3.38-3.42 (m, 1H), 4.34 (dd, 1H, J= 5.8 and 12.1 Hz), 4.57 (dd, 1H, J= 3.6 and 12.1 Hz), 6.94 (t, 1H, J= 4.7 Hz), 8.50 (d, 2H, J= 4.7 Hz). ESI-MS m/z 153 (M+H)$^+$, ESI-MS/MS m/z 135 (5), 97 (100).

3-[(Oxiran-2-yl)methoxy]pyridazine (36). 10% Yield. ^{1}H NMR (CDCl$_3$): δ 2.74-2.77 (m, 1H), 2.91 (t, 1H, J= 4.7 Hz), 3.41-3.47 (m, 1H), 4.32 (dd, 1H, J= 6.6 and 12.1 Hz), 4.92 (dd, 1H, J= 2.8 and 12.1 Hz), 7.03 (dd, 1H, J= 1.4 and 9.1 Hz), 7.39 (dd, 1H, J= 4.4 and 9.1 Hz), 8.84 (dd, 1H, J= 1.4 and 4.4 Hz). ESI-MS m/z 153 (M+H)$^+$. ESI-MS/MS m/z 135 (22), 123 (44), 97 (100).

2-[(Oxiran-2-yl)methoxy]pyrazine (37). 21% Yield. ^{1}H NMR (CDCl$_3$): δ 2.74-2.76 (m, 1H), 2.90 (t, 1H, J= 4.7 Hz), 3.36-3.41 (m, 1H), 4.21 (dd, 1H, J= 6.3 and 12.1 Hz), 4.65 (dd, 1H, J= 3.0 and

12.1 Hz), 8.06 (t, 1H, J= 1.4 Hz), 8.15 (d, 1H, J= 2.8 Hz), 8.28 (d, 1H, J= 1.4 Hz). ESI-MS m/z 153 (M+H)$^+$, ESI-MS/MS m/z 123 (16), 97 (100).

(R)-2-[(Oxiran-2-yl)methoxy]pyrazine ((R)-37). 24% Yield. ^{1}H NMR (CDCl$_3$): δ 2.76 (dd, 1H, J= 2.5 and 4.7 Hz), 2.87-2.92 (m, 1H), 3.36-3.42 (m, 1H), 4.22 (dd, 1H, J= 6.1 and 12.1 Hz), 4.66 (dd, 1H, J= 3.0 and 12.1 Hz), 8.06 (dd, 1H, J= 1.4 and 3.0 Hz), 8.14 (d, 1H, J= 3.0 Hz), 8.28 (d, 1H, J= 1.4 Hz). ESI-MS m/z 153 (M+H)$^+$. ESI-MS/MS m/z 123 (14), 97 (100). [α]$_D$: - 28.1° (c= 1.5, MeOH)

(S)-2-[(Oxiran-2-yl)methoxy]pyrazine ((S)-37). 24% Yield. ^{1}H NMR (CDCl$_3$): δ 2.75 (dd, 1H, J= 2.5 and 4.7 Hz), 2.90 (t, 1H, J= 4.7 Hz), 3.36-3.41 (m, 1H), 4.22 (dd, 1H, J= 6.3 and 12.1 Hz), 4.65 (dd, 1H, J= 3.0 and 12.1 Hz), 8.06 (dd, 1H, J= 1.4 and 2.8 Hz), 8.14 (d, 1H, J= 3.0 Hz), 8.28 (d, 1H, J= 1.1 Hz). ESI-MS m/z 153 (M+H)$^+$. ESI-MS/MS m/z 123 (14), 97 (100). [α]$_D$: + 28.1° (c= 1.5, MeOH)

General Procedure for the Preparation of the Chiral Epoxides ((R)- and (S)-34).

To a suspension of NaH (1.1 mmol) in anhydrous DMF, cooled at 0 °C, a solution of 4-methoxyphenol (0.19 g, 1.5 mmol) and (R)-or (S) glycidol nosylate (0.41 g, 1.5 mmol) in the same solvent was added dropwise. The reaction mixture was stirred at room temperature overnight, quenched with H$_2$O and extracted with AcOEt (3 x 20 mL). The organic layers were collected, dried over Na$_2$SO$_4$ and concentrated under reduced pressure. The crude was purified on a silica gel column (n-hexane/AcOEt, 7:3 as eluent) to give pure compound as a white solid.

(R)-2-[(4-Methoxyphenoxy)methyl]oxirane ((R)-34). 66% Yield. ^{1}H NMR (CDCl$_3$): δ 2.75 (dd, 1H, J = 2.8 and 4.9 Hz), 2.88-2.91 (m, 1H), 3.31-3.37 (m, 1H), 3.77 (s, 3H), 3.92 (dd, 1H, J = 5.5 and 11.0 Hz), 4.17 (dd, 1H, J = 3.0 and 11.0 Hz), 6.74-6.82 (m, 2H), 6.83-6.89 (m, 2H). ESI$^+$/MS m/z 153 (MH$^+$). ESI$^+$/MS/MS m/z 135 (22), 123 (44), 97 (100). [α]$_D$: - 10.8° (c= 1.0, MeOH)

(S)-2-[(4-Methoxyphenoxy)methyl]oxirane ((S)-34) 73% Yield. ^{1}H NMR (CDCl$_3$): δ 2.75 (dd, 1H, J = 2.5 and 4.7 Hz), 2.90 (app t, 1H), 3.32-3.37 (m, 1H), 3.76 (s, 3H), 3.90 (dd, 1H, J = 5.8 and 11.0

Hz), 4.17 (dd, 1H, J = 3.0 and 11.0 Hz), 6.78-6.88 (m, 4H). ESI⁺/MS *m/z* 153 (MH⁺). ESI⁺/MS/MS *m/z* 135 (22), 123 (44), 97 (100). [α]$_D$: + 11.0° (c= 1.0, MeOH)

General Procedure for the Preparation of Compounds 7-16.

A mixture of the appropriate 1-arylpiperazine (1.2 mmol) and the appropriate epoxide (1.0 mmol) in 20 mL of ethanol was refluxed for 5 hours. After cooling, the solvent was removed in vacuo. The crude residue was chromatographed as detailed below to give desired pure compound.

3-[4-(2-Biphenyl)piperazin-1-yl]-1-phenoxy-2-propanol (7). Eluted with CHCl$_3$/AcOEt, 1:1. 54% Yield. ^{1}H NMR (CDCl$_3$): δ 2.37-2.38 (m, 3H, 1H D$_2$O exchanged), 2.55-2.61 (m, 4H), 2.82-2.92 (m, 4H), 3.95-3.92 (m, 2H), 4.01-4.10 (m, 1H), 6.89-6.98 (m, 3H), 7.03-7.11 (m, 2H), 7.24-7.33 (m, 5H), 7.37-7.43 (m, 2H), 7.61-7.65 (m, 2H). GC/MS *m/z* 389 (M⁺+1, 3), 388 (M⁺, 8), 251 (100), 180 (43). The hydrochloride salt melted at 146-148 °C (from CHCl$_3$/*n*-hexane). Anal. (C$_{25}$H$_{28}$N$_2$O$_2$) C, H, N.

1-(4-Methoxyphenoxy)-3-[4-[3-(2-pyridyl)-2-pyridyl]piperazin-1-yl]-2-propanol (8). Eluted with CHCl$_3$/MeOH, 98:2. 94% Yield. ^{1}H NMR (CDCl$_3$): δ 2.40-2.47 (m, 3H, 1H D$_2$O exchanged), 2.50-2.57 (m, 2H), 2.61-2.68 (m, 2H), 3.17 (br s, 4H), 3.76 (s, 3H), 3.92 (d, 2H, *J*= 4.9 Hz), 4.01-4.09 (m, 1H), 6.79-6.86 (m, 4H), 6.97 (dd, 1H, *J*= 4.7 and 7.5 Hz), 7.20-7.24 (m, 1H), 7.71 (dt, 1H, *J*= 1.7 and 7.4 Hz), 7.83 (dt, 1H, *J*= 1.9 and 7.7 Hz), 7.89-7.92 (m, 1H), 8.27 (dd, 1H, *J*= 1.9 and 4.7 Hz), 8.69-8.72 (m, 1H). ESI-MS *m/z* 421 (M+H)⁺. ESI-MS/MS *m/z* 198 (100). The hydrochloride salt melted at 146-148 °C (from CH$_3$OH/diethyl ether). Anal. (C$_{24}$H$_{28}$N$_4$O$_3$•3HCl) C, H, N.

1-(4-Methoxyphenoxy)-3-[4-[3-(3-pyridyl)-2-pyridyl]piperazin-1-yl]-2-propanol (9). Eluted with CHCl$_3$/MeOH, 98:2. 80% Yield. ^{1}H NMR (CDCl$_3$): δ 2.38-2.44 (m, 3H, 1H D$_2$O exchanged), 2.51-2.55 (m, 2H), 2.58-2.65 (m, 2H), 3.12 (br s, 4H), 3.76 (s, 3H), 3.93 (d, 2H, *J*= 4.9 Hz), 3.99-4.05 (m, 1H), 6.79-6.86 (m, 4H), 6.98 (dd, 1H, *J*= 4.9 and 7.4 Hz), 7.34-7.38 (m, 1H), 7.47 (dd, 1H, *J*= 1.9 and 7.5 Hz), 7.94 (dt, 1H, *J*= 1.7 and 8.0 Hz), 8.28 (dd, 1H, *J*= 1.7 and 4.7 Hz), 8.57 (dd, 1H, *J*= 1.7 and 4.7 Hz), 8.84-8.85 (m, 1H). ESI-MS *m/z* 421 (M+H)⁺. ESI-MS/MS *m/z* 366 (19), 198 (100). The hydrochloride salt melted at 164-166 °C (from CH$_3$OH/diethyl ether). Anal. (C$_{24}$H$_{28}$N$_4$O$_3$•3HCl) C, H, N.

1-(4-Methoxyphenoxy)-3-[4-[3-(4-pyridyl)-2-pyridyl]piperazin-1-yl]-2-propanol (10). Eluted with CHCl$_3$/AcOEt, 1:1. 50% Yield. ^{1}H NMR (CDCl$_3$): δ 2.38-2.45 (m, 3H, 1H D$_2$O exchanged), 2.52-2.56 (m, 2H), 2.58-2.62 (m, 2H), 3.14 (br t, 4H), 3.76 (s, 3H), 3.92 (d, 2H, *J*= 4.9 Hz), 4.02-4.07 (m, 1H), 6.82-6.87 (m, 4H), 6.96 (dd, 1H, *J*=7.4 Hz), 7.48 (dd, 1H, *J*= 1.9 and 7.4 Hz), 7.54-7.56 (m, 2H), 8.28 (dd, 1H, *J*= 1.9 and 4.9 Hz), 8.65-8.67 (m, 2H). ESI-MS *m/z* 421 (M+H)$^+$. ESI-MS/MS *m/z* 378 (19), 198 (100). Mp: 131-133 °C (from CHCl$_3$/n-hexane). Anal. (C$_{24}$H$_{28}$N$_4$O$_3$) C, H, N.

1-(4-Methoxyphenoxy)-3-[4-[2-(2-pyridyl)-3-pyridyl]piperazin-1-yl]-2-propanol (11). Eluted with CHCl$_3$/MeOH, 19:1. 46% Yield. ^{1}H NMR (CDCl$_3$): δ 2.42-2.45 (m, 3H, 1H D$_2$O exchanged), 2.53-2.56 (m, 2H), 2.60-2.66 (m, 2H), 2.87-2.97 (m, 4H), 3.76 (s, 3H), 3.92 (d, 2H, *J*= 4.9 Hz), 4.00-4.08 (m, 1H), 6.80-6.87 (m, 4H), 7.19-7.28 (m, 2H), 7.39 (d, 1H, *J*= 8.3 Hz), 7.76 (dt, 1H, *J*= 8.0 Hz), 7.94 (d, 1H, *J*= 8.0 Hz), 8.41 (d, 1H, *J*= 4.7 Hz), 8.76-8.78 (m, 1H). ESI-MS *m/z* 421 (M+H)$^+$. ESI-MS/MS *m/z* 198 (100), 183 (15).

1-(4-Methoxyphenoxy)-3-[4-[2-(3-pyridyl)-3-pyridyl]piperazin-1-yl]-2-propanol (12). Eluted with CHCl$_3$/MeOH, 98:2. 62% Yield. ^{1}H NMR (CDCl$_3$): δ 2.46-2.49 (m, 3H, 1H D$_2$O exchanged), 2.54-2.57 (m, 2H), 2.64-2.68 (m, 2H), 2.90-2.92 (m, 4H), 3.76 (s, 3H), 3.92 (d, 2H, *J*= 4.7 Hz), 4.01-4.07 (m, 1H), 6.80-6.87 (m, 4H), 7.22-7.25 (m, 1H), 7.35-7.42 (m, 2H), 8.25 (d, 1H, *J*= 8.0 Hz), 8.39 (d, 1H, *J*= 4.7 Hz), 8.59 (d, 1H, *J*= 4.7 Hz), 9.27 (d, 1H, *J*= 1.9 Hz). ESI-MS *m/z* 421 (M+H)$^+$. ESI-MS/MS *m/z* 366 (100), 238 (4). The hydrochloride salt melted at 173-175 °C (from CH$_3$OH/diethyl ether). Anal. (C$_{24}$H$_{28}$N$_4$O$_3$•3HCl) C, H, N.

1-(4-Methoxyphenoxy)-3-[4-[2-(4-pyridyl)-3-pyridyl]piperazin-1-yl]-2-propanol (13). Eluted with CHCl$_3$/MeOH, 98:2. 55% Yield. ^{1}H NMR (CDCl$_3$): δ 2.49-2.54 (m, 3H, 1H D$_2$O exchanged), 2.57 (app t, 2H), 2.64-2.69 (m, 2H), 2.92 (br s, 4H), 3.76 (s, 3H), 3.92 (d, 2H, *J*= 4.9 Hz), 4.03-4.10 (m, 1H), 6.80-6.87 (m, 4H), 7.27-7.29 (m, 1H), 7.41 (dd, 1H, *J*= 1.4 and 8.3 Hz), 7.91-7.93 (m, 2H), 8.39 (dd, 1H, *J*= 1.4 and 4.7 Hz), 8.68-8.70 (m, 2H). ESI-MS *m/z* 421 (M+H)$^+$. ESI-MS/MS *m/z* 378 (100), 366 (57). The hydrochloride salt melted at 151-154 °C (from CH$_3$OH/diethyl ether). Anal. (C$_{24}$H$_{28}$N$_4$O$_3$•3HCl) C, H, N.

1-[4-[2-(4-Methoxyphenyl)phenyl]piperazin-1-yl]-3-(2-pyrimidinyloxy)-2-propanol (14).
Eluted with CHCl$_3$/MeOH, 98:2. 30% Yield. ^{1}H NMR (CDCl$_3$): δ 2.35-2.43 (m, 3H, 1H D$_2$O exchanged), 2.53-2.59 (m, 4H), 2.83-2.88 (m, 4H), 3.85 (s, 3H), 4.08-4.14 (m, 1H), 4.36-4.40 (m, 2H), 6.90-6.96 (m, 2H), 6.98-7.09 (m, 2H), 7.20-7.24 (m, 3H), 7.53-7.58 (m, 2H), 8.51 (d, 2H, *J*= 4.7 Hz). ESI-MS *m/z* 421 (M+H)$^+$. ESI-MS/MS *m/z* 325 (100), 281 (3). The hydrochloride salt melted at 80 °C dec (from CH$_3$OH/diethyl ether). Anal. (C$_{24}$H$_{28}$N$_4$O$_3$•2HCl) C, H, N.

1-[4-[2-(4-Methoxyphenyl)phenyl]piperazin-1-yl]-3-(3-pyridazinyloxy)-2-propanol (15). Eluted with CHCl$_3$/MeOH, 19:1. 40% Yield. ^{1}H NMR (CDCl$_3$): δ 2.38-2.46 (m, 3H, 1H D$_2$O exchanged), 2.48-2.52 (m, 2H), 2.56-2.60 (m, 2H), 2.83-2.88 (m, 4H), 3.85 (s, 3H), 4.09-4.17 (m, 1H), 4.43 (dd, 1H, *J*= 6.3 and 11.5 Hz), 4.64 (dd, 1H, *J*= 3.0 and 11.3 Hz), 6.90-6.95 (m, 2H), 7.00-7.09 (m, 2H), 7.19-7.24 (m, 3H), 7.37 (dd, 1H, *J*= 4.4 Hz), 7.53-7.59 (m, 2H), 8.83 (dd, 1H, *J*= 1.1 and 4.1 Hz). ESI-MS *m/z* 421 (M+H)$^+$. ESI-MS/MS *m/z* 325 (100), 153 (96). The tartrate salt melted at 115 °C dec (from CH$_3$OH/diethyl ether). Anal. (C$_{24}$H$_{28}$N$_4$O$_3$•C$_4$H$_6$O$_6$) C, H, N.

1-[4-[2-(4-Methoxyphenyl)phenyl]piperazin-1-yl]-3-(2-pyrazinyloxy)-2-propanol (16). Eluted with CHCl$_3$/MeOH, 98:2. 55% Yield. ^{1}H NMR (CDCl$_3$): δ 2.38-2.43 (m, 3H, 1H D$_2$O exchanged), 2.47-2.52 (m, 2H), 2.56-2.61 (m, 2H), 2.86-2.88 (m, 4H), 3.85 (s, 3H), 4.04-4.12 (m, 1H), 4.25-4.31 (m, 1H), 4.37-4.42 (m, 1H), 6.92-6.95 (m, 2H), 7.01-7.09 (m, 2H), 7.19-7.24 (m, 2H), 7.56-7.59 (m, 2H), 8.05 (dd, 1H, *J*= 1.1 and 2.9 Hz), 8.13 (d, 1H, *J*= 2.9 Hz), 8.28 (d, 1H, *J*= 1.1 Hz). ESI-MS *m/z* 421 (M+H)$^+$. ESI-MS/MS *m/z* 325 (100), 281 (12). The hydrochloride salt melted at 208-210 °C (from CH$_3$OH/diethyl ether). Anal. (C$_{24}$H$_{28}$N$_4$O$_3$•HCl) C, H, N.

(*R*)-1-[4-[2-(4-Methoxyphenyl)phenyl]piperazin-1-yl]-3-(2-pyrazinyloxy)-2-propanol ((*R*)-13).
Eluted with CHCl$_3$/MeOH, 98:2. 67% Yield. ^{1}H NMR (CDCl$_3$): δ 2.49-2.53 (m, 3H, 1H D$_2$O exchanged), 2.56-2.60 (m, 2H), 2.64-2.69 (m, 2H), 2.88-2.97 (m, 4H), 3.76 (s, 3H), 3.93 (d, 2H, *J*= 5.2 Hz), 4.02-4.10 (m, 1H), 6.80-6.87 (m, 4H), 7.26-7.29 (m, 1H), 7.41 (dd, 1H, *J*= 1.4 and 8.3 Hz), 7.92 (dd, 2H, *J*= 1.7 and 4.7 Hz), 8.39 (dd, 1H, *J*= 1.4 and 4.4 Hz), 8.69 (dd, 2H, *J*= 1.7 and 4.7 Hz). ESI-MS *m/z* 421 (M+H)$^+$. ESI-MS/MS *m/z* 378 (100), 366 (73). [α]$_D$: -3.5° (c=1.2, MeOH).

(*S*)-1-[4-[2-(4-Methoxyphenyl)phenyl]piperazin-1-yl]-3-(2-pyrazinyloxy)-2-propanol ((*S*)-13).
Eluted with CHCl$_3$/MeOH, 98:2. 42% Yield. ^{1}H NMR (CDCl$_3$): δ 2.49-2.53 (m, 3H, 1H D$_2$O

exchanged), 2.56-2.60 (m, 2H), 2.64-2.70 (m, 2H), 2.88-2.97 (m, 4H), 3.76 (s, 3H), 3.93 (d, 2H, *J*= 4.9 Hz), 4.02-4.10 (m, 1H), 6.80-6.88 (m, 4H), 7.26-7.29 (m, 2H), 7.41(dd, 1H, *J*= 1.4 and 8.3 Hz), 7.92 (dd, 2H, *J*= 1.7 and 4.7 Hz), 8.38 (dd, 1H, *J*= 1.4 and 4.7 Hz), 8.68-8.70 (m, 2H). ESI-MS *m/z* 421 (M+H)$^+$. ESI-MS/MS *m/z* 378 (100), 366 (73). [α]$_D$: +3.2° (c=1.5, MeOH).

(*R*)-1-[4-[2-(4-Methoxyphenyl)phenyl]piperazin-1-yl]-3-(2-pyrazinyloxy)-2-propanol   ((*R*)-16).
Eluted with CHCl$_3$/MeOH, 98:2. 46% Yield. ^{1}H NMR (CDCl$_3$): δ 2.39-2.45 (m, 3H, 1H D$_2$O exchanged), 2.48-2.52 (m, 2H), 2.56-2.61 (m, 2H), 2.87 (br s, 4H), 3.85 (s, 3H), 4.06-4.12 (m, 1H), 4.27 (dd, 1H, *J*= 5.8 and 11.3 Hz), 4.38 (dd, 1H, *J*= 3.6 and 11.3 Hz), 6.93 (d, 2H, *J*= 8.8 Hz), 7.01-7.09 (m, 2H), 7.21-7.24 (m, 2H), 7.58 (d, 2H, *J*= 8.8 Hz), 8.06 (dd, 1H, *J*= 1.4 and 2.7 Hz), 8.13 (d, 1H, *J*= 3.0 Hz), 8.28 (d, 1H, *J*= 1.4 Hz). ESI-MS *m/z* 421 (M+H)$^+$. ESI-MS/MS *m/z* 325 (100), 281 (11), 224 (6). [α]$_D$: -7.5° (c=1.1, MeOH).

(*S*)-1-[4-[2-(4-Methoxyphenyl)phenyl]piperazin-1-yl]-3-(2-pyrazinyloxy)-2-propanol   ((*S*)-16).
Eluted with CHCl$_3$/MeOH, 98:2. 60% Yield. ^{1}H NMR (CDCl$_3$): δ 2.39-2.44 (m, 3H, 1H D$_2$O exchanged), 2.48-2.53 (m, 2H), 2.57-2.63 (m, 2H), 2.83-2.93 (m, 4H), 3.85 (s, 3H), 4.05-4.12 (m, 1H), 4.26 (dd, 1H, *J*= 5.8 and 11.3 Hz), 4.39 (dd, 1H, *J*= 3.8 and 11.3 Hz), 6.92-6.96 (m, 2H), 7.01-7.09 (m, 2H), 7.21-7.24 (m, 2H), 7.55-7.60 (m, 2H), 8.06 (dd, 1H, *J*= 1.4 and 2.8 Hz), 8.13 (d, 1H, *J*= 2.8 Hz), 8.28 (d, 1H, *J*= 1.4 Hz). ESI-MS *m/z* 421 (M+H)$^+$. ESI-MS/MS *m/z* 325 (100), 281 (9). [α]$_D$: -7.8° (c=1.5, MeOH).

1-[2-(4-Hydroxyphenyl)phenyl]piperazine   (38). A solution of 1-(4-methoxybiphenyl-2-yl)piperazine (0.16 g, 0.6 mmol) in 5 mL of 48% HBr was refluxed overnight. After cooling, the reaction mixture was neutralized with conc. NH$_4$OH and extracted with AcOEt (3 x 20 mL). The organic layers were washed with brine, dried over Na$_2$SO$_4$ and concentrated under reduced pressure to yield pure compound as a brownish solid (0.10 g, 65% yield). ^{1}H NMR (CDCl$_3$): δ 1.71 (br s, 1H, D$_2$O exchanged), 2.99 (br s, 8H), 6.86 (d, 2H, *J*= 8.3 Hz), 6.99 (d, 1H, *J*= 7.7 Hz), 7.07-7.10 (m, 1H), 7.12-7.22(m, 2H), 7.45 (d, 2H, *J*= 8.5 Hz), 8.10 (br s, 1H, D$_2$O exchanged), 8.28 (d, 1H, *J*= 1.4 Hz). GC/MS *m/z* 255 (M$^+$+1, 9), 254 (M$^+$, 56), 212 (100), 197 (44), 196 (55).

(*R*)-1-[4-[2-(4-Hydroxyphenyl)phenyl]piperazin-1-yl]-3-(2-pyrazinyloxy)-2-propanol ((*R*)-39).

The compound was prepared as reported for (*R*)-**16** starting from (*R*)-**37** and piperazine **38**. Eluted with CHCl$_3$/MeOH, 98:2. 56% Yield. ^{1}H NMR (CDCl$_3$): δ 2.42-2.62 (m, 7H, 1H D$_2$O exchanged), 4.09-4.13 (m, 1H), 4.29 (dd, 1H, *J*= 5.8 and 11.3 Hz), 4.40 (dd, 1H, *J*= 3.6 and 11.0 Hz), 6.85 (d, 2H, *J*= 8.5 Hz), 7.01 (d, 1H, *J*= 8.0 Hz), 7.07 (d, 1H, *J*= 7.7 Hz), 7.20-7.23 (m, 2H), 7.50 (d, 2H, *J*= 8.5 Hz), 8.07-8.08 (m, 1H), 8.13 (d, 1H, *J*= 2.8 Hz), 8.28 (br s, 1H). ESI-MS *m/z* 405 (M+H)$^+$. ESI-MS/MS *m/z* 308 (100), 215 (36), 204 (31).

Radiochemistry

General. Chemicals were purchased from Acros, Fluka, Sigma, Tocris, or Merck. Unless otherwise stated, all chemicals were used without further purification. Thin layer chromatography (TLC) was performed using plates from Merck (silica gel 60 F$_{254}$ and aluminium oxide 60 F$_{254}$). Analytical high performance liquid chromatography (HPLC) measurements were performed on a Dionex system consisting of a P680A pump, a UVD 170U detector and a Scansys radiodetector. Chemical purity was checked either by HPLC or by GC. [^{11}C]Methane was produced via the ^{14}N(p,α)^{11}C reaction by bombardment of an [^{14}N]N2 containing 10% H$_2$ target with a 17 MeV proton beam in a Scanditronix MC32NI cyclotron. Radioactive syntheses were carried out on an automated Scansys module.

1. **Radioligand preparation.** [^{11}C]methyl iodide ([^{11}C]MeI) produced using a fully automated system was transferred in a stream of helium to a 1.1-mL vial containing the labeling precursor (1.3–1.4 mg), 2 M NaOH (2 µL) and DMF (300 µL). The resulting mixture was heated at 180 °C for 2 min and then purified by HPLC on an Onyx Monolithic C18 column (Phenomenex Inc.) (100 x 10 mm; 20:80 EtOH: 0.1% phosphoric acid at a flow rate of 9 mL/min, retention times: [^{11}C](*R*)-**16** = 1000 s; precursor = 200 - 400 s). The fraction corresponding to the labeled product (6 mL) was collected into a 20-mL vial containing phosphate buffer (9 mL, 100 mM, pH 7), giving a 15 mL solution of [^{11}C](R)-**17** with a pH of approximately 7.

2. Determination of radiochemical purity and specific radioactivity. Chemical and radiochemical purities were assessed on the same aliquot by HPLC analysis. Specific activity of the radiotracers were calculated from three consecutive HPLC analyses (average) and determined by the area of the UV absorbance peak corresponding to the radiolabeled product on the HPLC chromatogram and compared to a standard curve relating mass to UV absorbance (λ = 225 µm).

Column used for $[^{11}C](R)$-**16**: Agilent Eclipse XDB 5 μm C18 column (Agilent) (150 x 4.6 mm (35:65 acetonitrile0.1% phosphoric acid; at a flow rate: 1 mL/min. retention times: $[^{11}C](R)$-**16** = 4.6 min, precursor ((R)-**39**): 2.0 min).

Biological Methods

General. Human recombinant serotonin 5-HT$_7$ receptors expressed in CHO-K1 cells, human recombinant serotonin 5-HT$_{1A}$ receptors expressed in HEK293-EBNA cells, $[^3H]$-5-CT, and $[^3H]$-8-OH-DPAT were obtained from PerkinElmer Life and Analytical Sciences (Boston, MA, USA). 5-CT and SB-269970 were purchased from Tocris Bioscience (Bristol, UK). 8-OH-DPAT hydrobromide was from Sigma-Aldrich (Milan, Italy).

1. Radioligand binding assay at human cloned 5-HT$_7$ receptors. Binding of $[^3H]$-5-CT at human cloned 5-HT$_7$ receptor was performed according to Jasper et al.[43] with minor modifications. In 0.5 mL of incubation buffer (50 mM Tris-HCl, 10 mM MgSO$_4$ and 0.5 mM EDTA, pH 7.4) were suspended 34 μg of membranes, 1.5 nM $[^3H]$-5-CT, the drugs, or reference compound (six to nine concentrations). The samples were incubated for 120 min at 27 °C. The incubation was stopped by rapid filtration on Whatman GF/C glass microfiber filters (pre-soaked in 0.3% polyethylenimine for 30 min). The filters were washed with 3 × 1 mL of ice-cold buffer (50 mM Tris-HCl, pH 7.4). Nonspecific binding was determined in the presence of 10 μM 5-CT. Approximately 90% of specific binding was determined under these conditions. Concentrations required to inhibit 50% of radioligand specific binding (IC$_{50}$) were determined by using six to nine different concentrations of the drug studied in two or three experiments with sample duplicate. Apparent inhibition constants (K_i) values were determined by nonlinear curve fitting, using the Prism, version 3.0, GraphPad software.

2. Radioligand binding assay at human cloned 5-HT$_{1A}$ receptors. Human 5-HT$_{1A}$ serotonin receptors stably expressed in HEK293-EBNA cells were radiolabeled with 1.0 nM $[^3H]$-8-OH-DPAT[44]. Samples containing 32 μg of membrane protein, different concentrations of each compound ranging from 0.1 nM to 10 μM were incubated in a final volume of 500 μL of 50 mM Tris-HCl pH 7.4, 5 mM MgSO$_4$ for 120 min at 37 °C. After this incubation time, samples were filtered through Whatman GF/C glass microfiber filters pre-soaked in polyethylenimine 0.5% for at least 30 min prior to use. The filters were washed twice with 1 mL of ice-cold buffer (50 mM Tris-

HCl, pH 7.4). Nonspecific binding was determined in the presence of 10 μM 5-HT. Approximately 90% of specific binding was determined under these conditions. Concentrations required to inhibit 50% of radioligand specific binding (IC_{50}) were determined by using six to nine different concentrations of the drug studied in two or three experiments with sample duplicate. Apparent inhibition constants (K_i) values were determined by nonlinear curve fitting, using the Prism, version 3.0, GraphPad software.

3. *In vivo* experiments

Three female Danish Landrace pigs (mean weight ± S.D., 17 ± 0.75 kg) were used for *in vivo* PET imaging. Tranquillization, anaesthesia, monitoring and sacrifice of animals were performed as previously described[41, 45]. All animal procedures were approved by the Danish Council for Animal Ethics (journal no. 2012-15-2934-00156).

[^{11}C](R)-**16** was given as an intravenously (i.v.) bolus injection and the injected dose was 334 ± 217 MBq (n=5). The pigs were subsequently scanned for 90 min in list-mode with a high resolution research tomography (HRRT) scanner (Siemens AG, Munich, Germany), where scanning started at the time of injection (0 min). Immediately after the baseline scan of [^{11}C](R)-**16**, **1** was given as intravenous bolus infusion (1 mg/kg/hr) and rescanning started after 30 min of pretreatment. After one [^{11}C](R)-**16** scan. CsA (Sandimmun, Novartis 22.5 mg/kg i.v. bolus, 7.5 mg/kg/h i.v. bolus infusion started immediately after the bolus and continuing for the duration of the scan) was administered, and this pig was scanned again 30 min later with a second injection of [^{11}C](*R*)-**16** using the same PET protocol.

During the first 30 min of the scans, radioactivity in the whole blood was continuously measured using an ABSS autosampler (Allogg Technology, Mariefred, Sweden) counting coincidences in a lead-shielded detector. Concurrently, arterial whole blood was sampled manually at time 2.5, 5, 10, 20, 30, 40, 50, 70 and 90 minutes after injection and radioactivity was measured in whole blood and plasma using a well counter (Cobra 5003, Packard Instruments, PerkinElmer, Waltham, USA), which was cross-calibrated to the HRRT scanner and to the autosampler.

Ninety-minute list-mode PET data were reconstructed into 38 dynamic frames of increasing length (6x10, 6x20, 4x30, 9x60, 2x180, 8x300, and 3x600 seconds). Images consisted of 207 planes of 256 x 256 voxels of 1.22 x 1.22 x 1.22 mm. A summed picture of all counts in the 90-min scan was reconstructed for each pig and used for co-registration to a standardized MRI-based atlas of the Danish Landrace pig brain, similar to that previously published[45, 46]. The time activity curves

(TACs) were calculated for the following volumes of interest (VOIs): cerebellum, cortex, hippocampus, lateral and medial thalamus, caudate nucleus, and putamen. Striatum is defined as the mean radioactivity in caudate nucleus and putamen. The radioactivity in thalamus is calculated as the mean radioactivity in the lateral and medial thalamus. Radioactivity in all VOIs was calculated as the average of radioactive concentration (Bq/mL) in the left and right sides. Outcome measure in the time-activity curves (TACs) was calculated as radioactive concentration in VOI (in kBq/mL) normalized to the injected dose corrected for animal weight (in kBq/kg), yielding standardized uptake values (g/mL).

Distribution volumes (V_T) for the VOIs were calculated for $[^{11}C](R)$-**16** with the one-tissue compartment (1-TC). The V_T of baseline and blocked conditions were used to determine the non-displaceable distribution volume (V_{ND}) by use of the Lassen plot[40], and thereby allow for calculation of the non-displaceable binding potential (BP_{ND})[40]. All modelling was initiated with same starting parameters, and standard deviation coefficient variance (COV) was below 15 % for macroparameters (K_1 and V_T). Data sets that did not fulfil this criterion were not included in the results.

Radiolabeled parent compound and metabolites were measured in plasma using HPLC with online radioactivity detection. In short, $[^{11}C](R)$-**16** were separated from their respective radiolabeled metabolite(s) by direct injection of plasma in a column switching HPLC system. Whole blood samples were centrifuged (3500 rpm, 7 min) and the supernatant plasma fraction was collected and filtered through a 0.45 µM syringe filter prior to analysis with online radioactive detection, as previously described[47]. For the late blood samples collected 40 to 90 min post dosing, where radioactivity was too low for accurate measurement with online radioactive detection, fractions of HPLC eluent were collected and counted in a gamma counter (2480 Wizard2, Perkin Elmer, Waltham, USA).

REFERENCES

1. Bard, J. A.; Zgombick, J.; Adham, N.; Vaysse, P.; Branchek, T. A.; Weinshank, R. L. Cloning of a novel human serotonin receptor (5-HT7) positively linked to adenylate cyclase. *Journal of Biological Chemistry* **1993,** 268, 23422-6.

2. Lovenberg, T. W.; Baron, B. M.; de Lecea, L.; Miller, J. D.; Prosser, R. A.; Rea, M. A.; Foye, P. E.; Racke, M.; Slone, A. L.; Siegel, B. W.; Danielson, P. E.; Sutcliffe, J. G.; Erlander, M. G. A novel adenylyl cyclase-activating serotonin receptor (5-HT7) implicated in the regulation of mammalian circadian rhythms. *Neuron* **1993,** 11, 449-458.

3. Ruat, M.; Traiffort, E.; Leurs, R.; Tardivel-Lacombe, J.; Diaz, J.; Arrang, J. M.; Schwartz, J. C. Molecular cloning, characterization, and localization of a high-affinity serotonin receptor (5-HT7) activating cAMP formation. *Proc Natl Acad Sci U S A* **1993,** 90, 8547-51.

4. Leopoldo, M.; Lacivita, E.; Berardi, F.; Perrone, R.; Hedlund, P. B. Serotonin 5-HT7 receptor agents: Structure-activity relationships and potential therapeutic applications in central nervous system disorders. *Pharmacol Ther* **2011,** 129, 120-48.

5. Matthys, A.; Haegeman, G.; Van Craenenbroeck, K.; Vanhoenacker, P. Role of the 5-HT7 receptor in the central nervous system: from current status to future perspectives. *Mol Neurobiol* **2011,** 43, 228-53.

6. Roth, B. L.; Craigo, S. C.; Choudhary, M. S.; Uluer, A.; Monsma, F. J., Jr.; Shen, Y.; Meltzer, H. Y.; Sibley, D. R. Binding of typical and atypical antipsychotic agents to 5-hydroxytryptamine-6 and 5-hydroxytryptamine-7 receptors. *J Pharmacol Exp Ther* **1994,** 268, 1403-10.

7. Abbas, A. I.; Hedlund, P. B.; Huang, X. P.; Tran, T. B.; Meltzer, H. Y.; Roth, B. L. Amisulpride is a potent 5-HT7 antagonist: relevance for antidepressant actions in vivo. *Psychopharmacology (Berl)* **2009,** 205, 119-28.

8. Cates, L. N.; Roberts, A. J.; Huitron-Resendiz, S.; Hedlund, P. B. Effects of lurasidone in behavioral models of depression. Role of the 5-HT receptor subtype. *Neuropharmacology* **2013,** 70C, 211-217.

9. Ishibashi, T.; Horisawa, T.; Tokuda, K.; Ishiyama, T.; Ogasa, M.; Tagashira, R.; Matsumoto, K.; Nishikawa, H.; Ueda, Y.; Toma, S.; Oki, H.; Tanno, N.; Saji, I.; Ito, A.; Ohno, Y.; Nakamura, M. Pharmacological profile of lurasidone, a novel antipsychotic agent with potent 5-hydroxytryptamine 7 (5-HT7) and 5-HT1A receptor activity. *J Pharmacol Exp Ther* **2010,** 334, 171-81.

10. Speranza, L.; Chambery, A.; Di Domenico, M.; Crispino, M.; Severino, V.; Volpicelli, F.; Leopoldo, M.; Bellenchi, G. C.; di Porzio, U.; Perrone-Capano, C. The serotonin receptor 7 promotes neurite outgrowth via ERK and Cdk5 signaling pathways. *Neuropharmacology* **2013,** 67, 155-67.

11. Kobe, F.; Guseva, D.; Jensen, T. P.; Wirth, A.; Renner, U.; Hess, D.; Muller, M.; Medrihan, L.; Zhang, W.; Zhang, M.; Braun, K.; Westerholz, S.; Herzog, A.; Radyushkin, K.; El-Kordi, A.; Ehrenreich, H.; Richter, D. W.; Rusakov, D. A.; Ponimaskin, E. 5-HT7R/G12 signaling regulates neuronal morphology and function in an age-dependent manner. *J Neurosci* **2012,** 32, 2915-30.

12. Bonaventure, P.; Kelly, L.; Aluisio, L.; Shelton, J.; Lord, B.; Galici, R.; Miller, K.; Atack, J.; Lovenberg, T. W.; Dugovic, C. Selective blockade of 5-hydroxytryptamine (5-HT)7 receptors enhances 5-HT transmission, antidepressant-like behavior, and rapid eye movement sleep suppression induced by citalopram in rodents. *J Pharmacol Exp Ther* **2007,** 321, 690-8.

13. Hedlund, P. B.; Huitron-Resendiz, S.; Henriksen, S. J.; Sutcliffe, J. G. 5-HT7 receptor inhibition and inactivation induce antidepressantlike behavior and sleep pattern. *Biol Psychiatry* **2005,** 58, 831-7.

14. Wesolowska, A.; Tatarczynska, E.; Nikiforuk, A.; Chojnacka-Wojcik, E. Enhancement of the anti-immobility action of antidepressants by a selective 5-HT7 receptor antagonist in the forced swimming test in mice. *Eur J Pharmacol* **2007,** 555, 43-7.

15. Wesolowska, A.; Nikiforuk, A.; Stachowicz, K.; Tatarczynska, E. Effect of the selective 5-HT7 receptor antagonist SB 269970 in animal models of anxiety and depression. *Neuropharmacology* **2006,** 51, 578-86.

16. Guscott, M.; Bristow, L. J.; Hadingham, K.; Rosahl, T. W.; Beer, M. S.; Stanton, J. A.; Bromidge, F.; Owens, A. P.; Huscroft, I.; Myers, J.; Rupniak, N. M.; Patel, S.; Whiting, P. J.; Hutson, P. H.;

Fone, K. C.; Biello, S. M.; Kulagowski, J. J.; McAllister, G. Genetic knockout and pharmacological blockade studies of the 5-HT7 receptor suggest therapeutic potential in depression. *Neuropharmacology* **2005,** 48, 492-502.

17.   Lee, C. M.; Farde, L. Using positron emission tomography to facilitate CNS drug development. *Trends Pharmacol Sci* **2006,** 27, 310-6.

18.   Zhang, M. R.; Haradahira, T.; Maeda, J.; Okauchi, T.; Kida, T.; Obayashi, S. Synthesis and preliminary PET study of the 5-HT(7) receptor antagonist [11C]DR4446. *J. Labelled Cpd. Radiopharm.* **2002,** 45, 857-866.

19.   Herth, M. M.; Hansen, H. D.; Ettrup, A.; Dyssegaard, A.; Lehel, S.; Kristensen, J.; Knudsen, G. M. Synthesis and evaluation of [(11)C]Cimbi-806 as a potential PET ligand for 5-HT(7) receptor imaging. *Bioorg Med Chem* **2012,** 20, 4574-81.

20.   Lemoine, L.; Andries, J.; Le Bars, D.; Billard, T.; Zimmer, L. Comparison of 4 Radiolabeled Antagonists for Serotonin 5-HT7 Receptor Neuroimaging: Toward the First PET Radiotracer. *J Nucl Med* **2011**.

21.   Hansen, H. D.; Herth, M. M.; Ettrup, A.; Lehel, S.; Dyssegaard, A.; Kristensen, J. L.; Knudsen, G. M. In vivo PET imaging of cerebral 5-HT7 recptors with novel radioligands. *Journal of Cerebral Blood Flow and Metabolism* **2012,** 32, S126.

22.   Perrone, R.; Berardi, F.; Colabufo, N. A.; Lacivita, E.; Leopoldo, M.; Tortorella, V. Synthesis and structure-affinity relationships of 1-[omega-(4-aryl-1-piperazinyl)alkyl]-1-aryl ketones as 5-HT(7) receptor ligands. *J Med Chem* **2003,** 46, 646-9.

23.   Leopoldo, M.; Berardi, F.; Colabufo, N. A.; Contino, M.; Lacivita, E.; Perrone, R.; Tortorella, V. Studies on 1-arylpiperazine derivatives with affinity for rat 5-HT7 and 5-HT1A receptors. *J Pharm Pharmacol* **2004,** 56, 247-55.

24.   Leopoldo, M.; Berardi, F.; Colabufo, N. A.; Contino, M.; Lacivita, E.; Niso, M.; Perrone, R.; Tortorella, V. Structure-affinity relationship study on N-(1,2,3,4-tetrahydronaphthalen-1-yl)-4-aryl-1-piperazinealkylamides, a new class of 5-hydroxytryptamine7 receptor agents. *J Med Chem* **2004,** 47, 6616-24.

25.   Leopoldo, M.; Lacivita, E.; Contino, M.; Colabufo, N. A.; Berardi, F.; Perrone, R. Structure-activity relationship study on N-(1,2,3,4-tetrahydronaphthalen-1-yl)-4-aryl-1-piperazinehexanamides, a class of 5-HT7 receptor agents. 2. *J Med Chem* **2007,** 50, 4214-21.

26.   Andersson, J. D.; Leopoldo, M.; Finnema, S.; Lacivita, E.; Nakao, R.; De Giorgio, P.; Krasikova, R.; Varnas, K.; Halldin, C. Development of a PET radioligand for the 5-HT7 receptor. Preliminary characterizaion using autoradiography. In *The 19th International Symposium on Radiopharmaceutical Sciences*, Amsterdam, NL, 2011.

27.   Herth, M. M.; Volk, B.; Pallagi, K.; Kofoed Bech, L.; Antoni, F. A.; Knudsen, G. M.; Kristensen, J. L. Synthesis and in vitro evaluation of oxindole derivatives as potential radioligands for 5-HT(7) receptor imaging with PET. *ACS Chem Neurosci* **2012,** 3, 1002-7.

28.   Waterhouse, R. N. Determination of lipophilicity and its use as a predictor of blood-brain barrier penetration of molecular imaging agents. *Mol Imaging Biol* **2003,** 5, 376-89.

29.   Pike, V. W. PET radiotracers: crossing the blood-brain barrier and surviving metabolism. *Trends Pharmacol Sci* **2009,** 30, 431-40.

30.   Badescu, V. C. A. M. C., B. P.; Cohen, M, P.; Filla, S. A.; Gallagher, P. T.; Hellman, S. L.; Mazanetz, M. P.; Pineiro-Nunez, M. M.; Schaus, J. M.; Spinazze, P. G.; Whatton, M. A. 2-[4-(pyrazol-4-ylalkyl)piperazin-1-yl]-3-phenyl pyrazines and pyridines and 3-[4-(pyrazol-4-ylalkyl)piperazin-1-yl]-2-phenyl pyridines as 5-HT7 receptor antagonists. WO2008141020, CAN149:556666, 2008.

31.   Kaczmarek, L. Bipyridines. Part XVII. On the synthesis of [2,2'-bipyridin]-3-ol and other novel 2,2'-bipryridine derivatives from [2,2'-bipyridine]-3,3'-diamine. *Bulletin of the Polish Academy of Sciences, Chemistry* **1985,** 33, 441-409.

32.   Leahy, J. W.; Buhr, C. A.; Johnson, H. W.; Kim, B. G.; Baik, T.; Cannoy, J.; Forsyth, T. P.; Jeong, J. W.; Lee, M. S.; Ma, S.; Noson, K.; Wang, L.; Williams, M.; Nuss, J. M.; Brooks, E.; Foster, P.; Goon, L.; Heald, N.; Holst, C.; Jaeger, C.; Lam, S.; Lougheed, J.; Nguyen, L.; Plonowski, A.; Song, J.; Stout, T.; Wu, X.; Yakes, M. F.; Yu, P.; Zhang, W.; Lamb, P.; Raeber, O. Discovery of a novel series of potent and orally bioavailable phosphoinositide 3-kinase gamma inhibitors. *J Med Chem* **2012,** 55, 5467-82.

33.   Erhardt, P. W.; Woo, C. M.; Gorczynski, R. J.; Anderson, W. G. Ultra-short-acting beta-adrenergic receptor blocking agents. 1. (Aryloxy)propanolamines containing esters in the nitrogen substituent. *J Med Chem* **1982,** 25, 1402-7.

34.   Martinez, A.; Dutasta, J.-P. Hemicryptophane–oxidovanadium(V) complexes: Lead of a new class of efficient supramolecular catalysts. *Journal of Catalysis* **2009,** 267, 188-192.

35.   Caccia, S. N-dealkylation of arylpiperazine derivatives: disposition and metabolism of the 1-aryl-piperazines formed. *Curr Drug Metab* **2007,** 8, 612-22.

36.   Hedlund, P. B.; Leopoldo, M.; Caccia, S.; Sarkisyan, G.; Fracasso, C.; Martelli, G.; Lacivita, E.; Berardi, F.; Perrone, R. LP-211 is a brain penetrant selective agonist for the serotonin 5-HT(7) receptor. *Neurosci Lett* **2010,** 481, 12-6.

37.   Cohen, M. P. F., S. A.; Hellman, S. L.; Hollinshead, S. P.; Tidwell, M. W. Substituted piperazinyl pyrazines and pyridines as 5-HT7 receptor antagonists. WO2009029439, 2009.

38.   Lacivita, E.; Patarnello, D.; Stroth, N.; Caroli, A.; Niso, M.; Contino, M.; De Giorgio, P.; Di Pilato, P.; Colabufo, N. A.; Berardi, F.; Perrone, R.; Svenningsson, P.; Hedlund, P. B.; Leopoldo, M. Investigations on the 1-(2-biphenyl)piperazine motif: identification of new potent and selective ligands for the serotonin(7) (5-HT(7)) receptor with agonist or antagonist action in vitro or ex vivo. *J Med Chem* **2012,** 55, 6375-80.

39.   Varnas, K.; Thomas, D. R.; Tupala, E.; Tiihonen, J.; Hall, H. Distribution of 5-HT7 receptors in the human brain: a preliminary autoradiographic study using [3H]SB-269970. *Neurosci.Lett.* **2004,** 367, 313-316.

40.   Cunningham, V. J.; Rabiner, E. A.; Slifstein, M.; Laruelle, M.; Gunn, R. N. Measuring drug occupancy in the absence of a reference region: the Lassen plot re-visited. *J Cereb Blood Flow Metab* **2010,** 30, 46-50.

41.   Ettrup, A.; Mikkelsen, J. D.; Lehel, S.; Madsen, J.; Nielsen, E. O.; Palner, M.; Timmermann, D. B.; Peters, D.; Knudsen, G. M. 11C-NS14492 as a novel PET radioligand for imaging cerebral alpha7 nicotinic acetylcholine receptors: in vivo evaluation and drug occupancy measurements. *J Nucl Med* **2011,** 52, 1449-56.

42.   Bertani, B. B., G.; Capelli A. M.; Checchia, A.; Di Fabio, R.; Gentile, G.; Micheli, F.; Pasquarello, A.; Tedesco, G.; Terreni, S. Azabicyclo [3.1.0] hexyl derivatives as modulators of dopamine D3 receptors. WO2007113232, CAN147:448793, 2007.

43.   Jasper, J. R.; Kosaka, A.; To, Z. P.; Chang, D. J.; Eglen, R. M. Cloning, expression and pharmacology of a truncated splice variant of the human 5-HT7 receptor (h5-HT7b). *Br J Pharmacol* **1997,** 122, 126-32.

44.   Fargin, A.; Raymond, J. R.; Regan, J. W.; Cotecchia, S.; Lefkowitz, R. J.; Caron, M. G. Effector coupling mechanisms of the cloned 5-HT1A receptor. *J Biol Chem* **1989,** 264, 14848-52.

45.   Ettrup, A.; Palner, M.; Gillings, N.; Santini, M. A.; Hansen, M.; Rasmussen, L. K.; Någren, K.; Madsen, J.; Begtrup, M.; Knudsen, G. M. Radiosynthesis and evaluation of [11C]Cimbi-5: A high affinity 5-HT2A receptor agonist radioligand for use with positron emission tomography. *J Nucl Med* **2010**.

46.   Kornum, B. R.; Lind, N. M.; Gillings, N.; Marner, L.; Andersen, F.; Knudsen, G. M. Evaluation of the novel 5-HT4 receptor PET ligand [11C]SB207145 in the Gottingen minipig. *J.Cereb.Blood Flow Metab* **2009,** 29, 186-196.

47.   Gillings, N. A restricted access material for rapid analysis of [(11)C]-labeled radiopharmaceuticals and their metabolites in plasma. *Nucl Med Biol* **2009,** 36, 961-5.
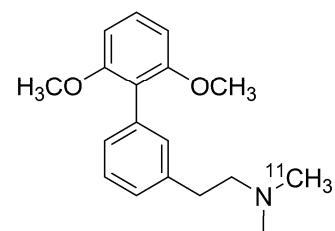
FIGURES AND FIGURE LEGENDS
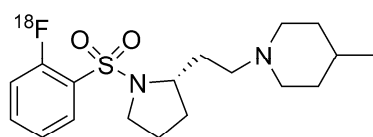
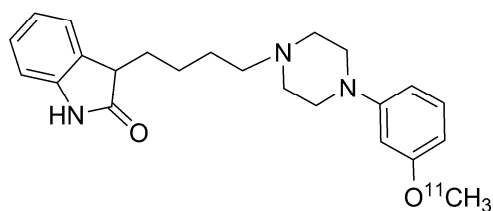**Figure 1.** Structures of 5-HT$_7$ PET radioligands.
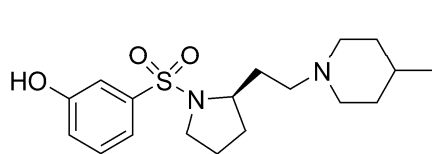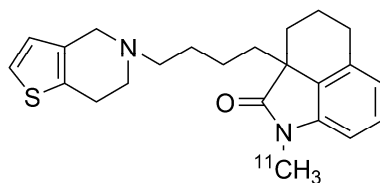
1 (SB-269970)   **2** ([^{11}C]DR4446   **3** ([^{11}C]Cimbi-806)
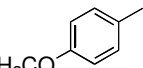
4 ([^{18}F]2FP3)   **5** ([^{11}C]Cimbi-717)   **6** ([^{11}C]PM20)
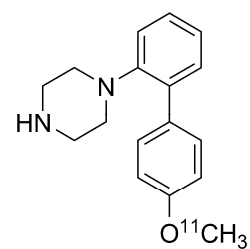
Table 1.
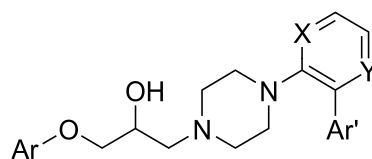
Comp.	Ar	X	Y	Ar'	$ClogD_{7.4}{}^{a}$	K_i, nM	
						5-HT$_7$	**5-HT$_{1A}$**
7	Ph	CH	CH	Ph	5.30	1.31 ± 0.2	113 ± 8.0
8	4-OCH$_3$-Ph	N	CH	2-Py	3.18	86.1 ± 2.4	134 ± 6.3
9	4-OCH$_3$-Ph	N	CH	3-Py	3.13	19.3 ± 1.1	98 ± 2.0
10	4-OCH$_3$-Ph	N	CH	4-Py	3.07	22.1 ± 0.1	22 ± 0.4
11	4-OCH$_3$-Ph	CH	N	2-Py	3.16	>1000	> 2000
12	4-OCH$_3$-Ph	CH	N	3-Py	3.20	57.0 ± 1.7	23 ± 0.9
13	4-OCH$_3$-Ph	CH	N	4-Py	3.12	16.8 ± 3.5	368 ± 25
14		CH	CH	4-OCH$_3$-Ph	3.73	1.72 ± 0.2	1184 ± 45
15		CH	CH	4-OCH$_3$-Ph	2.91	5.83 ± 1.1	255 ± 11
16		CH	CH	4-OCH$_3$-Ph	3.72	0.82 ± 0.1	119 ± 9.0
(R)-13		CH	N	4-Py	3.12	15.1 ± 2.2	50 ± 5.1
(S)-13		CH	N	4-Py	3.12	67.2 ± 5.1	1212 ± 60
(R)-16		CH	CH	4-OCH$_3$-Ph	3.72	1.1 ± 0.3	242 ± 10
(S)-16		CH	CH	4-OCH$_3$-Ph	3.72	3.4 ± 0.5	197 ± 9.5

[a]Values calculated by ACD LABS (version 9.0, NETWORK).

Scheme 1. General Synthesis of 1-[(pyridyl)-2-pyridyl]piperazines.[a]

17   →(a)→   **18**

↓(b)

19   →(c)→   **20**: Ar= 2-Py
21: Ar= 3-Py
22: Ar= 4-Py
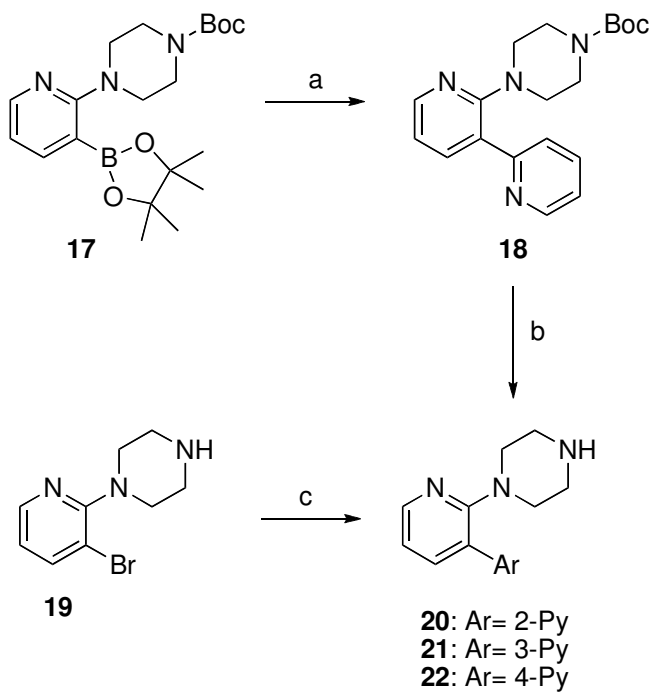
[a]Reagents and conditions: (a) 2-bromopyridine, Pd(PPh$_3$)$_4$, K$_2$CO$_3$, DME/H$_2$O, microwave irradiation, 3 min at 100 °C, quantitative yield; (b) TFA, DCM, rt, 3h, 90%; (c) 3- or 4-pyridineboronic acid, Pd(PPh$_3$)$_4$, 2 M K$_2$CO$_3$, reflux, 18 h, 50-55% yield.

Scheme 2. General Synthesis of 1-[(pyridyl)-3-pyridyl]piperazines.[a]

23

24

25: Ar= 3-Py
26: Ar= 4-Py

27: Ar= 2-Py
28: Ar= 3-Py
29: Ar= 4-Py
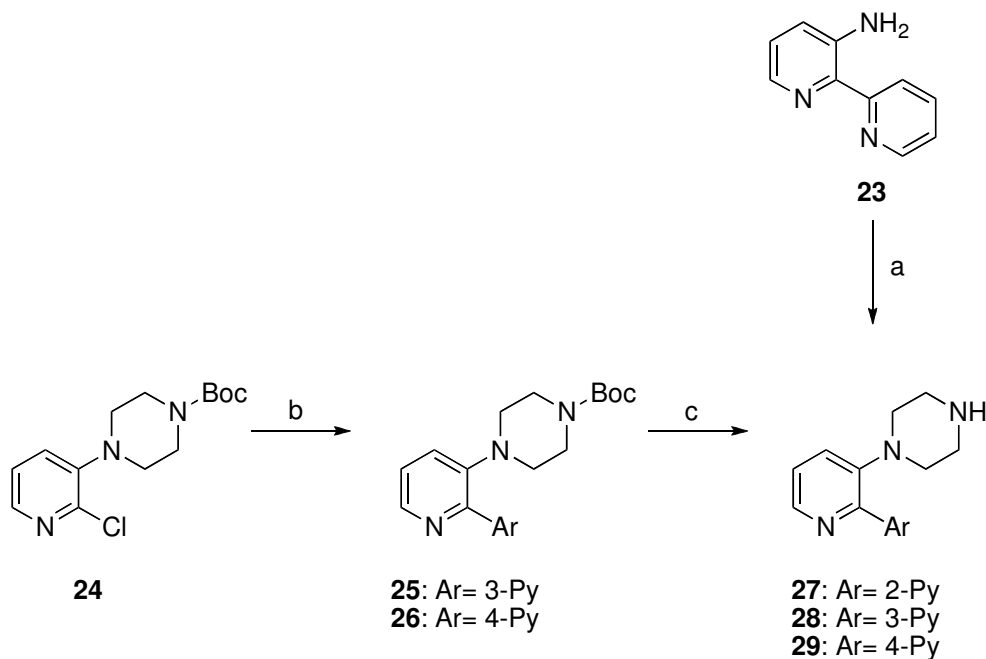
[a]Reagents and conditions: (a) bis 1-(2-chloroethyl)amine, K_2CO_3, KI, xylene, reflux, 48 h, 21% yield; (b) 3- or 4-pyridineboronic acid, $Pd(PPh_3)_4$, K_2CO_3, DME, 100 °C, 22h, 35-50% yield; (c) TFA, DCM, rt, 3h, 90% yield.

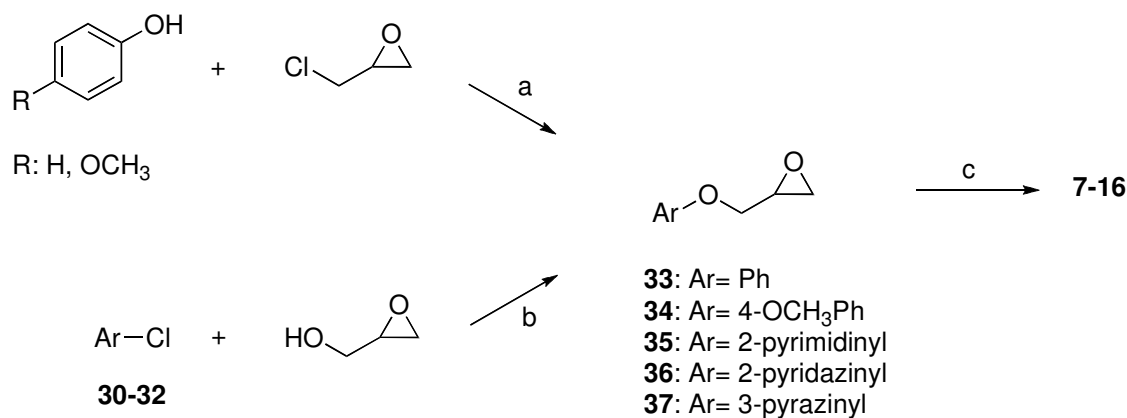**Scheme 3.** General Synthesis of Racemic Target Compounds.[a]

R: H, OCH_3

30-32

33: Ar= Ph
34: Ar= 4-OCH_3Ph
35: Ar= 2-pyrimidinyl
36: Ar= 2-pyridazinyl
37: Ar= 3-pyrazinyl

7-16

[a]Reagents and conditions: (a) NaOH, H_2O, 100 °C, 3h, 50-55% yield; (b) NaH, DMF, 0 °C to rt, overnight, 10-90% yield; (c) 1-arylpiperazine, EtOH, reflux, 3-5h, 30-90% yield.

Scheme 4. Synthesis of Enantiomerically Pure Target Compounds.[a]

(R)-(-)glycydyl nosilate

a

(R)-**34**

b

(R)-**13**

a

(S)-(+)glycydyl nosilate

(S)-**34**

b

(S)-**13**

(R)-(+)glycydol

a

(S)-**37**

b

(S)-**16**

a

(S)-(-)glycydol

(R)-**37**

b

(R)-**16**
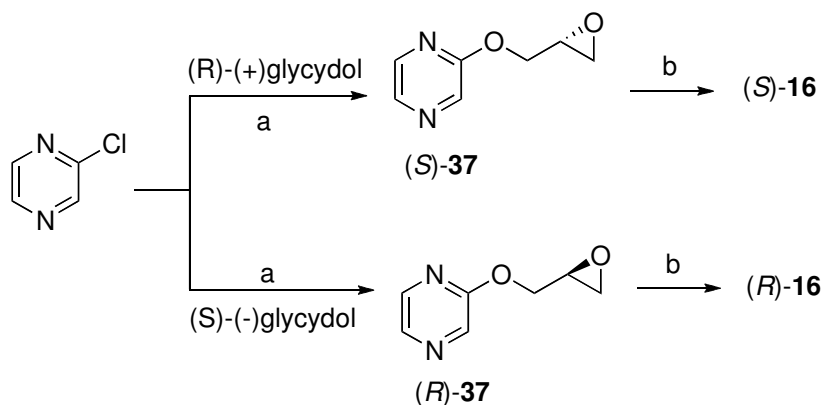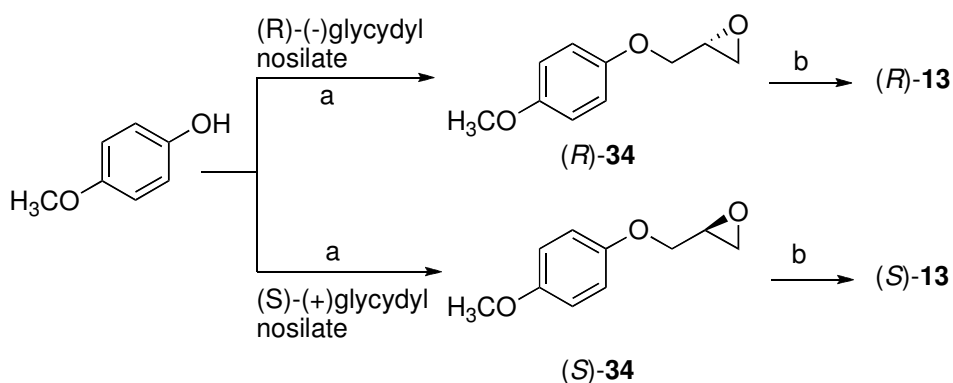
[a]Reagents and conditions: (a) NaH, DMF, 0 °C to rt, overnight, 22-73% yield; (b) 1-[2-(4-pyridyl)-3-pyridyl]piperazine or 1-[2-(4-methoxyphenyl)phenyl]piperazine, EtOH, reflux, 3-4h, 42-67% yield.

Scheme 5. Radiosynthesis of [^{11}C](R)-16.[a]

a

38

b

(R)-**39**

c

[^{11}C]-(R)-**16**
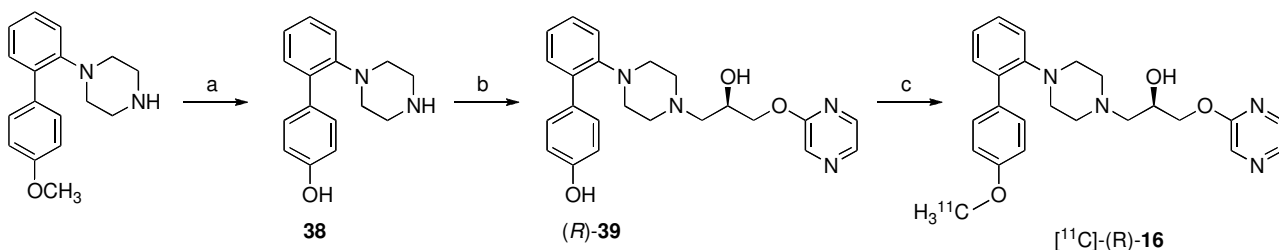
[a]Reagents and conditions: (a) HBr 48%, reflux, overnight, 65% yield; (b) (R)-**38**, EtOH, reflux, 4h, 56% yield; (c) [^{11}C]CH$_3$I, DMF, 2 M NaOH, 180 °C, 2 min.

Figure 2. Time-activity curves of $[^{11}C](R)$-**16.**
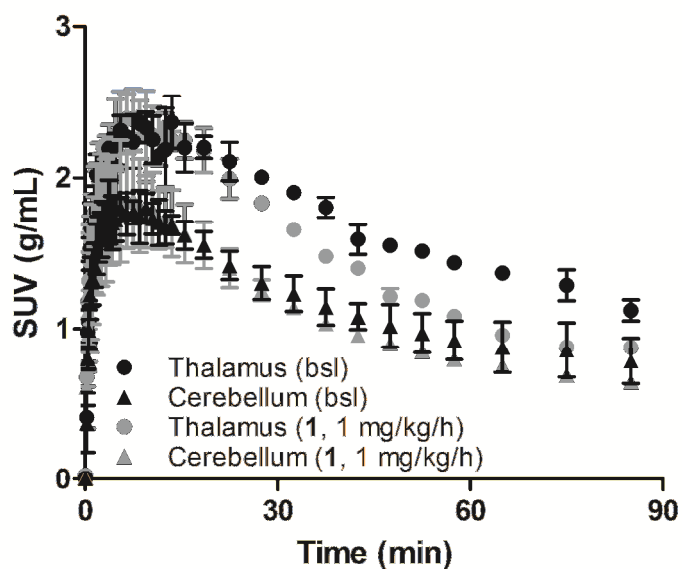
Regional time-activity curves of $[^{11}C](R)$-**16** for thalamus (circles) and cerebellum (triangles) at baseline (black symbols) and after pre-treatment with SB-269970 (**1,** 1 mg/kg/h, grey symbols). SUV = standardized uptake value. Error bars represent standard deviation (n=2) of both baseline and pre-treatment experiments.

Figure 3. Summed PET images of the pig brain
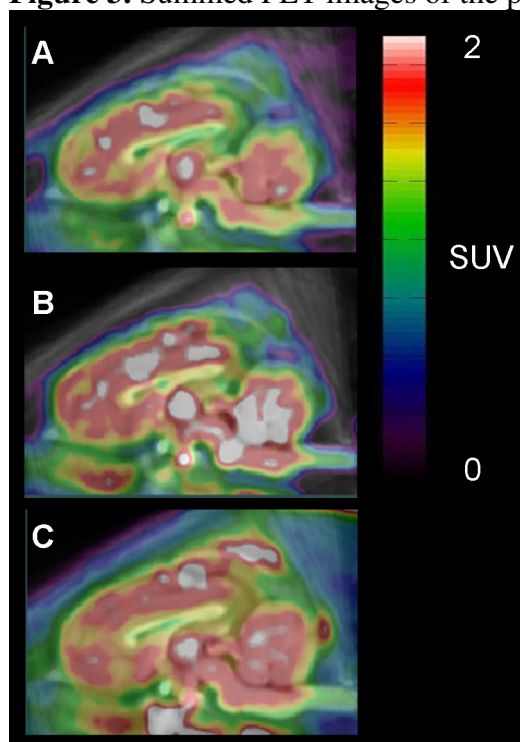
Summed PET sagittal images of the pig brain after injection of $[^{11}C](R)$-**16** at A) baseline, B) pretreatment with the PgP transporter inhibitor cyclosporine A (22.5 mg/kg + 7.5 mg/kg/h) C) pretreatment with the 5-HT$_7$ receptor selective antagonist **1** (1 mg/kg/h).

Figure 4. Quantification of $[^{11}C](R)$-**16** binding
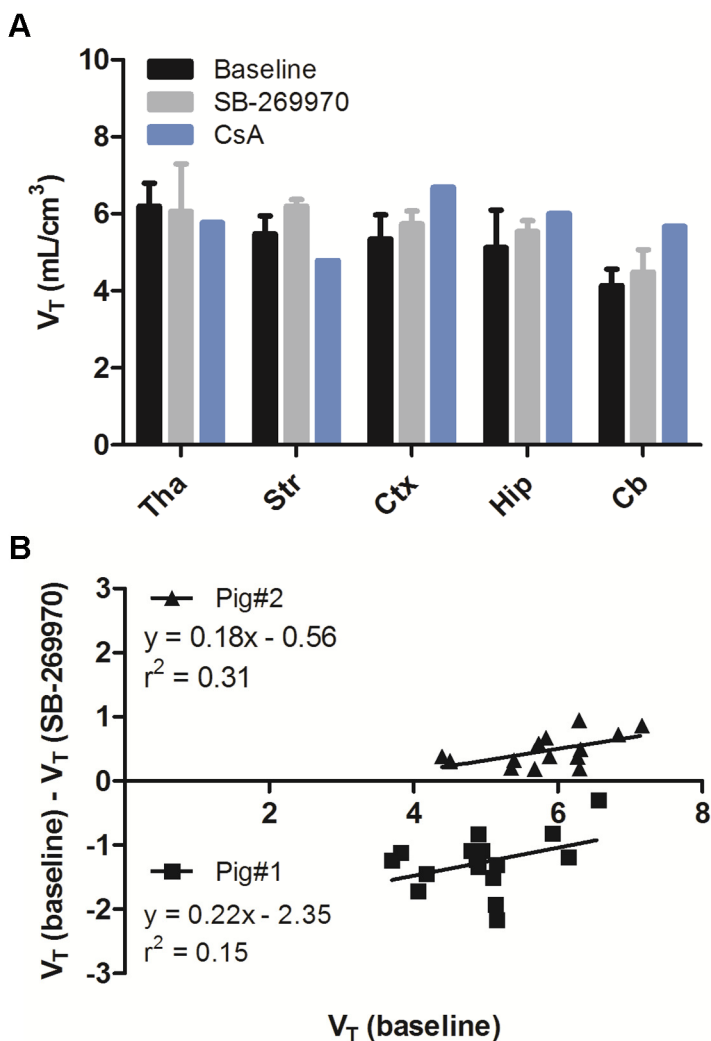
A) Distribution volumes (V_T) of $[^{11}C](R)$-**16** at baseline (n=2, black), after pretreament with **1** (n=2, grey) and after pretreatment with Cyclosporine A (CsA) (n=1, blue). **B**) Occupancy plots for $[^{11}C](R)$-16. Linear regression and goodness-of-fit (R^2) are indicated in the plot. Tha: thalamus, Str: striatum, Ctx: cortex, Hip: hippocampus, Cb: cerebellum.

Figure 5. Metabolism of [^{11}C](R)-**16**
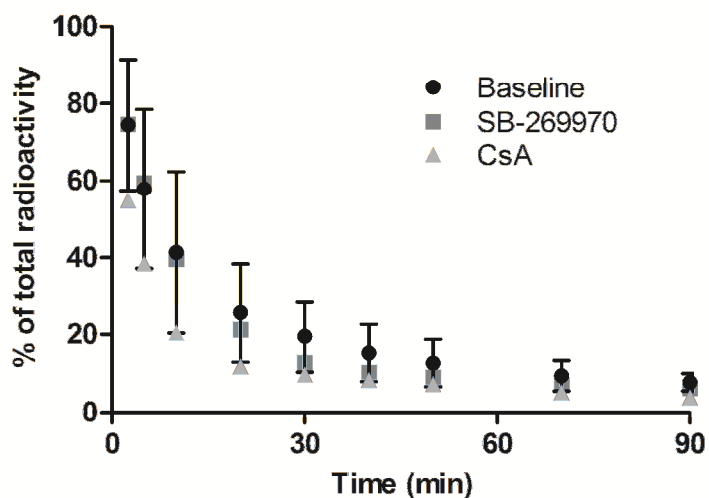
HPLC analysis of parent compound in pig plasma after i.v. injection of [^{11}C](R)-**16** at baseline (circles, n=2), pretreatment with cyclosporine A (CsA, triangles, n=1), and after pretreatment with **1** (squares, n=1). Parent compound is given as percent of total radioactivity.

SUPPLEMENTARY FIGURES

Supplementary Figure 1: Semi-preparative HPLC chromatograms of the [^{11}C](R)-**16**
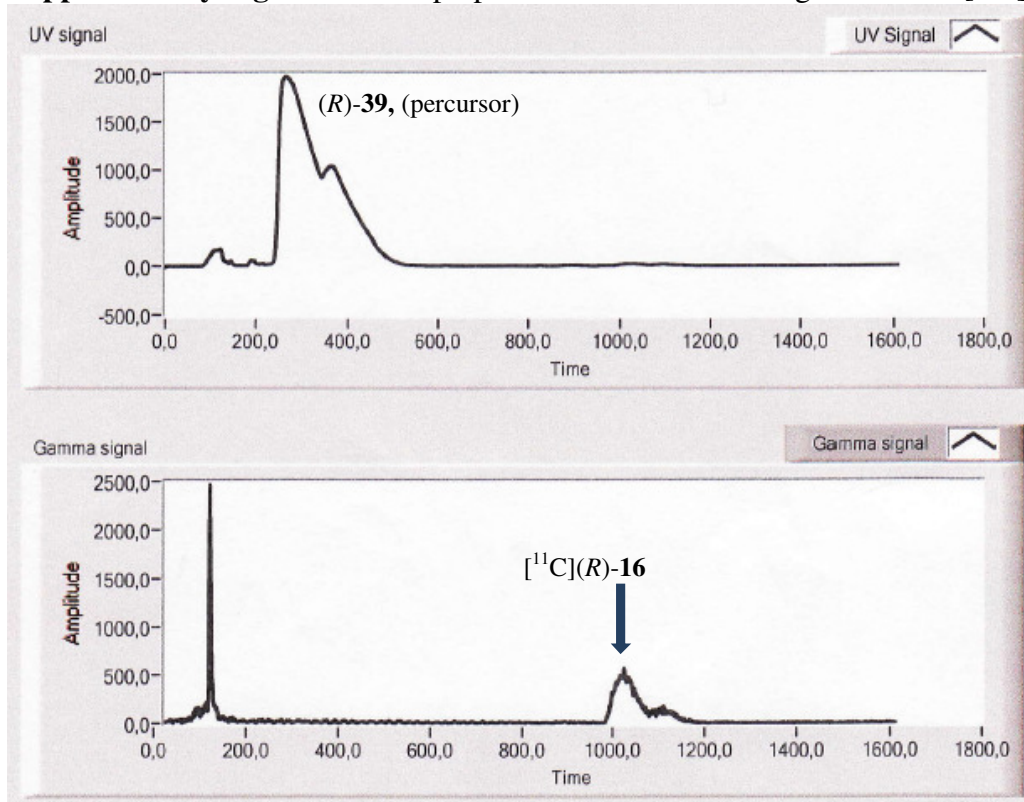
Supplementary Figure 2: Analytical HPLC chromatograms of (*R*)-**16** (BA10 in the figure) and the precursor (*R*)-**39** (EL-418 in the figure).
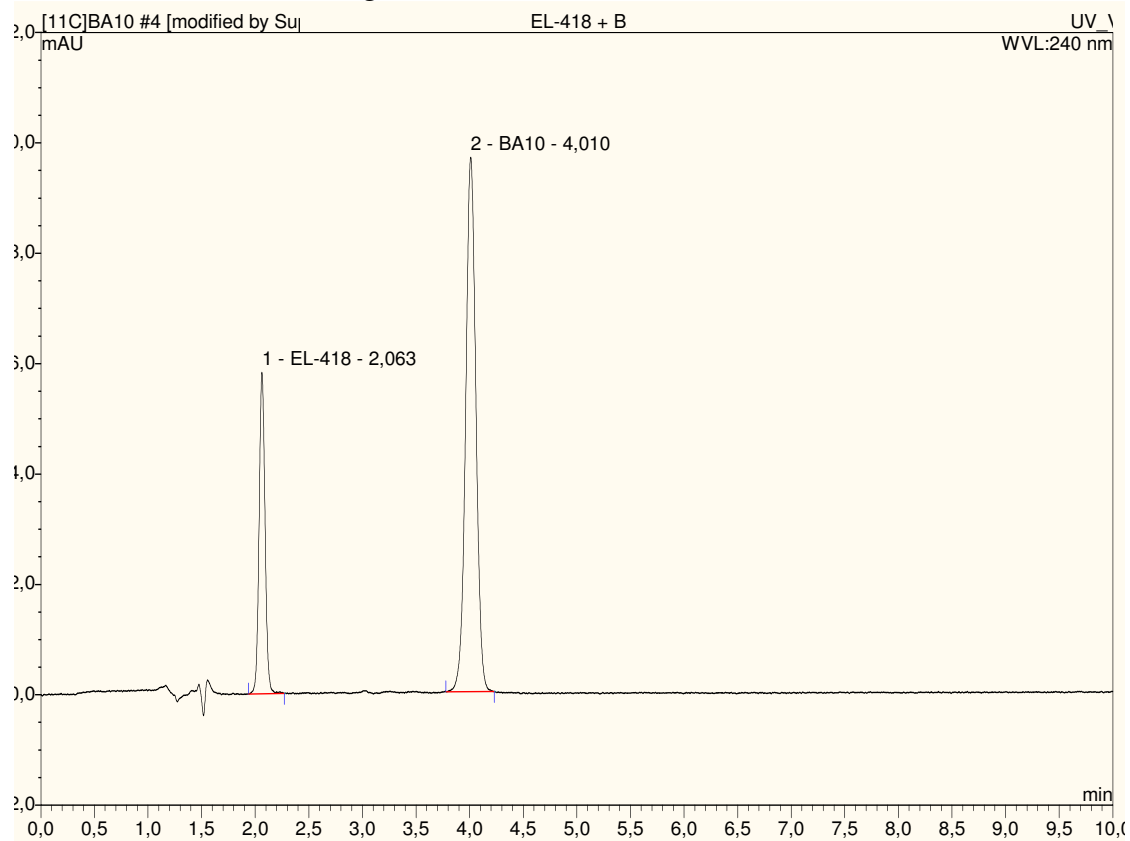
Supplementary Figure 3: HPLC chromatograms of (*R*)-**16** (grey) and [^{11}C](*R*)-**16** (black)
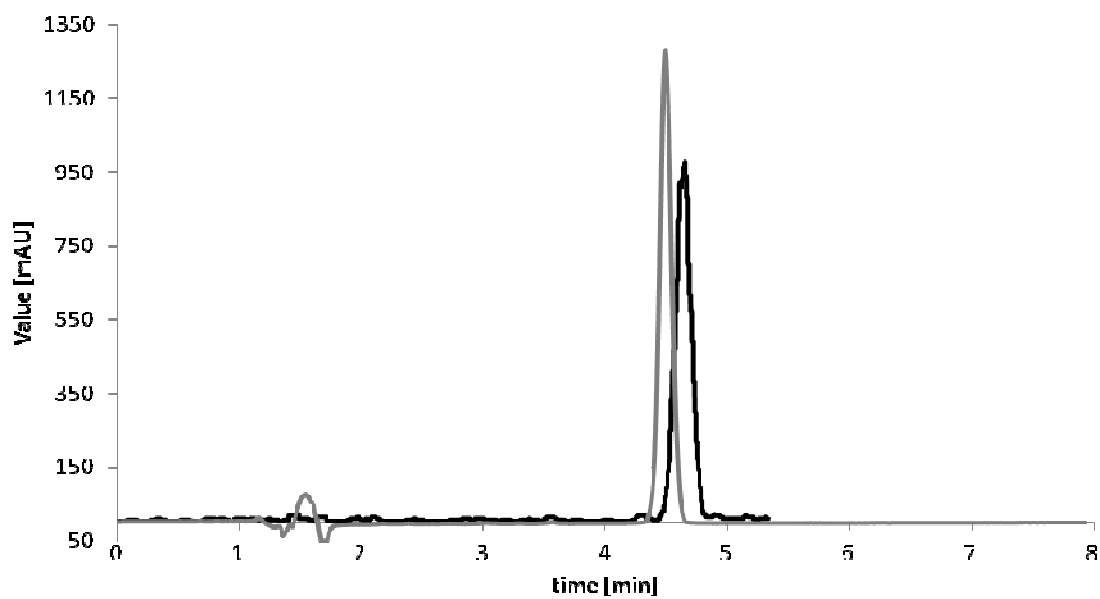
Paper III

Herth MM*, **Hansen HD***, Ettrup A, Dyssegaard A,
Lehel S, Kristensen J, and Knudsen GM.

Synthesis and evaluation of [^{11}C]Cimbi-806 as a potential
PET ligand for 5-HT$_7$ receptor imaging.

* Equal contributions.

Synthesis and evaluation of [11C]Cimbi-806 as a potential PET ligand for 5-HT7 receptor imaging

Matthias M. Herth [a,b,c,†], Hanne D. Hansen [a,†], Anders Ettrup [a], Agnete Dyssegaard [a], Szabolcs Lehel [c], Jesper Kristensen [b], Gitte M. Knudsen [a,*]

[a] Center for Integrated Molecular Brain Imaging, Rigshospitalet and University of Copenhagen, Blegdamsvej 9, DK-2100 Copenhagen, Denmark
[b] Institute for Medicinal Chemistry, The Faculty of Pharmaceutical Sciences, University of Copenhagen, Universitetsparken 2, DK-2100 Copenhagen, Denmark
[c] PET and Cyclotron Unit, Rigshospitalet, Blegdamsvej 9, DK-2100 Copenhagen, Denmark

ABSTRACT

2-(2′,6′-Dimethoxy-[1,1′-biphenyl]-3-yl)-N,N-dimethylethanamine has been identified as a potent ligand for the serotonin 7 (5-HT7) receptor. In this study, we describe the synthesis, radiolabeling and in vivo evaluation of [11C]2-(2′,6′-dimethoxy-[1,1′-biphenyl]-3-yl)-N,N-dimethylethanamine ([11C]Cimbi-806) as a radioligand for imaging brain 5-HT7 receptors with positron emission tomography (PET). Precursor and reference compound was synthesized and subsequent 11C-labelling with [11C]methyltriflate produced [11C]Cimbi-806 in specific activities ranging from 50 to 300 GBq/μmol. Following intravenous injection, brain uptake and distribution of [11C]Cimbi-806 was assessed with PET in Danish Landrace pigs. The time–activity curves revealed high brain uptake in thalamic and striatal regions (SUV ∼2.5) and kinetic modeling resulted in distribution volumes (V_T) ranging from 6 mL/cm³ in the cerebellum to 12 mL/cm³ in the thalamus. Pretreatment with the 5-HT7 receptor antagonist SB-269970 did not result in any significant changes in [11C]Cimbi-806 binding in any of the analyzed regions. Despite the high brain uptake and relevant distribution pattern, the absence of appropriate in vivo blocking with a 5-HT7 receptor selective compounds renders the conclusion that [11C]Cimbi-806 is not an appropriate PET radioligand for imaging the 5-HT7 receptor in vivo.

© 2012 Elsevier Ltd. All rights reserved.

1. Introduction

The brain serotonin (5-HT) system is known to be involved in various central nervous system (CNS) disorders, for example, depression,[1] and drugs with pharmacological effects on the 5-HT system are among the most frequently used for brain disorders. The most recently discovered receptor in the 5-HT receptor family, the 5-HT7 receptor, is also considered associated with depression. The atypical antipsychotic drug amisulpride has antidepressive effects[2,3] and studies in 5-HT7 receptor knock-out mice support that the 5-HT7 receptor antagonism of amisulpride causes this effect.[4] Other atypical antipsychotics also have relative high affinity for the 5-HT7 receptor although their direct involvement in alleviating depressive symptoms through 5-HT7 antagonism remains to be investigated.[5,6] Furthermore, there is also evidence that the 5-HT7 receptor is involved in psychosis, circadian rhythm, and sleep architecture (for review see[7]).

In vivo studies of cerebral 5-HT7 receptor binding in humans would provide a significant advance in the understanding of the above mentioned physiology and pathophysiology. Positron emission tomography (PET) is used to non-invasively quantify neuroreceptor binding in vivo and the availability of an appropriate PET radiotracer for the 5-HT7 receptor would be of particular interest. Previous attempts to develop a 5-HT7 receptor PET radioligand have been made but unfortunately so far with limited success.[8,9] Most recently, an 18F-labeled SB-269970 derivative was synthesized and evaluated[10,11] but in this study the arterial input function was not determined and in the absence of a valid reference region, the 5-HT7 receptor selectivity in vivo of this PET radioligand still remains to be determined.

In the past years, several lead structures of 5-HT7 receptor binding ligands have been identified within different structural classes.[12] Among these lead structures, biphenethylamines represent an easy moiety for both organic synthesis and radiochemical labelling and in addition has an interesting selectivity profile.[13,14] Especially, 2-(2′,6′-dimethoxy-[1,1′-biphenyl]-3-yl)-N,N-dimethylethanamine (Cimbi-806) is of interest, because of its simple synthesis and its favorable dissociation constant (K_i) for the 5-HT7 receptor (K_i = 8.6 nM) over the 5-HT1A receptor (K_i = 4826 nM).[13] This large

* Corresponding author. Tel.: +45 3545 6720; fax: +45 3545 6713.
  E-mail address: gmk@nru.dk (G.M. Knudsen).
† Both authors have contributed equally.

difference in K_i is necessary because of the relative low 5-HT$_7$ receptor density (B_{max}) in the brain and also because 5-HT$_7$ and 5-HT$_{1A}$ receptors are located in similar brain regions, such as the hippocampus and cortical areas.[15,16] Based on the literature values,[15,16] one can compute that in order to ensure that less than 10% PET signal from the 5-HT$_{1A}$ receptors, a selectivity of at least 350-fold (based on B_{max} values in relevant regions) is required for specific imaging the cerebral 5-HT$_7$ receptor binding.

In this study, we synthesized the precursor for [^{11}C]Cimbi-806 radiolabelling and subsequently evaluated its in vivo brain uptake and binding characteristics in the pig.

2. Results and discussion

2.1. Organic chemistry

Bisphenylethylamines were synthesized a similar manner as previously described.[13] The method involves formation of 2,6-dimethoxybenzeneboronic acid (**4**) and bromoethylamine derivatives, which were consequently reacted via Suzuki-cross-coupling to form the bisphenylethylamine matrix of [^{11}C]Cimbi-806. The Suzuki reaction was performed in good yields (>80%) under inert conditions in a microwave in 2–4 h. Reaction times of the cross-coupling varied and therefore, the completion of reaction was checked by thin layer chromatography. However, conventional heating for 12 h lead mainly to the reduced phenethylamine derivative rather than the bisphenylethylamine. Syntheses of precursor and reference compound of Cimbi-806 are summarized in Scheme 1.

To minimize synthesis efforts, both precursor and the reference compound of [^{11}C]Cimbi-806 was produced in an one-reaction sequence. Thus, 3-bromophenethylamine was not directly bismethylated, but Boc-protected which resulted in an almost complete conversion. 2,6-dimethoxybenzeneboronic acid (**4**) was synthesized in moderate yields (~30%) by lithiating 1,3-dimethoxybenzene and then reacting with B(OMe)$_3$. Afterwards, the Boc-protected derivative (**1**) and the boronic acid (**4**) were cross-coupled in excellent yields (~90%).

Several unsuccessful attempts were made to synthesize the precursor (**6**) from this cross-coupled intermediate (**5**). Reduction of the carbamate to the mono-methylated secondary amine with 4 equiv of LiAlH failed and only trace amounts of the precursor (**6**) could be detected via gas chromatography. In addition, methylation of (**5**) by activating the amine with NaH and reacting with MeI followed by TFA Boc-deprotecting only resulted in primary amine (**8**), probably since the alkylation was hindered by the Boc-group. However, Boc-deprotection of (**5**) leads to yields close to 80% and consequently reductive alkylation with aqueous formaldehyde resulted in the reference compound (Cimbi-806) in excellent yields (~80%).

Two strategies were applied to synthesize the precursor: Monomethylated bromophenylethylamine was produced starting either by reacting 3-bromophenethylbromide with aqueous methylamine in a condensation reaction or by nosylation and methylation of 3-bromophenethylamine in a one-pot reaction. The condensation reaction only resulted in poor amounts (~10%) of (**2**) even when different bases or varying temperatures were applied. However, the Nosyl-protection followed by base activated methylation with MeI resulted in complete conversion to (**3**).

Cross-coupling of (**2**) and (**3**) with 2,6-dimethoxybenzeneboronic acid (**4**) under microwave yielded in the precursor (**6**) or the intermediate (**7**) (~80–90%). The following thiolysis of (**7**) to the precursor (**6**) succeeded in 52% without any attempts to optimize this deprotection step, such as using higher concentration of thiol groups or increasing the reaction temperature. We isolated (**6**) in sufficient amounts for labelling purposes as well as for synthesising Cimbi-806 via reductive alkylation. Taken together, the

precursor (**6**) and the reference compound of [^{11}C]Cimbi-806 were synthesized in sufficient amounts in overall chemical yields of 43% and 28%, respectively.

2.2. Lipophilicity

The lipophilicities of promising compounds were determined using the HPLC method according to Krass et al.[17] The log$D$ of Cimbi-806 was determined to be 4.4. This value may appear a little high compared to the optimal log$D$ interval for small molecules to penetrate the blood–brain-barrier (BBB) as suggested by Rowley et al.[18] to be 2–3. But in our set-up other known CNS-PET ligands (e.g., MDL 100907, altanserin or WAY 100635) show similar high values. This fact gives rise to the assumption that [^{11}C]Cimbi-806 may have similarly good properties for molecular imaging.

2.3. In vitro autoradiography

The in vitro dissociation constant (K_i) for Cimbi-806 displacement of [^{3}H]SB-269970 binding on pig brain sections was 8.82 ± 0.04 nM (Fig. 1), in accordance with the previously reported K_i-value.[13] The displacement of [^{3}H]SB-269970 by Cimbi-806 was encouraging for in vivo PET experiments.

2.4. Radiochemistry

Radiolabeling of [^{11}C]Cimbi-806 (Scheme 2) using only 0.3 mg precursor (**6**) and [^{11}C]CH$_3$OTf was done with a fully automated system (RCY ~95%).[19] [^{11}C]Cimbi-806 at ~400 s was the only radioactive peak that was observed. Precursor (**6**) eluted 80 s prior to the radiolabelled product as indicated by the UV-absorption (data not shown). The radiosynthesis including HPLC purification and formulation generated an injectable solution of [^{11}C]Cimbi-806 (radiochemical purity >96%) within 80–90 min. Typically, 0.6–1.8 GBq of [^{11}C]Cimbi-806 was isolated with a specific activities (A_s) of 50–300 GBq/µmol at end of synthesis.

2.5. In vivo PET imaging

After intravenous injection of [^{11}C]Cimbi-806, a rapid and high uptake in the pig brain was observed (Fig. 2). Time-activity curves (TACs) and summed PET images show highest [^{11}C]Cimbi-806 uptake in the thalamus and the striatum and lowest uptake in the cerebellum. The TACs showed reversible kinetics of [^{11}C]Cimbi-806 with peak SUV at ~20 min followed by a relative fast decline in tissue activity.

With the high uptake of Cimbi-806 as seen in these experiments, the relatively high lipophilicity value for Cimbi-806 does not seem to be a problem. This outcome also holds true for many other CNS-PET ligands (e.g., MDL 100907, altanserin, and WAY 100635) where high values are determined, but the tracers have good brain uptake.

To investigate the selectivity of [^{11}C]Cimbi-806 in vivo, blocking experiments was performed in three pigs after the baseline scan. Pre-treatment followed by continuous infusion throughout the scan with 0.5 or 1.0 mg/kg/h of SB-269970 did not result in any significant changes in [^{11}C]Cimbi-806 distribution volumes. Contrary to the expected displacement, and increased uptake of [^{11}C]Cimbi-806 was observed in the thalamus, as seen on the TACs (Fig. 2B). This effect was only observed in the thalamus region and not in any other region investigated. All metabolite corrected plasma input functions were analyzed but no significant changes were observed in input function between baseline and blocked (SB-269970) conditions. The difference in uptake cannot be ascribed to blocking of peripheral 5-HT$_7$ receptor sites by the SB-269970 compound.
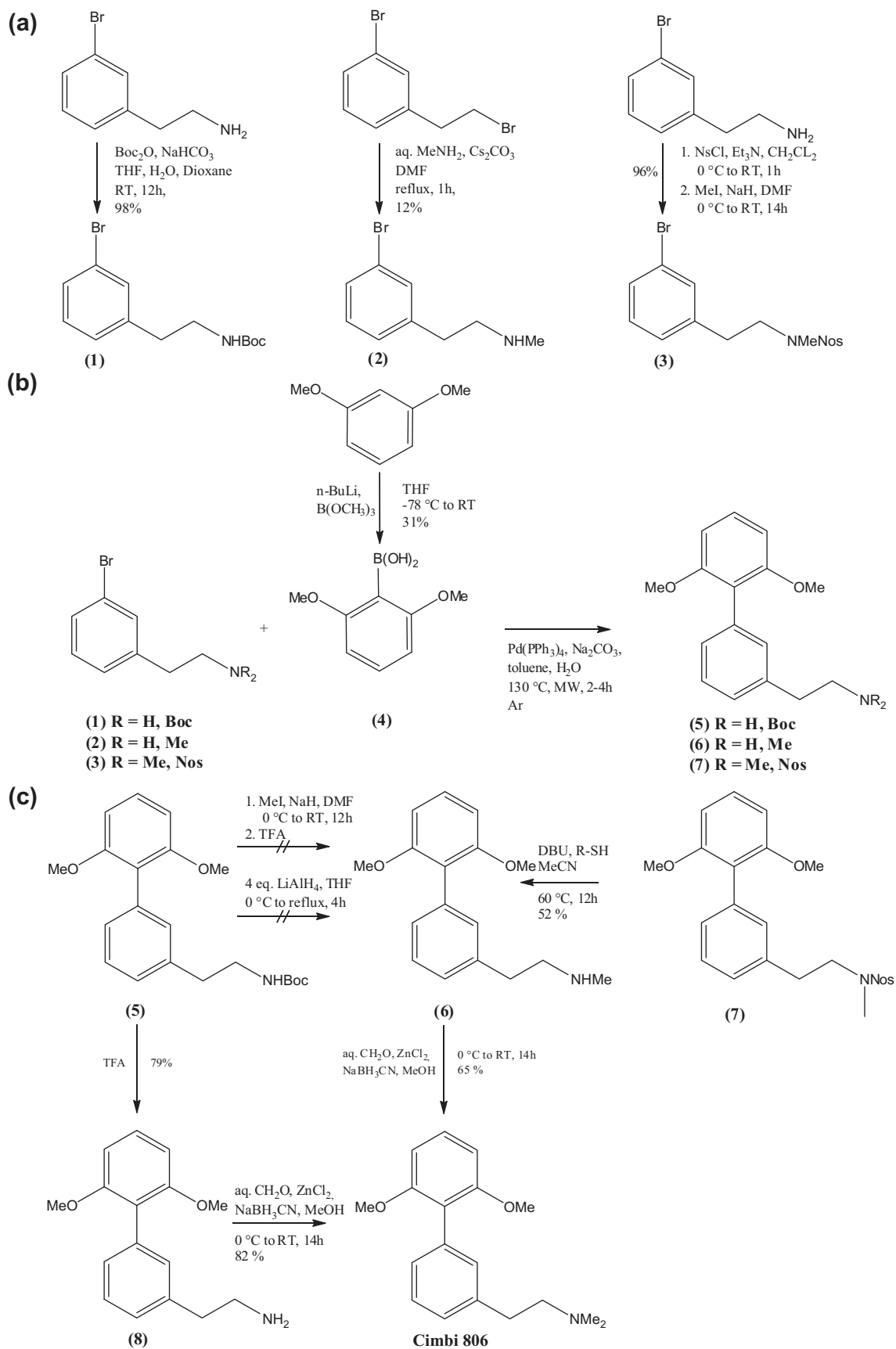
Scheme 1. Chemical syntheses: (a) Synthesis of 3-bromophenethylamine derivatives (b) Synthesis route for the biphenyl core (c) Synthesis of precursor and reference compound of [^{11}C]Cimbi-806.
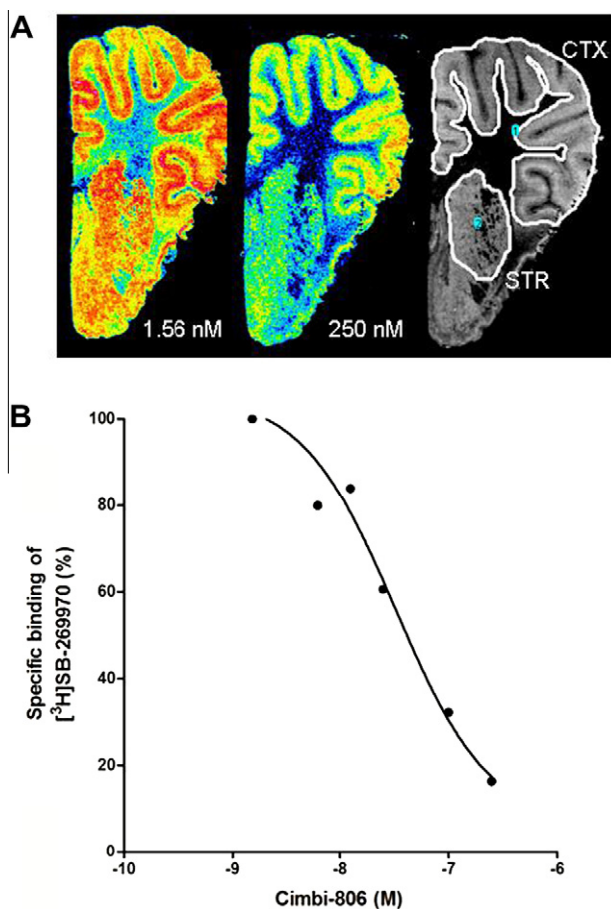
Figure 1. (A) In vitro competition autoradiography images with [³H]SB-269970 and two concentrations of **Cimbi-806** (left: 1.56 nM, right: 250 nM). (B) Inhibition of [³H]SB-269970 binding to pig brain sections by **Cimbi-806**.

In all pigs, full arterial plasma parent compound input curves were measured and these were used to calculate the distribution volumes (V_T) of [¹¹C]Cimbi-806 in volumes of interest (VOIs) using a one-tissue compartment (1-TC) model. An averaged metabolite curve (based on seven separate injections) was used to correct plasma activity for parent compound fraction as previously described[20]

No significant changes in V_T after SB-269970 pre-treatment was found in any region ($P > 0.5$, 2-way analysis of variance (ANOVA), Bonferroni post-test) (Fig. 3). High similarity between the deduced amino acid sequences of human and pig 5-HT₇ receptors[21] and a pharmacokinetic study confirming BBB penetration of SB-269970

in rat,[22] makes it unlikely that the lack of blockade in this study is caused by insufficient BBB penetration of the blocking agent. Thus, since it was not displaced by the selective compound SB-269970, we could not determine if [¹¹C]Cimbi-806 in vivo binding is selective for the 5-HT₇ receptor. The lack of displacement by SB-269970 could also be due to the radioligand having non-target affinity or because of high non-specific binding in the brain.

An autoradiographic study with [³H]SB-269970 to visualize the distribution of 5-HT₇ receptors in human whole hemisphere brain sections found that binding was mainly found in the thalamus, hypothalamus and hippocampal formation of the human brain,[16] which was in good agreement with autoradiographic studies carried out on rat and guinea-pig brain sections.[23,24] However differences were found when looking at the striatum, where the 5-HT₇ selective radioligand [³H]SB-269970 shows low binding and the less selective radioligand [³H]mesulergine found high binding.[25] The autoradiographic experiments carried out on pig brain sections in this study showed high binding in the cortical areas but also relatively high binding in the striatum (Fig. 1A). With this in mind we expect high binding of [¹¹C]Cimbi-806 in the thalamus and medium binding in the striatum and cortex. Binding in the cerebellum is expected, as 5-HT₇ receptors have been found in pig cerebellum.[21] V_T values were indeed higher in thalamus and striatum and lower in the cerebellum (Fig. 3). Compared to human data, high striatal binding was not expected but as seen on the autoradiographic images it is likely that a higher density of 5-HT₇ receptors can be found in the pig striatum, and thereby accounting for the unexpected high uptake of [¹¹C]Cimbi-806.

2.6. In vivo metabolism of [¹¹C]Cimbi-806

After intravenous injection, [¹¹C]Cimbi-806 was rapidly metabolized (Fig. 4) and this generated two radiolabelled metabolites that both were less lipophilic than [¹¹C]Cimbi-806. The parent compound fraction at baseline and pre-treatment conditions, showed no significant difference, indicating that pretreatment with SB-269970 did not affect [¹¹C]Cimbi-806 metabolism. The free fraction of [¹¹C]Cimbi-806 in plasma (f_P) was 23.5 ± 5.0% (mean ± SD, $n = 10$) after 3 h when equilibrium between the dialysis chambers was reached.

3. Conclusion

Cimbi-806 and its desmethyl precursor were synthesized in sufficient yields, and ¹¹C-radiolabeling produced [¹¹C]Cimbi-806 in high specific radioactivity, high radiochemical purity and yield. Evaluation of [¹¹C]Cimbi-806 in pigs with PET scanning revealed high brain uptake, and appropriate radiometabolism with only two polar metabolites, unlikely to cross the BBB, appearing in pig plasma. Since [¹¹C]Cimbi-806 could not be displaced by the
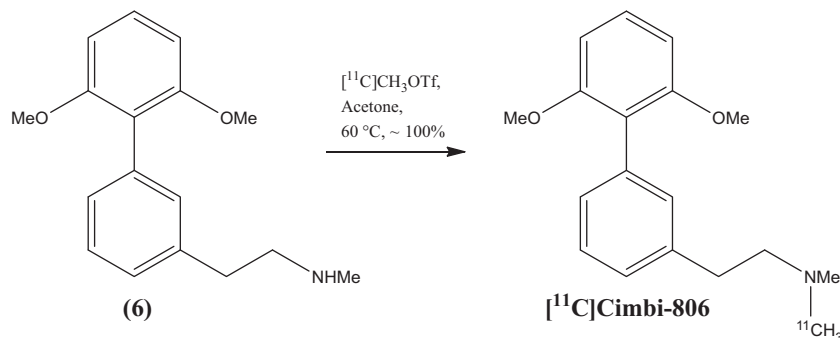
Scheme 2. Radiosynthesis of [¹¹C]Cimbi-806.

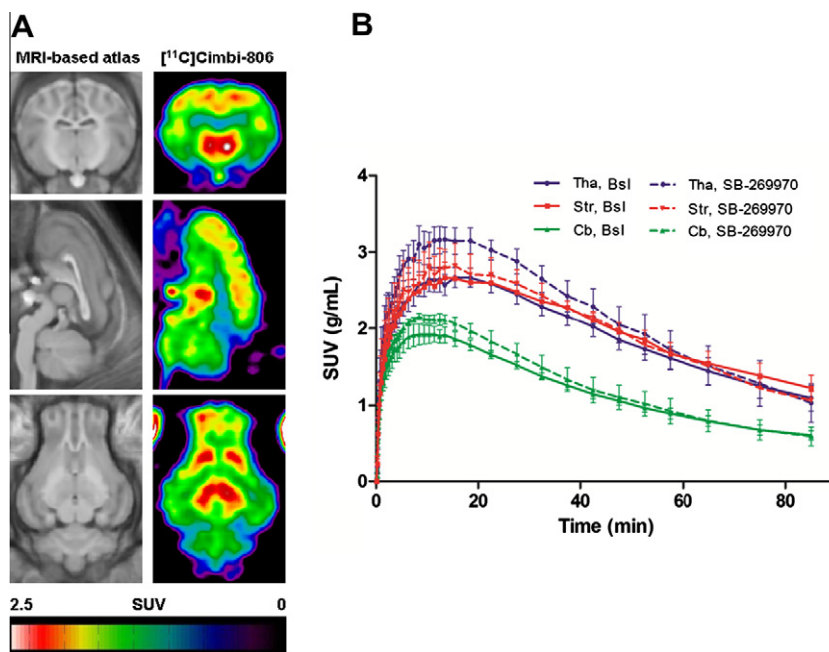**Figure 2.** (A) Representative PET images summed from 0 to 90 min scanning showing regional uptake of [¹¹C]Cimbi-806 (right column) and the standardized MRI-based atlas for the pig brain to which the PET images are co-registered (left column). (B) Time-activity curves at baseline (solid lines, $n = 5$) and blocked (dashed lines, $n = 3$) conditions. Bsl = baseline, Tha = thalamus, Str = striatum, Cb = Cerebellum, TACs are represented as standardized uptake value (SUV) ± S.E.M.
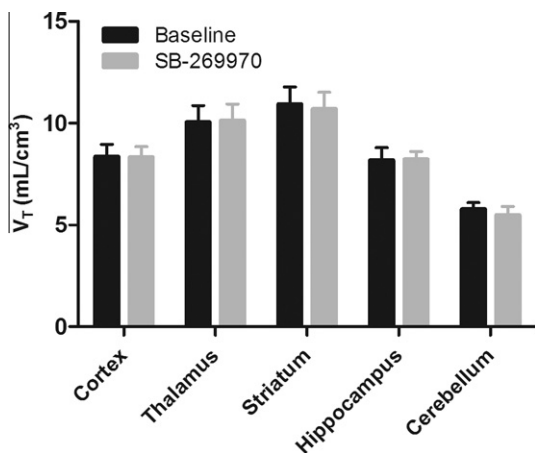
Figure 3. Distribution volumes (V_T) of [¹¹C]Cimbi-806. Mean ± S.E.M. distribution volumes for one-tissue compartment (1TC) modeling of baseline ($n = 4$) and blocked ($n = 3$) for the different brain regions.
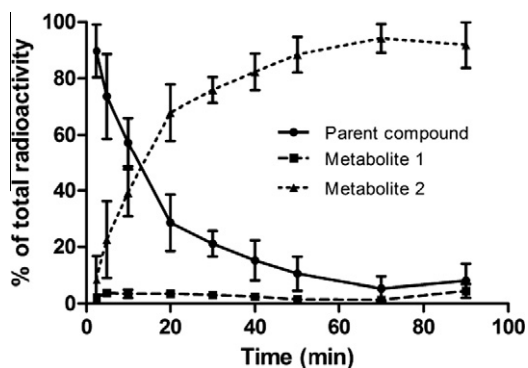
Figure 4. [¹¹C]Cimbi-806 (solid line) and metabolites (dashed lines) as a function of time after intravenous injection. The graph shows the average of measurements from seven experiments, error bars represent S.D.

selective 5-HT$_7$ receptor antagonist SB-269970 in vivo, we do not find this PET radioligand to be suitable for imaging the 5-HT$_7$ receptor.

4. Experimental details

4.1. Chemicals and equipment

Chemicals were purchased from Acros, Fluka, Sigma, Tocris, ABX or Merck. Unless otherwise stated, all chemicals were used without further purification. [³H]SB-269970 was purchased from PerkinElmer. Microwave-assisted synthesis was carried out in a Biotage Initiator apparatus operating in single mode; the microwave cavity producing controlled irradiation at 2.45 GHz (Biotage AB, Uppsala, Sweden). The reactions were run in sealed vessels (0.5–2.0 mL). These experiments were performed by employing magnetic stirring and a fixed hold time using variable power to reach (during 1–2 min) and then maintain the desired temperature in the vessel for the programmed time period. The temperature was monitored by an IR sensor focused on a point on the reactor vial glass. The IR sensor was calibrated to internal solution reaction temperature by the manufacturer. GC–MS were performed on a Shimadzu. For Solid Phase Extraction (SPE), Sep-Pak®-C18-cartridges (Waters, USA) were used. Thin Layer Chromatography (TLC) was performed using plates from Merck (Silicagel 60 F254 and Alumina oxide 60 F254). ¹H-NMR spectra were recorded using a Bruker AC 300 spectrometer. Chemical shifts are quoted as δ-values (ppm) downfield from tetramethylsilane (TMS). Field desorption (FD) mass spectra were recorded using a Finnigan MAT90 spectrometer. Analytical and preparative high performance liquid chromatography (HPLC) were performed on a Dionex system consisting of a pump P680A pump, a UVD 170U detector and a Scansys radiodetector. Metabolite analysis of pig plasma was performed using a Dionex Ultimate 3000 HPLC system consisting of a DGP-3600SD pump and an online Posi-Ram Radio Flow-Through Detector. Brain slices were cut on a HM500OM Cryostat (Microm Intl GmbH). Fuji imaging plates (IP) were scanned by a Fuji BAS-2500 scanner. PET scanning was

performed with a high-resolution research tomography scanner (HRRT, Siemens AG). [^{11}C]Methane was produced via the ^{14}N(p,α)^{11}C reaction by bombardment of an [^{14}N]N$_2$ containing 10% H$_2$ target with a 17 MeV proton beam in a Scanditronix MC32NI cyclotron.

4.2. Organic synthesis

4.2.1. [2-(3-Bromo-phenyl)-ethyl]-carbamic acid *tert*-butyl ester (1)

To a solution of 3-bromophenethylamine (3.12 g, 15.7 mmol) and NaHCO$_3$ (2.3 g, 27.38 mmol) in THF (50 mL), H$_2$O (50 mL) and dioxane (50 mL) were added (Boc)$_2$O (4.1 g, 18.8 mmol). This mixture was stirred for 12 h and then extracted with CH$_2$Cl$_2$. The combined organic layers were dried, filtered and evaporated to yield **1** (4.66 g 98%) as a colorless liquid. ^{1}H NMR (300 MHz, CDCl$_3$): δ 7.30–7.27 (m, 2H, ArH) 7.11–7.07 (m, 2H, ArH), 3.30 (q, J = 6 Hz, 2H, NCH$_2$), 2.72 (t, J = 9 Hz, 2H, ArCH$_2$), 1.40 (s, 9H, *tert*-butyl); TLC R_f: 0.52 (Heptane/EtOAc 3:1) (full analytical data are reported in[26]).

4.2.2. 2-(3-Bromophenyl)-*N*-methylethanamine (2)

To a solution of 3-bromophenethylbromide (1 g, 3.83 mmol) in DMF (10 mL) was added 40% aqueous methylamine (2.97 mL, 38.3 mmol), followed by Cs$_2$CO$_3$ (1.625 g, 5 mmol). After the reaction mixture was refluxed for 1 h, it was cooled to room temperature and the solvent was removed. The residue was dissolved in ethyl acetate (30 mL), and the organic layer was washed with water (3 × 20 mL) and dried over Na$_2$SO$_4$. The solvent was removed in vacuo, and the oily residue was further purified using flash column chromatography (CHCl$_3$/MeOH 5:2) yielding in **2** (100 mg, 12%) as a colorless liquid. ^{1}H NMR (300 MHz, CDCl$_3$): δ 7.26–7.23 (m, 2H, ArH), 7.06–7.04 (m, 2H, ArH), 2.78–2.74 (m, 4H), 2.30 (s, 3H, NCH$_3$); TLC R_f: 0.2 (CHCl$_3$/MeOH 5:2); GC–MS (EI) *m/z* (% rel Int.): 214 (100.0 [M]$^+$), rt: 7.240 min (full analytical data are reported in[27]).

4.2.3. *N*-(3-Bromophenethyl)-*N*-methyl-2-nitrobenzenesulfonamide (3)

2-(3-Bromophenyl)ethanamine (2 g, 10.05 mmol) were dissolved in anhydrous CH$_2$Cl$_2$ (50 mL) and Et$_3$N (2 g, 20 mmol, 2.77 mL) and cooled to 0 °C. 2-nosylchloride (2.21 g, 10 mmol) was added dropwise and the mixture was warmed to rt and stirred for 1 h. The mixture was diluted with Et$_2$O, quenched with 10% aq HCl and washed successively with sat. NaHCO$_3$ and brine. After drying with Na$_2$SO$_4$, the solvent was evaporated to yield 3.8 g of crude product (~100%) which was used without any further purification and dissolved in DMF (10 mL). NaH (60% dispersion in mineral oil, 397.2 mg, 10 mmol) and after 15 min, MeI (0.91 g, 5.28 mmol, 0.4 mL) were added at 0 °C. The mixture was stirred at room temperature for 14 h, hereafter, DMF was removed. The resultant mixture was diluted in a mixture of EtOAc/H$_2$O and extracted with ethyl acetate three times. The combined organic layers were dried over Na$_2$SO$_4$ and concentrated. The residue was purified by flash chromatography on silica gel with EtOAc/Heptane (2:1) yielding in **3** (3.87 g, 96%) as a yellowish liquid. ^{1}H NMR (300 MHz, CDCl$_3$): δ 7.95–7.92 (m, 1H, ArH), 7.70–7.60 (m, 3H, ArH), 7.37–7.27 (m, 2H, ArH), 7.19–7.11 (m, 2H, ArH), 3.51–3.46 (m, 2H, NCH$_2$), 2.99–2.87 (m, 5H, NCH$_3$ and ArCH$_2$); ^{13}C NMR (75 MHz, CDCl$_3$): δ 148.15, 140.49, 133.84, 132.47, 132.00, 131.93, 130.80, 130.43, 130.01, 127.79, 124.36, 122.71, 51.81, 35.32, 34.69; TLC R_f: 0.8 (Heptane/EtOAc 2:1); GC–MS (EI) *m/z* (% rel Int.): 398.0 (100.0 [M]$^+$), rt: 22.298 min.

4.2.4. 2,6-Dimethoxybenzeneboronic acid (4)

2,6-Dimethoxybenzeneboronic acid was synthesized as reported.[28]

4.2.5. General procedure for the Suzuki cross-coupling

The appropriate phenylbromide (0.517 mmol), 2,6-dimethoxybenzeneboronic acid (170 mg, 0.9 mmol) and Na$_2$CO$_3$ (137.65 mg, 1.29 mmol) were dissolved in a mixture of toluene/H$_2$O (10:1) (5.5 mL) and sparged with argon for at least 30 min to assure all oxygen is removed from the reaction mixture. Pd(PPh$_3$)$_4$ (29.86 mg, 0.026 mmol) were added and heated for 2–4 h in a microwave oven (Initiator, Biotage) at 130 °C. The resulting reaction mixture was quenched with water and extracted by diethylether. After drying with MgSO$_4$ the united organic layers were reduced and the crude mixture was purified by column chromatography yielding in the desired product.

4.2.6. *tert*-Butyl (2-(2′,6′-dimethoxy-[1,1′-biphenyl]-3-yl)ethyl) carbamate (5)

Colorless liquid (173 mg 94%); ^{1}H NMR (300 MHz, CDCl$_3$): δ 7.30–7.12 (m, 5H, ArH), 6.67–7.07 (d, *J* = 9 Hz 2H, ArH), 3.75 (s, 6H, OCH$_3$), 3.45 (q, *J* = 6 Hz 2H, NCH$_2$), 2.85 (t, *J* = 9 Hz 2H, ArCH$_2$), 1.48 (s, 9H, *tert*-butyl); ^{13}C NMR (75 MHz, CDCl$_3$): δ 157.72, 156.04, 138.27, 134.41, 131.61, 129.17, 128.88, 128.15, 127.45, 119.44, 104.39, 79.44, 56.29, 42.00, 35.47, 28.84; TLC R_f: 0.31 (Heptane/EtOAc 3:1); GC–MS (EI) *m/z* (% rel Int.): 357 (100.0 [M]$^+$), rt: 16.307 min.

4.2.7. 2-(2′,6′-Dimethoxy-[1,1′-biphenyl]-3-yl)-*N*-methylethanamine (6)

Colorless liquid (116 mg; 83%); ^{1}H NMR (300 MHz, CDCl$_3$): δ 7.31–7.14 (m, 5H, ArH), 6.63 (d, J = 6 Hz 2H, ArH), 3.71 (s, 6H, OCH$_3$), 2.89–2.81 (m, 4H, ArCH$_2$CH$_2$N), 2.43 (s, 3H, NCH$_3$), 1.64 (br s, 1H, NH); TLC R_f: 0.15 (EtOAc/Et$_3$N 3:1); GC–MS: 271 g/mol, rt: 12.806 min, purity: 100% (full analytical data are reported in[29]).

4.2.8. *N*-(2-(2′,6′-Dimethoxy-[1,1′-biphenyl]-3-yl)ethyl)-*N*-methyl-2-nitrobenzenesulfonamide (7)

White solide (205 mg; 87%); mp: 128–129 °C; ^{1}H NMR (300 MHz, CDCl$_3$): δ 7.90–7.87 (m, 1H, ArH), 7.63–7.54 (m, 3H, ArH), 7.28–7.26 (m, 2H, ArH), 7.20–7.17 (m, 2H, ArH), 7.11–7.09 (m, 1H, ArH), 6.63 (d, *J* = 9 Hz 2H, ArH), 3.71 (s, 6H, OCH$_3$), 3.49 (t, *J* = 9 Hz, 2H, NCH$_2$), 2.95–2.90 (m, 5H, NCH$_3$ and ArCH$_2$); ^{13}C NMR (75 MHz, CDCl$_3$): δ 157.73, 137.32, 134.66, 133.48, 132.84, 131.74, 131.64, 130.95, 129.48, 128.94, 128.14, 127.41, 125.58, 124.18, 119.33, 104.40, 56.23, 56.13, 35.36, 35.29; TLC R_f: 0.5 (Heptane/EtOAc 1:1).

4.2.9. 2-(2′,6′-Dimethoxy-[1,1′-biphenyl]-3-yl)-*N*-methylethanamine (6)

A 100 mL round-bottom flask was charged with of 1-dodecylmercaptan (0.722 g, 3.57 mmol, 0.854 mL) and acetonitrile (25 mL). The mixture is cooled in an ice-water bath and of DBU (0.542 g, 3.57 mmol, 0.533 mL) was added over a period of 10 min. After 5 min, the ice-water bath was removed, and **7** (791 mg, 1.785 mmol) in acetonitrile (20 mL) is added and the mixture was heated to 60 °C for 12 h. The crude mixture was taken up in EtOAc and washed with Na$_2$CO$_3$ and dried over MgSO$_4$, filtered, and concentrated under reduced pressure. The residue was purified by column chromatography on silica. First the column was flushed with (Heptane/EtOAc 1:1) to remove all byproducts and then with EtOAc/ET$_3$N (2:0.3) to yield the desired secondary amine as a colorless oil (250 mg, 52%). (See above for analytical data)

4.2.10. 2-(2′,6′-Dimethoxy-[1,1′-biphenyl]-3-yl)ethanamine (8)

Compound **5** (0.105 mg, 0.294 mm) were carefully dissolved in TFA (5 mL). The resulting mixture was stirred for 4 h. Afterwards, TFA was removed in vacuo and the resulting mixture solved in diethylether. Then the pH was set to 8 by addition of 1 M NaHCO$_3$ and then extracted with diethylether (3×). After drying with

Na_2SO_4 the united organic layers were reduced to yield in the desired product (60 mg, 79%) as a colorless liquid. ^{1}H NMR (300 MHz, $CDCl_3$): δ 7.34–7.10 (m, 5H, ArH), 6.50 (d, J = 6 Hz, 2H, ArH), 4.79 (br s, 2H, NH_2), 3.71 (s, 6H, OCH_3), 3.04 (t, J = 6 Hz, 2H NCH_2), 2.87 (t, J = 6 Hz, 2H, $ArCH_2$); ^{13}C NMR (75 MHz $CDCl_3$): δ 157.67, 138.01, 134.50, 131.64, 129.33, 128.93, 128.17, 127.51, 111.34, 104.40, 56.18, 42.89, 38.16; TLC R_f: 0.01 (Heptane/EtOAc 3:1); GC–MS (EI) m/z (% rel Int.): 257 (100.0 [M][+]), rt 12.467 min.

4.2.11. General procedure to synthesize 2-(2′,6′-dimethoxy-[1,1′-biphenyl]-3-yl)-N,N-dimethylethanamine (Cimbi-806)

To a stirred solution of the appropriate amine (1.32 mmol), zinc chloride (90 mg, 0.65 mmol), and 37% aqueous formaldehyde (0.4 mL, 5.28 mmol) in MeOH (10 mL) was added sodium cyanoborohydride (99.64 mg, 1.584 mmol) at 0 °C. The resulting mixture was stirred at room temperature for 14 h and then quenched by addition of 1 N NaOH and extracted with ethyl acetate. The combined organic layers were dried over Na_2SO_4 and concentrated. The residue was purified by flash chromatography on silica gel with $EtOAc/Et_3N$ (10:0.1) to yield in a colorless oil. Method A: Starting from **6** resulting in Cimbi-806 (244 mg, 65%). Method B: Starting from **8** resulting in the desired product (319 mg, 82%). ^{1}H NMR (300 MHz, $CDCl_3$): δ 7.36–7.25 (m, 2H, ArH), 7.20–7.18 (m, 3H, ArH), 6.65 (d, J = 6 Hz, 2H, ArH), 3.74 (s, 6H, OCH_3), 2.87–2.81 (m, 2H, NH_2), 2.64–2.58 (m, 2H, $ArCH_2$), 2.32 (s, 6H, NCH_3); ^{13}C NMR (75 MHz, $CDCl_3$): δ 157.99, 139.67, 134.39, 131.67, 129.00, 128.99, 128.09, 127.54, 104.57, 99.38; 61.93, 56.30, 44.61, 34.88; TLC R_f: 0.2 (Heptane/Et_3N 10:0.1); GC–MS (EI) m/z (% rel Int.): 285 (100.0 [M][+]), rt: 11.513 min, purity: >99%.

4.3. Radiolabeling of [^{11}C]Cimbi-806

[11]C-methyl trifluoromethanesulfonate ([^{11}C]MeOTf) produced using a fully automated system was transferred in a stream of helium to a 1.1-mL vial containing the labeling precursor **6** (0.3–0.4 mg) and acetone (300 µL). The resulting mixture was heated at 60 °C for 180 s and then purified by HPLC on a Luna 5 µm C18(2) 100 Å column (Phenomenex Inc.) (250 × 10 mm; 25:75 acetonitrile: 0.1% phosphoric acid; and flow rate, 6 mL/min, retention times: [^{11}C]Cimbi-806 = 7 min; precursor (6) = 5.4 min). The fraction corresponding to the labeled product (11.5 min) was collected in sterile water (150 mL), and the resulting solution was passed through a solid-phase C18 Sep-Pak extraction column (Waters Corp.), which had been preconditioned with ethanol (10 mL), followed by isotonic sodium chloride solution (20 mL). The column was flushed with sterile water (3 mL). Then, the trapped radioactivity was eluted with ethanol (3 mL), followed by isotonic sodium chloride solution (3 mL) into a 20-mL vial containing phosphate buffer (9 mL, 100 mM, pH 7), giving a 15 mL solution of [^{11}C]Cimbi-806 with a pH of approximately 7. In a total synthesis time of 80–90 min, 0.6–1.8 GBq of [^{11}C]Cimbi-806 was produced.

4.3.1. Determination of radiochemical purity and specific radioactivity

The radiotracer preparation was visually inspected for clarity, and absence of color and particles. Chemical and radiochemical purities were assessed on the same aliquot by HPLC analysis. Specific activity (A_s) of the radiotracers were calculated from three consecutive HPLC analyses (average) and determined by the area of the UV absorbance peak corresponding to the radiolabeled product on the HPLC chromatogram and compared to a standard curve relating mass to UV absorbance (λ = 225 µm). Column used for [^{11}C]Cimbi-806: Luna 5 µm C18(2) 100 Å column (Phenomenex Inc.) (150 × 4.6 mm (25:75 acetonitrile: 0.1% phosphoric acid; and flow rate: 2 mL/min. retention times: [^{11}C]Cimbi-806 = 2.618 min; precursor (6) = 2.247 min).

4.4. Lipophilicity

Lipophilicites were determined using a Dionex Ultimate 3000 HPLC equipped with de-gasser, autosampler, column-oven and UV-detector. The eluent was 50:50 (v/v) 25 mM sodium phospaht$_e$-buffer (pH = 7.4) and MeOH. Injected volumes were 100 µL with a flow rate of 2 mL/min. The column was a Zorbax SB-C8 (250 mm × 4.6 mm, 5 µm). The column oven was kept at 37 °C and detection was at 254 nm. The logarithm of retention factor of reference compounds (phenol, acetophenone, p-cresol, benzene, toluene, chlorobenzene, benzophenone, naphthalene, diphenyl and phenanthrene) and tested compounds was calculated, and a plot of the reference values against their known log D values was used to calculate log D values for tested compounds.

4.5. Animal procedures

Five female Danish Landrace pigs were used in this study (weight 19 kg). After arrival, animals were housed under standard conditions and were allowed to acclimatize for one week before scanning. To minimize stress, the animals were provided with straw bedding and environment enrichment, in the form of plastic balls and metal chains. On the scanning day, pigs were tranquilized by intramuscular (im) injection of 0.5 mg/kg midazolam. Anesthesia was induced by im injection of a Zoletil veterinary mixture (1.25 mg/kg tiletamin, 1.25 mg/kg zolazepam, and 0.5 mg/kg midazolam; Virbac Animal Health, France). Following induction, anesthesia was maintained by intravenous (iv) infusion of 15 mg/kg/h propofol (B. Braun Melsugen AG). During anesthesia, animals were endotracheally intubated and ventilated (volume 250 mL, frequency 16 per min). Venous access was granted through two catheters (Becton Dickinson) in the peripheral milk veins, and an arterial line for blood sampling measurement was obtained by a catheter in the femoral artery after a minor incision. Vital signs including blood pressure and heart rate were monitored throughout the duration of the PET scanning. Immediately after scanning, animals were sacrificed by iv injection of pentobarbital/lidocain. All animal procedures were approved by the Danish Council for Animal Ethics (Journal No. 2007/561-1320).

4.6. PET scanning protocol

[^{11}C]Cimbi-806 (n = 7) was given as intravenous bolus injections, and the pigs were subsequently PET-scanned for 90 min in list mode with the HRRT scanner. Scanning began at the time of injection. After the baseline scan, pigs were maintained in anesthesia and scanned a second time using the same PET-protocol. The 5-HT_7 antagonist, SB-269970 was administered 30 min prior to the second scan (0.5–1.0 mg/kg/h infusion). Infusion was continued for the remaining of the scan. An average of 468 ± 31 MBq was injected of [^{11}C]Cimbi-806, the average specific activity at the time of injection was 123 GBq/µmol (range: 30–215 GBq/µmol), and the average mass injected 1.6 µg (range: 0.61–4.3 µg). During the first 30 min of scanning, radioactivity in whole blood was continuously measured using an ABSS autosampler (Allog Technology) counting coincidences in a lead-shielded detector. Concurrently, blood samples were manually drawn at 2.5, 5, 10, 20, 30, 40, 50, 70, and 90 min and the radioactivity in whole blood was measured using a well counter (Cobra 5003, Packard Instruments) that was cross-calibrated to the HRRT scanner and autosampler.

4.7. Quantification of PET data

90-minute HRRT list-mode PET data were reconstructed into 38 dynamic frames of increasing length (6 × 10, 6 × 20, 4 × 30, 9 × 60, 2 × 180, 8 × 300, and 3 × 600 s). Images consisted of 207 planes and 256 × 256 voxels of 1.22 × 1.22 × 1.22 mm. A summed

picture of all counts in the 90-min scan was reconstructed for each pig and used for co-registration to a standardized MRI-based atlas of the Danish Landrace pig brain, similar to that previously published.[30,31] The temporal radioactivity in volumes of interest (VOIs), including the cerebellum, cortex, hippocampus, lateral and medial thalamus, caudate nucleus, and putamen, was extracted. Activity in the striatum was averaged over the caudate nucleus and putamen. Activity in the thalamus was averaged over the lateral and medial thalamus. Radioactivity in all VOIs was calculated as the average of radioactive concentration (Bq/mL) in the left and right sides. Outcome measure in the time-activity curves was calculated as radioactive concentration in VOI (in kBq/mL) normalized to the injected dose corrected for animal weight (in kBq/kg), yielding standardized uptake values (SUV, in the unit of g/mL).

In all pigs, full arterial function was measured. A population-based averaged metabolite curve of the seven scans was constructed and subsequently used to correct plasma activity in the individual scans for parent compound fraction. We calculated the distribution values (V_T) VOIs for [^{11}C]Cimbi-806 using plasma corrected for parent compound as arterial input function. The one-tissue compartment (1TC) model was chosen for quantitative analysis the data Kinetic modeling was done with PMOD software (version 3.0; PMOD Technologies Inc.).

4.8. HPLC analysis of pig plasma

[^{11}C]Cimbi-806 was separated from its radio-labelled metabolite(s) by direct injection of plasma in a column switching HPLC system. Whole blood samples were centrifuged (3500 rpm, 7 min) and the supernatant plasma fraction was collected and filtered through a 0.45 μM syringe filter prior to analysis with online radioactive detection, as previously described.[32]

4.9. Protein binding

The free fraction of [^{11}C]Cimbi-806 in plasma, f_p, was estimated using an equilibrium dialysis chamber method as previously described.[31] Briefly, the dialysis was conducted in chambers (Harvard Biosciences) separated by cellulose membrane with a protein cut-off of 10,000 Da. Small amounts of [^{11}C]Cimbi-806 (~5 MBq) were added to 5 mL plasma sample from the pig. Plasma (500 μL) was then dialyzed at 37 °C against an equal volume of buffer (135 mM NaCl, 3.0 mM KCl, 1.2 mM CaCl$_2$, 1.0 mM MgCl$_2$, and 2.0 mM KH$_2$PO$_4$, pH 7.4). Counts per minute in 400 μL of plasma and buffer were determined in a well counter after various dialysis times, and f_p of [^{11}C]Cimbi-806 was calculated as the ratio of radioactivity in buffer and plasma. The samples were measured after equilibrium had been obtained between the two chambers.

4.10. In vitro autoradiography

Twenty micrometers coronal sections of pig brain (weight ~19 kg) were cut on a HM500OM Cryostat (Microm Intl GmbH) and thawed-mounted on super frost plus glass slides, air-dried and stored at −80 °C until use. Sections were cut so both cortical and striatal areas were visible. Autoradiography was performed with 5 nM [^{3}H]SB-269970 (PerkinElmer, Inc.) and with increasing competing concentrations of Cimbi-806 (1.56–250 nM). Non-specific binding was determined with 5 μM SB-258719 (Tocris Bioscience). Two separate experiments were carried out on adjacent sections from the same pig. Assay buffer used consistend of 50 mM Tris–HCl, pH 7.4, and an incubation time of 2 h was used. Sections were washed 3 × 5 min in ice-cold assay buffer with a subsequent dip in ice-cold dH$_2$O. Sections were dried and exposed to Fujifilm tritium-sensitive imaging plates for 14 days. Specific radioligand binding (total minus non-specific binding) was plotted as a function of concentration of Cimbi-806 and regressed using Prism 4.0 software to obtain K_i.

A. Supplementary data

Supplementary data associated with this article can be found, in the online version, at http://dx.doi.org/10.1016/j.bmc.2012.05.005.

References and notes

1. Carr, G. V.; Lucki, I. *Psychopharmacology (Berl)* **2011**, *213*, 265.
2. Cassano, G. B.; Jori, M. C. *Int. Clin. Psychopharmacol.* **2002**, *17*, 27.
3. Lecrubier, Y.; Boyer, P.; Turjanski, S.; Rein, W. *J. Affect. Disord.* **1997**, *43*, 95.
4. Abbas, A. I.; Hedlund, P. B.; Huang, X. P.; Tran, T. B.; Meltzer, H. Y.; Roth, B. L. *Psychopharmacology (Berl)* **2009**, *205*, 119.
5. Ishibashi, T.; Horisawa, T.; Tokuda, K.; Ishiyama, T.; Ogasa, M.; Tagashira, R.; Matsumoto, K.; Nishikawa, H.; Ueda, Y.; Toma, S.; Oki, H.; Tanno, N.; Saji, I.; Ito, A.; Ohno, Y.; Nakamura, M. *J. Pharmacol. Exp. Ther.* **2010**, *334*, 171.
6. Smith, C.; Rahman, T.; Toohey, N.; Mazurkiewicz, J.; Herrick-Davis, K.; Teitler, M. *Mol. Pharmacol.* **2006**, *70*, 1264.
7. Matthys, A.; Haegeman, G.; Van Craenenbroeck, K.; Vanhoenacker, P. *Mol. Neurobiol.* **2011**, *43*, 228.
8. Zhang, M. R.; Haradahira, T.; Maeda, J.; Okauchi, T.; Kida, T.; Obayashi, S. *J. Labelled Compd. Radiopharm.* **2002**, *45*, 857.
9. Andries, J.; Lemoine, L.; Mouchel-Blaisot, A.; Tang, S.; Verdurand, M.; Le, B. D.; Zimmer, L.; Billard, T. *Bioorg. Med. Chem. Lett.* **2010**, *20*, 3730.
10. Lemoine, L.; Becker, G.; Vacher, B.; Billard, T.; Lancelot, S.; Newman-Tancredi, A.; Zimmer, L. *J. Nucl. Med.* **2011**, *52*, 1811.
11. Andries, J.; Lemoine, L.; Le Bars, D.; Zimmer, L.; Billard, T. *Eur. J. Med. Chem.* **2011**, *46*, 3455.
12. Leopoldo, M.; Lacivita, E.; Berardi, F.; Perrone, R.; Hedlund, P. B. *Pharmacol Ther* **2011**, *129*, 120.
13. Paillet-Loilier, M.; Fabis, F.; Lepailleur, A.; Bureau, R.; Butt-Gueulle, S.; Dauphin, F.; Lesnard, A.; Delarue, C.; Vaudry, H.; Rault, S. *Bioorg. Med. Chem. Lett.* **2007**, *17*, 3018.
14. Badarau, E.; Bugno, R.; Suzenet, F.; Bojarski, A. J.; Finaru, A. L.; Guillaumet, G. *Bioorg. Med. Chem.* **1958**, *2010*, 18.
15. Hall, H.; Lundkvist, C.; Halldin, C.; Farde, L.; Pike, V. W.; McCarron, J. A.; Fletcher, A.; Cliffe, I. A.; Barf, T.; Wikstrom, H.; Sedvall, G. *Brain Res.* **1997**, *745*, 96.
16. Varnas, K.; Thomas, D. R.; Tupala, E.; Tiihonen, J.; Hall, H. *Neurosci. Lett.* **2004**, *367*, 313.
17. Krass, J. D.; Jastorff, B.; Genieser, H. G. *Anal. Chem.* **1997**, *69*, 2575.
18. Rowley, M.; Kulagowski, J. J.; Watt, A. P.; Rathbone, D.; Stevenson, G. I.; Carling, R. W.; Baker, R.; Marshall, G. R.; Kemp, J. A.; Foster, A. C.; Grimwood, S.; Hargreaves, R.; Hurley, C.; Saywell, K. L.; Tricklebank, M. D.; Leeson, P. D. *J. Med. Chem.* **1997**, *40*, 4053.
19. Jewett, D. M. *Int. J. Rad. Appl. Instrum. A* **1992**, *43*, 1383.
20. Ettrup, A.; Mikkelsen, J. D.; Lehel, S.; Madsen, J.; Nielsen, E. O.; Palner, M.; Timmermann, D. B.; Peters, D.; Knudsen, G. M. *J. Nucl. Med.* **2011**, *52*, 1449.
21. Bhalla, P.; Saxena, P. R.; Sharma, H. S. *Mol. Cell Biochem.* **2002**, *238*, 81.
22. Hagan, J. J.; Price, G. W.; Jeffrey, P.; Deeks, N. J.; Stean, T.; Piper, D.; Smith, M. I.; Upton, N.; Medhurst, A. D.; Middlemiss, D. N.; Riley, G. J.; Lovell, P. J.; Bromidge, S. M.; Thomas, D. R. *Br. J. Pharmacol.* **2000**, *130*, 539.
23. Gustafson, E. L.; Durkin, M. M.; Bard, J. A.; Zgombick, J.; Branchek, T. A. *Br. J. Pharmacol.* **1996**, *117*, 657.
24. To, Z. P.; Bonhaus, D. W.; Eglen, R. M.; Jakeman, L. B. *Br. J. Pharmacol.* **1995**, *115*, 107.
25. Martin-Cora, F. J.; Pazos, A. *Br. J. Pharmacol.* **2004**, *141*, 92.
26. Broo, A.; Holm, P.; Judkins, R.; Li, L.; Lindstedt-Alstermark, E.-L.; Sandberg, P.; Swanson, M.; Weidolf, L.; Brickmann, K.; Patent number: EP1838687 (A1); 2006.
27. Cheshire, D.; Cladingboel, D.; Hirst, S.; Manners, C.; Stocks, M. **2001**.
28. Fukuda, T.; Sudo, E.-I.; Shimokawa, K.; Iwao, M. *Tetrahedron* **2008**, *64*, 328.
29. Romero Alonso, L.; Zamanillo Castanedo, D.; Vela Hernández, J. M.; Buschmann, H. H.; Patent number EP1997493; 2008.
30. Ettrup, A.; Palner, M.; Gillings, N.; Santini, M. A.; Hansen, M.; Rasmussen, L. K.; Nàgren, K.; Madsen, J.; Begtrup, M.; Knudsen, G. M. *J. Nucl. Med.* **2010**, *51*, 1763.
31. Kornum, B. R.; Lind, N. M.; Gillings, N.; Marner, L.; Andersen, F.; Knudsen, G. M. *J. Cereb. Blood Flow Metab.* **2009**, *29*, 186.
32. Gillings, N. *Nucl. Med. Biol.* **2009**, *36*, 961.

Paper IV

Hansen HD, Herth MM, Ettrup A, Andersen VL, Lehel S, Dyssegaard A, Kristensen JL, and Knudsen GM.

Radiosynthesis and in vivo evaluation of novel radioligands for PET imaging of 5-HT$_7$ receptors.

RADIOSYNTHESIS AND IN VIVO EVALUATION OF NOVEL RADIOLIGANDS FOR PET IMAGING OF CEREBRAL 5-HT$_7$ RECEPTORS.

Hanne D. Hansen[a,b], Matthias M. Herth[a,b,c,d], Anders Ettrup[a,b], Valdemar L. Andersen[a,b,c,d], Szabolcs Lehel[c], Agnete Dyssegaard[a,b], Jesper L. Kristensen[b], and Gitte M. Knudsen[a,b].

a) Center for Integrated Molecular Brain Imaging, Copenhagen University Hospital Rigshospitalet, Blegdamsvej 9, 2100 Copenhagen, Denmark

b) Neurobiology Research Unit, Rigshospitalet and University of Copenhagen, Blegdamsvej 9, 2100 Copenhagen, Denmark

c) Department of Drug Design and Pharmacology, Faculty of Health and Medical Sciences, University of Copenhagen, Universitetsparken 2, 2100 Copenhagen, Denmark

d) PET and Cyclotron Unit, Copenhagen University Hospital Rigshospitalet, Blegdamsvej 9, 2100 Copenhagen, Denmark

CORRESPONDING AUTHOR FOOTNOTE

Gitte M. Knudsen
Center for Integrated Molecular Brain Imaging
Copenhagen University Hospital, Rigshospitalet
Blegdamsvej 9
DK-2100 Copenhagen, Denmark
Phone: (+45) 3545 6720   Fax: (+45) 3545 6713
Email: gmk@nru.dk

FIRST AUTHOR

Hanne D. Hansen, Ph.D. Student
Center for Integrated Molecular Brain Imaging
Copenhagen University Hospital, Rigshospitalet
Blegdamsvej 9
DK-2100 Copenhagen, Denmark
Phone: (+45) 35 45 67 06
Email: hanne.d.hansen@nru.dk

ABSTRACT

Rationale: The 5-HT$_7$ receptor is the most recently discovered 5-HT receptor, and its physiological and possible pathophysiological roles are not fully elucidated. So far, no suitable 5-HT$_7$ receptor PET radioligand is available thus limiting the investigation of this receptor in the living brain. Here, we present the radiosynthesis and in vivo evaluation of [^{11}C]Cimbi-712 and [^{11}C]Cimbi-717 as selective 5-HT$_7$ receptor PET radioligands in the pig brain. The 5-HT$_7$ receptor distribution in the post-mortem pig brain is also assessed.

Methods: In vitro autoradiography with the 5-HT$_7$ receptor selective radioligand [^{3}H]SB-269970 was carried out on pig brain sections to establish the 5-HT$_7$ receptor binding distribution. Radiolabeling of 5-HT$_7$ receptor selective compounds were carried out in an automated synthesis module where we conducted either palladium-mediated cross coupling ([^{11}C]Cimbi-712) or conventional O-methylation ([^{11}C]Cimbi-717). After intravenous injection of the radioligands, the in vivo brain distribution of the ligands was studied in Danish Landrace pigs. Specific binding of [^{11}C]Cimbi-712 and [^{11}C]Cimbi717 to the 5-HT$_7$ receptor was investigated by intravenous administration of SB-269970 prior to a second scan of the animal.

Results: High 5-HT$_7$ receptor distribution was found in the thalamus and cortical regions of the pig brain by autoradiography. The radiosynthesis of both radioligands succeeded after optimisation efforts (RCY ~ 20 – 30 % at EOS). Time-activity curves of [^{11}C]Cimbi-712 and [^{11}C]Cimbi-717 both showed high brain uptake and distribution according to 5-HT$_7$ receptors, but the tracer kinetics of [^{11}C]Cimbi-717 were more reversible than [^{11}C]Cimbi-712. Both radioligands were specific for the 5-HT$_7$ receptor, as they could be displaced by pre-treatment with SB-269970, for [^{11}C]Cimbi-717 in a dose-dependent fashion. For [^{11}C]Cimbi-717, binding potentials (BP$_{ND}$) of 6.4 ± 1.2 (n=6) were calculated in the thalamus.

Conclusion: [^{11}C]Cimbi-712 and [^{11}C]Cimbi-717 both generated a specific binding in accordance with 5-HT$_7$ receptor distribution and are both potential PET radioligands for the 5-HT$_7$ receptor. [^{11}C]Cimbi-717 is the better candidate because of the reversible tracer kinetics and this radioligand showed a dose-dependent decline in cerebral binding following receptor blockade. Thus, [^{11}C]Cimbi-717 is currently the most promising radioligand for investigation of 5-HT$_7$ receptor binding in the living human brain.

INTRODUCTION

The serotonergic system plays a key modulatory role in the brain and is a target for many drug treatments for brain disorders either through reuptake blockade or via interactions with the 14 subtypes of serotonin (5-HT) receptors. Our knowledge about the behaviour of the 5-HT system in vivo is still scattered and most of the understanding is derived from animal models. However, the development of imaging techniques such as positron emission tomography (PET) and the increasing number of radioligands for the 5-HT receptors enable in vivo investigation of the 5-HT system in the human brain.

The 5-HT$_7$ receptor is an interesting target for the development of novel radioligands. Along with the role of 5-HT$_7$ receptors in the pathophysiology of brain disorders such as schizophrenia, depression, and control of circadian rhythm (reviewed in (*1*)), currently no well-validated radioligand is available for in vivo imaging of this receptor. Interestingly, the 5-HT$_7$ receptor and the 5-HT$_{1A}$ receptor are the receptors for which 5-HT has the highest affinity. This is relevant for the aim of developing a radioligand that is sensitive to changes in cerebral levels of endogenous 5-HT. If the competition model applies, the probability of measuring a signal change in response to a pharmacologic challenge that changes 5-HT levels, will solely depend on the affinity of 5-HT to the target receptor (*2*).

Several potent and selective ligands for the 5-HT$_7$ receptor have been developed, but so far a very limited number of PET radioligands have been evaluated in vivo. [^{11}C]DR4446 had good blood-brain barrier permeability and was metabolically stable, but it only showed a minimal specific binding component (*3*). The 5-HT$_7$ receptor antagonist SB-269970 has been used as lead structure for developing ^{18}F-labeled radioligands. [^{18}F]1-{2-[(2S)-1-(phenylsulfonyl)pyrrolidin-2-yl]ethyl}piperidin-4-yl 4-fluorobenzoate and [^{18}F]2FP3 was evaluated ex vivo in rats and in vivo in cats (*4, 5*), however no input function was obtained while evaluating ^{18}F-2FP3. Furthermore, the 5-

HT$_7$ receptor binding distribution was not evaluated in cats, thus making it difficult to verify if the binding of [^{18}F]2FP3 was specific to 5-HT$_7$ receptors. We recently also reported the evaluation of a 5-HT$_7$ receptor PET radioligand, [^{11}C]Cimbi-806, which displayed selectivity in vitro but the lack of displacement by SB-269970 in vivo led us to conclude that this compound does not selectively image 5-HT$_7$ receptors in vivo (*6*).

Despite high sequence similarity in the transmembrane domains (the putative binding site) of the 5-HT$_{1A}$ and 5-HT$_7$ receptor (*7, 8*), oxindole derivatives (reported as antagonists) displayed high selectivity to the 5-HT$_7$ receptor (*9*). Because of the relatively low 5-HT$_7$ receptor density (B$_{max}$) in the brain and because of co-localization of the 5-HT$_7$ and 5-HT$_{1A}$ receptors, a high selectivity for the 5-HT$_7$ receptor will be a requirement for a PET radioligand to be successful. In the temporal cortex and insula of post mortem human tissue, the specific binding of 5-HT$_{1A}$ receptors is 78.6 fmol/mg as measured with [^{3}H]WAY100635 (*10*) and 44.5 fmol/mg/tissue as measured with [^{3}H]CUMI-101 (*11*). In the same region, the specific binding of 5-HT$_7$ receptors is 2.3 fmol/mg (*12*), giving a density ratio of 19-34 depending on the 5-HT$_{1A}$ receptor radioligand. In order to allow only 10 percent of signal arising from binding to 5-HT$_{1A}$ receptors, a 190-340-fold difference in K$_D$ of the 5-HT$_{1A}$ and 5-HT$_7$ receptor is necessary.

Further work with the oxindole compound class led to the synthesis of a group of compounds including Cimbi-712 (3-{4-[4-(4-Methylphenyl)piperazine-1-yl]butyl}p-1,3-dihydro-2H-indol-2-one) and Cimbi-717 (3-{4-[4-(3-Methoxyphenyl)piperazine-1-yl]butyl}-1,3-dihydro-2H-indol-2-one) (*13*). The in vitro selectivity profile for both compounds showed the desired 5-HT$_7$ receptor selectivity against the 5-HT$_{1A}$ and adrenergic alpha1 receptors; with Cimbi-712 displaying a little higher selectivity for the 5-HT$_7$ receptor as compared to Cimbi-717.

Here, we report the ^{11}C-radiolabeling and in vivo evaluation including receptor occupancy measurements with two novel 5-HT$_7$ selective PET radioligands in Danish Landrace pigs. For

comparison between in vivo and post-mortem receptor distribution, we also investigated the distribution of 5-HT$_7$ receptors in the pig brain.

MATERIALS AND METHODS

In vitro autoradiography

One brain hemisphere of a 30 kg Danish Landrace pig was sliced on a HM500OM cryostat (Microm Intl GmbH, Walldorf, Germany) in 20 µm coronal sections except for cerebellum which was sliced in the sagittal plane. Sections were thaw-mounted on superfrost plus glass slides (Thermo Scientific, Braunschweig, Germany) and stored at -80 degrees until use. Autoradiography was carried out at room temperature (RT) in 50 mM Tris-HCl buffer (pH 7.4) with 5 nM [^{3}H]SB-269970 (PerkinElmer, Skovlunde, Denmark). Non-specific binding was determined by adding 10 µM SB-258719 (Tocris Bioscience, Bristol, United Kingdom). Sections were pre-incubated in buffer for approximately 30 min and then incubated with radioactive buffer for two hours. Sections were hereafter washed for 1 x 5 min and for 2 x 10 min, rinsed in dH$_2$O for twenty seconds and lastly dried before exposure to Fujifilm tritium sensitive plates (Fujifilm Europe GmbH, Düsseldorf, Germany) for nineteen days.

Calibration, quantification and data evaluation of all autoradiography images were done with ImageJ analysis software (http://rsb.info.nih.gov/ij/). Regions of interest were hand-drawn around anatomical landmarks, e.g. borders of sections, for each brain region and the mean pixel density was measured in each brain region as outcome. A third-degree exponential calibration function of decay-corrected ^{3}H-microscales (Amersham Biosciences, GE Healthcare, Piscataway, USA) and specific activity of [^{3}H]SB-269970 was used to convert the mean pixel density to receptor binding measured in fmol/mg tissue equivalents (TE).

Organic synthesis

The precursors as well as the reference compounds were synthesized as previously described (*13, 14*).

Radioligand preparation

[^{11}C]Cimbi-717: ^{11}C-methyl trifluoromethanesulfonate ([^{11}C]MeOTf), produced using a fully automated system, was transferred in a stream of helium to a 1.1-mL vial containing the labeling precursor (0.3– 0.4 mg), 0.5 M K_2CO_3 (14 µL) and MeCN (300 µL). The resulting mixture was heated at 60 °C for 5 min and then purified by HPLC on a Luna 5 µm C18(2) 100Å column (Phenomenex Inc., Værløse, Denmark) (250 x 10 mm; 50:50 acetonitrile: 0.01M borax buffer; at a flow rate of 6 mL/min, retention times: [^{11}C]Cimbi-717 = 610 s; precursor = 300 s). The fraction corresponding to the labeled product was collected in sterile water (150 mL), and the resulting solution was passed through a solid-phase C18 Sep-Pak extraction column (Waters Corp., Saint-Quentin, France), which had been preconditioned with ethanol (10 mL), followed by isotonic sodium chloride solution (20 mL). The column was flushed with sterile water (3 mL). Then, the trapped radioactivity was eluted with ethanol (3 mL), followed by isotonic sodium chloride solution (3 mL) into a 20-mL vial containing phosphate buffer (9 mL, 100 mM, pH 7), giving a 15 mL solution of [^{11}C]Cimbi-717 with a pH of approximately 7.

[^{11}C]Cimbi-712: [^{11}C]Cimbi-712 was produced as described (*14*). The HPLC fraction corresponding to the labeled product was collected in sterile water (150 mL), and the resulting solution was passed through a solid-phase C18 Sep-Pak extraction column, which had been preconditioned with ethanol (10 mL), followed by water (20 mL). The trapped radioactivity was eluted with ethanol (3 mL) into a 20-mL vial containing phosphate buffer (9 mL, 100 mM, pH ~ 7), giving a 12 mL solution of [^{11}C]Cimbi-712 with a pH of approximately 7.

Determination of radiochemical purity and specific radioactivity

Chemical and radiochemical purities were assessed on the same aliquot by HPLC analysis. Specific activity of the radioligands were calculated from three consecutive HPLC analyses (average) and determined by comparing the area of the UV absorbance peak corresponding to the radiolabeled product on the HPLC chromatogram and compared to a standard curve relating mass to UV absorbance (λ = 225 μm). [^{11}C]Cimbi-712 and [^{11}C]Cimbi-717 were analyzed with HPLC using a Luna 5 μm C18(2) 100Å column (Phenomenex Inc., Værløse, Denmark) (150 x 4.6 mm (50:50 acetonitrile: 0.01M borax buffer; at a flow rate of 2 mL/min. retention times: [^{11}C]Cimbi-717 = 2.978 min, [^{11}C]Cimbi-712: 4.790 min).

Animal procedure

Eight female Danish Landrace pigs (mean weight ± S.D., 19 ± 2.0 kg) were used for in vivo PET imaging. Tranquillization, anaesthesia, monitoring and euthanasia of animals were performed as previously described (*15*). All animal procedures were approved by the Danish Council for Animal Ethics (journal no. 2012-15-2934-00156).

PET protocol

[^{11}C]Cimbi-712 was given as an intravenously (i.v.) bolus injection and the injected dose was 155 and 110 MBq for baseline scans (n=2) and 123 and 73 MBq for scans where SB-269970 was pre-administered (n=2). [^{11}C]Cimbi-717 was also given as an i.v. bolus and the injected dose (mean ± S.D.) was 236 ± 117 MBq for baseline scans (n=6, range: 115-435 MBq) and 147 ± 82.1 MBq for scans where a pre-blocking agent was administered (n=6, range, 40-277 MBq). The pigs were subsequently scanned for 90 min in list-mode with a high resolution research tomography (HRRT)

scanner (Siemens AG, Munich, Germany), where scanning started at the time of injection (0 min). Immediately after the baseline scan (90 min), SB-269970 (Tocris Bioscience, Bristol, United Kingdom) was given i.v. as bolus infusion (0.2, 1.0 or 4.2 mg/kg/h) and rescanning started after 30 min of pre-treatment with SB-269970. In one pig, 0.5 mg/kg prazosin (Sigma Aldrich, St. Louis, USA) was given as an i.v. infusion prior to injection of [^{11}C]Cimbi-717. During the first 30 min of the scans, radioactivity in the whole blood was continuously measured using an ABSS autosampler (Allogg Technology, Mariefred, Sweden) counting coincidences in a lead-shielded detector. Concurrently, arterial whole blood was sampled manually at time 2.5, 5, 10, 20, 30, 40, 50, 70 and 90 minutes after injection and radioactivity was measured in whole blood and plasma using a well counter (Cobra 5003, Packard Instruments, PerkinElmer, Waltham, USA), which was cross-calibrated to the HRRT scanner and to the autosampler. Radiolabeled parent compound and metabolites were measured in plasma using HPLC with online radioactivity detection. In short, [^{11}C]Cimbi-712 and [^{11}C]Cimbi-717 were separated from their respective radiolabeled metabolite(s) by direct injection of plasma in a column switching HPLC system. Whole blood samples were centrifuged (3500 rpm, 7 min) and the supernatant plasma fraction was collected and filtered through a 0.45 µM syringe filter prior to analysis with online radioactive detection, as previously described (*16, 17*). The free fraction (f_p) of [^{11}C]Cimbi-717 in pig plasma was measured using an equilibrium dialysis method as previously described (*18*) and calculated as the ratio between radioactivity in a buffer and plasma compartment after equilibrium between the chambers was reached after 3 hours.

Quantification of PET data

Ninety-minute list-mode PET data were reconstructed into 38 dynamic frames of increasing length (6x10, 6x20, 4x30, 9x60, 2x180, 8x300, and 3x600 seconds). Images consisted of 207 planes

of 256 x 256 voxels of 1.22 x 1.22 x 1.22 mm. A summed picture of all counts in the 90-min scan was reconstructed for each pig and used for co-registration to a standardized MRI-based atlas of the Danish Landrace pig brain, similar to that previously published (*17, 18*). The time activity curves (TACs) were calculated for the following volumes of interest (VOIs): cerebellum, cortex, hippocampus, lateral and medial thalamus, caudate nucleus, and putamen. Striatum is defined as the mean radioactivity in caudate nucleus and putamen. The activity in thalamus is calculated as the mean radioactivity in the lateral and medial thalamus. Radioactivity in all VOIs was calculated as the average of radioactive concentration (Bq/mL) in the left and right sides. Outcome measure in the time-activity curves (TACs) was calculated as radioactive concentration in VOI (in kBq/mL) normalized to the injected dose corrected for animal weight (in kBq/kg), yielding standardized uptake values (g/mL).

Distribution volumes (V_T) for the VOIs were calculated on the basis of three different models: The one-tissue compartment (1-TC), two-tissue compartment (2-TC) and the Logan linearization models. The parent compound fraction was fitted to a bi-exponential function for both baseline and blocked (SB-269970 and prazosin) conditions of [^{11}C]Cimbi-717 and used to generate a metabolite corrected arterial plasma input function. The V_T of baseline and blocked conditions was used to determine the non-displaceable distribution volume (V_{ND}) by use of the Lassen plot, and thereby allow for calculation of the non-displaceable binding potential BP_{ND} (*19*). All modelling was initiated with same starting parameters, and standard deviation coefficient variance (COV) was below 15 % for macroparameters (K_1 and V_T). Data sets that did not fulfil this criterion were not included in the results. Of the 176 fittings for [^{11}C]Cimbi-717, 2 failed for 1-TC, 31 failed for 2-TC, and 7 failed for Logan linearization model. Of the 40 attempts for [^{11}C]Cimbi-712, 2 failed for 1-TC, 12 failed for 2-TC, and 11 failed for Logan linearization model.

RESULTS

5-HT$_7$ receptor distribution in the pig brain

Regional specific 5-HT$_7$ receptor binding was measured with [^{3}H]SB-269970 autoradiography on the pig brain sections (TABLE 1 and FIGURE 1). Highest binding was found in small subregions of the thalamus, amygdala, and the occipital cortex. Low binding was found in striatum and especially in the cerebellum. In the cortical regions binding increased towards the posterior parts of the pig brain, with highest cortical binding found in the occipital lobe (see also Supplementary Figure 1).

Radiochemistry

Radiolabeling of [^{11}C]Cimbi-712 has previously been described (*14*). In brief, [^{11}C]Cimbi-712 was labeled with a RCY of 0.3-0.5 GBq and with a specific activity (A$_S$) of 106 ± 68 GBq/µmol (n=4) in a total synthesis time of 80-90 min.

Radiolabeling of [^{11}C]Cimbi-717 underwent extensive optimization as compared to [^{11}C]Cimbi-712 (*14*), now using 0.3 mg precursor, 14 µL 0.5M K$_2$CO$_3$ (1 equiv.) and [^{11}C]CH$_3$OTf on a fully automated system (RCY ~ 20%) (SCHEME 1). Two major radioactive peaks were detected. The minor peak corresponded to [^{11}C]Cimbi-717 (~600 sec) (for further information, see supporting information). The precursor eluted ~300 sec prior to the radiolabeled product as indicated by the UV-absorption chromatogram (Supplementary Figure 2). The radiosynthesis including HPLC purification and formulation generated an injectable solution of [^{11}C]Cimbi-717 (radiochemical purity > 97%) within 70-80 min. Typically, 0.2–0.4 GBq of [^{11}C]Cimbi-717 was isolated with a A$_S$ of 69.7 ± 41.0 GBq/µmol (n=12) at the end of synthesis.

In vivo distribution

With [^{11}C]Cimbi-712, the highest brain uptake was observed in the thalamus and lowest uptake in the cerebellum. TACs display slow kinetics with peak uptake after approximately 50 minutes (FIGURE 2A). Pre-treatment of the animals with 1.0 mg/kg/h SB-269970 decreased binding equally in all regions. Like [^{11}C]Cimbi-712, [^{11}C]Cimbi-717 showed the highest brain uptake in thalamus and lowest uptake in the cerebellum (FIGURE 2D). The [^{11}C]Cimbi-717 TACs indicated reversible binding in the pig brain with fast brain uptake and a more pronounced decline in tissue TACs as compared to [^{11}C]Cimbi-712 (FIGURE 2B). Pre-treatment of the animal with SB-269970 (1.0 mg/kg/h and 4.2 mg/kg/h) decreased [^{11}C]Cimbi-717 uptake and increased the rate of washout in all brain regions.

Since no significant changes were observed between baseline and blocking experiments in the metabolic rate of parent fraction (data not shown), a population based metabolism of [^{11}C]Cimbi-717 was computed and used to generate arterial plasma input TACs. Receptor binding of [^{11}C]Cimbi-717 quantified with the 1-TC model, and here the distribution volumes (V_T) were highest in thalamus (16 ± 2.5 mL/cm^3) and lowest in the cerebellum (6.6 ± 1.2 mL/cm^3) indicating good regional separation, as also confirmed by the TACs (FIGURE 2B). V_T was also calculated for all doses of SB-269970 and prazosin (FIGURE 3C). A dose-dependent reduction in V_T was observed with SB-269970, with significant reductions with the doses 1.0 mg/kg/h ($p < 0.01$) and 4.2 mg/kg/h ($p < 0.001$) in all regions, except the cerebellum. The slope of the occupancy curve for prazosin was not significantly different from 0, supporting that prazosin does not alter the binding of the [^{11}C]Cimbi-717 in vivo.

Receptor binding of [^{11}C]Cimbi-712 was quantified with the 1-TC model. V_Ts were as with [^{11}C]Cimbi-717 highest in the thalamus (87.5 and 54.9 mL/cm^3) and lowest in the cerebellum (35.2 and 32.1 mL/cm^3). The V_Ts of the pre-treated scans revealed a decrease in binding, although it could not be reliably statistically assessed (FIGURE 3A). The slope of the occupancy slopes were,

however, significantly different from 0, verifying that SB-269970 did block the binding of [^{11}C]Cimbi-712.

Based on occupancy plots of [^{11}C]Cimbi-717 (FIGURE 3D), the non-displaceable distribution volume (V_{ND}) and occupancy were extracted from the linear regression. The [^{11}C]Cimbi-717 V_{ND} was on average 2.1 ± 0.8 ml/cm^3 (mean $\pm$ SD, n=5) and i.v. pre-treatment with 0.2 mg/kg/h SB-269970 resulted in 25.4% occupancy, whereas pre-treatment with the higher doses of 1.0 and 4.2 mg/kg/h resulted in 59.9% and 75.4% occupancy, respectively (Table 2). Consequently, the non-displaceable binding potential (BP_{ND}) of [^{11}C]Cimbi-717 at baseline in the thalamus and cerebellum were calculated to 6.4 ± 1.2 and 2.1 ± 0.6 (n=6), respectively.

Treatment with 1.0 mg/kg/h SB-269970 prior to [^{11}C]Cimbi-712 injection resulted in an occupancy of 75.3% and a V_{ND} of 8.57 mL/cm^3 (FIGURE 3B). Consequently, the BP_{ND} of [^{11}C]Cimbi-712 in the thalamus is 7.3 based on average V_{T}s and V_{ND}s.

Comparison of the in vitro and in vivo binding data revealed significant positive correlations between [^{3}H]SB-269970 binding in vitro and [^{11}C]Cimbi-712 (p = 0.016) and [^{11}C]Cimbi-717 (p < 0.001) binding in vivo (FIGURE 4).

Metabolism

Radio-HPLC analysis of pig plasma revealed that after i.v. injection, the parent compound of [^{11}C]Cimbi-717 was relatively slowly metabolized (50% remaining after 30 min) and two radiometabolites were observed (FIGURE 5). The polar metabolite fraction increased during the 90 min scanning time. The other more lipophilic metabolite was detected in relatively low amounts (approximately 15%). However, this metabolite was less lipophilic than [^{11}C]Cimbi-717. The free fraction of [^{11}C]Cimbi-717 in plasma was measured to be on average 6.7% at equilibrium.

DISCUSSION

Here we present the radiosyntheses and in vivo evaluation of two novel 5-HT$_7$ receptor radioligands, [^{11}C]Cimbi-712 and [^{11}C]Cimbi-717. In order to enable comparisons between in vitro and in vivo data we also assessed for the first time the cerebral 5-HT$_7$ receptor distribution in the pig brain.

Consistent with observations in the human brain (*12, 20*) and brain membrane binding assays in different species (*21*), in vitro data with [^{3}H]SB-269970 showed that 5-HT$_7$ receptor distribution in the pig brain was fairly homogenous across brain regions. Our data also showed that hypothalamus, thalamus, and amygdala are areas with high 5-HT$_7$ receptor distribution, which is in line with the involvement of the 5-HT$_7$ receptor in circadian rhythm controlled by the suprachiasmatic nucleus (*22, 23*). As described for human brain tissue, [^{3}H]SB-269970 binding in the pig striatum was low. We found low 5-HT$_7$ receptor binding in the pig cerebellum, corresponding to a study showing low amounts of 5-HT$_7$ receptor mRNA in cerebellum in pigs (*24*). We found a general high binding in the cerebral cortex of the pig brain as reported earlier by membrane binding assays (*21*). Although the cortical binding pattern did not resemble that of 5-HT$_{2A}$ or 5-HT$_{1A}$ receptor binding (*25*), we confirmed the specificity of [^{3}H]SB-269970 through autoradiographic blocking experiments with the specific 5-HT$_{1A}$ and 5-HT$_{2A}$ receptor antagonist WAY-100635 and MDL-100907 (data not shown). No displacement was found with WAY-100635, but in accordance with the affinity of MDL-100907 (K$_i$ ~50 nM) towards the 5-HT$_7$ receptor (*26*), a 40% displacement was observed.

Although [^{11}C]Cimbi-717 were successfully labeled in sufficient RCY for the PET experiments, we did not succeed in further optimising the RCY. We speculate that the major radioactive side-product is due to methylation of the oxindole moiety and if so, the introduction of a

protecting-group at the N-1 position of the oxindole may reduce the formation of the observed side-product.

In vivo evaluation of [^{11}C]Cimbi-717 demonstrated a high brain uptake and a binding distribution similar to the 5-HT$_7$ receptor distribution found in vitro; thalamus has the highest and cerebellum the lowest V$_T$, consistent with the [^{3}H]SB-269970 autoradiography. [^{11}C]Cimbi-717 binding in the striatum was not quite in line with the correlation between in vivo binding in other regions to the in vitro autoradiography binding. Further analysis of these differences revealed that this discrepancy between 5-HT$_7$ receptor binding in vivo and in vitro was larger for the putamen than for caudate nucleus, thus the discrepancy could be due to binding to an unknown target, for which [^{11}C]Cimbi-717 has affinity. However, the occupancy plot did not reveal lower displacement in the striatal regions. We suspect that the difference observed between the in vitro and in vivo results are due to inhomogeneity in the autoradiography experiments. With autoradiography, only a few cross sections were evaluated whereas in PET, binding in the whole region is evaluated. The putamen is in proximity of the amygdala in the pig brain, and partial volume effects may affect the signal from this high binding region, leading to an overestimation of the [^{11}C]Cimbi-712 and [^{11}C]Cimbi-717 binding in the putamen. The correlation between in vitro and in vivo binding was not as strong for [^{11}C]Cimbi-712 as for [^{11}C]Cimbi-717. Along with the difference in binding in striatum, [^{11}C]Cimbi-712 also displayed equal uptake in hippocampus and cerebellum, which is not in line with what we find with [^{3}H]SB-269970 autoradiography. Highest binding is however still observed in the thalamus, consistent with the autoradiography results.

Pre-treatment with SB-269970 resulted in a dose-dependent decrease in [^{11}C]Cimbi-717 binding in the pig brain supporting the 5-HT$_7$ receptor selectivity in vivo for [^{11}C]Cimbi-717. V$_T$ decreased in all regions examined including the cerebellum. Although this decrease in binding in the cerebellum was not statistically significant, it confirms the in vitro autoradiography data and the

literature data in 5-HT$_7$ receptors being present in the cerebellum (*24*). This also invalidates cerebellum as reference region for reference tissue model analysis of the PET data. In the absence of a reference region, we determined the non-displaceable binding using the occupancy plot. Because of the affinity profile of Cimbi-717 (*13*), we ensured that pre-treatment with prazosin, a alpha-1 adrenergic receptor ligand, did not result in any significant decrease in [^{11}C]Cimbi-717 V$_T$. [^{11}C]Cimbi-712 binding was blocked with SB-269970, supporting that this radioligand also labels the 5-HT$_7$ receptor specifically. The slow kinetics of [^{11}C]Cimbi-712, however, complicates modelling of the binding, which results in large variations in the outcome measures (V$_T$) and consequently also larger uncertainties in the calculated occupancy and V$_{ND}$.

The average non-specific binding in the pig brain, V$_{ND}$, of [^{11}C]Cimbi-717 as determined by the occupancy plot was 2.1 mL/cm^3 and thus comprised of about 15 % of the V$_T$ in the high-binding regions. This ratio of specific-to non-specific binding is larger than what is obtained by other PET ligands evaluated in the same species, e.g. app. 50% for [^{11}C]NS14492 and app. 35% for [^{11}C]SB2047145 (*15, 18*).

Modelling of the [^{11}C]Cimbi-717 data was done with the 1-TC model because of the simplicity of the model and because more regions converged with this model compared to 2-TC (99 % vs. 82 %). Also, the Akaike Information Criterion was generally lower for the 1-TC than for the 2TC, hence also in favour of choosing the 1-TC. Although the Logan linearization model had 96 % success in modelling the data, this model was not chosen because of 10-15 % underestimation of the V$_T$ compared to both 1-TC and 2-TC (data not shown). The slow tracer kinetics of [^{11}C]Cimbi-712 complicated the kinetic modelling. The 1-TC was chosen as a consequence of too few regions converging with the Logan linearization model and the 2-TC was also less successful than the 1-TC model.

The systemic metabolism of [11C]Cimbi-717 was relatively slow compared with other radioligands evaluated in pigs (*6, 17, 18*) with approximately 60 % of the total plasma activity arising from the parent compound left after 20 minutes. Metabolism was non-significantly faster after blockade with SB-269970, which could be explained by an increased availability in the blood, and thus an increased availability to enzymatic degradation. No effects on metabolism were observed with prazosin.

CONCLUSION

[11C]Cimbi-712 and [11C]Cimbi-717 were both successfully radiolabeled in sufficient RCYs for in vivo evaluation in the pig. Of the two novel radioligands for brain imaging of the 5-HT$_7$ receptor, [11C]Cimbi-717 generated the highest high brain uptake and contrary to [11C]Cimbi-712 showed reversible kinetics, which is important for quantification. Both [11C]Cimbi-712 and [11C]Cimbi-717 had a regional distribution pattern compatible with 5-HT$_7$ receptor distribution in the pig brain, as assessed independently by autoradiography. Finally, [11C]Cimbi-717 showed a dose-dependent decrease in binding after pre-treatment with the 5-HT$_7$ receptor specific antagonist SB-269970. We conclude that based on these preclinical data, [11C]Cimbi-717 may be a useful radioligand for in vivo imaging of 5-HT$_7$ receptor binding sites in the human brain.

ACKNOWLEDGEMENTS

REFERENCES

1. Matthys A, Haegeman G, Van Craenenbroeck K, Vanhoenacker P. Role of the 5-HT7 receptor in the central nervous system: from current status to future perspectives. *Mol Neurobiol.* Jun 2011;43(3):228-253.

2. Paterson LM, Tyacke RJ, Nutt DJ, Knudsen GM. Measuring endogenous 5-HT release by emission tomography: promises and pitfalls. *J Cereb Blood Flow Metab.* Oct 2010;30(10):1682-1706.

3. Zhang M-R, Haradahira T, Maeda J, et al. Synthesis and preliminary PET study of the 5-HT7 receptor antagonist [11C]DR4446. *J Labelled Cpd Radiopharm.* 2002;45(10):857-866.

4. Andries J, Lemoine L, Mouchel-Blaisot A, et al. Looking for a 5-HT7 radiotracer for positron emission tomography. *Bioorg Med Chem Lett.* 2010;20(12):3730-3733.

5. Lemoine L, Andries J, Le Bars D, Billard T, Zimmer L. Comparison of 4 Radiolabeled Antagonists for Serotonin 5-HT7 Receptor Neuroimaging: Toward the First PET Radiotracer. *J Nucl Med.* 2011;52(11):1811-1818.

6. Herth MM, Hansen HD, Ettrup A, et al. Synthesis and evaluation of [(11)C]Cimbi-806 as a potential PET ligand for 5-HT(7) receptor imaging. *Bioorg Med Chem.* Jul 15 2012;20(14):4574-4581.

7. Ruat M, Traiffort E, Leurs R, et al. Molecular cloning, characterization, and localization of a high-affinity serotonin receptor (5-HT7) activating cAMP formation. *Proc Natl Acad Sci U S A.* Sep 15 1993;90(18):8547-8551.

8. Leopoldo M, Lacivita E, Berardi F, Perrone R, Hedlund PB. Serotonin 5-HT7 receptor agents: Structure-activity relationships and potential therapeutic applications in central nervous system disorders. *Pharmacol Ther.* Feb 2011;129(2):120-148.

9. Volk B, Barkoczy J, Hegedus E, et al. (Phenylpiperazinyl-butyl)oxindoles as selective 5-HT7 receptor antagonists. *J Med Chem.* 2008;51(8):2522-2532.

10. Hall H, Lundkvist C, Halldin C, et al. Autoradiographic localization of 5-HT1A receptors in the post-mortem human brain using [3H]WAY-100635 and [11C]way-100635. *Brain Res.* Jan 16 1997;745(1-2):96-108.

11. Kumar JS, Parsey RV, Kassir SA, et al. Autoradiographic evaluation of [(3)H]CUMI-101, a novel, selective 5-HT1AR ligand in human and baboon brain. *Brain Res.* Apr 24 2013;1507:11-18.

12.   Varnas K, Thomas DR, Tupala E, Tiihonen J, Hall H. Distribution of 5-HT7 receptors in the human brain: a preliminary autoradiographic study using [3H]SB-269970. *Neurosci Lett.* 2004;367(3):313-316.

13.   Herth MM, Volk B, Pallagi K, et al. Synthesis and in vitro evaluation of oxindole derivatives as potential radioligands for 5-HT(7) receptor imaging with PET. *ACS Chem Neurosci.* Dec 19 2012;3(12):1002-1007.

14.   Andersen VL, Herth MM, Lehel S, Knudsen GM, Kristensen JL. Palladium-mediated conversion of para-aminoarylboronic esters into para-aminoaryl-11C-methanes. *Tetrahedron Lett.* 2013;54(3):213-216.

15.   Ettrup A, Mikkelsen JD, Lehel S, et al. 11C-NS14492 as a novel PET radioligand for imaging cerebral alpha7 nicotinic acetylcholine receptors: in vivo evaluation and drug occupancy measurements. *J Nucl Med.* Sep 2011;52(9):1449-1456.

16.   Gillings N. A restricted access material for rapid analysis of [(11)C]-labeled radiopharmaceuticals and their metabolites in plasma. *Nucl Med Biol.* Nov 2009;36(8):961-965.

17.   Ettrup A, Palner M, Gillings N, et al. Radiosynthesis and Evaluation of 11C-CIMBI-5 as a 5-HT2A Receptor Agonist Radioligand for PET. *J Nucl Med.* November 1, 2010 2010;51(11):1763-1770.

18.   Kornum BR, Lind NM, Gillings N, Marner L, Andersen F, Knudsen GM. Evaluation of the novel 5-HT4 receptor PET ligand [11C]SB207145 in the Gottingen minipig. *J Cereb Blood Flow Metab.* 2009;29(1):186-196.

19.   Cunningham VJ, Rabiner EA, Slifstein M, Laruelle M, Gunn RN. Measuring drug occupancy in the absence of a reference region: the Lassen plot re-visited. *J Cereb Blood Flow Metab.* Jan 2010;30(1):46-50.

20.   Hagan JJ, Price GW, Jeffrey P, et al. Characterization of SB-269970-A, a selective 5-HT(7) receptor antagonist. *Br J Pharmacol.* Jun 2000;130(3):539-548.

21.   Thomas DR, Atkinson PJ, Hastie PG, Roberts JC, Middlemiss DN, Price GW. [3H]-SB-269970 radiolabels 5-HT7 receptors in rodent, pig and primate brain tissues. *Neuropharmacology.* 2002;42(1):74-81.

22.   Lovenberg TW, Baron BM, de Lecea L, et al. A novel adenylyl cyclase-activating serotonin receptor (5-HT7) implicated in the regulation of mammalian circadian rhythms. *Neuron.* 1993;11(3):449-458.

23.   Sprouse J, Li X, Stock J, McNeish J, Reynolds L. Circadian rhythm phenotype of 5-HT7 receptor knockout mice: 5-HT and 8-OH-DPAT-induced phase advances of SCN neuronal firing. *J Biol Rhythms.* Apr 2005;20(2):122-131.

24.   Bhalla P, Saxena PR, Sharma HS. Molecular cloning and tissue distribution of mRNA encoding porcine 5-HT7 receptor and its comparison with the structure of other species. *Mol Cell Biochem.* Sep 2002;238(1-2):81-88.

25.   Ettrup A, Kornum BR, Weikop P, Knudsen GM. An approach for serotonin depletion in pigs: effects on serotonin receptor binding. *Synapse.* Feb 2011;65(2):136-145.

26.   Roth BL, Craigo SC, Choudhary MS, et al. Binding of typical and atypical antipsychotic agents to 5-hydroxytryptamine-6 and 5-hydroxytryptamine-7 receptors. *J Pharmacol Exp Ther.* Mar 1994;268(3):1403-1410.

FIGURES AND FIGURE LEGENDS
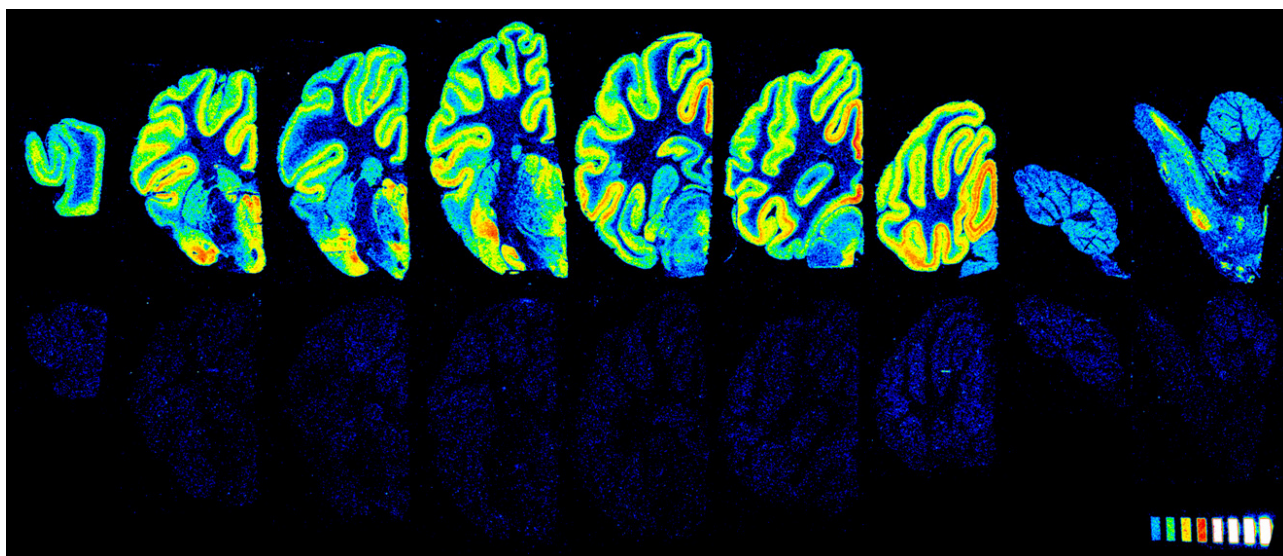
FIGURE 1 Representative sections of 5-HT$_7$ receptor autoradiography. Sections were incubated with 5 nM [^{3}H]SB-269970 to determine total binding (upper row) and with 10 µM SB-258719 to determine non-specific binding (lower row).
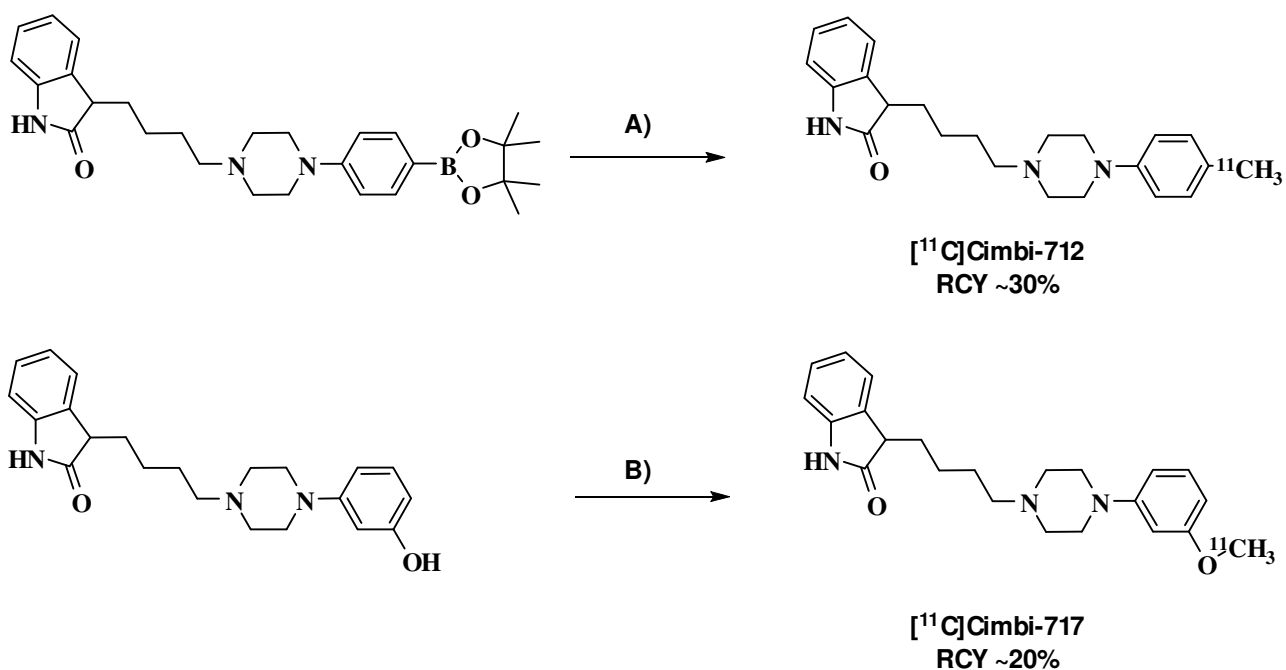
SCHEME 1 Radiosyntheses of [^{11}C]Cimbi-712 and [^{11}C]Cimbi-717. Reagents and conditions: A) [^{11}C]CH$_3$I, K$_2$CO$_3$, Pd$_2$(dba)$_3$, P(o-tolyl)$_3$, 60°C, DMF:H$_2$O (v:v 9:1). B) [^{11}C]CH$_3$OTf, 0.3 mg precursor, MeCN, K$_2$CO$_3$ (1 equiv.), 60°C, 5 min.
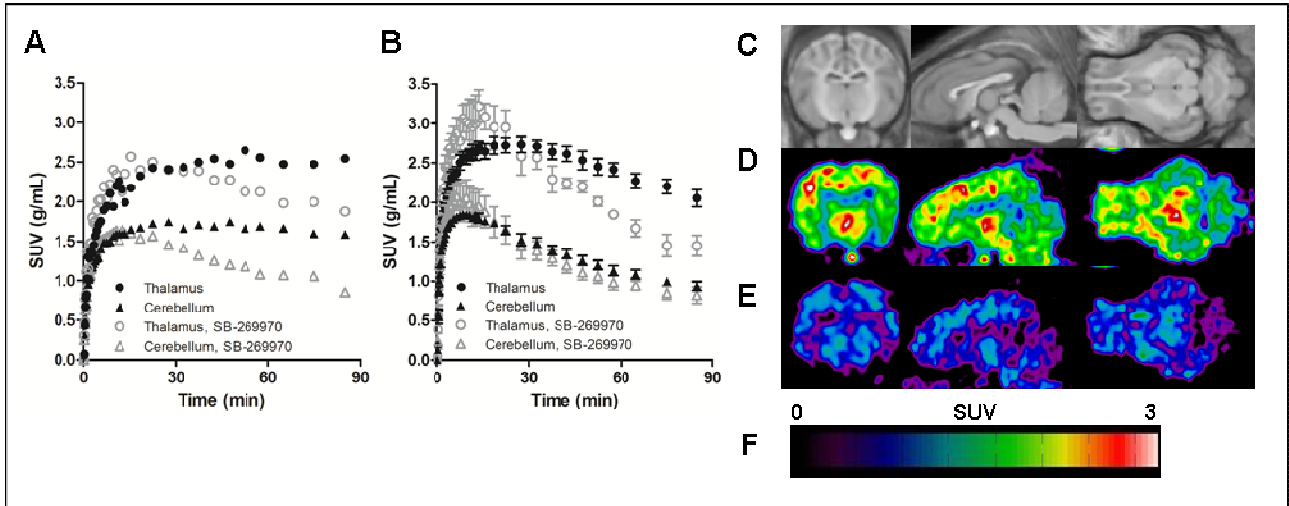
FIGURE 2   A) Time activity curves for [^{11}C]Cimbi-712 at baseline (black circles and triangles, n=2) and after blocking with 1.0 mg/kg/h SB-269970 (open circles and triangles, n=2) B) Time activity curves for [^{11}C]Cimbi-717 at baseline (black symbols, n=6) and after blocking with 1.0 mg/kg/h SB-269970 (open circles and triangles, n=3) C) MRI-based atlas of the pig brain. D) [^{11}C]Cimbi-717 baseline summed PET images from 0-90 min. E) SB-269970 pre-treated [^{11}C]Cimbi-717 summed PET images from 0-90 min. F) Color bar of standardized uptake value (SUV) (g/mL). Error bars: standard error of mean (SEM).
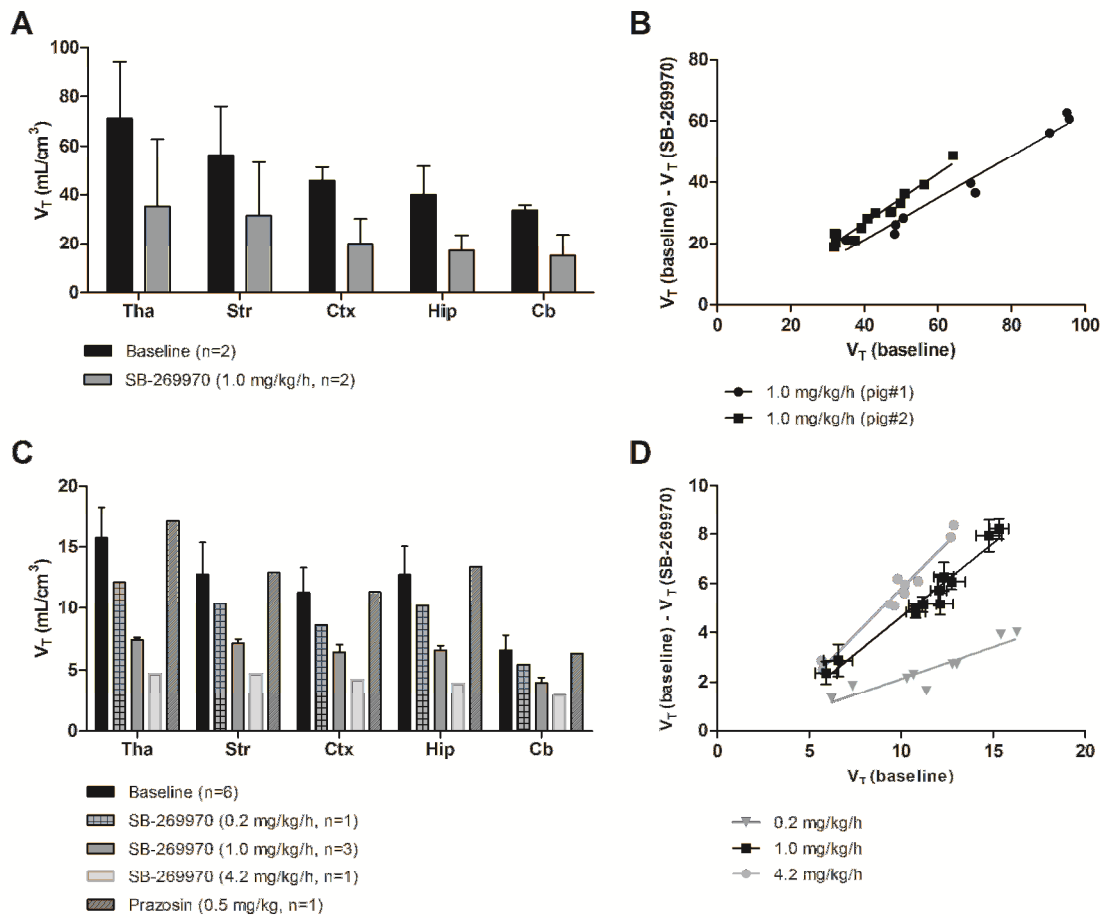
FIGURE 3   A) Distribution volumes (V_T) for [^{11}C]Cimbi-712 quantified by one-tissue compartment modelling. B) Occupancy plots for [^{11}C]Cimbi-712, where the V_Ts for the individual pigs are shown. C) Distribution volumes (V_T) for [^{11}C]Cimbi-717 quantified by one-tissue compartment modelling. D) Occupancy plots for [^{11}C]Cimbi-717 with three different doses of SB-269970. A) and C) Bars represent mean ± SD. B) and D) Bars represent mean ± SEM. ** $P<0.01$ and *** $P<0.001$ significance in comparison to baseline data within each volume of interest. Statistical analysis with two-way ANOVA amd Bonferroni posttest. Tha: Thalamus, Str: Striatum, Ctx: cortex, Hip: hippocampus, Cb: cerebellum.
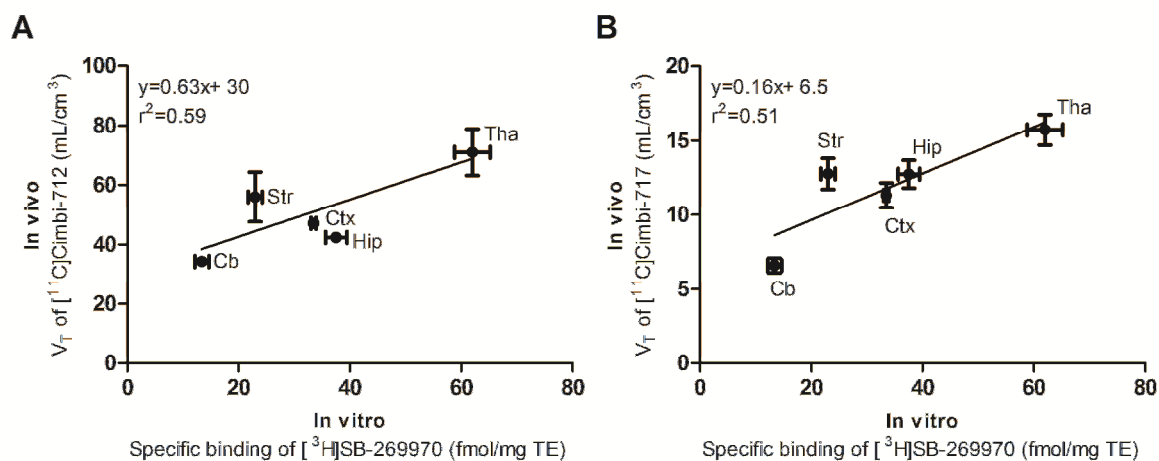
FIGURE 4   Comparison of 5-HT$_7$ receptor brain distribution determined by [^{3}H]SB-269970 autoradiography and determined by in vivo PET experiments using baseline distribution volumes (V$_T$) of [^{11}C]Cimbi-712 (A) and [^{11}C]Cimbi-717 (B). Tha: Thalamus, Str: Striatum, Ctx: cortex, Hip: hippocampus, Cb: cerebellum. Error bars represent mean ± SEM.
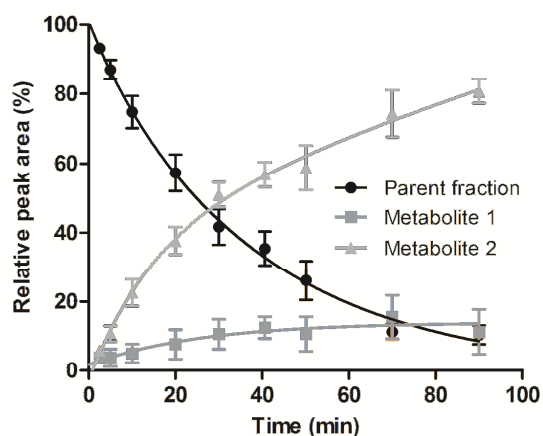
FIGURE 5   Metabolism of [^{11}C]Cimbi-717. Three radioactive compounds could be detected with the radio-HPLC: [^{11}C]Cimbi-717 (parent compound) and two radiolabeled metabolites, both of which had lower retention time than the parent compound. Data are presented as mean ± S.E.M.

TABLES

TABLE 1   5-HT$_7$ receptor distribution in different brain regions determined by autoradiography as specific binding of 5 nM [^{3}H]SB-269970 in fmol/mg tissue equivalent (TE). Average is determined of three independent experiments, values are given as mean ± S.D.

Region	Specific binding (fmol/mg TE)	Number of sections in region
Cortical regions		
Prefrontal cortex	32.7 ± 1.60	2
Frontal cortex	38.3 ± 2.68	5
Temporal cortex	41.0 ± 3.03	7
Cingulate cortex	44.9 ± 2.60	16
Occipital cortex	33.2 ± 2.40	4
Striatum		
Putamen	21.6 ± 1.64	5
Caudate	24.4 ± 2.81	5
Thalamus	45.6 ± 0.19	3
Thalamus (high binding subregion)	62.0 ± 5.53	2
Hypothalamus	43.0 ± 6.03	3
Hippocampus	37.5 ± 3.35	6
Amygdala	48.3 ± 5.01	4
Cerebellum	13.4 ± 2.22	2

SUPPLEMENTARY INFORMATION

General methods

Chemicals were purchased from Acros, Fluka, Sigma, Tocris, or Merck. Unless otherwise stated, all chemicals were used without further purification. Thin layer chromatography (TLC) was performed using plates from Merck (silica gel 60 F_{254} and aluminium oxide 60 F_{254}). Analytical high performance liquid chromatography (HPLC) measurements were performed on a Dionex system consisting of a P680A pump, a UVD 170U detector and a Scansys radiodetector. Chemical purity was checked either by HPLC or by GC. [^{11}C]Methane was produced via the ^{14}N(p,α)^{11}C reaction by bombardment of an [^{14}N]N2 containing 10% H_2 target with a 17 MeV proton beam in a Scanditronix MC32NI cyclotron. Radioactive syntheses were carried out on an automated Scansys module.

[³H]SB-269970 autoradiography
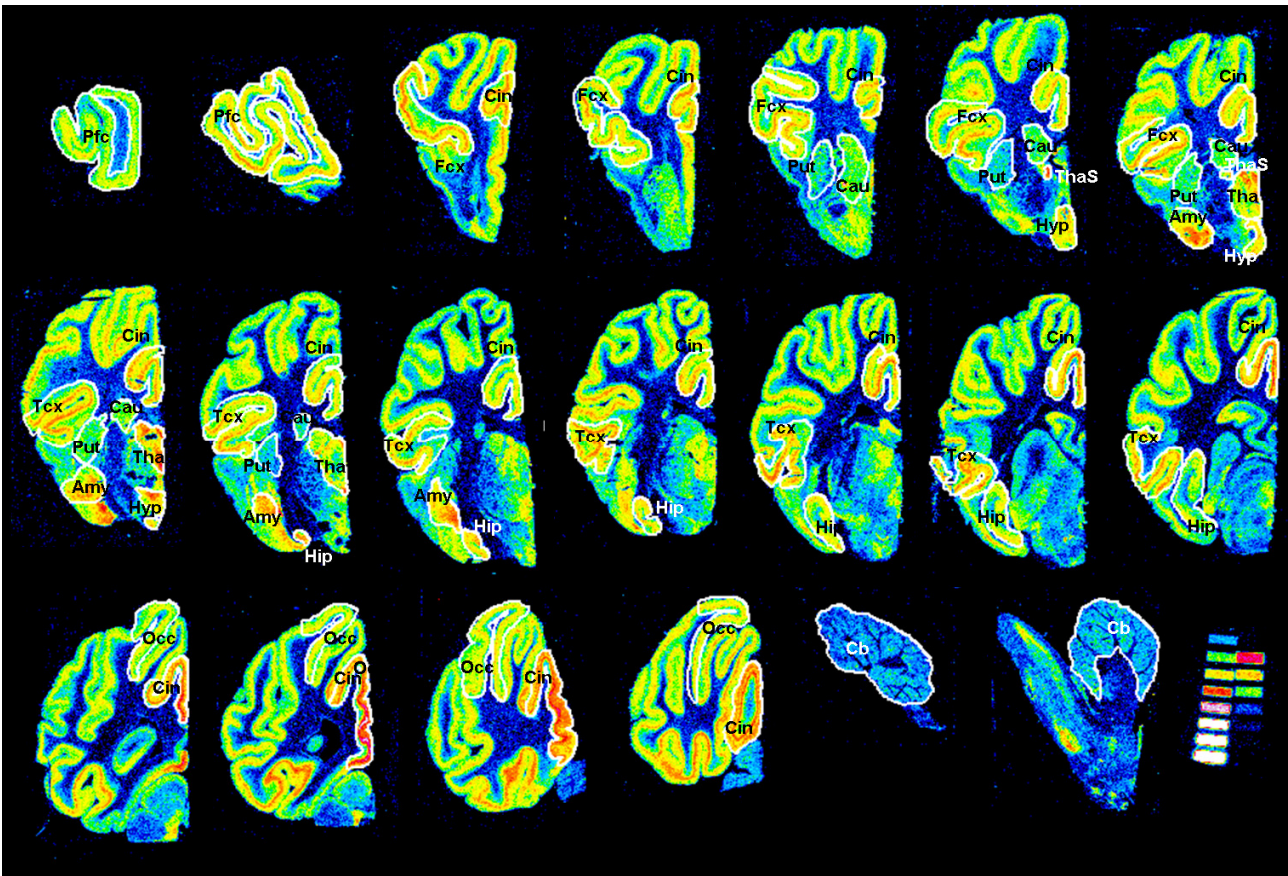
Supplementary Figure 1: Autoradiography with 5 nM [³H]SB-269970. One hemisphere of a pig brain was sliced into 20 different regions. All regions are cut coronal except the two cerebellar regions, which are sliced in the sagittal plane. ROIs are indicated on all regions. Radioactivity of the steps of the the left microscale used as internal standard are: 28, 40, 68, 101, 167, 248, 397, 630 fmol/mg TE (top to bottom).

Optimization of radiolabeling of [^{11}C]Cimbi-717

Supplementary Table 1: Tested radiolabeling conditions for the synthesis of [^{11}C]Cimbi-717.

Precursor	synthon	base	temperature	solvent	time	RCY
0.3 mg	[^{11}C]MeI	1 equiv. NaOH	60 °C	MeCN	5 min	8 %
0.3 mg	[^{11}C]MeOTf	1 equiv. K$_2$CO$_3$	60 °C	MeCN	5 min	27 %
0.3 mg	[^{11}C]MeOTf	1 equiv. K$_2$CO$_3$	60 °C	Acetone	5 min	18 %
0.3 mg	[^{11}C]MeOTf	1 equiv. Bu$_4$NOH	60 °C	MeCN	5 min	-
0.3 mg	[^{11}C]MeOTf	1 equiv. Cs$_2$CO$_3$	60 °C	MeCN	5 min	15 %
0.3 mg	[^{11}C]MeOTf	No base	60 °C	MeCN	5 min	2 %
0.3 mg	[^{11}C]MeOTf	2 equiv. NaOH	60 °C	MeCN	5 min	14 %
0.3 mg	[^{11}C]MeOTf	2 equiv. K$_2$CO$_3$	60 °C	MeCN	5 min	22%
0.5 mg	[^{11}C]MeOTf	1 equiv. K$_2$CO$_3$	60 °C	MeCN	5 min	23 %
0.3 mg	[^{11}C]MeOTf	1 equiv. K$_2$CO$_3$	60 °C	DMSO	5 min	12 %
0.3 mg	[^{11}C]MeOTf	1 equiv. K$_2$CO$_3$	60 °C	DMF	5 min	11 %
0.3 mg	[^{11}C]MeOTf	1 equiv. K$_2$CO$_3$	80 °C	MeCN	5 min	23 %
0.3 mg	[^{11}C]MeI	1 equiv. K$_2$CO$_3$	120 °C	MeCN	5 min	4 %

Radiolabeling of [11C]Cimbi-717
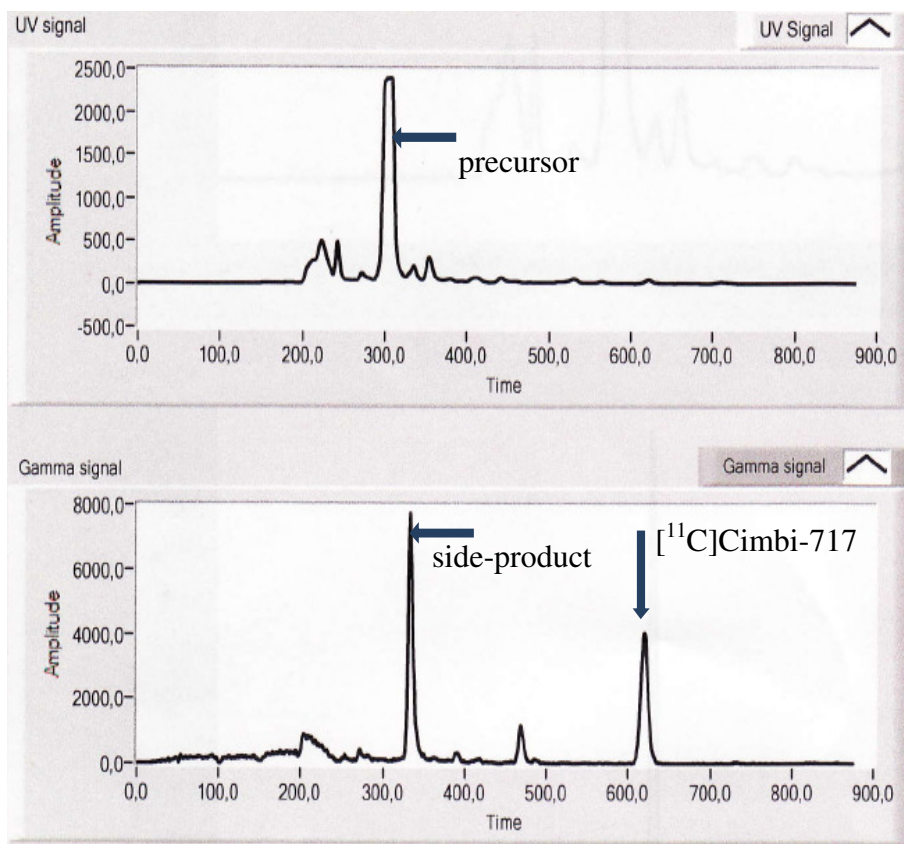
Supplementary Figure 2: Semi-preparative HPLC chromatograms of [11C]Cimbi-717.
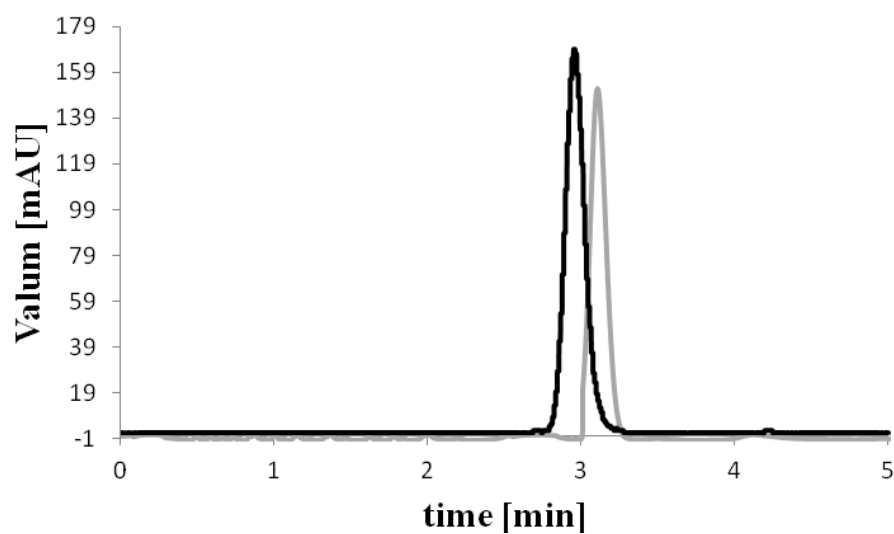
Supplementary Figure 3: Analytical HPLC chromatograms of Cimbi-717 (black) and [11C]Cimbi-717 (grey).

DECLARATION OF CO-AUTHORSHIP

This form must be filled in on the screen, printed, signed and sent to the Graduate School
- You can use the TAB-button to jump between the grey boxes.

Information on PhD student:

Name of PhD student	**Hanne Demant Hansen**
E-mail	**hanne.d.hansen@nru.dk**
Date of birth	**01-05-1985**
Work place	**Neurobiology Research Unit, Rigshospitalet**
Principal supervisor	**Gitte Moos Knudsen**

Title of PhD thesis:

Evaluation of PET radioligand for the cerebral 5-HT7 and 5-HT2A receptors

This declaration concerns the following article:

Direct comparison of [18F]MH.MZ and [18F]altanserin for 5-HT2A receptor imaging with PET.

The PhD student's contribution to the article:

(please use the scale (A,B,C) below as benchmark*)	(A,B,C)
1. Formulation/identification of the scientific problem that from theoretical questions need to be clarified. This includes a condensation of the problem to specific scientific questions that is judged to be answerable by experiments	B
2. Planning of the experiments and methodology design, including selection of methods and method development	C
3. Involvement in the experimental work	C
4. Presentation, interpretation and discussion in a journal article format of obtained data	C

*Benchmark scale of the PhD student's contribution to the article		
A. refers to:	Has contributed to the co-operation	0-33 %
B. refers to:	Has contributed considerably to the co-operation	34-66 %
C. refers to:	Has predominantly executed the work independently	67-100 %

Signature of the co-authors:

Date:	Name:	Title:	Signature:
29/5-13	Anders Ettrup	PHD, M.Sc.	*[signature]*
27/5-13	Matthias M. Herth	PhD	*[signature]*
8/5-13	Agnete Dyssegaard	MSc.	*Agnete Dyssegaard*

Signature of the PhD student and the principal supervisor:

Date: 8/5 - 2013	Date: 8/5-13
PhD student: *[signature] Hanne D. Hans*	Principal supervisor: *[signature]*

1/2

DECLARATION OF CO-AUTHORSHIP

This form must be filled in on the screen, printed, signed and sent to the Graduate School
- You can use the TAB-button to jump between the grey boxes.

Information on PhD student:	
Name of PhD student	Hanne Demant Hansen
E-mail	hanne.d.hansen@nru.dk
Date of birth	01-05-1985
Work place	Neurobiology Research Unit, Rigshospitalet
Principal supervisor	Gitte Moos Knudsen

Title of PhD thesis:
Evaluation of PET radioligand for the cerebral 5-HT7 and 5-HT2A receptors

This declaration concerns the following article:
Direct comparison of [18F]MH.MZ and [18F]altanserin for 5-HT2A receptor imaging with PET.

The PhD student's contribution to the article: *(please use the scale (A,B,C) below as benchmark*)*	(A,B,C)
1. Formulation/identification of the scientific problem that from theoretical questions need to be clarified. This includes a condensation of the problem to specific scientific questions that is judged to be answerable by experiments	
2. Planning of the experiments and methodology design, including selection of methods and method development	
3. Involvement in the experimental work	
4. Presentation, interpretation and discussion in a journal article format of obtained data	

*Benchmark scale of the PhD student's contribution to the article		
A. refers to:	*Has contributed to the co-operation*	0-33 %
B. refers to:	*Has contributed considerably to the co-operation*	34-66 %
C. refers to:	*Has predominantly executed the work independently*	67-100 %

Signature of the co-authors:			
Date:	Name:	Title:	Signature:
28/5/2013	Cecilia Ratner	Msc	*signature*
8/5/2013	Nic Gillings	Dr.	*signature*
8/5 -2013	Gitte M Knudsen	PROF	*signature*

Signature of the PhD student and the principal supervisor:	
Date:	Date:
PhD student:	Principal supervisor:

2/2

DECLARATION OF CO-AUTHORSHIP

This form must be filled in on the screen, printed, signed and sent to the Graduate School
- You can use the TAB-button to jump between the grey boxes.

Information on PhD student:

Name of PhD student	Hanne Demant Hansen
E-mail	hanne.d.hansen@nru.dk
Date of birth	01-05-1985
Work place	Neurobiology Research Unit, Rigshospitalet
Principal supervisor	Gitte Moos Knudsen

Title of PhD thesis:

Evaluation of PET radioligand for the cerebral 5-HT7 and 5-HT2A receptors

This declaration concerns the following article:

Synthesis, Radiolabeling and In Vivo Evaluation of [11C](R)-1-[4-[2-(4-methoxyphenyl)phenyl]piperazin-1-yl]-3-pyrazin-2-yloxy]-2-propanol, a Potential PET Radioligand for the 5-HT7 Receptor.

The PhD student's contribution to the article: *(please use the scale (A,B,C) below as benchmark*)*	(A,B,C)
1. Formulation/identification of the scientific problem that from theoretical questions need to be clarified. This includes a condensation of the problem to specific scientific questions that is judged to be answerable by experiments	A
2. Planning of the experiments and methodology design, including selection of methods and method development	B
3. Involvement in the experimental work	B
4. Presentation, interpretation and discussion in a journal article format of obtained data	B

*Benchmark scale of the PhD student's contribution to the article		
A. refers to:	Has contributed to the co-operation	0-33 %
B. refers to:	Has contributed considerably to the co-operation	34-66 %
C. refers to:	Has predominantly executed the work independently	67-100 %

Signature of the co-authors:

Date:	Name:	Title:	Signature:
16.05.2013	Enza Lacivita	Ph D	*signature*
16.05.2013	Pantaleo Di Pilato		*signature*
28.05.13	Matthias M. Herth	Ph D	*signature*

Signature of the PhD student and the principal supervisor:

Date: 8/5 - 2013	Date: 8/5 - 2013
PhD student: *Hanne D. Hansen*	Principal supervisor: *signature*

¹/₅

DECLARATION OF CO-AUTHORSHIP

This form must be filled in on the screen, printed, signed and sent to the Graduate School
- You can use the TAB-button to jump between the grey boxes.

Information on PhD student:

Name of PhD student	Hanne Demant Hansen
E-mail	hanne.d.hansen@nru.dk
Date of birth	01-05-1985
Work place	Neurobiology Research Unit, Rigshospitalet
Principal supervisor	Gitte Moos Knudsen

Title of PhD thesis:

Evaluation of PET radioligand for the cerebral 5-HT7 and 5-HT2A receptors

This declaration concerns the following article:

Synthesis, Radiolabeling and In Vivo Evaluation of [11C](R)-1-[4-[2-(4-methoxyphenyl)phenyl]piperazin-1-yl]-3-pyrazin-2-yloxy]-2-propanol, a Potential PET Radioligand for the 5-HT7 Receptor.

The PhD student's contribution to the article: *(please use the scale (A,B,C) below as benchmark*)*	(A,B,C)
1. Formulation/identification of the scientific problem that from theoretical questions need to be clarified. This includes a condensation of the problem to specific scientific questions that is judged to be answerable by experiments	
2. Planning of the experiments and methodology design, including selection of methods and method development	
3. Involvement in the experimental work	
4. Presentation, interpretation and discussion in a journal article format of obtained data	

*Benchmark scale of the PhD student's contribution to the article		
A. refers to:	Has contributed to the co-operation	0-33 %
B. refers to:	Has contributed considerably to the co-operation	34-66 %
C. refers to:	Has predominantly executed the work independently	67-100 %

Signature of the co-authors:

Date:	Name:	Title:	Signature:
28/5-2013	Szabolcs Lehel	Ph. D.	*Szabolcs Lehel*
29/5-13	Anders Ettrup	PHD, MSC	*signature*
29/5-13	Valdemar L. Andersen	MSc	*signature*

Signature of the PhD student and the principal supervisor:

Date:	Date:
PhD student:	Principal supervisor:

DECLARATION OF CO-AUTHORSHIP

This form must be filled in on the screen, printed, signed and sent to the Graduate School
- You can use the TAB-button to jump between the grey boxes.

Information on PhD student:

Name of PhD student	Hanne Demant Hansen
E-mail	hanne.d.hansen@nru.dk
Date of birth	01-05-1985
Work place	Neurobiology Research Unit, Rigshospitalet
Principal supervisor	Gitte Moos Knudsen

Title of PhD thesis:

Evaluation of PET radioligand for the cerebral 5-HT7 and 5-HT2A receptors

This declaration concerns the following article:

Synthesis, Radiolabeling and In Vivo Evaluation of [11C](R)-1-[4-[2-(4-methoxyphenyl)phenyl]piperazin-1-yl]-3-pyrazin-2-yloxy]-2-propanol, a Potential PET Radioligand for the 5-HT7 Receptor.

The PhD student's contribution to the article: *(please use the scale (A,B,C) below as benchmark*)*	(A,B,C)
1. Formulation/identification of the scientific problem that from theoretical questions need to be clarified. This includes a condensation of the problem to specific scientific questions that is judged to be answerable by experiments	
2. Planning of the experiments and methodology design, including selection of methods and method development	
3. Involvement in the experimental work	
4. Presentation, interpretation and discussion in a journal article format of obtained data	

*Benchmark scale of the PhD student's contribution to the article		
A. refers to:	Has contributed to the co-operation	0-33 %
B. refers to:	Has contributed considerably to the co-operation	34-66 %
C. refers to:	Has predominantly executed the work independently	67-100 %

Signature of the co-authors:

Date:	Name:	Title:	Signature:
8/5-13	Agnete Dyssegaard	Msc pharm	*Agnete Dyssegaard*
16/5-13	Paola DeGeorgio	Ph D	*Paolo De Giorpo*
17/5-13	Roberto Perrone	Professor	*Perrone*

Signature of the PhD student and the principal supervisor:

Date:	Date:
PhD student:	Principal supervisor:

DECLARATION OF CO-AUTHORSHIP

This form must be filled in on the screen, printed, signed and sent to the Graduate School
- You can use the TAB-button to jump between the grey boxes.

Information on PhD student:

Name of PhD student	Hanne Demant Hansen
E-mail	hanne.d.hansen@nru.dk
Date of birth	01-05-1985
Work place	Neurobiology Research Unit, Rigshospitalet
Principal supervisor	Gitte Moos Knudsen

Title of PhD thesis:

Evaluation of PET radioligand for the cerebral 5-HT7 and 5-HT2A receptors

This declaration concerns the following article:

Synthesis, Radiolabeling and In Vivo Evaluation of [11C](R)-1-[4-[2-(4-methoxyphenyl)phenyl]piperazin-1-yl]-3-pyrazin-2-yloxy]-2-propanol, a Potential PET Radioligand for the 5-HT7 Receptor.

The PhD student's contribution to the article: *(please use the scale (A,B,C) below as benchmark*)*	(A,B,C)
1. Formulation/identification of the scientific problem that from theoretical questions need to be clarified. This includes a condensation of the problem to specific scientific questions that is judged to be answerable by experiments	
2. Planning of the experiments and methodology design, including selection of methods and method development	
3. Involvement in the experimental work	
4. Presentation, interpretation and discussion in a journal article format of obtained data	

*Benchmark scale of the PhD student's contribution to the article		
A. refers to:	Has contributed to the co-operation	0-33 %
B. refers to:	Has contributed considerably to the co-operation	34-66 %
C. refers to:	Has predominantly executed the work independently	67-100 %

Signature of the co-authors:

Date:	Name:	Title:	Signature:
16/05/2013	F Beradi	professor	
16/05/201	N A Colabufo	Professor	
16/05/2013	Mauro Niso	PhD	

Signature of the PhD student and the principal supervisor:

Date:	Date:
PhD student:	Principal supervisor:

4/5

DECLARATION OF CO-AUTHORSHIP

This form must be filled in on the screen, printed, signed and sent to the Graduate School
- You can use the TAB-button to jump between the grey boxes.

Information on PhD student:	
Name of PhD student	Hanne Demant Hansen
E-mail	hanne.d.hansen@nru.dk
Date of birth	01-05-1985
Work place	Neurobiology Research Unit, Rigshospitalet
Principal supervisor	Gitte Moos Knudsen

Title of PhD thesis:

Evaluation of PET radioligand for the cerebral 5-HT7 and 5-HT2A receptors

This declaration concerns the following article:

Synthesis, Radiolabeling and In Vivo Evaluation of [11C](R)-1-[4-[2-(4-methoxyphenyl)phenyl]piperazin-1-yl]-3-pyrazin-2-yloxy]-2-propanol, a Potential PET Radioligand for the 5-HT7 Receptor.

The PhD student's contribution to the article: *(please use the scale (A,B,C) below as benchmark*)*	(A,B,C)
1. Formulation/identification of the scientific problem that from theoretical questions need to be clarified. This includes a condensation of the problem to specific scientific questions that is judged to be answerable by experiments	
2. Planning of the experiments and methodology design, including selection of methods and method development	
3. Involvement in the experimental work	
4. Presentation, interpretation and discussion in a journal article format of obtained data	

*Benchmark scale of the PhD student's contribution to the article		
A. refers to:	Has contributed to the co-operation	0-33 %
B. refers to:	Has contributed considerably to the co-operation	34-66 %
C. refers to:	Has predominantly executed the work independently	67-100 %

Signature of the co-authors:			
Date:	Name:	Title:	Signature:
8/5 -2013	Gitte M. Knudsen	PROF	
16/5/2013	Marcello Leopoldo	PROF.	

Signature of the PhD student and the principal supervisor:	
Date:	Date:
PhD student:	Principal supervisor:

DECLARATION OF CO-AUTHORSHIP

This form must be filled in on the screen, printed, signed and sent to the Graduate School
- You can use the TAB-button to jump between the grey boxes.

Information on PhD student:	
Name of PhD student	Hanne Demant Hansen
E-mail	hanne.d.hansen@nru.dk
Date of birth	01-05-1985
Work place	Neurobiology Research Unit, Rigshospitalet
Principal supervisor	Gitte Moos Knudsen

Title of PhD thesis:

Evaluation of PET radioligand for the cerebral 5-HT7 and 5-HT2A receptors

This declaration concerns the following article:

Synthesis and evaluation of [11C]Cimbi-806 as a potential PET ligand for 5-HT7 receptor imaging.

The PhD student's contribution to the article: *(please use the scale (A,B,C) below as benchmark*)*	(A,B,C)
1. Formulation/identification of the scientific problem that from theoretical questions need to be clarified. This includes a condensation of the problem to specific scientific questions that is judged to be answerable by experiments	B
2. Planning of the experiments and methodology design, including selection of methods and method development	C
3. Involvement in the experimental work	C
4. Presentation, interpretation and discussion in a journal article format of obtained data	B

*Benchmark scale of the PhD student's contribution to the article		
A. refers to:	*Has contributed to the co-operation*	*0-33 %*
B. refers to:	*Has contributed considerably to the co-operation*	*34-66 %*
C. refers to:	*Has predominantly executed the work independently*	*67-100 %*

Signature of the co-authors:			
Date:	Name:	Title:	Signature:
27/5- 13	Matthias M. Herth	PhD	*signature*
29/5 -13	Anders Ettrup	PhD, M.Sc.	*signature*
8/5- 13	Agnete Dyssegaard	M.Sc.	Agnete Dyssegaard *signature*

Signature of the PhD student and the principal supervisor:	
Date: 8/5 -2013	Date: 8/5
PhD student: *Hanne D. Hansen*	Principal supervisor: *signature*

DECLARATION OF CO-AUTHORSHIP

This form must be filled in on the screen, printed, signed and sent to the Graduate School
- You can use the TAB-button to jump between the grey boxes.

Information on PhD student:	
Name of PhD student	**Hanne Demant Hansen**
E-mail	**hanne.d.hansen@nru.dk**
Date of birth	**01-05-1985**
Work place	**Neurobiology Research Unit, Rigshospitalet**
Principal supervisor	**Gitte Moos Knudsen**

Title of PhD thesis:

Evaluation of PET radioligand for the cerebral 5-HT7 and 5-HT2A receptors

This declaration concerns the following article:

Synthesis and evaluation of [11C]Cimbi-806 as a potential PET ligand for 5-HT7 receptor imaging.

The PhD student's contribution to the article: *(please use the scale (A,B,C) below as benchmark*)*	(A,B,C)
1. Formulation/identification of the scientific problem that from theoretical questions need to be clarified. This includes a condensation of the problem to specific scientific questions that is judged to be answerable by experiments	
2. Planning of the experiments and methodology design, including selection of methods and method development	
3. Involvement in the experimental work	
4. Presentation, interpretation and discussion in a journal article format of obtained data	

*Benchmark scale of the PhD student's contribution to the article		
A. refers to:	Has contributed to the co-operation	0-33 %
B. refers to:	Has contributed considerably to the co-operation	34-66 %
C. refers to:	Has predominantly executed the work independently	67-100 %

Signature of the co-authors:			
Date:	Name:	Title:	Signature:
28/5-13	Szabolcs Lehel	Ph.D.	*Szabolcs Lehel*
29/5-13	Jesper L. Kristensen	Ph.D.	*signature*
8/5-13	Gitte M. Knudsen	PROF	*signature*

Signature of the PhD student and the principal supervisor:	
Date:	Date:
PhD student:	Principal supervisor:

DECLARATION OF CO-AUTHORSHIP

This form must be filled in on the screen, printed, signed and sent to the Graduate School
- You can use the TAB-button to jump between the grey boxes.

Information on PhD student:	
Name of PhD student	Hanne Demant Hansen
E-mail	hanne.d.hansen@nru.dk
Date of birth	01-05-1985
Work place	Neurobiology Research Unit, Rigshospitalet
Principal supervisor	Gitte Moos Knudsen

Title of PhD thesis:

Evaluation of PET radioligand for the cerebral 5-HT7 and 5-HT2A receptors

This declaration concerns the following article:

Radiosynthesis and in vivo evaluation of novel radioligands for PET imaging of 5-HT7 receptors

The PhD student's contribution to the article: *(please use the scale (A,B,C) below as benchmark*)*	(A,B,C)
1. Formulation/identification of the scientific problem that from theoretical questions need to be clarified. This includes a condensation of the problem to specific scientific questions that is judged to be answerable by experiments	B
2. Planning of the experiments and methodology design, including selection of methods and method development	C
3. Involvement in the experimental work	C
4. Presentation, interpretation and discussion in a journal article format of obtained data	C

*Benchmark scale of the PhD student's contribution to the article		
A. refers to:	Has contributed to the co-operation	0-33 %
B. refers to:	Has contributed considerably to the co-operation	34-66 %
C. refers to:	Has predominantly executed the work independently	67-100 %

Signature of the co-authors:			
Date:	Name:	Title:	Signature:
27.5.13	Matthias M. Herth	PhD	
29/5-13	Anders Ettrup	PHD, M.Sc.	
27/5-13	Valdemar L. Andersen	M.Sc	

Signature of the PhD student and the principal supervisor:	
Date: 8/5 -2013	Date: 8/5 - 2013
PhD student: Hanne D. Hansen	Principal supervisor:

1/3

DECLARATION OF CO-AUTHORSHIP

This form must be filled in on the screen, printed, signed and sent to the Graduate School
- You can use the TAB-button to jump between the grey boxes.

Information on PhD student:	
Name of PhD student	**Hanne Demant Hansen**
E-mail	**hanne.d.hansen@nru.dk**
Date of birth	**01-05-1985**
Work place	**Neurobiology Research Unit, Rigshospitalet**
Principal supervisor	**Gitte Moos Knudsen**

Title of PhD thesis:
Evaluation of PET radioligand for the cerebral 5-HT7 and 5-HT2A receptors

This declaration concerns the following article:
Radiosynthesis and in vivo evaluation of novel radioligands for PET imaging of 5-HT7 receptors

The PhD student's contribution to the article: *(please use the scale (A,B,C) below as benchmark*)*	(A,B,C)
1. Formulation/identification of the scientific problem that from theoretical questions need to be clarified. This includes a condensation of the problem to specific scientific questions that is judged to be answerable by experiments	
2. Planning of the experiments and methodology design, including selection of methods and method development	
3. Involvement in the experimental work	
4. Presentation, interpretation and discussion in a journal article format of obtained data	

*Benchmark scale of the PhD student's contribution to the article		
A. refers to:	*Has contributed to the co-operation*	0-33 %
B. refers to:	*Has contributed considerably to the co-operation*	34-66 %
C. refers to:	*Has predominantly executed the work independently*	67-100 %

Signature of the co-authors:			
Date:	Name:	Title:	Signature:
28/5-2013	Szabolcs lehel	Ph.D.	*Szabolcs Lehel*
8/5-13	Agnete Dyssegaard	MSc.	*Agnete Dyssegaard*
29/5-13	Jesper L. Kristensen	Ph.D.	*[signature]*

Signature of the PhD student and the principal supervisor:	
Date:	Date:
PhD student:	Principal supervisor:

2/3

DECLARATION OF CO-AUTHORSHIP

This form must be filled in on the screen, printed, signed and sent to the Graduate School
- You can use the TAB-button to jump between the grey boxes.

Information on PhD student:	
Name of PhD student	**Hanne Demant Hansen**
E-mail	**hanne.d.hansen@nru.dk**
Date of birth	**01-05-1985**
Work place	**Neurobiology Research Unit, Rigshospitalet**
Principal supervisor	**Gitte Moos Knudsen**

Title of PhD thesis:

Evaluation of PET radioligand for the cerebral 5-HT7 and 5-HT2A receptors

This declaration concerns the following article:

Radiosynthesis and in vivo evaluation of novel radioligands for PET imaging of 5-HT7 receptors

The PhD student's contribution to the article: *(please use the scale (A,B,C) below as benchmark*)*	(A,B,C)
1. Formulation/identification of the scientific problem that from theoretical questions need to be clarified. This includes a condensation of the problem to specific scientific questions that is judged to be answerable by experiments	
2. Planning of the experiments and methodology design, including selection of methods and method development	
3. Involvement in the experimental work	
4. Presentation, interpretation and discussion in a journal article format of obtained data	

*Benchmark scale of the PhD student's contribution to the article		
A. refers to:	Has contributed to the co-operation	0-33 %
B. refers to:	Has contributed considerably to the co-operation	34-66 %
C. refers to:	Has predominantly executed the work independently	67-100 %

Signature of the co-authors:			
Date:	Name:	Title:	Signature:
8/5 -13	Gitte M. Knudsen	PROF	

Signature of the PhD student and the principal supervisor:	
Date:	Date:
PhD student:	Principal supervisor:

3/3